Fabrication of electrochemical biosensors for detection of microorganisms

Asif Ahmed

Submitted in accordance with the requirements for the degree of

Doctor of Philosophy

The University of Leeds

School of Biomedical Sciences

Faculty of Biological Sciences

January, 2015

Declaration

The candidate confirms that the work submitted is his/her own, except where work which has formed part of jointly-authored publications has been included. The contribution of the candidate and the other authors to this work has been explicitly indicated below. The candidate confirms that appropriate credit has been given within the thesis where reference has been made to the work of others.

Jointly authored publications:

1) Parts of Chapter One of the thesis has appeared in the following publication: Biosensors for whole-cell bacterial detection, 2014, **Ahmed A,** Rushworth JV, Hirst NA, Millner PA.; Clinical Microbiology Reviews, 27 (3): 631-646.

All authors contributed equally. Asif Ahmed and Dr. Jo V. Rushworth are joint first authors in this publication.

2) Some parts of Chapter One have also appeared in monograph co-authored by the candidate; Impedimetric biosensors for medical applications: current progress and challenges, 2013, Rushworth JV, Hirst NA, Goode JA, Pike DJ, **Ahmed A**, Millner PA.; ASME, 2 Park Avenue, NY.

Asif Ahmed contributed equally with other authors in this publication.

3) Some parts of Chapter Three and Chapter Four have been published in Novel impedimetric immunosensor for detection of pathogenic bacteria *Streptococcus pyogenes* in human saliva, 2013, **Ahmed A,** Rushworth JV, Wright JD, Millner PA.; Analytical Chemistry, 85:12118-12125.

Asif Ahmed contributed all of the research work and writing in this research paper. Service technician Mr. John Wright provided heat inactivated pathogenic bacterial

strains. Dr. Jo V. Rushworth and Prof. Paul A. Millner helped with research planning, provided critical feedback and editorial support.

4) Some parts of Chapter Three and Chapter Four were published in Midland blotting: a rapid, semi-quantitative method for biosensor surface characterization, 2013, Rushworth JV, **Ahmed A**, Millner PA.; Journal of Biosensors and Bioelectronics 4:1-7.

Asif Ahmed performed parts of the research work, particularly on-sensor detection of polytyramine and immobilized bioreceptors and contributed to editorial support. Dr. Jo V. Rushworth prepared the manuscript and conducted part of research work. Prof. Paul A. Millner gave critical feedback and editorial support. This is an open access article.

Publications involving works that does not appear in this thesis:

1) Comparative electrochemical analysis of two flow cell systems, 2014, Goode JA, **Ahmed A,** Pike D, Millner PA, Kapur N, Stewart D.; Journal of The Electrochemical Society 161:B143-B146.

The work was done in collaboration with Prof Nik Kapur, Faculty of Engineering, University of Leeds. Asif Ahmed and Jack A Goode contibuted equally in lab work and writing the manuscript. Other authors helped in flow cells design, editorial support and critical discussions.

2) A label-free electrical impedimetric biosensor for the specific detection of Alzheimer's amyloid-beta oligomers, 2014, Rushworth JV, **Ahmed A,** Griffiths HH, Pollock NM, Hooper NM, Millner PA.; Biosensors and Bioelectronics 56:83-90.

Asif Ahmed helped with his biosensor expertise in optimized polymer, biosensor fabrication and impedance spectroscopy in this work. Dr. Jo V Rushworth planned and conducted all the experiments and prepared the manuscript. Prof Paul A Millner and Asif Ahmed contributed in editorial support.

"***There are two pillars of happiness. One is love. The other is finding a way of coping with life that does not push love away***."

-Prof. George Eman Vaillant, Harvard Medical School.

Acknowledgements

First, I would like to thank University of Leeds for supporting my PhD research with Fully International Research Scholarship (FIRS). Without this, it would be hard task for me to concentrate on full time research. My supervisor, Prof. Paul A Millner has always extended his encouraging words, love, humour and both science and non-science suggestions. His style of supervision has inspired me to become an academic like him in my future career. My co-supervisor, Dr. Lars Jeuken has kindly helped me whenever needed, especially with his electrochemistry lectures. I am also very grateful to my academic assessor Prof. Andrew Nelson, for his patient style of teaching me electrochemistry in the very beginning. That was so helpful when I was baffled by the electrochemistry theories for the first time in my life.

Collaboration in science is very powerful and engaging, working with Dr. Jo Rushworth has undoubtedly proved that concept. It was amazing experience to work with her, all the brainstorming meetings, experimental planning, critical discussions, proof reading, philosophical discussions and funny moments made my PhD journey easier than I thought. I have learned from her how one should be devoted and joyful in one's work. I also acknowledge her great tips during SDS-PAGE experiments.

Thanks to Dr. Tim Gibson for sharing his long and rich biosensor research experience with me. Special thanks to Mr. John Wright for his microbiological support which helped me to focus on electrochemistry part. Mr. Martin Fuller was very helpful to teach SEM with all his enthusiasm and expertise. Special thanks to project student Charlotte West, who was a delight to guide. I appreciate your attention and dedication.

Thanks to all the previous and present Millner group members I have met during my PhD. All of you have made my journey smooth some way or other, with your lunch and coffee moments, special dinners, fun and so on. Thanks to Dr. Vas Poonambalam and his group for their all kind of support.

I also acknowledge the love and inspiration of my teachers, colleagues and students from Khulna University, Bangladesh. Specially, Dr. Md. Morsaline Billah who encouraged me all the way in my career. Being a senior, teacher and colleague you have played a fantastic role.

My family members were always beside me, my parents, brothers and sisters, their kids with all of their love and care. My beloved wife Kamrun Nahar and loving son Ayman Ahmed have made my every tough day easier with their love , affection and presence. Last but not least, all my friends, well-wishers, seniors and juniors, you all mean a lot to me. Lots of love to you all for being with me.

Abstract

Pathogenic bacteria are responsible for around two million deaths and many reported hospitalization per year worldwide. *Streptococcus pyogenes* is a Gram +ve bacteria responsible for invasive and non-invasive infections. Traditional molecular and immunological detection systems are usually time consuming, require well equipped laboratory facilities and skilled personnel. Biosensors are ideal for the early detection of microorganisms because of their on-site, sensitive and rapid detection capability and electrochemical impedance offers a highly sensitive signal following target analyte interaction.

In this study, immunosensors were fabricated on commercial screen printed gold electrodes to detect *S. pyogenes*. Electrochemical impedance spectroscopy (EIS) was carried out as the primary technique with other supporting methods including cyclic voltammetry (CV), on-sensor chemiluminescence characterization (termed 'Midland blotting') and fluorescence microscopy to successfully detect bacteria. With unstable impedance using conducting polymer and inconsistent signal using self-assembled monolayer (SAM), a non-conducting polymer, polytyramine was selected and optimized. Polyclonal antibodies against heat killed intact *S. pyogenes* was immobilized using two methods. First, biotinylated antibodies were immobilized via biotin-NeutrAvidin; second, reduced half antibody fragments were coupled using a bifunctional linker. The latter produced a higher signal due to the oriented half antibodies and close distance from the sensor surface. The surface density of antibodies was found to be critically important to get optimum signal. *S. pyogenes* cell surface proteins M and H, contributed towards the non-specific signal and this was reduced using protein A/ G as specific blocking agents. In addition, an attempt was made to polymerize novel phenolic copolymers in order to minimize non

relevant protein interference from biological samples. The optimized full antibody based sensors detected *S. pyogenes* both in buffer to 10^4 cells/ml and in spiked 50% human saliva in PBS (v/v) with high specificity and selectivity.

Abbreviations

2-ABA	2-aminobenzylamine
2-MEA	2-mercaptoetylamine HCl
*C*dl	Double layer capacitance
CPE	Constant phase element
CV	Cyclic voltammetry
DMSO	Dimethyl sulfoxide
DS	DropSens
DTT	Dithothreitol
E	Potential
ECL	Enhanced chemiluminescence
EIS	Electrochemical impedance spectroscopy
ELISA	Enzyme linked immunosorbent assay
GAS	Group A streptococcus
GCE	Glassy carbon electrode
GOx	Glucose oxidase
HRP	Horseradish peroxidase
i	Current
IgG	Immunoglobulin
IHP	Inner Helmholtz plane
ISE	Ion selective electrodes
ITO	Indium tin oxide
LSPR	Localized surface plasmon resonance
mSAM	Mixed self-assembled monolayer
NET	Neutrophil extracellular traps
NHS	N-hydroxysuccinimide ester
OHP	Outer Helmholtz plane
PANI	polyaniline
Ptyr	Polytyramine
QCM	Quartz crystal microbalance
*R*ct	Charge transfer resistance
*R*p	Polarization resistance
*R*s	Solution resistance
SAM	Self-assembled monolayer
ScFv	Single chain variable fragment

Sda1	Streptodornase A
SEM	Scanning electron microscopy
SERS	Surface enhanced Raman scattering
SLS	Streptolysin S
SNR	Signal to noise ratio
SpeA	Exotoxin type A
SPR	Surface plasmon resonance
STSS	Streptococcal toxic shock like syndrome
TCEP	Tris (2-carboxyethyl) phosphine
TIRE	Total internal reflection ellipsometry
Z’	Real impedance
-Z’’	Imaginary impedance
W	Warburg component

Contents

List of Tables

List of Figures

Chapter One

Introduction

Chapter 1 Introduction

1.1 Overview

Bacterial infections are one of the major reasons behind hospitalization, mortality and morbidity every year worldwide. In spite of many detection techniques being developed, their complicated nature, long processing time and multiple steps trigger the need for a quick point-of-care detection method. Biosensors can be an attractive option providing rapid and sensitive detection of infectious bacteria in food, environmental, security and medical sectors. However, research to develop stand-alone sensor chips to detect whole bacteria without any pre-processing step is in its infancy and many development and optimization steps are required to take a finished product to market.

A biosensor uses different output signals, e.g. optical, mechanical, electrochemical and others which correlate with the binding interaction on its surface and can be presented as a quantitative value. In this study, an electrochemical technique, electrochemical impedance spectroscopy (EIS) was used as the primary detection method. EIS has several benefits including precise information on surface electrochemistry, high sensitivity, label free detection, the potential to be miniaturized and to be used in a point-of-care device. Although, EIS is particularly helpful during research and development, an ideal device would in reality use single frequency to measure the component of impedance. This research work was exclusively focused on screen printed commercial electrodes as a starting transducer as this type of single use electrode format is suitable for use in home or medical facilities.

Initially, electrodes were well characterized and a base polymer with stable electrochemical properties was optimized. Then, *Streptococcus pyogenes* was selected and used as a pathogenic bacterial model. Antibodies generated against this bacteria were used to construct immunosensors using full antibodies and reduced antibody fragments. Strict optimization was practiced at every step of immobilization to enhance binding. As bacteria are µm in size (typically 0.5 µm to 2 µm) and contain complex surface proteins and glycoproteins, non-specific interactions were also observed. These non-specific binding issues were minimized by targeting the specific reasons for them. In addition, novel copolymers of phenolic compounds have been examined in an attempt to minimize the non-specific signal due to presence of various interfering proteins in real sample like human serum. In the introduction chapter, brief overview of *S. pyogenes,* different biosensor techniques and research highlights of sensor development strategies to detect whole bacteria have been presented. Then general methods are presented followed by the research data. An overall general discussion is presented at the end with a focus on key future possibilities. Overall, the information and primary findings presented here will aid biosensor research in the fabrication of electrode surfaces to detect specific bacteria.

1.2 Bacteria as biomarkers

Bacterial infections and their associated diseases are one of the leading causes of mortality and morbidity worldwide resulting in millions of death and hospitalization. In 2011, WHO identified infectious and parasitic diseases as second highest cause of worldwide death, with lower tract infections (third), diarrheal disease (fourth) and tuberculosis (seventh) in the list. These infections are equally lethal in both low income or high-income countries. The low income countries suffer more due to the lack of, or delayed identification, poor management and treatment. However, in high income countries food borne pathogens cause around 76 million cases of illness, 300,000 hospitalizations and 5,000 deaths per year (Scallan et al., 2011; Sharma and Mutharasan, 2013c).

For these reasons, bacteria are important target for detection and identification in food safety, medicine, public health, environment and security. The choice of detection method and its suitability vary from case to case, depending on the sample, type of bacteria and particular target area of bacterial cells to be detected. Before discussing conventional bacterial detection methods in practice (**section 1.3**) and development of biosensors to detect whole bacterial cells (**section 1.10**) the general structure and possible analytical targets in a bacterial cell are presented.

Bacteria are usually 0.5 to 5 µm in size, with different shapes including spherical cocci, rod-shaped bacilli and spiral shaped spirilla. Generally, most bacteria are covered by a cell wall surrounding the cell membrane (**Figure 1.1**). The main component of cell wall is peptidoglycan, a negatively charged polymer comprising linked *N*-acetylglucosamine and *N*-acetylmuramic acid. Bacteria containing a thick

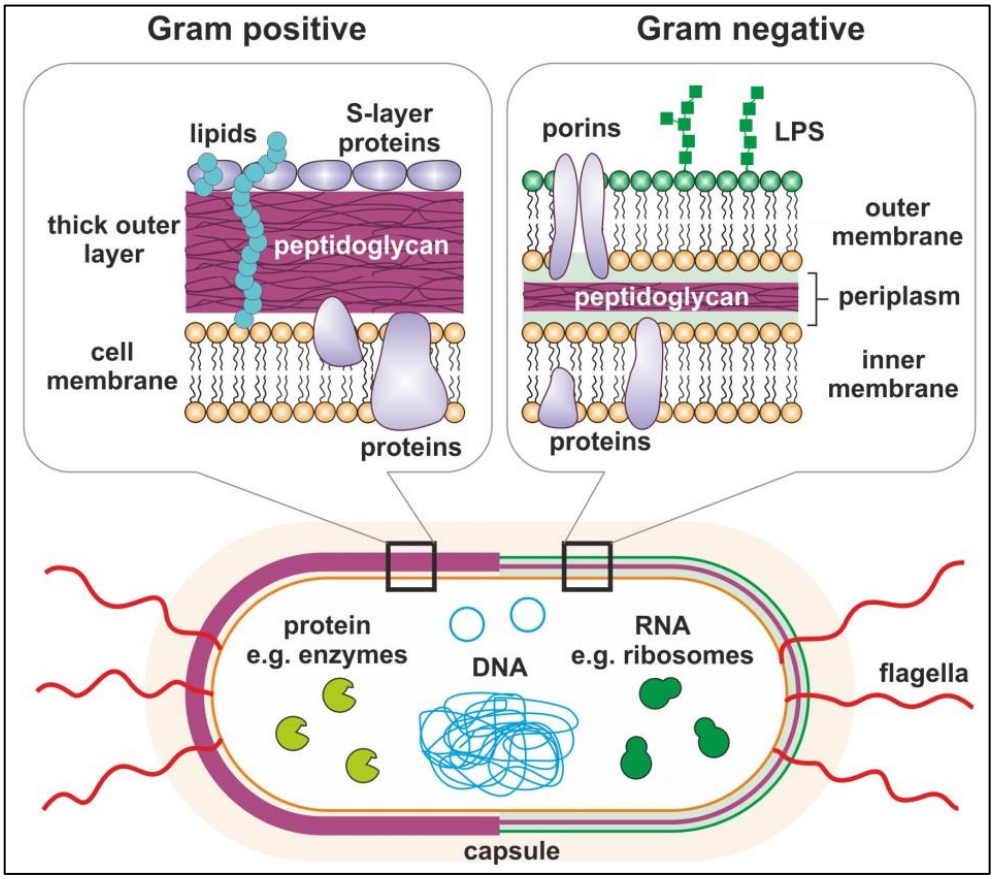

Figure 1.1: Bacterial architecture and targets for biosensing

The cell wall of Gram-positive bacteria comprises of a thick layer of peptidoglycan, which also contains lipids and other protein components, surrounding a lipid membrane. In contrast, Gram-negative bacteria possess a much thinner peptidoglycan layer sandwiched in between two cell membranes. The outer membrane contains proteins, such as porins, as well as lipopolysaccharides (LPS), also known as endotoxin. The inner membranes of both types of bacteria contain various proteins. Both types of bacteria may have flagella. Intracellular targets for biosensing include proteins, DNA and RNA. Image reproduced from (Ahmed et al., 2014).

peptidoglycan layer are termed as Gram positive and can retain the violet Gram stain. On the other hand, Gram negative bacteria can not pick this stain as they have a very thin layer of peptidoglycan. The Gram positive bacterial cell surface also contain lipids and other proteins. Gram negative bacteria contain lipopolysaccharides (LPS) which act as endotoxins and various proteins like porins which cause immune reaction in humans. These lipids, proteins or LPS can be a suitable target for bacterial detection as they present unique characteristics.

Other targets in bacteria are DNA, RNA, intracellular proteins, enzymes and exotoxins. However, most of these components are internal and cell disruption is a prerequisite to release these before identification. In this thesis, identification of whole bacterial cells will be focused on, which deals with whole cell detection thus avoiding any processing step to extract cellular materials. Thus cell surface biomarkers will be discussed as they are targeted to detect whole bacterial cells.

.

1.3 Conventional bacterial detection methods

Conventional bacterial detection methods include microscopy, cell culture, biochemical assays, immunological tests and genetic analysis. **Table 1.1** presents some common bacterial diseases, their conventional detection methods and strategies. Typically specimens (e.g. blood, saliva, urine, food or environmental sample) are processed in laboratory by the methods mentioned above. Morphological identification can be achieved by microscopy but gives less specificity. Bacterial culture in selective media is another option. However, the long incubation time (often over days) and inability of many bacteria to be cultured limit this method. Bacterial surface epitopes can be specifically detected by enzyme linked immunosorbent assays (ELISAs) in the laboratory.

Genetic analysis has taken the identification further. For example, PCR can handle very tiny sample and give highly specific detection, although it is expensive (Croxen et al., 2013). However, false positive can arise due to incorrect PCR primer pair selection and mutated strains can result in inactive primer pairing with false negatives. Molecular detection also needs cell disruption and isolation of target to be detected. Finally, a further problem with PCR based detection is its extreme sensitivity. Many bacteria that cause disease are normal commensal organism, and only cause disease when they are presented to a particular site. But whether latent or virulent they are always sensitive to PCR based detection.

For some strains, detection time is very crucial as it has strong correlation with patient survival. An example here is the Meningococcal meningitis when a delay of a few hours can mean death or severe disability for the patient. Thus point-of-care biosensor devices can play a major role in detection of bacteria where rapid detection is very important and can save life. Point-of-care detection chips are not

only a good alternative due to potentially low price but it can also help in regular monitoring of food and beverages and environmental monitoring in remote places. In **section 1.10** the main focus will be on whole bacterial cell detection with a special focus on electrochemical impedimetric biosensors.

Table 1.1: Common global diseases of bacterial infection, burden and their conventional detection methods

Disease(s)	Causative bacterial agent(s)	Disease burden (DALY), millions	Annual deaths, millions	Annual cases, millions	Conventional method of diagnosis	Diagnosis time critical?	Spread prevention critical?	Ref(s)
Lower respiratory infections (e.g. pneumonia)	*Streptococcus pneumoniae* *Haemophilus influenzae*	94.5	4.2	430	Physical examination, chest X-ray, sputum and blood cultures, PCR.	No	No	(a)
Diarrheal diseases	*Shigellae* *Campylobacter* *Salmonellae* *Escherichia coli O157:H7*	72.8	2.1	4,620	Microbiology (culture on Gram-negative selective media), PCR, ELISA, particle agglutination assay	Possibly	Yes	(b,c)
TB	*Mycobacterium tuberculosis*	34.2	1.5	7.8	Chest X-ray, blood test, Mantoux TST, sputum smear and culture, staining and microscopy	No	Yes	(d)
Meningitis	*Neisseria meningitides,* *Streptococcus pneumonia,* *Escherichia coli*	11.4	0.34	0.7	Lumbar puncture, blood cultures, PCR	Yes	No	(e)

Disease(s)	Causative bacterial agent(s)	Disease burden (DALY), millions	Annual deaths, millions	Annual cases, millions	Conventional method of diagnosis	Diagnosis time critical?	Spread prevention critical?	Ref(s)
Sexually transmitted infections (excluding HIV)	*Treponema pallidum* (Syphilis), *Chlamydia trachomatis* (Chlamydia)*, Neisseria gonorrhoeae* (Gonorrhoea)	10.4	0.13	222	Urethral/vaginal swab and culture, Gram staining and microscopy, immunoassay, particle agglutination assay	No	Yes	(f,g)

Abbreviations: DALY, disability-adjusted life years i.e. number of years lost due to disease; ELISA, enzyme-linked immunosorbent assay; TB, Tuberculosis; TST, tuberculin skin test; HIV, human immunodeficiency virus; PCR, polymerase chain reaction. **References:** a (Carroll, 2002), b (Barletta et al., 2013), c (Boehme et al., 2013; Pfeiffer et al., 2012), d (Boehme et al., 2013), e (Bamberger, 2010), f (Su et al., 2011b) and g (Read and Donovan, 2012). The table is adapted from (Ahmed et al., 2014).

1.4 The pathogenic bacteria *Streptococcus pyogenes*

Streptococcus pyogenes, the Gram-positive beta haemolytic bacterium (**Figure 1.2**), also known as group A *Streptococcus* (GAS), is a human pathogen that is responsible for numerous superficial and invasive diseases with diverse clinical manifestations (Cole et al., 2011). Worldwide, estimated 700 million cases of mild, non-invasive infections are found each year, of which near 650,000 progress to serious invasive infections. The mortality rate due to invasive infection is approximately 25% (Carapetis et al., 2005). In the UK, a widespread increase in invasive group A streptococcal (*S. pyogenes*) infections was identified in December 2010, beyond the seasonal expectation (Lamagni et al., 2008; Report, 2011; Zakikhany et al., 2011).

GAS associated diseases can be classified according to their pathology. This can be localized, invasive and non-suppurative post infection sequelae. They form colonies in the oropharynx and skin, and have got the ability to invade the epithelia causing invasive diseases e.g. bacteraemia, cellulitis and necrotizing fasciitis. Further complications arise due to development of streptococcal toxic shock-like syndrome (STSS). Other common symptoms are abscesses, septic arthritis and meningitis (Cunningham, 2000). After successful colonization of the epithelial cells, GAS penetrates further where it faces resistance from the innate immune system and other different cell types. It has acquired several virulence determinants which allow it to survive the human defence mechanisms.

GAS strains are classified into serotypes according to their surface protein M, which is encoded by the *emm* gene. More than 200 strains have been typed by sequence variance in the *emm* gene, in a process known as *emm* typing (Smeesters et al., 2010). The most frequently identified virulent invasive strain worldwide is M1 and

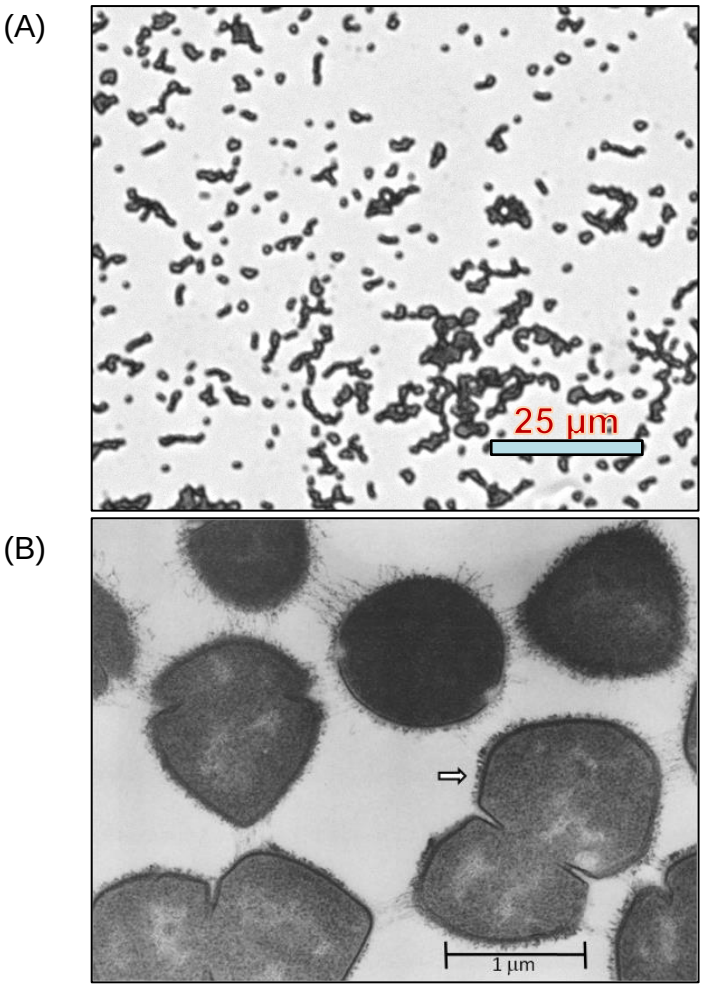

Figure 1.2: Light and electron micrograph of *S. pyogenes*

(A) Light micrograph of *S. pyogenes* cells. They can aggregate to form small chain like structures. The cells were Gram stained before imaging. (B) SEM image of *S. pyogenes* outer surface showing plenty of surface proteins (marked with arrow) which have a role in pathogenesis and can be used as targets for developing bioreceptors against them. Figure B was adapted from (Fischetti, 1989).

the unusual revival of infection in the last 30 years was found to be associated with globally distributed clone M1T1. The distinguishing factors of M1T1 are bacteriophage encoded virulence factors, extracellular streptodornase D (Sda1) and exotoxin type A (SpeA) which might have key roles in its virulence potential (Sumby et al., 2005). In general, most GAS strains show repeating emergence in a particular community at times, whereas M1T1 has shown persistence globally, both in invasive and non-invasive forms (Aziz and Kotb, 2008).

1.4.1 GAS epidemiology and virulence factor

There are several virulence factors responsible for different stages of GAS infection. These factors help the bacteria in activities like colonization, adhesion to epithelial cells, anti-phagocytic effects, invasion, spread and systemic toxicity (**Figure 1.3**). Surface anchored M protein mediates adhesion to the epithelial cell and helps the bacteria survive neutrophils and neutrophil extracellular traps (NETs). The Sda1 of M1T1 is a DNase that degrades the DNA of NETs and enables the bacterium to escape the killing by immune cells. Invasive GAS strains are coated with a capsule composed of hyaluronic acid which gives resistance to opsophagocytosis. The M protein and capsule jointly help in the invasion process. Research suggests that Sda1, M protein and capsule together promote M1T1 resistance to NET based killing in the host (Cole et al., 2011).

Extracellular products also confer the virulence of GAS. Streptolysin O (SLO) is a cholesterol dependent cytolysin that forms oligomers to create pores in the host membrane. It induces apoptosis in epithelial cells, neutrophils and macrophages. Streptolysin S (SLS) is another type of cytolysin capable of damaging membranes of platelets, leukocytes and subcellular organelles.

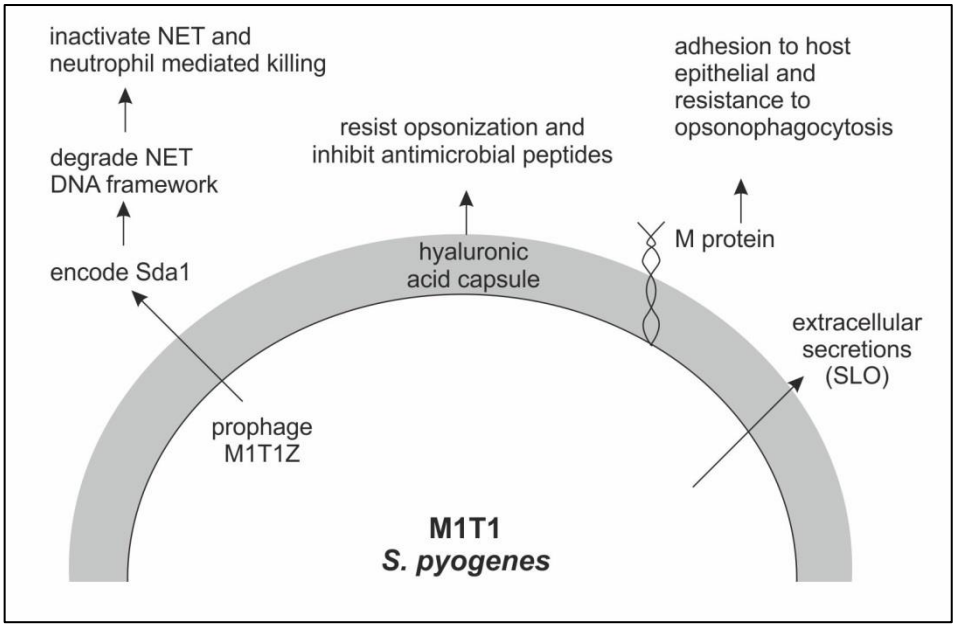

Figure 1.3: Schematics of *S. pyogenes* M1T1 strain virulence factors

The virulent strain M1T1 confers adhesion, colonization, invasion and resistance towards the immune system via extracellular secretions, M protein mediated adhesion and hyaluronic acid capsule. All of these factors, alone or cooperatively, take part in pathogenesis and survival mechanism inside host. The image is drawn based on the literature from (Cole et al., 2011).

Streptococcal pyrogenic exotoxins are family of bacterial super antigens that triggers STSS. These super antigens bind to the T cells via MHC and cause over production of interleukins. These over expressed modulators activate the complement system leading to hypotension and multi-organ failure which are typical characteristics of STSS (Bisno et al., 2003).

1.4.2 Current methods to detect *S. pyogenes*

For many years, throat swab culture from pharyngitis patients was the only way for the detection of *S. pyogenes*. Usually throat swab from suspected patients are cultured in blood agar medium. The main disadvantages of this procedure is the long incubation time (usually one to two days) involved in obtaining the result. In early 1980s, the rapid antigen test became available as commercial choice (Gerber and Shulman, 2004). The first of this type was latex agglutination test (Gerber et al., 1984) which became obsolete due to unclear results (Schwabe et al., 1991).

Commercially available products now use lateral flow strips where pre incubation of specimen is done to dissolve cell wall to release carbohydrates. These cell wall carbohydrates are specifically detected by antibodies immobilized to these strips. Most of the commercial test kits provide colour based qualitative detection, e.g. OSOM® Ultra Strep A Test (Sekisui Diagnostics, UK), BD check™ Group A Strep Test (Beckton Dickinson, NJ, USA), QuickVue In-line Strep A Test (Quiden Corporation, San Diego, USA). However, these commercial strips are still need to be coupled with follow up culture results as false positive and false negative results are often reported. As a safe and efficacious GAS vaccine is still to be developed, research has focused on early detection of the strain. Specific, cost effective and rapid point-of-care label free detection would be an advantage for better management of this disease.

1.5 Bacteriophage MS2 and *E. coli* as model microbes

Bacteriophage MS2 is ~27 nm RNA virus that can infect male *E. coli* (Stockley et al., 1994). Because of its simple structural composition, small size and ease of propagation, MS2 is considered a good model organism. The genome (3569 nucleotide) has been sequenced and it encodes the coat protein, a maturation protein (also known as A protein), a replicase subunit and a lysis protein. MS2 coat protein is the main structural unit. The A protein helps MS2 to bind to the bacterial pillus. The replicase and lysis protein take part in viral replication and lysis of bacterial cells respectively. The high resolution 3D structure of MS2 resolved its icosahedral capsid shape composed of 90 coat protein homodimers (Golmohammadi et al., 1993).

E. coli is gram negative rod shaped bacterium commonly found in the lower intestine of warm blooded organisms. The average length is 2 µm and diameter around 0.5 µm and a few strains contain flagella that help in their motility and attachment. Most strains can be grown at 37° C with minimal media. The majority of the strains are harmless to humans except a few which can cause food contamination. It has been widely used as model organism as it can be grown quickly and easily in laboratory. Some strains have been adapted for laboratory use so that they have lost their ability to thrive in intestines like the wild type. In this thesis, beside MS2 and *E. coli, S. pneumoniae* (another pathogenic *streptococcus*) was also used as model or control microorganism. In practice, MS2 pure culture has been used, whereas in case of bacteria heat killed strains were applied onto biosensor.

1.6 Biosensors

1.6.1 Overview

A biosensor is composed of a biological recognition system, known as the bioreceptor, a transducer and read out system e.g. a computer (**Figure 1.4**). The component to be analysed, termed the analyte, interacts with the bioreceptor and produces a signal. Then transducer converts the information into a measurable effect, e.g. an electrical signal which can be interpreted by computer (Vo-Dinh and Cullum, 2000). The type of biosensor depends on the combination of bioreceptor and transducer.

An ideal biosensor should have some key properties to be commercially viable. They include a low detection limit, species and strain selectivity, low assay time and good precision, the ability to discriminate viable from non-viable cells and ease of assay protocol. Their packaging into user-friendly and compact devices is also a prerequisite to take a sensor into market (Grieshaber et al., 2008; Ivnitski et al., 1999).

Biosensors are generally classified depending on the choice of bioreceptor or type of transduction method. Biosensor research incorporates different transduction modes including non-electrochemical processes such as optical, mechanical and electrochemical methods e.g. amperometric, potentiometric and impedimetric. Sometimes multiple transduction modes can be coupled to construct efficient biosensing. In the following section different transduction methods will be discussed in brief, which will be followed by a further detailed discussion of impedance spectroscopy (**section 1.7**) and cyclic voltammetry (**section 1.8**) which are key techniques underpinning the work in this thesis. Specific applications of different transducers in detecting whole bacterial cells will be discussed in **section 1.10**.

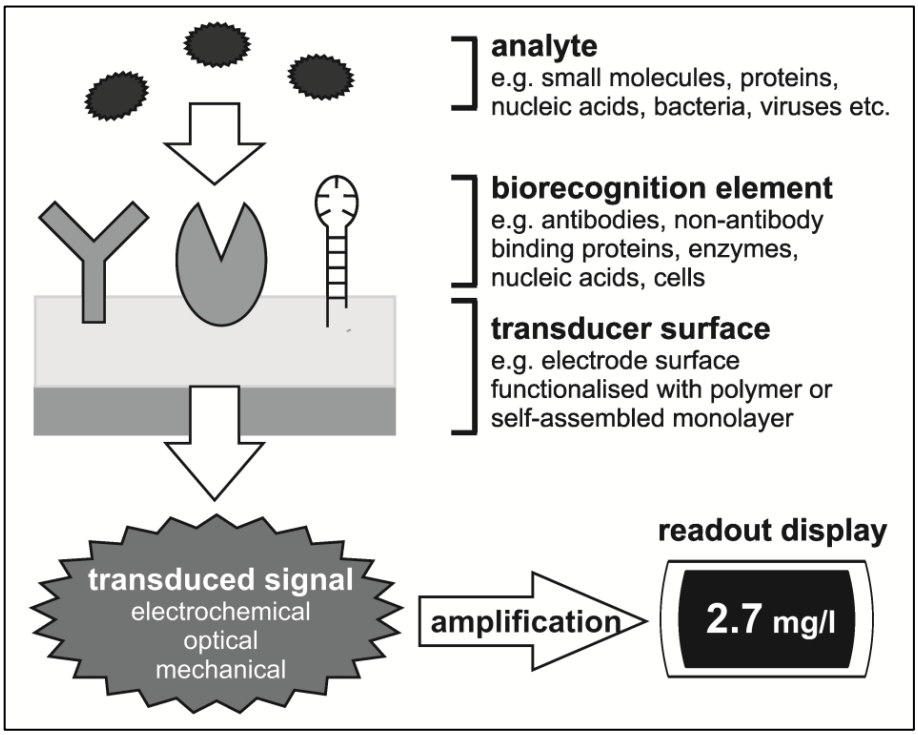

Figure 1.4: General schematic of a biosensor

The three basic components of a biosensor are a bio-recognition element, a transducer and a readout display. Analyte binding to the bioreceptors within the bio-recognition element causes a difference in signal to be transduced through to the readout display (Rushworth et al., 2013b).

1.6.2 Non-electrochemical transduction

1.6.2.1 Optical

Optical biosensors use a range of techniques including measurement of absorbance, fluorescence, refractive index, in the UV or visible light (Borisov and Wolfbeis, 2008). The general benefits of optical transduction includes non-interference from electromagnetic fields, remote sensing and multiplexing (Fan et al., 2008). Optical biosensors can be label free or labelled, e.g. using fluorescence or dye tagged analyte or secondary binding molecule. Although labelled optical biosensors are very sensitive, they are less suitable to be translated as point of care device due to their overall system complexity.

Surface plasmon resonance (SPR), is the most widely used label free optical transduction method where a surface resonance plasmon wave is measured on metal on a dielectric surface. The surface plasmon wave can be generated by different approaches including prisms, waveguides, and fibre optic coupling. Although SPR based detection can be highly sensitive, turbid media can decrease the detection sensitivity (Fan et al., 2008). Ellipsometry is an optical technique where dielectric properties of thin layers are examined by reflection. When this is combined with SPR detection, the technique is called total internal reflection ellipsometry (TIRE) and gives better performance as it can be used in opaque media (Arwin et al., 2004).

Other emerging optical phenomena include bio-layer interferometry, where multiple wavelengths with the same frequency are superimposed and their phase shift is analysed, and optical ring resonators, which is based on a whispering gallery effect of light waves. Upon analyte binding the light wave resonance drifts (Salleh et al., 2013).

1.6.2.2 Mechanical

Mechanical biosensors use the change in mechanical properties on nano surfaces due to biological binding events. These include changes in surface stress and surface oscillation due to mass deposition on the surface (Arlett et al., 2011). The use of nano-mechanical biosensors have increased due to the progress in micro and nano material fabrication processes (Tamayo et al., 2013). Changes in surface stress can be of two types, static and dynamic which can be measured on functionalized micro cantilever fingers. The quartz crystal microbalance (QCM) is a widely used biosensing technique where nanoscale mass deposition is monitored on a quartz crystal surface. In brief, a metal surface is assembled on an AT-cut quartz crystal and the resonance frequency drops with increasing binding on the surface. Non-specific deposition brings a critical issue which sometimes can be reduced by fast flow and appropriate washing inside the flow system. Mechanical sensors are particularly less sensitive towards small molecules and protein, but they can be used in large analytes including viruses and bacteria.

1.6.3 Electrochemical transduction

1.6.3.1 Potentiometric

Potentiometric biosensors measure the charge potential between working and reference electrode in electrochemical cells with zero current flow. The sensors are based on ion-selective electrodes (ISE) and ion-sensitive field effect transistors (ISFET) and the output is due to ion accumulation at a membrane surface (Chaubey and Malhotra, 2002). In potentiometric measurements, the relationship between free ion concentration and potential is governed by the Nernst equation (**equation 1.1**)

$$\mathbf{EMF\ or\ E_{cell} = E^{0}_{cell} - \frac{RT}{nF} \ln Q} \qquad \text{..... 1.1}$$

[20]

Where,

E_{cell} represents the observed cell potential at zero current, sometimes mentioned as electromotive force (EMF),
E^0_{cell} is constant potential contribution to the cell,
R the universal gas constant,
T the absolute temperature in degree Kelvin,
n is the charge number of electrode reaction,
F is the Faraday constant and
Q is the ratio of ion concentration at the anode to cathode.

1.6.3.2 Amperometric

Amperometric biosensors measure the continuous current produced by electroactive species in any biochemical reaction and usually the potential is kept constant during the measurement (Grieshaber et al., 2008). When the potential varies during the process it is called voltammetric analysis (**section 1.8**). Clark and Lyons glucose electrode (Clark and Lyons, 1962) was the model example of an amperometric biosensors. The sensor was used to monitor the oxygen consumption (**equation 1.2**) and relative change in current by the enzyme catalysed reaction of glucose oxidase (GOx).

$$\mathbf{glucose + oxygen \overset{GOx}{\longleftrightarrow} gluconic\ acid + hydrogen\ peroxide} \quad \textbf{..... 1.2}$$

This was further developed so that determination of blood glucose was done based on amperometric determination of liberated hydrogen peroxide oxidation (**equation 1.3**).

$$\mathbf{H_2O_2 \rightarrow O_2 + 2H^+ + 2e^-} \qquad \textbf{..... 1.3}$$

In the second generation amperometric detection, redox mediator such as ferrocene was used to accept electrons from enzyme reaction and in the third generation, the enzymes are directly immobilized onto electrode surface to exchange electron to and from the electrodes. Although indirect sensing is done, amperometric sensors show high sensitivity over potentiometric sensors and have successfully been used for sensing glucose in microbial growth (Tothill et al., 1997) and other metabolites such as lactate (Hirst et al., 2013) and cholesterol (Chiang et al., 2011). The glucose biosensors are regularly used by diabetes patients to monitor their blood glucose level.

1.6.3.3 Impedimetric

Impedimetric sensors measure impedance, or resistance and capacitance which are the result of a complex interaction with a small amplitude voltage signal as a function of frequency. The common formats for impedance data presentation are the Nyquist and Bode plots. In the Nyquist plot, the imaginary part of impedance (-Z``, out of phase) is plotted against the real component (Z`, in phase) at each excitation frequency. By comparison, the Bode plot shows the logarithm of absolute impedance and phase shift (ϕ) versus the log of excitation frequency. As compared to amperometric and potentiometric system, impedimetric system does not rely on enzymes, instead, antibodies or any other binding molecule can be used. This makes impedance as a convenient choice in electrochemical sensing platform. Although fabrication of impedimetric sensors can be low cost, compared to other types of sensors, in terms of performance they still demand further development (Prodromidis, 2010). More details of impedimetric transduction method will be discussed in **section 1.7**.

1.7 Electrochemical impedance spectroscopy

1.7.1 Electrochemistry at sensor surface

Electrochemistry deals with the interrelation of electrical and chemical changes. The chemical changes can be due to the passage of electron or electrical charges can be produced by certain chemical reactions. In an electrochemical cell, the factors affecting the transfer of charges across different chemical phases are monitored. Basically electrochemical studies deal with the changes in the electrode/electrolyte interface (Wang, 2006).

To collect the electrochemical information on a bare or functionalized electrode surface-solution interface, the electrode is typically connected to a potentiostat using three electrode system (**Figure 1.5**). The working area upon which biosensor is fabricated is known as working electrode (WE). Reference electrodes (RE) usually comprises Ag/AgCl and are either printed on the same electrode surface with working electrode or can be provided external. The RE helps to fix and determine the potential. Counter electrodes (CE) are also used and are typically made of gold or platinum, and usually have a much large surface area than WE. The CE is used to maintain the current flow between WE and CE in the electrochemical cell (Bard and Faulkner, 2001).

At the electrode-solution interface, two types of reaction can occur. Electrons can pass through the electrodes as a result of oxidation or reduction at the electrode-solution interface. This is known as a Faradaic process as it follows Faraday's law. In other condition, charges cannot transfer across the surface, a transient electricity can flow in such environment behaving as a capacitor and this is known as a non-Faradaic process.

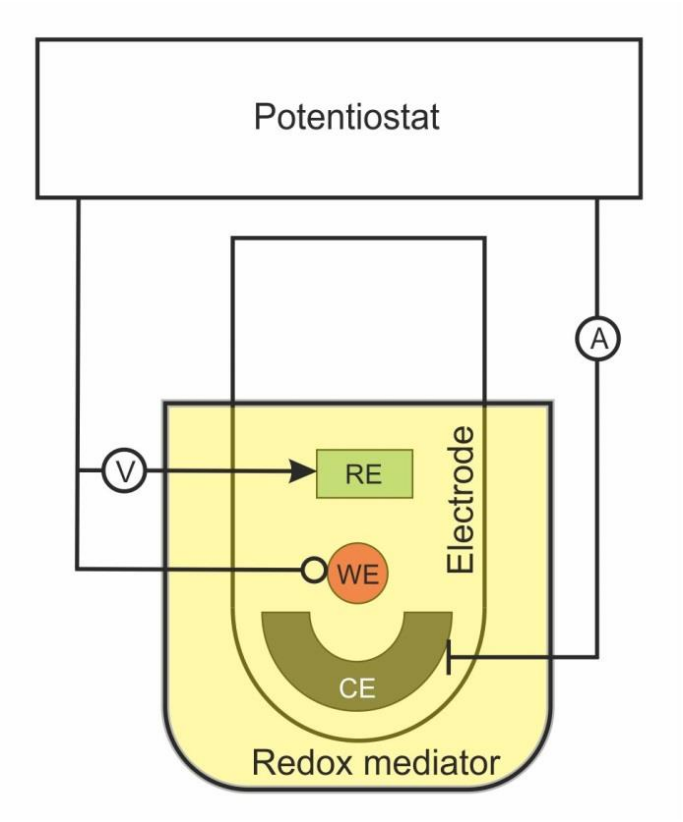

Figure 1.5: Schematic of three electrode electrochemical cell used in biosensor application

In three electrode system working electrode (WE), reference electrode (RE) and counter electrode (CE) are connected to potentiostat. CE maintain current between CE and WE. The RE on the other hand helps to maintain potential between RE and WE. A= ampere, measurement unit of current flow, V= unit of voltage/potential. The three electrodes are submerged into some measuring solution which constitutes the three cell system (shown in yellow).

To have an electrode reaction, reactants must follow few steps in the reaction pathway to reach the surface. Mass transfer allows the movement of reactant from bulk solution to the electrode surface (**Figure 1.6**). The zone between bulk solution and electrode surface is termed as diffusion layer. Major rate determining factors in this zone include the rate of electron transfer near surface, chemical reactions before and after the electron transfer and surface adsorption or desorption. A number of variables also determine the reaction rate in an electrochemical cell. These include external forces (pressure, temperature), electrode material (surface area, roughness), electrical variables (potential, current), mode of mass transfer and solution composition (concentration of electroactive species, pH). Solvents and ions are absorbed onto the surface and construct the double layer. The closest layer to the electrode surface is called inner Helmhotz plane (IHP) and the immediate layer is known as outer Helmhotz plane (OHP). In electrochemical study, the behaviour of a particular layer on the electrode is represented by its total resistance, capacitance and overall impedance. These can be numerically extracted from experimental data and can be used to explain surface behaviour in biosensor applications.

Physical design and dimension of electrode can also influence diffusion properties. Diffusion pattern near large planar electrode surface tends to be linear, whereas, in microelectrode (one dimension at least 10-50 μm) the diffusion is radial to and from the solution (Davis and Higson, 2013). The radial diffusion is more efficient in mass transport and helps to reduce double layer capacitance. However, due to very small size the change in current is low and hard to get the signal. In case of bacterial detection it can also limit the range of detection due to the size of bacterial cells. Efficiency of microelectrodes can be further enhanced by constructing interdigitated electrode surface.

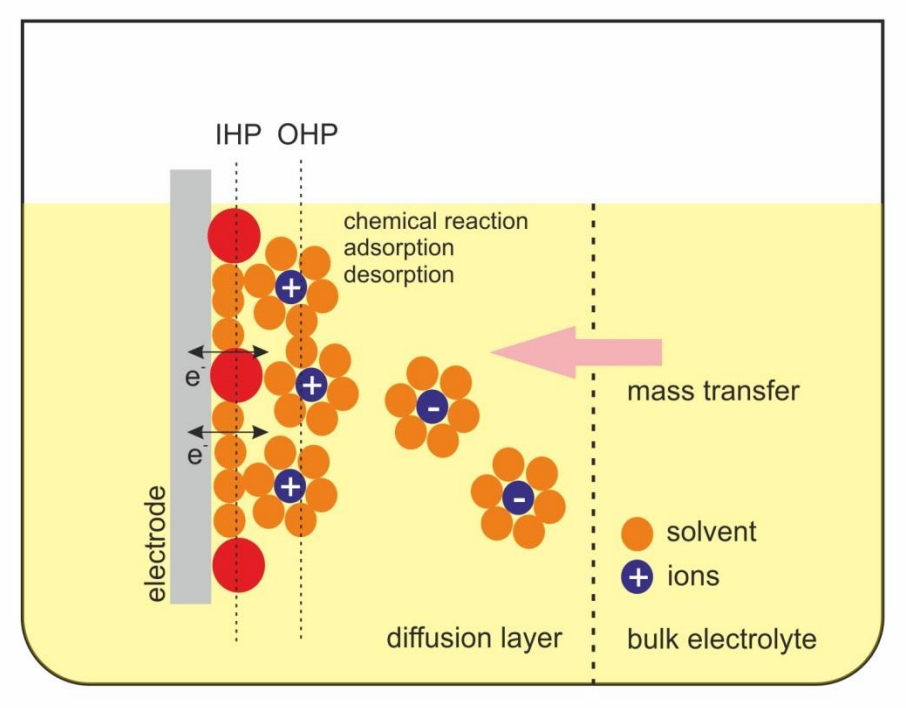

Figure 1.6: General events and diffusion pattern near the electrode solution interface

When electrodes are immersed into electrolyte solution (yellow), solvent molecules travel towards the electrode surface from bulk solution via mass transfer. Depending on the electrode charge, oppositely charged ions are absorbed onto surface. This is known as the double layer. The closest layer to surface is called inner Helmhotz plane (IHP) and the next immediate layer is called outer Helmholtz plane (OHP). Chemical reactions, adsorption and desorption take place in the diffusion layer (around 50-100 µm). Electrons can travel to, or from the electrode depending on the type of reaction.

1.7.2 Impedance theory

In EIS, a small amplitude sinusoidal voltage is applied over a range of frequencies. The impedance is calculated as the ratio of voltage time function and current time function (**equation 1.4**), taking into account the phase shift (Lisdat and Schafer, 2008). Bulk impedance is expressed according to **equation 1.4**.

$$\mathbf{Z} = \frac{\mathbf{V}(\mathbf{t})}{\mathbf{I}(\mathbf{t})} = \frac{\mathbf{V_m}\ \mathbf{sin}(\omega \mathbf{t})}{\mathbf{I_m}\ \mathbf{sin}(\omega \mathbf{t} + \boldsymbol{\phi})} \qquad \textbf{..... 1.4}$$

Where, Z is impedance,

V_m and I_m are the maximum voltage and current, at a specific frequency,

t is the time, and

ω is angular frequency or $2\pi f$ where f is the frequency and

ϕ the phase shift between voltage and current time function.

When an alternating perturbation voltage (AC voltage) is applied to the system and the corresponding behaviour of the current is observed information on resistance and capacitance can be obtained. A typical sine wave curve has positive and negative peaks, where one complete rotation covers 2π or 360^o when plotted on polar coordinates (**Figure 1.7, A**). The peak in phasor diagram is known as its amplitude. At a particular frequency, it has specific amplitude and each point in the sine wave can be plotted in a phasor circle (2π). When a surface acts as a pure resistor, both the current and voltage stay in-phase and they do not have any phase angle difference. They only differ in their magnitude (**Figure 1.7, B**).

At a particular frequency

$$\mathbf{V} = \mathbf{V_m}\ \mathbf{sin}\ \boldsymbol{\omega}\mathbf{t} \qquad \textbf{..... 1.5}$$

and according to Ohm's law,

$$\mathbf{I} = \frac{\mathbf{V}}{\mathbf{R}} = \frac{\mathbf{V_m sin}\ \boldsymbol{\omega}\mathbf{t}}{\mathbf{R}} = \mathbf{I_m sin}\ \boldsymbol{\omega}\mathbf{t} \quad \left[\mathbf{I_m} = \frac{\mathbf{Vm}}{\mathbf{R}}\right] \quad \textbf{..... 1.6}$$

From these equations (**equation 1.5 and 1.6**), it can be seen that in a pure resistor, both voltage and current follow the same equation and stay in phase. In contrast, in a pure capacitor, the voltage lags current by 90º and stays completely out of phase (**Figure 1.7, C**). In a pure capacitor, when the capacitor is fully charged, there is no current flow, but during charging and discharging the flow of current takes place. In a capacitor, capacitance is the ratio of charge to voltage,

$$\mathbf{C = \frac{Q}{V}} \quad \text{..... 1.7}$$

$$\mathbf{or\ Q = CV = CV_m \sin \omega t} \quad (\mathbf{from\ eq.\ 1.5}) \qquad \text{..... 1.8}$$

In the circuit with capacitor, the current is the ratio of charge difference over time

$$\mathbf{I = \frac{dQ}{dt} = \frac{d(CV_m \sin \omega t)}{dt}} \quad \text{..... 1.9}$$

$$\mathbf{= CV_m \frac{d}{dt}(\sin \omega t) = CV_m\, \omega \cos \omega t}$$

$$\mathbf{= \frac{V_m}{1/\omega C} \sin\left(\omega t + \frac{\pi}{2}\right)}$$

The term $1/\omega C$ is known as capacitive reactance (X_C) expressed in Ohms. So, equation 1.9 can be rewritten as

$$\mathbf{I = I_m \sin\left(\omega t + \frac{\pi}{2}\right)} \qquad \left[\mathbf{\frac{V_m}{X_c} = I_m}\right] \qquad \text{..... 1.10}$$

From **equation 1.10** it can be stated that in purely capacitive surface, the current wave has the sine wave with difference of $\pi/2$ with that of voltage, thus it is always out of phase. In a real world biosensor surface, a pure resistor or capacitor does not exist (**Figure 1.7, D**). That is why the phase shift falls between 0º to 90º and the imperfect capacitance is often termed as double layer capacitance (*C*dl) or sometimes a constant phase element (CPE).

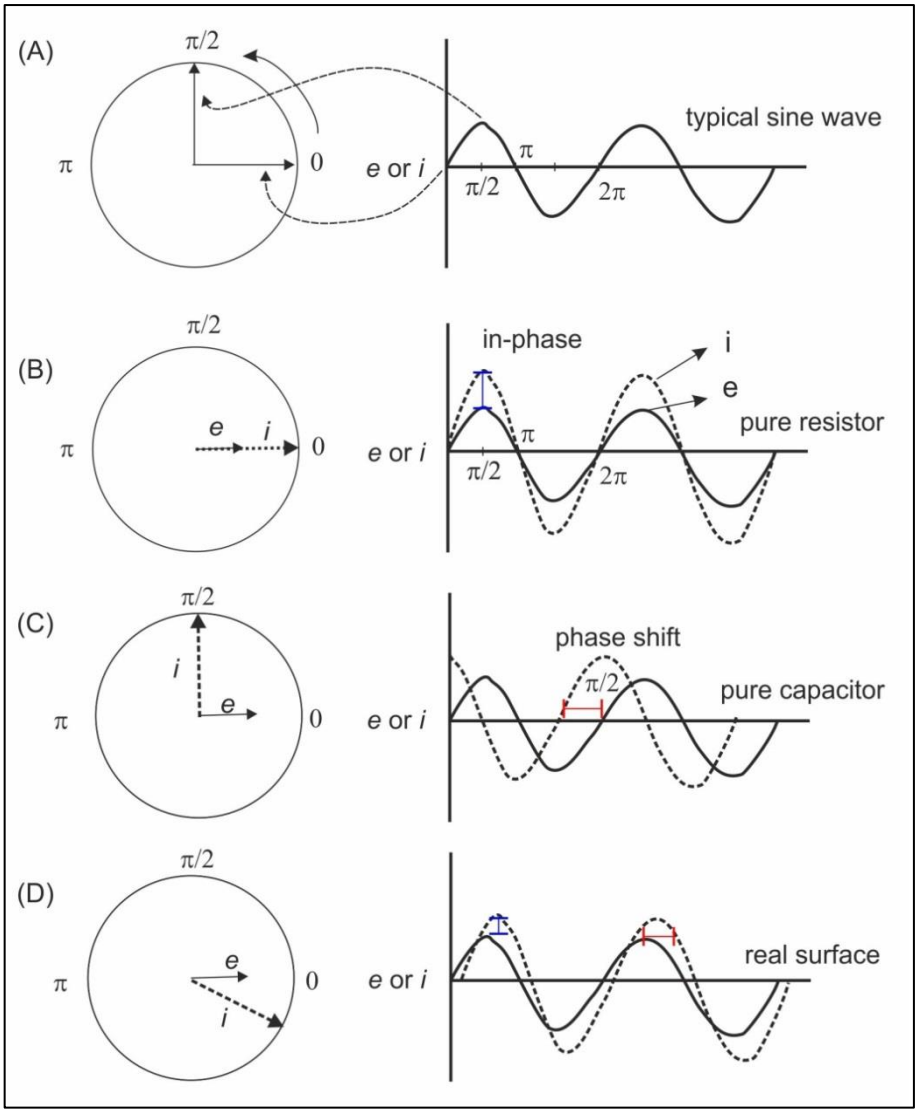

Figure 1.7: Phasor diagram of different sine waves

(A) A general sine wave and corresponding position in polar coordinates. A single wave moves total 2π distance, equal to a circle, (B) phasors in pure resistor, both current (i) and voltage (e) are in-phase, only difference is in their magnitude, (C) phasors of a pure capacitor, where at a fixed point in the wave, i and e are separated by π/2 or 90º phase shift and known as out-of-phase and (D) in real sensor surface they do not act like pure resistor or capacitor, rather the phase shift is observed somewhere between 0 to 90º with a difference in magnitude.

The relationship of voltage and current in a rotating phasor diagram is further presented using complex notation. The x-axis components are assigned as real and the components on the y-axis are assigned as imaginary, and multiplied by the value j (i.e. $\sqrt{-1}$). Although mathematically they are termed as real and imaginary, both of them are real and can be calculated from the phase angle.

When a resistance *R* and capacitance *C*, are in series and a potential V is applied across them, at every moment the voltage will be equal to the sum of individual voltage drop in resistor and capacitor. Thus,

$$\mathbf{V = V_R + V_C} \quad \text{..... 1.11}$$

Where,

V_R and V_C voltage drops in resistor and capacitor respectively.

The equation 1.9 can be further written using imaginary components

$$\mathbf{V = IR + IX_C(-j)} \quad \text{..... 1.12}$$

$$\mathbf{= IR - jX_C I}$$

$$\mathbf{= I(R - jX_C) = IZ}$$

Z or impedance=R-jX_C which is a vector that relates current and voltage.

This is in general represented as,

$$\mathbf{Z(\omega) = Z_{real} - jZ_{imaginary}} \quad \text{..... 1.13}$$

Where, Z_{real} and $Z_{imaginary}$ are the resistive and capacitive components of impedance respectively.

For example for a circuit with series resistor and capacitor Z_{real}=*R* and $Z_{imaginary}$=X_C=1/ω*C*. The magnitude of Z or absolute impedance is represented as

$$\mathbf{|Z| = \sqrt{(Z_{real})^2 + (Z_{imaginary})^2}} \quad \text{..... 1.14}$$

And the phase angle is expressed as,

$$\tan \phi = \frac{Z_{imaginary}}{Z_{real}} = \frac{X_C}{R} = 1/\omega RC \quad \text{..... 1.15}$$

Using these relationships, the complex impedance is typically represented as Nyquist plot where the imaginary impedance ($Z_{imaginary}$ or -Z'', as in electrochemistry capacitance is always negative) is plotted against the real impedance (Z_{real} or Z') for each frequency analysed (**Figure 1.8, A and B**). At high frequencies a semicircle is observed and this part is kinetically controlled. At lower frequencies the process is controlled by mass transfer, to and from the sensor surface.

From the Nyquist plot, *R*s, *R*ct and *C*dl can be derived. *R*s is the solution resistance from conductance of ions in bulk solution. This is usually observed at very high frequency. *C*dl or CPE arises from the absorbed oppositely charged ions across the interface acting as a double layer and has been modelled by Helmholtz. It can be calculated from the frequency at the maximum amplitude of the semi-circle. At low frequency a 45° line intersection of the straight line indicates the Warburg impedance (W), which is mass transfer controlled. For analytical purposes, usually the Warburg impedance is neglected. *R*ct is the resistance from the surface to charge transfer across the electrode. When the *R*ct is comparatively bigger, it indicates the slow kinetics of electron transfer near surface. In contrast, a bigger Warburg component with smaller *R*ct is an indication of very active kinetics at surface (Bard and Faulkner, 2001).

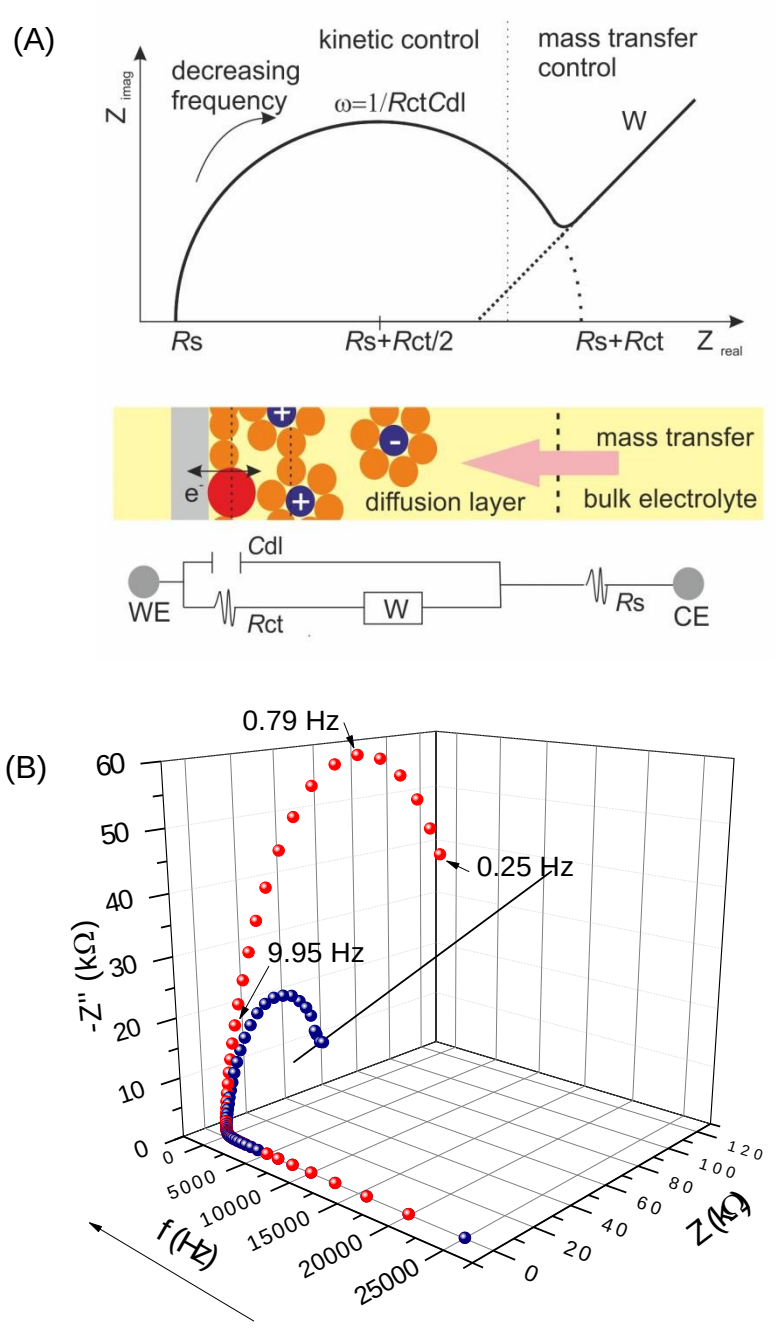

Figure 1.8: Impedance data presentation by Nyquist plot

(A) A typical complex 2D Nyquist plot shown with different components of a system and their origin in solution-surface interface. The equivalent circuit can be drawn comprising all components (B) 3D Nyquist plot showing the change in Z' and -Z'' with respect to frequency. At 9.95 Hz (low frequency, arrow marked) two different layers (blue full sensor and red analyte bound) starts to separate.

1.7.3 Equivalent circuit and data presentation

After the introduction of simple equivalent circuit designs by Randle in 1947 (Randles, 1947), it became a regular practice to draw equivalent circuit elements while discussing any particular biosensor construction. However, equivalent circuit is not a model of experimental data as this is not directly derived from it, instead it is considered as an analogue, which requires in depth surface electrochemistry wisdom to draw and interpret equivalent circuit (Macdonald, 2006). It is also useful to compare already stablished models with experimental fitting to draw a new model but care should be taken as multiple designs can fit a single dataset. Advanced algorithm has enabled electrochemistry software to have many pre-set designs which can be tested and the best fit can be selected if logical parameters does match with it.

The Randle's equivalent circuit can be simulated using impedance data to describe the electronic components of the cell. *C*dl and *R*ct are in parallel to each other, with *Rs* in series with them. W is sometimes found in series with *R*ct. In a capacitive biosensor, the surface will be pinhole free, fully covered with bioreceptor so that no electrons can be transferred. In immunosensors, Faradaic sensors are closer to reality, where upon binding of analyte, the resistance to the transfer of electrons can be easily measured by a change in *R*ct. As this circuit design can be very powerful to isolate individual component in the process and to know the distinctive property of any component in a particular biosensor, it has been suggested to use electrochemical knowledge and pay extra attention while modelling the equivalent circuit (Uygun and Uygun, 2014).

When impedance spectroscopy is used to report a biosensor performance, data can be presented in different ways (Rushworth et al., 2013b). The most common way of presenting impedance data is to present the change or percent change of

*R*ct over biosensor surface with increasing concentration of analyte. However, other parameters like imaginary impedance –Z'', absolute impedance $|Z|$, double layer properties (*C*dl or CPE) are also presented. These data can be extracted directly from Nyquist plot data. When only one or few frequencies are used, the effective frequencies where the maximum changes among different surfaces are observed can be picked and presented. In some potentiostat, real time impedance can be recorded, which is particularly useful when used with flow cell systems and when binding parameters are analysed.

1.8 Cyclic voltammetry

Voltammetric methods are used to analyse the electrolysis mechanism. There are three types of voltammetric analysis; potential step, linear sweep and cyclic voltammetry. In potential sweep, applied voltage is suddenly shifted from E_1 to E_2, and the changing current is measured. In the case of linear sweep, the potential is swept from lower potential to a higher one and current measured. Cyclic voltammetry (CV) is close to linear sweep voltammetry, with the only difference being that, in CV a reverse scan is done to get both oxidation and reduction peaks (Fisher, 1996).

$$[\mathbf{Fe(CN)_6}]^{\mathbf{4-}} \leftrightarrow [\mathbf{Fe(CN)_6}]^{\mathbf{3-}} + \mathbf{e^-} \qquad \text{..... 1.16}$$

For a reversible reaction (**equation 1.16**), the potential is swept from E1 to E2 (in this case from -0.4 V to +0.7 V). As the potential approaches more positive value during forward scan, $[Fe(CN)_6]^{4-}$ starts to oxidise and reaches its maximum peak. At the peak, complete oxidation of $[Fe(CN)_6]^{4-}$ is accomplished and the amount of $[Fe(CN)_6]^{4-}$ near surface starts to deplete. At this point the peak starts to fall from its maximum. When the potential is reversed, reduction of the oxidation product $[Fe(CN)_6]^{3-}$ can be accomplished and a reduction peak is observed (**Figure 1.9**).

The peak potential and peak current reflect the reversible nature of redox couple. The peak currents for oxidation at anode (i_{pa} oxidation) and reduction in cathode (i_{pc} reduction) in a reversible redox reaction are important. The potential difference between oxidation and reduction peak ($E_{pa} - E_{pc}$) is ideally 59 mV at 25° C and the ratios of peak currents (i_p ox/ i_p red) for one electron oxidation/ reduction are equal to 1. In a complete reversible CV, the ratio of oxidation current and reduction

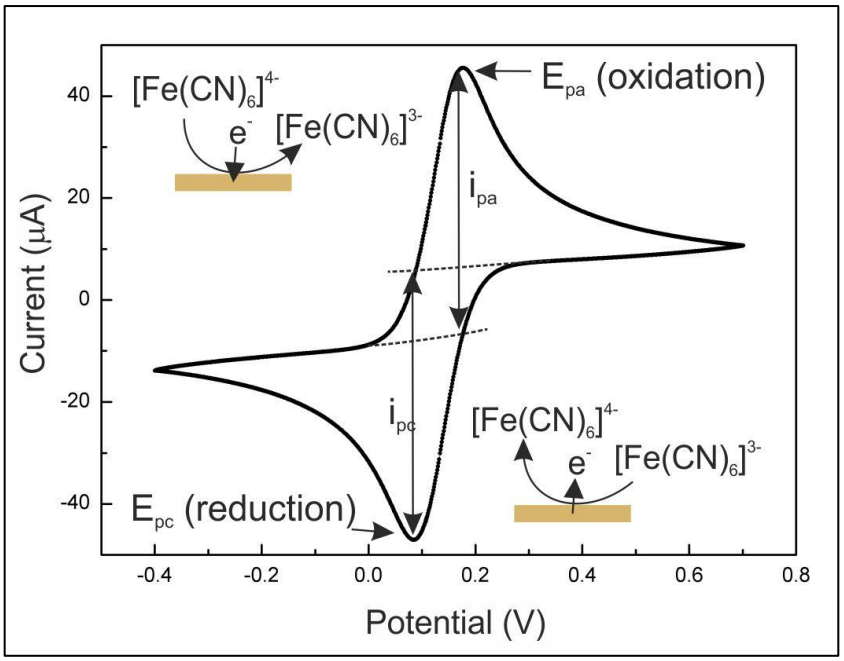

Figure 1.9: A typical cyclic voltammogram

Usually electrodes are cycled from one potential to another and reversed back to the initial point. Here, in the example bare gold surface was scanned in the presence of 10 mM [Fe(CN)6]3-/4- redox couple in 10 mM PBS, pH 7.0. When electrode was cycled to positive potential it reached a potential where oxidation of one species released electrons and was measured at electrode surface. Epa is anodic potential where maximum oxidation was observed. When the cycle was reversed back to negative potential, the oxidized species reduced back to the initial state. Electrons were consumed by this process thus current dropped. Epc is cathode potential where reduction peak was observed. Insets show process of electron transfer on electrode surface at both oxidation and reduction process.

current will be one. When the electron transfer is very fast and reversible at electrode surface the process is only limited by diffusion from bulk.

When something is deposited on the surface, the fast reaction on surface is slowed down and the reversible peaks start to deviate and separate from each other. At that stage the peaks are often termed as quasi reversible or completely irreversible. CV method is also performed for polymer deposition and regularly used in biosensor research. CV during polymer formation provide valuable information of oxidation and reduction peaks in the subsequent cycles. It is also useful to compare CV data before and after polymer or SAM deposition on surface. CV can be used to monitor layer by layer sensor fabrication, however the sensitivity decreases when peaks tend to separate from each other and quasi-reversible or completely reversible peaks are formed.

1.9 Biosensor construction

1.9.1 Electrode materials and design

Biosensor electrode chips are constructed using wide a range of materials including gold, platinum, carbon, silver, copper, indium tin oxide (ITO) and porous or non-porous alumina. The choice of material is important as the conductivity and surface properties such as roughness can influence sensor performance especially in electrochemical biosensors. In a comparative study, the effectiveness of four surfaces (platinum, gold, palladium and glassy carbon) for the sensitive amperometric detection of glutamate was reported (O'Neill et al., 2004). Glutamate oxidase was cross-linked with poly(o-phenylenediamine) and sensor performance was best in Pt (Pt>Au>Pd>>glassy carbon).

Sensor base is typically deposited onto substrates like silicon wafers, glass or ceramic using lithographic deposition or screen printing. However, depending on the deposition method the surface roughness can vary from a few nm to µm. Often, three electrodes; working, counter and reference are deposited onto the same surface producing a stand-alone electrode system that is easy to use. If only the working electrode is manufactured, external counter and reference electrodes are used. The working electrode can be circular, rectangular or interdigitated. Printing of all three electrodes on same surface ensures the fixed 3D positioning of each of and gives good reproducibility. When external counter and reference electrodes are used, during multiple analyses their inter-distance can vary and affect the reproducibility of the signal. Micrographs of some custom-made and commercial electrodes are shown in **Figure 1.10**.

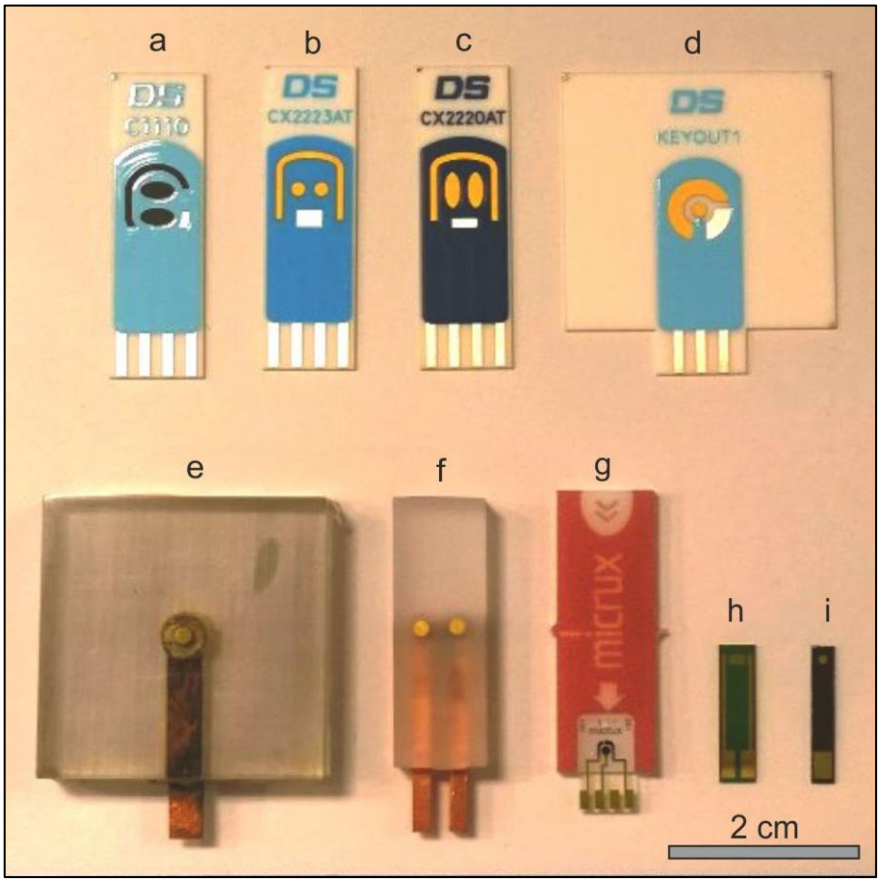

Figure 1.10: Photograph of different commercial and custom made electrodes Screen printed electrodes commercially produced by DropSens; (a), dual oval carbon; (b), dual round gold; (c), dual oval gold and (d), single circular gold designed to work in a flow cell. All these electrodes have reference and counter electrodes printed beside working electrode(s). Lower panel are either disk or lithographic gold surfaces; (e), custom made disk single for flow cell; (f), dual for flow cell; (g), commercial electrode from Micrux; (h), custom made interdigitated and (i), single gold electrodes produced by Tyndall institute, Ireland. Scale is shown to show comparative sizes of the electrodes.

Sometimes, further modifications of surfaces can be achieved by incorporating nanoparticles, magnetic beads, nano-fibre, nanotubes, graphene sheets and polymers during the manufacturing of electrodes. These additional modification facilitate increase of surface area and improvement of conductivity or incorporation of desired chemical groups. A good number of commercial companies are coming forward to produce electrodes with diverse design and materials. They include Metrohm USA Inc. (United States), DropSens S. L. (Spain), Gwent Sensors Ltd. (United Kingdom), BVT Technologies Ltd. (Czech Republic), and Quasense Company Ltd. (Thailand).

1.9.2 Base layers

1.9.2.1 Self-assembled monolayers

For biosensor construction, an organic base layer on metal transducer is often used to immobilize the bioreceptors. This facilitates the correct orientation of the biomolecules on the sensor surface and increase bio-stability. Self-assembled monolayers (SAMs) are widely used to construct these base layers for sensor fabrication. A SAM layer is formed by spontaneous adsorption of surfactant molecules in a monolayer fashion on any surface. Silanes are able to form SAMs on metal surface, but the predominant SAM format is to use thiol compounds, such as 4-ATP or MHDA on gold, due to their ability to chemisorb onto gold.

The attraction of thiol towards gold substrates and their stability over a range of different environmental condition makes them amenable to widespread use. The useful properties of SAMs are their ordered structure and orientation and self-organising nature. Other benefits include ease of preparation and scope for changing surface structure according to the requirements of the system (Schreiber, 2000).

Several approaches can be adopted to make a SAM which can be functionalized before or after adsorption, so that the functionalized group does not react with the end thiol or substrate. For example, incorporation of long chain molecules such as phospholipids with different termini made it possible to create a mixed SAM (mSAM) (Billah et al., 2008; Hays et al., 2006; Mandler and Kraus-Ophir, 2011). Although SAMs provide a suitable platform to detect small analytes (Conroy et al., 2010), they may not be suitable for larger analytes like microorganisms (Caygill, 2012; Shahidan, 2012).

1.9.2.2 Polymers

In the field of biosensors, conducting polymers are another good choice for biomolecule immobilization. They are organic conjugated polymers with unusual electrochemical properties such as a low ionisation potential and high electrical conductivity (Macdiarmid et al., 1987). Since its appearance, polyaniline (PANI) has been a widely used polymer. PANI can stay as a base or protonated form in acid. It can be fully oxidised (pernigraniline) or reduced (leucoemeraldine) or can have equal mixture of both (emeraldine). The major limitation of using PANI in biosensing systems is the lack of functional groups to add sensing bioreceptors. To solve this problem several approaches have been taken. One is to co-polymerize aniline with its derivatives (Caygill et al., 2012). The benefit of using an aniline derivative is that additional pendant amine or other groups can be provided to facilitate biomolecule coupling.

Non-conducting polymers are also a good choice for the sensor base layer. Usually non-conducting polymers exhibit self limiting growth behavior during deposition. This turns these polymers into insulating thin layers with the desired chemical groups e.g. -COOH, -NH_2, -SH to facilitate bioreceptor immobilization. One of the most widely used non-condting polymer is polytyramine. This polymer has been mainly used in enzyme sensors, however, use of polytyramine has been reported in impedimetric sensors (Pournaras et al., 2008). In this thesis, polytyramine has been used and more detail about this polymer is discussed in **section 3.6**. Proposed tyramine polymerization mechanism is shown in **Figure 1.11** and a general schematic of different types of base layers and their interaction with bioreceptors is shown in **Figure 1.12**.

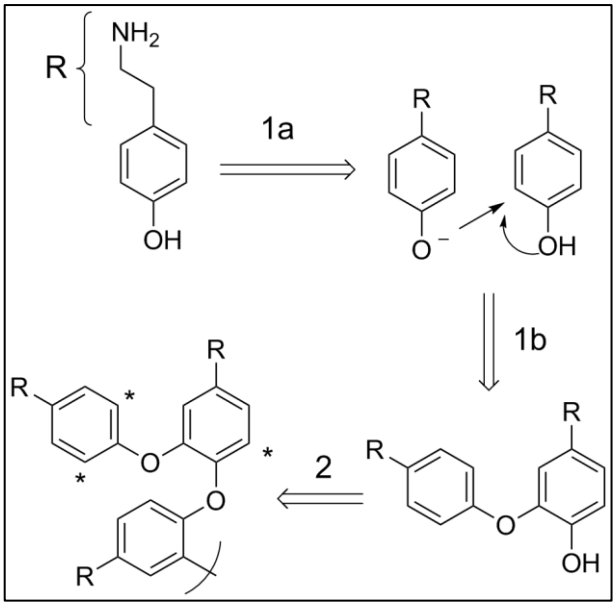

Figure 1.11: Theoretical polymerization mechanism for tyramine

First, a dimer is formed via ether formation (1a and 1b), in the second phase, trimer can be formed (2). Later on, more branches can be generated in other available ring positions (marked *). The mechanism is adapted from (Tenreiro et al., 2007).

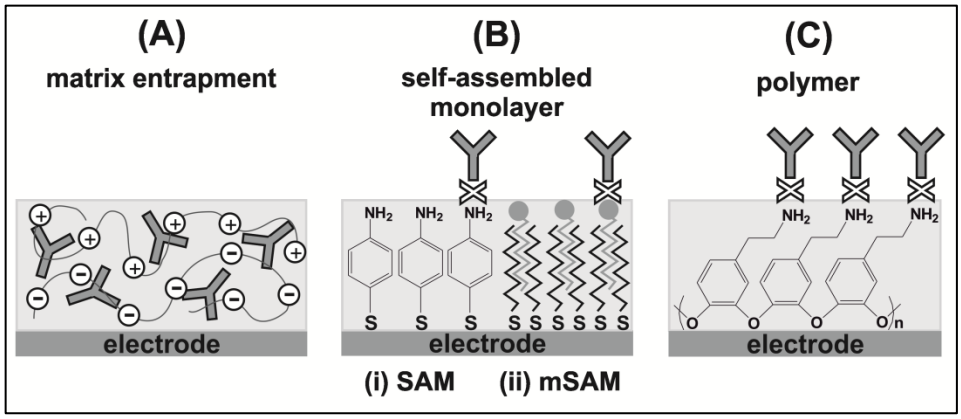

Figure 1.12: General approaches to construct base layers on electrode surface

(A) Bioreceptors can be entrapped inside a matrix by charge interaction or just physical encapsulation, (B) self-assembled monolayers with functional groups can be used as a base support and (C) conducting or non-conducting polymers with desired chemical moiety to immobilize bioreceptors. Adapted from (Rushworth et al., 2013b).

1.9.3 Bioreceptors

1.9.3.1 Antibodies

Overall, there are five isotypes of immunoglobulins, namely IgA, IgD, IgE, IgG and IgM. They have individual roles in the immune system. Immunoglobulin G (IgG) is a large protein (~150 kDa) secreted by plasma cells in response to invasion of foreign molecules, and cells including bacteria and viruses (antigens). In analytical chemistry and diagnostics, antibodies have been widely used because of their high specificity towards a particular antigen. Use of antibodies have been explored in all types of analytical systems including ELISA, immunoblotting, optical, mechanical and electrochemical systems.

Structurally, an IgG comprises of two identical heavy chains and two identical light chains interconnected via disulphide bridges forming a Y shaped structure (**Figure 1.13, A**). Both the heavy and light chain have variable and constant region. The variable region is capable of binding a specific region of antigen, called an epitope. The part of variable region that binds to epitope is known as the paratope. Each paratope consists of three loops, known as complementary determining region (CDR) that interact with epitope.

Large scale production of antibodies can be done in two ways. Specific antigens can be injected to an animal (e.g. rabbit, mouse, sheep) triggering production of a mixed antibody population. The serum can then be collected and purified to isolate IgG. These are called polyclonal antibodies (pAb), as they have specificity towards a number of epitopes. The process is comparatively easy and as the antibodies can bind different parts of a single analyte, their use in analytical chemistry has excelled. When antibodies are generated against a specific antigenic epitope, they are called monoclonal antibodies (mAbs).

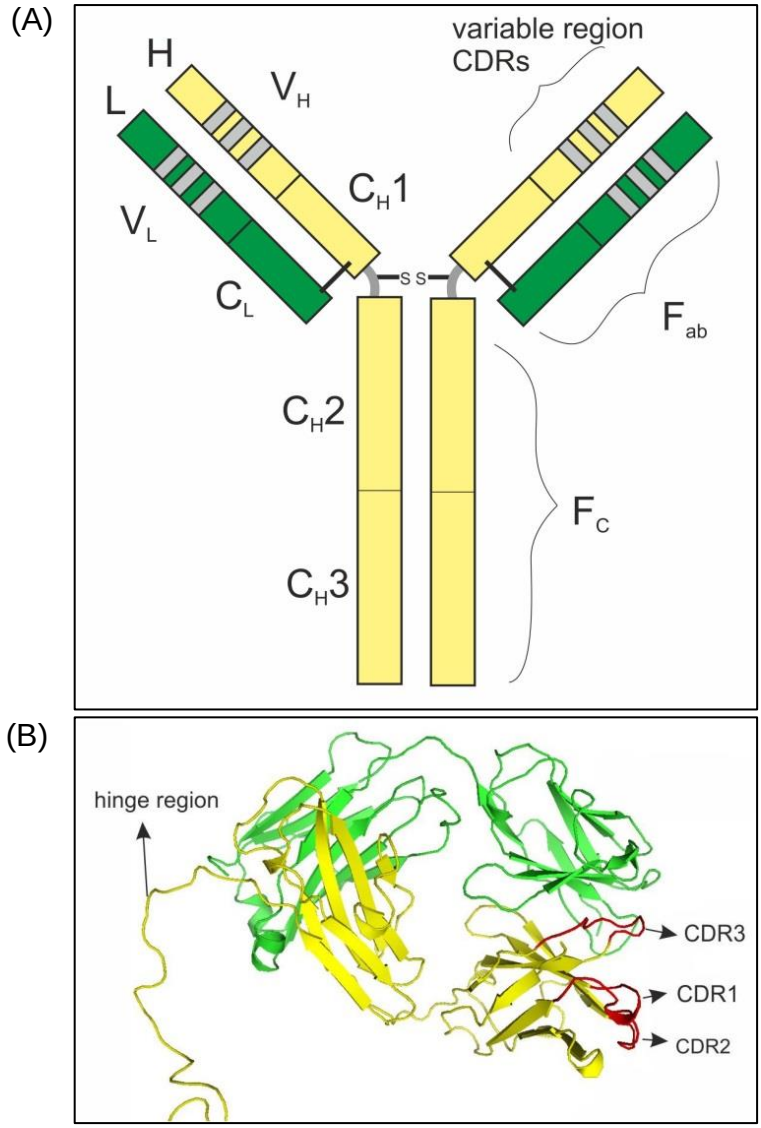

Figure 1.13: General schematic of IgG structure

(A) Schematic of IgG showing two identical heavy chains (yellow) and light chains (green). Heavy chain has one variable region and three constant regions (CH1-CH3). Light chain has one variable (VL) and one constant part (CL). Variable regions contribute to antigen binding with three complement determining regions (CDR) on each (grey rectangles). The upper part of the hinge region is called antigen binding fragment (Fab) and the lower part is called the constant fragment (Fc) and (B) ribbon structure of Fab showing CDRs in red (adapted PDB ID 1IGT).

The production of mAb is much more complex and expensive and involves fusion of myeloma cells with spleen cells. The fused hybridoma cells are grown in culture to generate specific antibodies. As they do not bind multiple sites on an antigen and due to their expense, their use is limited.

Human polyclonal IgGs have four subclasses, mouse IgGs have five, whereas rabbit IgGs has only one subclass, making the rabbit a good host animal as most of the IgG collected is of same type. As different subclasses have structural variability in hinge region and number of disulphide bond between the heavy chains, antibody from other sources will have a combination of all subclasses making antibody fragmentation technically challenging.

Besides the use of whole antibodies, antibody fragments are also a good option for use as bioreceptors (Saerens et al., 2008). There are different types of enzymes and reducing agents that target specific parts of an antibody. The protease pepsin, can digest the Fc portion leaving $F(ab')_2$, this can be further cleaved by a reducing agent to open the disulphide bridge. Fab' can be directly immobilized onto a gold surface (Brogan et al., 2003) or can be linked to surface moieties via its SH group (Tedeschi et al., 2003). Papain digestion, on the other hand, produces two Fab fragments without any SH group and an intact Fc, from which Fab can be purified by passing through a protein A/G column which selectively bind Fc. However, in biosensor applications due to the ease of conjugation, Fab' is considered a better choice over Fab.

Generation of antibody fragments by reducing agents is also routine. The commonly used reducing agents to break disulphides bonds in antibody are 2-mercaptoethyamine.HCl (2-MEA), tris(2-carboxyethyl) phosphine (TCEP) and dithiothreitol (DTT). DTT is known to be very harsh, and in one study reduction over time indicated that, DTT attacks the disulphide between light chain and heavy chain

at a faster rate as compared to the disulphide between the two heavy chains (Hong et al., 2009). TCEP is a thiol free reducing agent, which is milder than DTT (Getz et al., 1999) but is still strong compared to 2-MEA. The reduction of antibodies using 2-MEA is comparatively mild. Detail reviews on antibody fragmentation and their use to fabricate biosensors can be found in the literature (Makaraviciute and Ramanaviciene, 2013; Manjappa et al., 2011).

1.9.3.2 Antibody mimetic and non-antibody binding proteins

Small size antibody mimetic can be produced keeping antigen binding properties intact. They offer small size and greater stability during and after immobilization on surface. The major engineered antibody alternatives include single chain variable fragments (ScFv) (Ahmad et al., 2012), camelid-derived heavy variable chain antibodies (VHH) or nanobodies (Hassanzadeh-Ghassabeh et al., 2013; Muyldermans, 2013), single chain antibodies expressed via yeast surface display (Richman et al., 2009), DARPins (Stumpp and Amstutz, 2007) and other artificial proteins with high temperature resistance like Adhiron (Tiede et al., 2014). They are derived from libraries of variants based around a core protein structure. Typically these display two or more randomized loops that create the binding pocket. These alternatives can be mass produced in bacterial culture avoiding the need for live animals for polyclonal antibody production or animal cell culture for monoclonal antibodies.

1.9.3.3 Enzymes

Enzymes have specific catalytic activity, and thus provide a specific interaction and reaction product to be detected. A prime example is glucose oxidase, which is the most stable and widely used enzyme in biosensor research. This enzyme tend to stay functional up to months in dry condition (Davis and Higson, 2012). However,

many enzyme based sensors suffer from loss of stability, interference by oxidisable species in the sample, loss of enzyme by leaching, enzyme poisoning, bio-fouling and sensitivity to pH. Thus for bacterial detection enzymes are not very popular.

1.9.3.4 Cells

Whole cells can be used directly as bioreceptors. Bacteriophage, is a virus which selectively infects bacteria is widely used as bioreceptors. There are a few advantages of using phage as recognition element including high specificity, their binding ability at variable pH and in presence of nucleases and proteolytic enzymes (Wang et al., 2012b). The additional benefit of phage is that they can infect bound bacteria and rupture them over time which is a good indication of the specific interaction.

Microorganisms are generally easier to grow compared to animal cells and thus a good choice to be used as bioreceptors. The cells are complex, thus tuning the cell to focus on a particular function is possible via genetic engineering. The complexity of a bacterial cell and its ability to interact with a wide variety of substrates enabled researchers to design the cells to detect wide variety of analytes. However, the efficiency and sensitivity depends on the type of analyte, immobilization strategy and detection principles (Su et al., 2011a).

1.9.3.5 Other bioreceptors

Other common bioreceptors include molecularly imprinted polymers (MIPS) (Schirhagl, 2014), DNA/RNA or peptide aptamers (Zhou et al., 2014) and nucleic acids (DNA or RNA) (Wang, 2002). However, use of nucleic acid demands the isolation of target nucleic acid from bacteria before interrogating onto sensor surface.

1.9.4 Conjugation chemistry

There are several ways to immobilize the bioreceptors to the sensor surface. Different conjugation chemistries can be used to link antibodies onto the sensor surface. Either full antibodies or reduced antibody fragments can be attached using an appropriate chemistry. The biotin-avidin interaction can be used to tether whole antibodies onto the sensor surface. For this purpose both the antibody and polymer layer need to be biotinylated before bridging with avidin or one of its homologues, e.g. NeutrAvidin. NeutrAvidin, like avidin is naturally tetrameric with four biotin binding sites which make it easy to link biotin tagged molecules. Bifunctional linker with biotin that can target amines can be used to link between polymer amines and NeutrAvidin.

Several methods can be applied to selectively cleave antibodies for specific linking to the biosensor surface. Cleaving IgG into half, in the hinge region by adding 2-mercaptoethylamine (2-MEA) has been reported which leaves unique free sulfhydryl groups. These can bind to linkers containing a maleimide group at one end with other reactive groups (typically amine reactive, e.g. sulfo-SMCC) attaching to the biosensor. The tendency of re-joining of the antibody fragments can be effectively reduced by using oxygen free buffers, as sulfhydryl groups are susceptible to oxidation. Also, the presence of EDTA in the buffer helps to chelate any metal ions which prevent metal catalysed oxidation of sulfhydryls. Removal of residual 2-MEA from the solution is important after the reduction otherwise it would interfere with the coupling reaction. The use of different conjugation chemistry is shown in **Figure 1.14**.

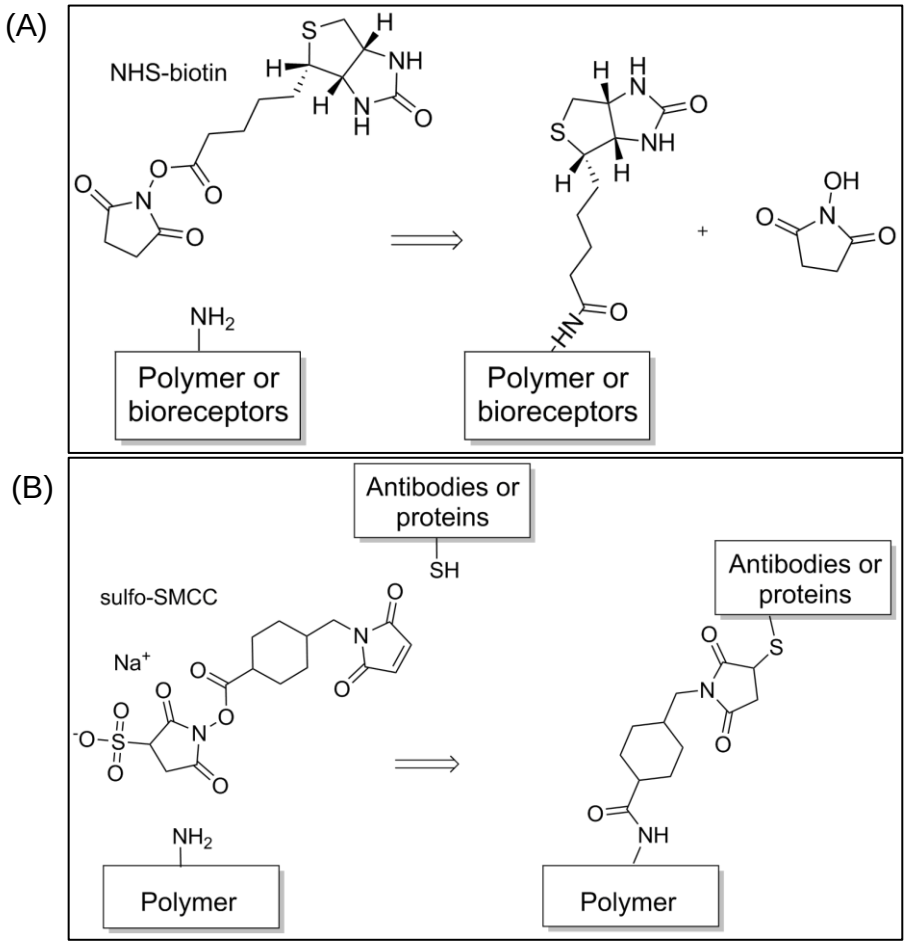

Figure 1.14: Conjugation chemistry of biotin-NHS and sulfo-SMCC

(A) Chemistry of biotinylation of polymer or bioreceptor amine. NHS-biotin reacts with primary amine and free pendant biotins are available. (B) chemistry of bi-functional sulfo-SMCC to link primary amine and sulfhydryl group. NHS group reacts with amine and maleimide reacts with free SH. Adapted from (Hermanson, 2008a; Hermanson, 2008b) and redrawn in ChemDraw.

1.10 Biosensors to detect whole bacterial cells

Biosensor research has excelled in past few decades. Affinity based biosensors have started to advance over enzymatic sensors because of their enhanced selectivity and specificity and the lack of any need for labelling. **Figure 1.15, A** shows the relative use of different biosensing techniques over the biosensor field in general. It can be seen that amperometric sensors are the leading ones followed by optical and SPR based techniques. However, other electrochemical techniques such as impedance and fibre optic based optical techniques are advancing in recent years. When analysing publications related to whole bacterial cell detection only, it emerged that impedimetric measurement is the leading technique followed by optical techniques (**Figure 1.15, B**).

From these data it becomes clear that with the advent of nanotechnology and electronics, impedimetric detection methods are being improved and applied in the field of biosensors. In the following sections, some of the techniques including optical, mechanical and electrochemical methods will be discussed with a focus on impedimetric biosensors to detect whole bacteria. As mentioned earlier, sensors can be categorised in various ways, according to their transducer material, base layer, immobilization process, choice of bioreceptors and overall electrode design. When each technique is discussed, care has been taken to sample all types of variations. It is worth mentioning that the examples are not exhaustive, but representative of their fields.

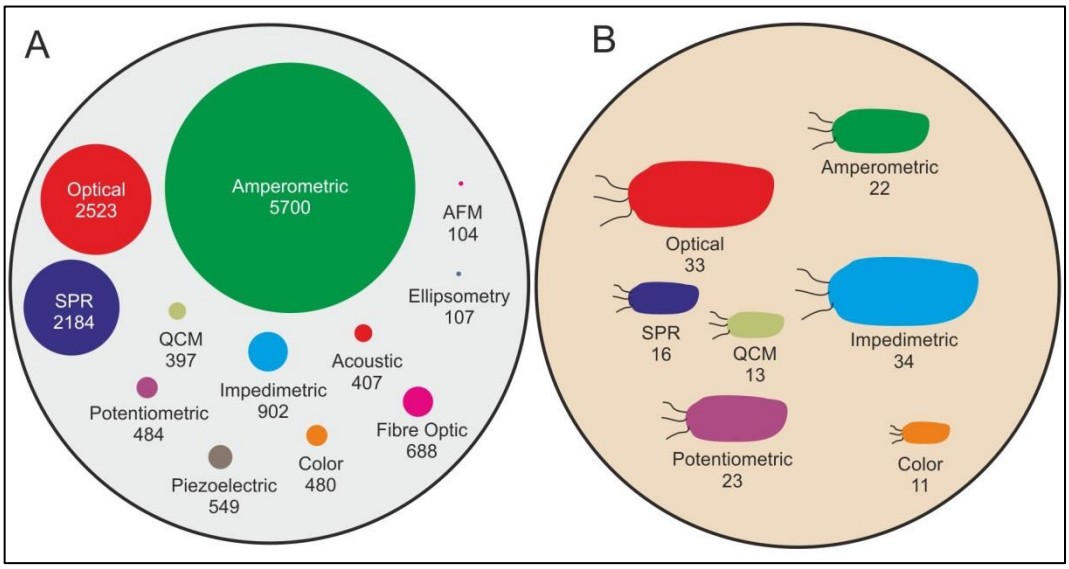

Figure 1.15: Publications on different biosensors in general compared with whole bacterial detection method

(A) Different detection methods being used in biosensing platforms; published literature were obtained via the ISI Web of Science using search terms 'biosensor' and 'used technique' from 1983 to 2013. (B) Different techniques used for the detection of whole bacteria. The size of circle or 'bacterium' is proportional to the number of publications associated with that technique (Ahmed et al., 2014).

1.10.1 Optical biosensors

Optical biosensors can be absorption, fluorescence or chemiluminescence based or can be label free. The intensity of fluorescence, luminescence or absorption of the light is directly proportional to analyte binding. Although this has been regularly practiced in 96 well plate format, using the same principle optical fibres have been used for the detection of whole bacteria (Geng et al., 2006; Ligler et al., 2007). Highly sensitive detection of 15 cells/ml *E. coli* was reported with fluorescence based biosensors (Mouffouk et al., 2011). First they used antibody coated magnetic beads to bind and isolated bacteria, then they used a pH sensitive capture antibody coated micelle to bind those bacteria. The fluorescent self-assembled micelle released dye when the pH was adjusted and the intensity was proportional to the captured bacterial concentration. However, the addition of fluorescence onto the system is an extra step and expensive.

Surface plasmon resonance (SPR) is another optical method used to detect different analytes including bacteria after the first commercial device launched by Bioacore (GE Healthcare) in 1990 (Owen, 1997). Various data has been published for whole cell detection using different bioreceptors, including antibodies (Baccar et al., 2010; Wang et al., 2012a), bacteriophages (Tawil et al., 2012; Tripathi et al., 2012) and lectins (Gasparyan and Bazukyan, 2013; Wang et al., 2013a). However, the bacterial detection by SPR is limited by low penetration of electromagnetic field through bacteria and similarity in refractive index of the bacterial cytoplasm and the surrounding aqueous environment (Torun et al., 2012).

Localized surface plasmon resonance (LSPR) uses noble metal nanoparticles to enhance the sensitivity of SPR (Sepulveda et al., 2009). Other strategies to improve the SPR signal include surface modification (Charlermroj et al., 2013), use of nanorods for multiple analyte detection (Wang and Irudayaraj, 2008), sandwich type

assays to boost signal amplification (Gasparyan and Bazukyan, 2013) and long range SPR which is more suitable for larger analytes (Wang et al., 2012a). However, to detect whole bacteria from biological sample LSPR are still less sensitive due to matrix density (Ray et al., 2012). Surface enhanced Raman scattering (SERS) is another kind of modification where the Raman intensity is enhanced and has been used in combination with other techniques for detection of bacterial cells in blood (Cheng et al., 2013). In most cases, optical biosensor platforms have yet to be miniaturized to be used in point-of-care with the ability to detect bacteria from a complex matrix i.e. blood. Representative examples of optical biosensors in the field of bacterial detection are presented in **Table 1.2**.

Table 1.2: Examples of optical biosensors for detection of whole bacterial cells

Target analyte(s)	Transducer signal	Sensor assembly	Bioreceptor(s)	LOD	Analyte(s)	Ref(s)
Escherichia coli	Fluorescence	Bio-conjugated magnetic beads for capture; fluorescent polymeric micelles for reporting	Polyclonal anti-*E. coli* antibodies	15 cells/ml	Bacteria in buffer	(a)
Escherichia coli	Thin-film optical interference spectroscopy	Antibody-functionalised nanostructured oxidized porous silicon ($PSiO_2$)	Anti-*E. coli* polyclonal antibody	10^4 cells/ml	Bacteria in buffer	(b)
Salmonella typhimurium	Light scattering	Immunoagglutination assay using anti-*Salmonella*-conjugated polystyrene microparticles	Anti-*Salmonella* polyclonal antibody	10 CFU/ml	Liquid from processed raw chicken	(c)
Shewanella oneidensis	SERS	Silver nanoparticles sandwiched by analyte bound on optical fibre tip	NA	10^6 cells/ml	Bacteria in buffer	(d)
Escherichia coli, Staphylococcus aureus, Bacillus subtilis	SPR	Lectin-functionalised anisotropic silver nanoparticles	Potato lectin	1.5×10^4 CFU/ml	Bacteria in serum-spiked buffer	(e)

Target analyte(s)	Transducer signal	Sensor assembly	Bioreceptor(s)	LOD	Analyte(s)	Ref(s)
Escherichia coli O157:H7	Long-range SPR	Antibodies on SAM- gold surface/ antibody-functionalised magnetic nanoparticles	Anti-*E. coli* antibody	50 CFU/ml	Bacteria in buffer	(f)
Escherichia coli	SPR	Bacteriophage covalently bound to SiO_2 optical fibres	T4 bacteriophage	10^3 CFU/ml	Bacteria in buffer	(g)

Abbreviations: SERS, surface enhanced Raman scattering; SPR, surface plasmon resonance; NA, not applicable. **References:** a (Mouffouk et al., 2011), b (Massad-Ivanir et al., 2011), c (Fronczek et al., 2013), d (Yang et al., 2011), e (Gasparyan and Bazukyan, 2013), f (Wang et al., 2012a) and g (Tripathi et al., 2012). Table is adapted from (Ahmed et al., 2014).

1.10.2 Mechanical biosensors

In the field of whole bacterial cell detection, mechanical biosensors offer high sensitivity and label free detection. Most commonly used approaches are the quartz crystal microbalance (QCM) and cantilever based technologies (**Table 1.3**). In QCM, quartz crystal resonators are used and typically the resonance frequency of these surfaces are monitored before and after the binding of target of interest. QCM has been successfully used to detect whole bacteria including *E. coli* (Guo et al., 2012a; Jiang et al., 2011), *Salmonella* Typhimurium (Salam et al., 2013), *Campylobacter jejuni* (Yakovleva et al., 2011) and *Bacillus anthracis* (Hao et al., 2009). Additional use of sandwich nanoparticles to enhance signal enabled the detection of as low as 10 CFU/ml in one study (Salam et al., 2013).

Another nano-mechanical approach is micro-cantilever technology which oscillates at a particular resonant frequency and the change in oscillation can be detected upon bacterial binding (Buchapudi et al., 2011; Lang and Gerber, 2008). This technique has been used to detect *E. coli* O157:H7 (Campbell and Mutharasan, 2005; Zhang and Ji, 2004), *Salmonella* Typhimurium (Zhu et al., 2007), *Vibrio cholera* (Sungkanak et al., 2010) and the bio-warfare agent *Francisella tularensis* (Ji et al., 2004). The recent development of piezoelectric excited millimetre size cantilevers (PEMC) was used to detect as low as one *E. coli* cell in buffer (Campbell and Mutharasan, 2007) and one hundred *Listeria monocytogenes* in milk (Sharma and Mutharasan, 2013b). As mechanical sensors show higher sensitivity than optical sensors for detecting bacteria, future point-of-care devices could be made using this technology if appropriately miniaturized and sensitivity in real sample can be retained.

Table 1.3: Examples of mechanical biosensors to detect whole bacterial cells

Target analyte	Transducer signal	Sensor assembly	Bioreceptor	LOD	Analyte	Ref
Bacillus anthracis	QCM	Protein A/antibody-functionalised SAM on gold	Anti-*B. anthracis* antibody	1×10^3 CFU or spores/ml	Vegetative cells and spores	(a)
Salmonella Typhimurium	QCM	Immunosensor sandwich assay using gold nanoparticles for signal amplification	Anti- *S. typhimurium* antibody	10 CFU/ml	Bacteria spiked into meat samples	(b)
E. coli O157:H7	PEMC	Antibody-functionalised cantilever	Anti-*E. coli* antibody	1 cell/ml	Bacteria in buffer	(c)
Vibrio cholerae O1	Micro-cantilever / DFM	Antibody-functionalised SAM on gold	Anti-*V. cholera* antibody (monoclonal)	1×10^3 CFU/ml	Bacteria in buffer	(d)
Listeria monocytogenes	PEMC	Protein G/antibody with post-capture antibody binding for signal amplification	Anti- *L. monocytogenes* antibody for capture; secondary antibody for signal amplification	1×10^2 cells/ml	Bacteria in milk	(e)

Abbreviations: QCM, quartz crystal microbalance; PEMC, piezoelectric-excited millimetre-size cantilever; DFM, dynamic force microscopy. **References:** a (Hao et al., 2009), b (Salam et al., 2013), c (Campbell and Mutharasan, 2007), d (Sungkanak et al., 2010) and e (Sharma and Mutharasan, 2013b). This table is adapted from (Ahmed et al., 2014).

1.10.3 Electrochemical biosensors

1.10.3.1 Potentiometric and amperometric sensors

The use of potentiometric biosensors to detect bacteria is limited compared to other electrochemical techniques. However, some innovative use of this technique has enabled reasonable limits of detection. Potential stripping analysis (PSA) is a chrono-potentiometric method, where at stripping potential the amount and rate of stripping of a deposited compound are measured. Sulphate reducing bacteria have been detected using potential stripping where bacterial samples were pre-incubated with lead and nitric acid to generate sulphide (Wan et al., 2010a). With increasing concentration of bacteria, the required time to strip also increases. Although it gives good detection, the pre-incubation steps with the bacterial sample make it difficult to apply on-site. Aptamer immobilized onto single-wall carbon nanotube was used to detect a skin commensal, *Staphylococcus aureus* (Zelada-Guillen et al., 2012). In this study real time electromotive force (EMF) was measured with increasing concentration of bacteria giving a detection limit of 8×10^2 cells/ml.

Amperometry is a widely used electrochemical method within the biosensor field due to its ease of operation, and simplicity. Although amperometric research is mainly focused on low molecular weight metabolites biosensor such as glucose and lactate, other analytes including whole bacteria have been detected. As the most favourable amperometric biosensors are enzyme based, this is one of the biggest limitations in the field of bacterial detection. Other limiting factors are the influence of operating potential range on selectivity and bioreceptor stability.

In a novel approach, haemolytic bacteria were selectively identified using an amperometric method (Kim et al., 2006). Electron mediator was trapped inside liposomes, which were selectively ruptured by haemolytic bacteria producing an

increased current signal. Control bacteria (non-haemolytic) were unable to break the liposomes which created significant signal difference between haemolytic and non-haemolytic strains. However, the detection range was limited and quite high at 5×10^5 to 2×10^7 CFU/ml.

In another study, *E. coli* was detected in a flow cell with the use of antibody coated magnetic beads (Laczka et al., 2011). These beads were accumulated magnetically just above the gold electrode surface and then a bacterial sample was passed through the flow cell. Bound bacteria were further labelled using HRP conjugated antibodies and the additional electron mediator hydroquinone was used to measure the current signal. As the antibody-magnetic beads were located over the electrode surface, the gold surface was free to generate a sensitive signal. Although the detection limit was as low as 55 cells/ml, the multistep labelling process and need for a flow cell limits its point-of-care use.

Bacteriophage mediated release of intracellular enzymes in *E. coli* K-12 cells on carbon electrodes enabled amperometric detection of 1 CFU/ml (Neufeld et al., 2003). The method is highly specific due to the use of strain specific phage but required pre-incubation of sample bacteria with enzyme enhancer and phage. In another study (Li et al., 2013), synthetic stool samples spiked with heat killed *E. coli* was analysed with a multistep and labelled amperometric detection This method was also very sensitive with low detection of 15 CFU/ml, but the extra complication of the construction and labelling was unattractive. A few examples of potentiometric and amperometric research toward bacterial cell detection are presented in **Table 1.4**.

Table 1.4: Examples of potentiometric and amperometric electrochemical biosensors for whole bacterial cell detection

Biosensor	Bacterium	Transducer	Technique	Bioreceptor	LOD	Ref(s)
Potentiometric	Sulphate reducing bacteria	Glassy carbon electrode	Potentiometric stripping analysis	None	2.3×10 - 2.3×10^7 CFU/ml	(a)
	Staphylococcus aureus	Single-walled carbon nanotubes	EMF	Aptamer	8×10^2 CFU/ml	(b)
Amperometric	*E. coli*	Photolithographic gold	Immunomagnetic/ amperometric in flow cells	Antibody	55 cells/ml in PBS and 100 cells/ml in milk	(c)
	E. coli K12	Screen printed carbon electrodes	Phage induced release and subsequent quantitation of bacterial intracellular enzyme	Bacteriophage	1 CFU/100 ml	(d)
	Heat-killed *E. coli*	SCE	Amperometric detection of secondary antibody with GOx	Biotinyl antibody	3×10^1 - 3.2×10^6 CFU/ml with LOD down to 15 CFU/ml	(e)
	Staphylococcus aureus	DropSens SPGE	HRP H_2O_2 mediated immunosensor	Antibody	1 CFU/ml in raw milk	(f)

Abbreviations: SCE, saturated calomel electrode; GOx, glucose oxidase; EMF, electron motive force; HRP, horseradish peroxidase. **References:** a (Wan et al., 2010a), b (Zelada-Guillen et al., 2012), c (Laczka et al., 2011), d (Neufeld et al., 2003), e (Li et al., 2013) and f (de Avila et al., 2012).Table is adapted from (Ahmed et al., 2014).

1.10.3.2 Impedimetric sensors

As discussed earlier, impedance measurement of biosensors offer label free detection of binding on to the sensor surfaces with considerable sensitivity. It also offers critical surface electrochemical information such as resistance, capacitance, overall impedance over a wide range of frequencies. These attributes have also enabled this technique to explore diverse range of bioreceptors against bacteria. Substantial research has been published over the last few decades to improve the detection system and the key factors have been explored, e.g. different electrode material, choice of base layers, different bioreceptors, choice of immobilization methods and format of data presentation. In this section, research themes will be presented with their unique use of manipulating the system for better impedimetric signals to detect bacteria.

Differentiating live from dead cells is sometimes useful to identify the real pathogen count in a sample. Viable *E. coli* has been successfully detected in a mixed population of dead and live cells (de la Rica et al., 2009). Initially, immunosensors were constructed onto silicon interdigitated electrodes; then as viable cells are voluminous compared to dead cells they produce a higher interference in an electric field. This enabled the researcher to detect as low as 3×10^2 CFU/ml when live cells were mixed with excess of dead cells. However, the detection ability of this system in complex media was not reported.

As a novel electrode material, reduced graphene oxide paper was used to detect *E. coli* with a nanoparticle based sensor (Wang et al., 2013b). Nanoparticles were electrodeposited onto graphene oxide paper and antibody immobilisation was performed using biotin-streptavidin link. The sensor showed a detection limit of 10^4 cells/ml and 10^3 cells/ml in contaminated ground beef and cucumber respectively.

Bacteriophages, as they are highly specific towards their host bacteria were used as a bioreceptor (Tlili et al., 2013). The phage were immobilized onto a SAM surface formed on a gold electrode. The detection limit was 8×10^2 CFU/ml in less than 15 min and further validation was done by amplifying and measuring the *E. coli tuf* gene which was released via phage mediated cell rupture.

In a novel approach, magnetic beads and a two compartment detection cell was designed to facilitate target bacterial flow towards an antibody functionalized surface (Chan et al., 2013). Two chambers were separated by silanised nonporous alumina, the upper chamber facing side of the membrane was functionalized with antibodies. Two platinum wires were used as working and reference electrode on upper and lower chamber respectively. Magnetic beads coated with antibodies were used to bind target bacteria and a magnetic field was created to bring these near to the alumina surface in the upper chamber. Upon immune binding, the magnetic field was withdrawn and the change in impedance was plotted between the two chambers. Although it had a low detection limit of 10 CFU/ml, the complicated nature of the system design makes it difficult to be used as a point-of-care device.

Detection of sulphate reducing bacteria (SRB) using porous nickel foam as a working electrode has been reported (Wan et al., 2010b). Gold nanoparticles were deposited inside the pores, followed by 11-mercaptoundecanoic acid (MPA) SAM tethered antibodies. The sensor showed selectivity over other strains with a detection range of 2.1×10^1 to 2.1×10^7 CFU/ml. In another approach a bacteria bio-imprinting technique was applied to selectively bind SRB (Qi et al., 2013). In short, reduced graphene sheets and chitosan were electrodeposited onto indium tin oxide (ITO) surface, which was followed by SRB adsorption and a thin layer of non-conducting chitosan. Then the SRB was washed off to leave a cellular imprint. This

surface was able to detect SRB over the range of 10^4 to 10^8 CFU/ml using EIS. Although the system could differentiate other bacteria of different size and shapes, the authors recommended the use of the system in combination with other bioreceptors.

Monoclonal antibodies were also used to detect *Salmonella* Typhimurium on a gold plated disposable circuit board. Antibodies were generated against one of the cell surface lipopolysaccharides (LPS) and the impedance signal was able to detect 10 bacteria in 100 ml sample. A selective collection of recent impedimetric sensor applications to detect whole bacteria is presented in **Table 1.5**. However, the challenge to take laboratory based sensors into the market are multidimensional. With the advancement of nanotechnologies and increased funding for impedimetric biosensor research could make such sensor a successful commercial point-of-care device for bacterial detection. This is particularly important where immediate detection, e.g. of sepsis, could help avoid severe morbidity or mortality.

Table 1.5: Examples of impedimetric biosensors to detect bacteria

Bacteria	Transducer	Chemistry	Bioreceptor(s)	LOD	Reference(s)
E. coli O157:H7	Gold	EDC/NHS	Antibody	2 CFU/ml	(Barreiros dos Santos et al., 2013)
E. coli O157:H7	Nanoporous aluminium oxide membrane	Trimethoxysilane-HA-EDC/NHS	Antibody	10 CFU/ml	(Joung et al., 2013)
E. coli O157:H7	Nanoporous aluminium oxide membrane	Silane-PEG	Antibody	10 CFU/ml	(Chan et al., 2013)
E. coli K12	Gold microelectrode, interdigitated	Physisorption	T4 bacteriophage	10^4 - 10^7 CFU/ml	(Mejri et al., 2010)
E. coli K12	boron-doped UNCD microelectrode array	Physisorption	Antibody	NA	(Siddiqui et al., 2012)
E. coli O157:H7	Gold microelectrode, interdigitated	Physisorption	Antibody	2.5×10^4 and 2.5×10^7 CFU/ml	(Dweik et al., 2012)
E. coli	Gold	SAM-EDC/NHS	Antibody	1.0×10^3 CFU/ml	(Geng et al., 2008)
E. coli	Gold electrode	SAM-biotin-NeutrAvidin	Biotinyl antibody	10 CFU/ml	(Maalouf et al., 2007)
E. coli	7% gold–tungsten plate wire	Polyethyleneamine-streptavidin	Biotinyl antibody	10^3 - 10^8 CFU/ml	(Lu et al., 2013)
E. coli	Gold disk	mSAM	Synthetic glycan	10^2 - 10^3 CFU/ml	(Guo et al., 2012b)
E. coli	Polysilicon interdigitated electrodes	Glutaraldehyde	Antibody	3×10^2 CFU/ml	(de la Rica et al., 2009)

Bacteria	Transducer	Chemistry	Bioreceptor(s)	LOD	Reference(s)
E. coli O157:H7	Gold	SAM-HA-EDC/NHS	Antibody	7 CFU/ml	(Joung et al., 2012)
E. coli	Gold	SAM-PDICT cross-linker	Bacteriophage	8×10^2 CFU/ml	(Tlili et al., 2013)
E. coli	Graphene paper	biotin-streptavidin	Antibody	1.5×10^2 CFU/ml	(Wang et al., 2013b)
E coli	Screen printed carbon microarrays	EDC/NHS	Bacteriophage	10^4 CFU/ml for 50 µl samples	(Shabani et al., 2008)
sulphate reducing bacteria	Glassy carbon	Reduced graphene sheet with chitosan plus 1% glutaraldehyde	Antibody	1.8×10^1 - 1.8×10^7 CFU/ml	(Wan et al., 2011)
sulphate reducing bacteria	ITO	Chitosan-reduced grapheme sheet	Bioimprint of bacteria	1.0×10^4 - 1.0×10^8 CFU/ml	(Qi et al., 2013)
Sulphate reducing bacteria	Foam Ni	Nanoparticle-SAM-EDC/NHS	Antibody	2.1×10^1 - 2.1×10^7 CFU/ml	(Wan et al., 2010b)
Salmonella Typhimurium	Gold	SAM-glutaraldehyde	Antibody	NA	(Mantzila et al., 2008)
Salmonella Typhimurium	Electroplated gold on disposable printed circuit board	16-MHDA-EDC-NHS	Monoclonal antibody	10 CFU in 100 ml	(La Belle et al., 2009)
Salmonella Typhimurium	Gold	Polytyramine-glutaraldehyde	Antibody	NA	(Pournaras et al., 2008)

Bacteria	Transducer	Chemistry	Bioreceptor(s)	LOD	Reference(s)
Campylobacter jejuni	Glassy carbon	Physisorped onto O-carboxymethylchitosan surface modified Fe_3O_4 nanoparticles	Monoclonal antibody	1.0×10^3 - 1.0×10^7 CFU/ml	(Huang et al., 2010)
Listeria innocua	Gold	SAM-EDC/NHS	Endolysin (phage peptidoglycan hydrolases)	1.1×10^4 and 10^5 CFU/ml	(Tolba et al., 2012)
Staphylococcus aureus	Nanoporous alumina	Silane- 1% GPMS	Antibody	10^2 CFU/ml	(Tan et al., 2011)
Porphyromonas gingivalis and *E. coli*	Microfluidic cell with hydrodynamic focusing	No immobilization/ impedance reading during flow of cells	None	10^3 cells/ml	(Zhu et al., 2010)

Abbreviations: EDC, ethyl(dimethylaminopropyl) carbodimide; PEG, plyethylene glycol; UNCD, ultrananocrystalline diamond; NA, not available; PDICT, 1,4-dithiocyanate; ITO, indium tin oxide; mSAM, mixed self-assembled monolayer; NHS, N-hydroxysuccinimide; SAM, self-assembled monolayer; MHDA, mercaptohexadecanoic acid; GPMS, (3-glycidoxypropyl)trimethoxysilane. Table adapted from (Ahmed et al., 2014).

1.11 Project aims

The overall objective of this project was to fabricate and optimize a commercial chip based impedimetric immunosensor for specific and selective detection of bacteria. The commercially printed electrode chips offer three electrodes (working, counter and reference) printed on a single surface, is small in size, comparatively cheap, easy to use and the design is closely compatible to be used in single use biosensing. Bacterial infections are associated with many human diseases, making whole bacterial cells as attractive biomarker. Although there are several qualitative and quantitative techniques available to detect bacterial presence, a quick point-of-care biosensor would speed up clinical decisions.

One main aspect of this project was to assess the feasibility of using commercially produced screen printed electrodes. The next focus was to optimize a polymer layer which is electrochemically suitable and rich in surface amines. After this, antibodies were immobilized via two different schemes and their effect on bacterial binding was observed. As bacteria are comparatively much larger than antibodies and contain multiple surface epitopes, the effect of sensor surface antibody density on binding was also examined. Different incubation strategies were also explored as part of sensor development. Further objective of the project was to develop quick and sensitive semi-quantitative method to confirm the presence of specific surface moieties in different sensor layers e.g. amine availability after polymer layer deposition and presence of immobilized antibodies, which is critical information during sensor fabrication.

In the later part of the project, non-specific binding of bacteria on control sensor surfaces was also investigated. The pathogenic bacteria *S. pyogenes* showed some unique non-specific binding to surfaces with non-relevant antibodies due to

the presence of its surface M and H protein. Different blocking agents have been explored to solve this problem. Then the effect of this blocking was compared in surfaces with antibodies immobilized in different ways. Attempts were also made to electropolymerize copolymers which could help to minimize non-specific signal in biological sample like human serum.

The key objectives can be summarized as

- Optimization of layer-by-layer sensor construction on commercial screen printed electrodes.
- Optimization of electrochemically deposited polymer base layer with abundant surface amines and stable electrochemical properties.
- To study the effect of surface bioreceptor density on analyte binding.
- To investigate different incubation strategies suitable for point-of-care use.
- Development of quick semi-quantitative on-sensor detection method (Midland blotting) to facilitate sensor fabrication
- To compare the electrochemical signal of sensors with immobilized biotinylated full antibody and reduced half antibody fragments.
- Reduction of non-specific signal due to *S. pyogenes* surface proteins and development of copolymer to supress non-specific interaction of human serum.

Chapter Two

Materials and methods

Chapter 2 Materials and methods

2.1 Materials

2.1.1 Inorganic chemicals

$K_3Fe(CN)_6$ (99%), $K_4Fe(CN)_6$ ($3H_2O$, 98%), 35% H_2O_2 (v/v), Na_2HPO_4 (99%), NaCl (99%), and NaH_2PO_4 (99%) were purchased from Fisher scientific (UK), NaOH (99%) was purchased from BDH laboratory supplies (Poole, Dorset, UK). H_2SO_4 (95%) was purchased from MERCK (Hoddesdon, Hertfordshire, UK). 2-mercaptoethylamine hydrochloride (2-MEA) (98%) was supplied by Alfa Aesar (Heysham, Lancashire, UK). Tris (2-carboxyethyl) phosphine hydrochloride (TCEP. HCl) was purchased from Fisher scientific, UK. $MgSO_4.H_2O$ was purchased from Sigma Aldrich (Poole, Dorset, UK). Agar was purchased from Oxoid Ltd (Basngstoke, Hampshire, UK).

2.1.2 Organic chemicals

16-mercaptohexadecanoic acid (MHDA), 4-aminothiophenol (4-ATP), 2-aminobenzylamine (2-ABA), tyramine hydrochloride (≥ 98%), 3-(4-hydroxyphenyl)propionic acid (phloretic acid or PA), 4-propylphenol (4-PP), propidium iodide, (+)-biotin N-hydroxysuccinimide ester (biotin-NHS), biotinamidohexanoic acid N-hydroxysuccinimide ester (long chain biotin-NHS), ethylenediaminetetraacetic acid disodium salt dehydrate (EDTA) and 4-(N-maleimidomethyl) cyclohexane-1-carboxylic acid 3-sulfo-N-hydroxysuccinimide ester sodium salt (sulfo-SMCC) were purchased from Sigma Aldrich (UK). Head group modified lipid 1,2-dipalmitoyl-sn-glycero-3-phosphoethanolamine-N-cap

biotinyl (biotin-cap DPPE) was purchased from Avanti Polar Lipids Inc. (USA). Aniline and Tween 20 was purchased from Fisher Scientific.

2.1.3 Solvents and buffers

Phosphate buffered saline (10 mM PBS; 0.9% (w/v) NaCl, pH 7.0) was prepared using appropriate mixture of mono and dibasic sodium salts and was used in all experiments unless otherwise mentioned. The same buffer was used as a solvent for redox mediator, antibody reduction buffer with EDTA and in washing and blocking buffer. Dimethyl sulfoxide (DMSO), methanol and ethanol were purchased from Sigma.

2.1.4 Proteins

NeutrAvidin was purchased from Invitrogen (Paisley, UK). Lyophilized protein A from *Staphylococcus aureus* (MW 42 kDa) was purchased from MP Biomedicals, UK. Recombinant protein G (MW 21.6 kDa) lacking the albumin binding region was obtained from Source Bioscience (Nottingham, UK). Bovine serum albumin (BSA), MW ~66 kDa was purchased from Sigma UK. Prediluted (10 µg/ml) high sensitivity streptavidin HRP (strep-HRP) was purchased from Thermo Scientific, USA.

2.1.5 Antibodies

Protein G purified anti-*S. pyogenes* polyclonal antibody (5 mg/ml) was raised in a rabbit host against heat-inactivated *S. pyogenes* (GenScript; NJ, USA). Anti- *E. coli* polyclonal antibodies (6.96 mg/ml) were produced against a heat killed mixture of five strains (35218, HB101, NCTC10418 and BL21) by GenScript and was kindly provided by Dr. Natalie Hirst. Lyophilized anti-MS2 polyclonal antibody was raised in rabbit against MS2 coat protein by GenScript and was a gift from Dr. Rebecca Caygill (Faculty of Biological Sciences, University of Leeds). Lyophilized anti-digoxin antibody was raised in sheep by Therapeutic Antibodies Ltd, UK. HRP-

conjugated anti-rabbit and anti-sheep antibodies were purchased from Sigma-Aldrich (Dorset, UK).

2.1.6 Electrodes

Gold screen printed electrodes (model CX223AT) were purchased from DropSens (Llanera, Asturias, Spain). Each chip (**Figure 2.1**) has two circular gold working electrodes, a small rectangular Ag/AgCl reference electrode and a U-shaped gold counter electrode fired onto a ceramic base. The sensor is 3.4 cm by 1 cm with four silver connectors to connect two working electrodes, one counter and one reference electrode. These configuration of the chip provides a three electrode system making its use easier without external reference and counter electrodes.

2.1.7 Bacterial and Viral strains

Bacterial cultures of *Streptococcus pyogenes* and *Streptococcus pneumoniae* were provided by Mr. John Wright, Faculty of Biological Sciences, University of Leeds and the detailed protocols are described in section 2.2.1. Bacteriophage MS2 was kindly provided by Dr. Rebecca Caygill in highly purified form at ~ 2×10^{15} p.f.u./ml. This stock was prepared using the ATCC strain (Virginia, USA). The titre of the stock was enumerated before testing on a biosensor.

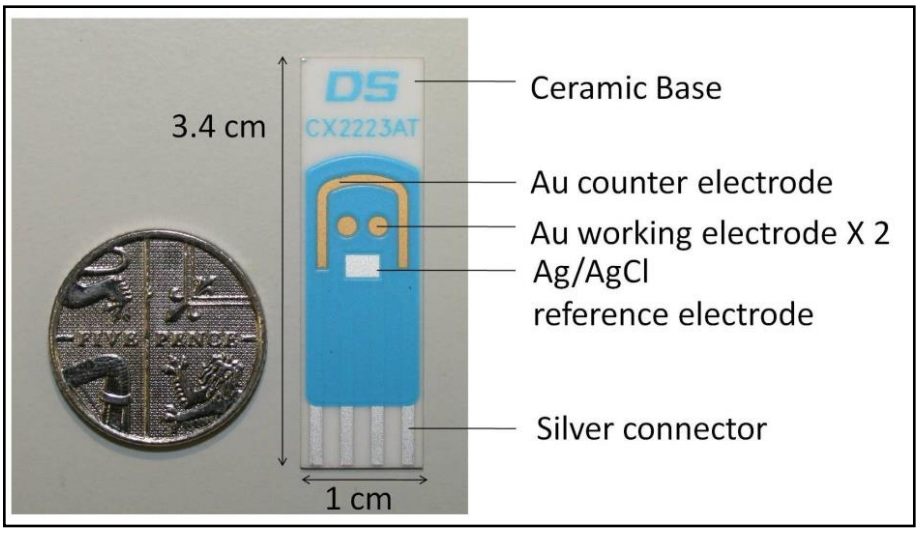

Figure 2.1: Photograph of DropSens gold screen printed electrodes

The electrode has two circular screen printed gold working electrodes, a small rectangular Ag/AgCl reference electrode and a U-shaped gold counter electrode fired onto a ceramic base. The blue dielectric material masks the connectors and prevents cross connections. Four silver connectors at bottom are used to connect the electrode to the potentiostat via an appropriate connector.

2.2 Standard methods

2.2.1 Bacterial culture

S. pyogenes (ATCC 19615) and *S. pneumoniae* bacteria were plated out onto heated blood agar (HBA) and incubated for 48 h at 37 °C. Cells were centrifuged at 3,600 *x g* for 10 min and cell pellets were suspended in sterile PBS. Heat killed cells were prepared by incubation at 70 °C for 2 h in a dry heat block. Successful heat killing was verified in triplicate by plating onto culture plates with no visible colonies grown. The final cell concentration of *S. pyogenes and S. pneumoniae* before heat killing was calculated to be 4.68×10^{8} and 2.4×10^{8} cells/ml, respectively.

2.2.2 Viral enumeration

Prior to use of MS2 on a biosensor, the viable number of particles were determined. A double agar layer plaque assay was used to enumerate the MS2 stock. An overnight culture of *E. coli* (ATCC-15597) was transferred to 50 ml LB liquid culture medium and kept in a shaker incubator at 37 °C. Bacteriophage MS2 stock was serially diluted tenfold from 10^{-2} to 10^{-15} using LB medium with 10 mM $MgSO_4$. Tubes with 3 ml LB medium with soft agar (0.7% w/v agar) corresponding to each dilution were kept in a water bath at 45 °C. From each viral dilution, 100 μl of sample was taken and mixed with 300 μl of bacterial culture (OD_{600} of 0.46) and incubated for 30 minutes at 37 °C. Then the mixture was transferred to the corresponding soft agar tubes in the water bath. The mixture from the soft agar tubes were then gently poured on top of premade LB agar plates (1.4% w/v agar) avoiding any air bubble. After the top soft agar had hardened, plates were

incubated overnight at 37 °C. The following day, plates containing 10-300 plaques were counted and used to calculate the phage titre.

2.2.3 Electrode cleaning

Several cleaning approaches were followed to evaluate the efficiency and effectiveness of the method for a particular application. Three different cleaning methods were employed; (1), sonication in 100% ethanol for 5 min in a water bath, the electrodes were dipped into the ethanol inside a Bijou tube and floated while sonication; (2), careful pipetting of 1.5 µl of piranha solution [3:7 mixture of 30% (v/v) H_2O_2 and 98% (v/v) H_2SO_4] onto each circular working electrode area for 2 min (please note that piranha solution is highly corrosive and proper care must be taken) and (3), electrochemical cleaning of the electrode surfaces by running 15 cyclic voltammetric (CV) cycles from 0 V to 1.4 V in 0.1 M H_2SO_4 solution at scan rate of 50 mV/s. The electrochemical parameters prior and after the cleaning were measured and compared (**section 3.2.2**).

2.2.4 Electrochemical polymerization

A copolymer of aniline and 2-aminobenzylamine (2-ABA) was electrochemically deposited on the working electrode from a solution containing 1:1 molar ratio. The solution (100 mM of each) was prepared in 1 M HCl and CV was run for 20 cycles from +0.0 V to +1.0 V and at 100 mV/s speed to ensure full coverage on the surface. Then the surface was washed several times with deionised water before drying in an argon stream.

CV was employed for the electropolymerization of tyramine, dissolved in different solvents, onto gold electrodes. Generally, tyramine was dissolved to a final concentration of 0.025 M in one of the following; 10 mM PBS, pH 7.0, methanol, 1 M HCl, 0.5 M H_2SO_4 or methanol containing 0.3 M NaOH. Electrodes were cycled

from +0.0 V to +1.6 V using a variable scan rates and number of cycles, as mentioned in individual figure captions. Deposition parameters of copolymer of tyramine and its acidic analogue will be described in detail in the relevant sections.

2.2.5 Self-assembled monolayer (SAM) formation

SAMs or mixed SAMs (mSAM) were deposited onto CV cleaned electrodes. For a 4-ATP SAM, freshly cleaned gold electrodes were immersed into 10 mM 4-ATP in ethanol for 4 h (Billah et al., 2010). Then the electrodes were washed with ethanol before immobilizing bioreceptors. For mSAM formation, first 0.05 mM biotin-cap DPPE was dissolved in 10 ml ethanol. Then 144 µl of MHDA (10 mg/ml solution in chloroform) was added to this solution to make 10:1 molar ratio of MHDA to biotin-cap DPPE. The electrodes were incubated overnight and then washed with copious amount of ethanol before further functionalization.

2.2.6 Biotinylation of whole antibodies

Antibodies (5 mg/ml) were incubated with biotinamidohexanoic acid N-hydroxysuccinimide ester (long chain biotin-NHS; 0.2 mg/ml) in PBS under gentle agitation for 1 h. Unbound NHS-biotin was removed by three rounds of centrifugation through a 30 kDa molecular weight cut-off filter (Millipore; Billerica, MA, USA) at 17, 000 *x g* for 2.5 min each time.

2.2.7 Full antibody sensor construction

Polymer or 4-ATP SAM modified electrodes with available surface amine were first equilibrated in PBS for 30 min before derivatisation. For surface biotinylation, working electrodes were incubated with 10 µl of biotin-NHS (1 mg/ml) in PBS for 30 min, prior to washing in PBS and dH_2O and gentle drying in a stream of argon. The biotinylated surfaces were incubated with 10 µg/ml of NeutrAvidin (diluted from stock solution of 1 mg/ml in PBS) for 45 min. This was followed by three, 5 min

washes in PBS and dH_2O and drying in argon. The NeutrAvidin functionalized surface was then incubated with biotinylated antibodies at varying concentrations for 1 h. Finally, the biosensor surfaces were washed extensively with PBS and dH_2O to remove non-specifically bound antibodies before drying in argon. When sensors surfaces were blocked, after antibody immobilization, they were incubated in 1 mg/ml BSA solution to block the surface for 30 min prior washing with buffer.

2.2.8 Antibody fragment generation by reductive cleavage

Antibodies (2.5 mg/ml) were incubated with 50 mM 2-MEA solution for 90 min in 37ºC water bath. PBS buffer with 10 mM EDTA, pH 7.0 was used. Centrifugal filters (50 kDa and 100 kDa cut off) were used to get rid of 2-MEA and/or purification of antibody fragments (**section 5.2.1**). For TCEP mediated reduction, different molar excess of TCEP to antibodies were incubated in room temperature for 30 min. Removal of TCEP and purification of reduced fragments were performed in the same way mentioned above. The fragments were immediately used for sensor application.

2.2.9 Half antibody sensor construction

Polymer surface amine was incubated with 5 mM sulfo-SMCC in PBS EDTA buffer (10 mM EDTA), pH 7.0 for 1 h. Then the freshly prepared antibody fragments with free sulfhydryl groups were incubated onto sulfo-SMCC functionalized surface for 1 h. These fully constructed sensor surfaces with or without blocking were ready to be tested for analyte binding.

2.2.10 Analyte addition

When sensors were fully constructed using full or reduced antibodies, increasing concentration of bacteria or a single concentration of bacterial sample in PBS were incubated on the working electrodes for 30 min. For a range of concentrations

tested, intermediate washing with PBS tween buffer (0.05 % Tween 20 (v/v)) was performed prior electrochemical testing. To test the sensor in biological media, functionalized immunosensors were incubated with varying concentrations of bacteria spiked in 50 % human saliva (v/v) in PBS.

2.2.11 Electrochemical measurement

Electrochemical analysis was performed in a three cell system (**Figure 2.2, A and B**) using an EcoChemie µAutolab Type III potentiostat (Metrohm Autolab B.V.; Utrecht, The Netherlands) with frequency response analyser FRA-2. Cyclic voltammetry (CV) and electrochemical impedance spectroscopy (EIS) were carried out in an electrolyte solution of 10 mM $K_3[Fe(CN)_6]$/ $K_4[Fe(CN)_6]$ (1:1 ratio) in 10 mM PBS, pH 7.0. EIS was recorded at 0 V potential over the frequency range of 0.25 Hz to 25 kHz with a modulation voltage of 10 mV. Autolab GPES and FRA software were used to record CV and EIS data, respectively. Usually 10 µl of solution were incubated over the two working electrode areas inside a moist chamber created in a petri dish (**Figure 2.2, C**). EIS readings were taken at each layer of sensor construction, and also before and after bacterial incubation. All the experiments were replicated (n ≥ 3) with independent sensor surfaces and change in impedance after analyte addition was normalized against sensor level impedance (with no bacteria incubated).

For each individual electrode, *R*ct values were obtained from individual Nyquist plots directly using Autolab software, both at the biosensor level and at each step of bacterial incubation. Then the change in *R*ct upon incubation with a particular concentration of bacteria was calculated and normalized to percentage change using the following equation:

$$\textbf{Change in Rct}\ (\%) = \frac{\textbf{Rct}\ (\textbf{bacteria}) - \textbf{Rct}\ (\textbf{biosensor})}{\textbf{Rct}\ (\textbf{biosensor})} \times \mathbf{100} \quad \textbf{.....}\ \ \textbf{2.1}$$

[79]

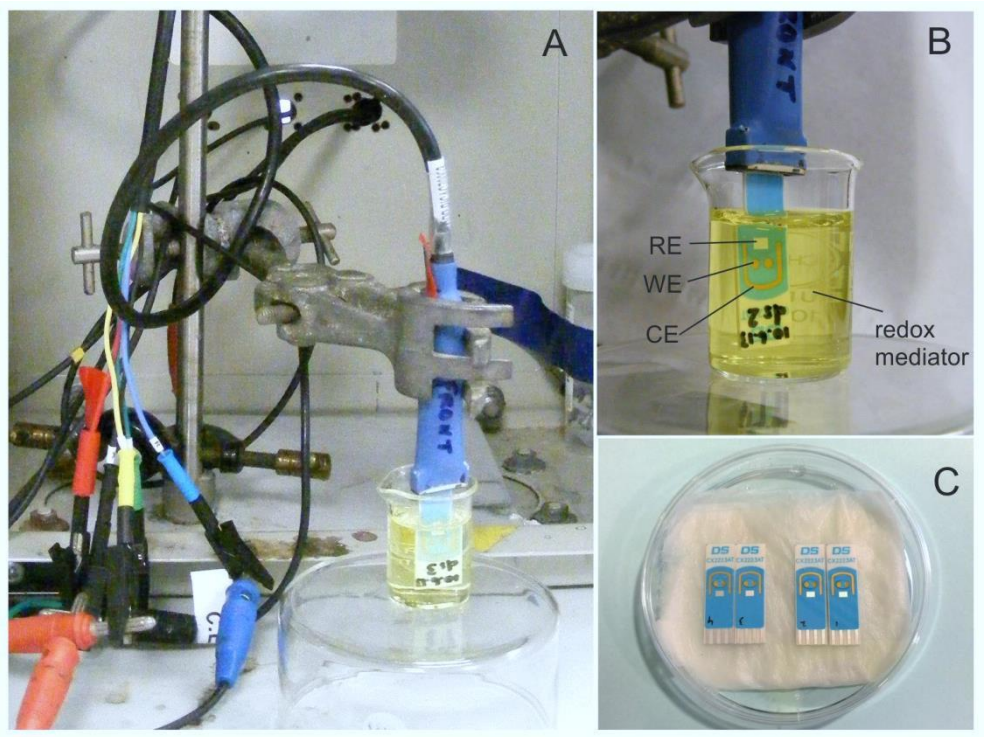

Figure 2.2: Electrochemical setup and incubation in wet chamber

(A) Electrochemical measurement of electrodes in redox mediator solution. The rig is shown outside its Faraday cage. Yellow and red cables are connectors for working electrodes, blue for reference, black for counter and green for earth. (B) Zoomed image of electrode in redox solution and (C) incubation of electrodes in a wet tissue chamber inside petri dish.

2.2.12 Midland blotting

On-sensor characterization was performed at different stages of sensor construction using targeted horseradish peroxidase conjugates followed by generation of light signal using enhanced chemiluminescence (ECL) reagent. This protocol (**Figure 2.3**) has been termed Midland blotting (Rushworth et al., 2013a). Here, appropriate HRP conjugated molecules can bind to a target moiety in the presence or absence of linker molecules and can generate a quantifiable light signal when imaged. In brief, to detect surface amine groups presented by Ptyr, polymer-coated electrodes were incubated in the presence or absence of biotin-NHS followed by streptavidin-HRP. Biotin-NHS couples to surface amine groups and the free biotin moiety can strongly bind streptavidin-HRP which then produces a light signal when exposed to ECL reagent. To detect the presence of bioreceptor (full Ab raised in rabbit) on the sensor surface, HRP conjugated anti-sheep Ab or anti-rabbit Ab were incubated and a subsequent ECL signal was generated. The light signal was imaged using a G:BOX imager and further processed with image processing software ImageJ (NIH; Bethesda, Maryland, USA). Images presented are either chemiluminescence (white light on a black background), or a superimposition of chemiluminescence on the bright-field image, where chemiluminescence has been false coloured cyan to aid viewing.

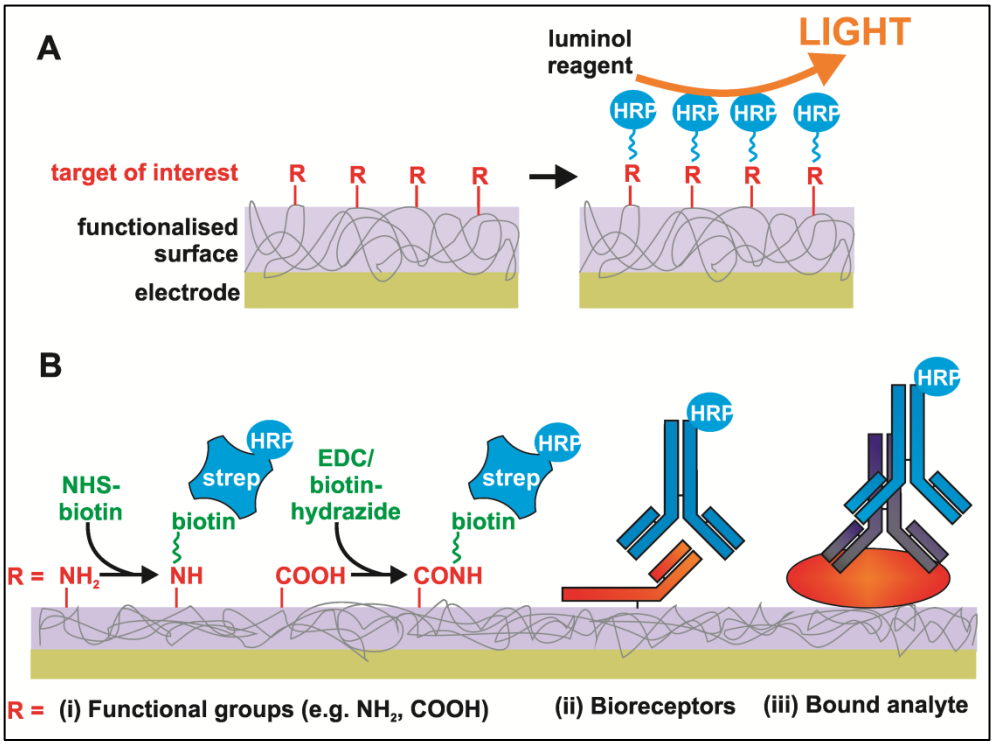

Figure 2.3: Midland blotting: a schematic overview

(A) An overview of midland blotting. The sensor is incubated in the presence of a horseradish peroxidase (HRP)-conjugated reagent which recognises a target group of interest (R) upon the biosensor surface. Upon addition of a luminol-based developing reagent, HRP catalyses a reaction which generates a chemiluminescent (light) signal, which is proportional to the amount of bound HRP. (B) Target groups can include: (i) functional groups upon polymers or self-assembled monolayers (SAM), such as amines (NH_2) or carboxyl groups (COOH), which can be detected by biotinylation and subsequent addition of HRP-streptavidin; (ii) bioreceptors, such as antibodies, which can be detected using HRP-conjugated secondary antibodies; (iii) bound analytes, which can be detected using primary antibodies coupled with HRP-conjugated secondary antibodies (Rushworth et al., 2013a)

2.2.13 SDS PAGE

Antibodies and reductively cleaved half antibodies (Billah et al., 2010) were analysed by sodium dodecyl sulphate-polyacrylamide gel electrophoresis (SDS-PAGE). Bio-Rad Mini Protean TGX gels (4-15% resolving gel, Herts, UK) were used with Bio-Rad Mini Protean Tetra cell system (Hertfordshire, UK). Antibody samples (untreated, treated with either 2-MEA or TCEP) were mixed with 5× SDS loading dye containing bromophenol blue (0.250 M Tris, pH 7.6, 50% (v/v) glycerol, 10% (w/v) SDS, 0.05% (v/v) bromophenol blue) prior to electrophoresis. Details of sample volumes and other parameters are indicated in individual figure legends.

Prestained molecular markers were also used as a molecular weight guideline. Precision Plus Protein all blue standards (10 kDa to 250 kDa) and Spectra multicolour broad range protein ladder (10 kDa to 260 kDa) were purchased from Bio-Rad (Herts, UK) and Thermo Fisher Scientific (USA). Electrophoresis was carried out in Tris-glycine running buffer (25 mM Tris, 192 mM glycine, 0.1% (w/v) SDS, pH 8.0, National diagnostics, USA) at 40 mA until the dye front reached bottom of the gel. After electrophoresis, gels were stained with Generon quick Coomassie stain (Berkshire, UK) for 30 min to 1 h. Then the gels were destained in deionised water before imaging. The imaging was done either in Fujifilm intelligent DARK box (LAS 3000, USA) or in Syngene G-Box imager (Cambridge, UK). Finally the images were optimized for better brightness and contrast in ImageJ software.

2.2.14 Dot blot

Samples (usually 2 µl) were applied carefully and at appropriated spacing onto nitrocellulose membrane and were allowed to dry completely before blocking. Typically used blocking buffer was 3% (w/v) BSA in 10 mM PBS, pH 7.0 containing 0.05% (v/v) Tween-20. Appropriate HRP conjugated binding molecules (streptavidin

or antibodies) were used to differentiate between specific and non-specific signal. Enhanced Chemiluminescence (ECL) reagents were then applied and the dot blot signal was imaged as described in **section 2.2.13**.

2.2.15 Scanning Electron Microscopy

To visualize the bare electrode surface before and after polymerization and sensors with bound bacteria Scanning electron microscopy (SEM) was performed using a Quanta 200F (FEI) in FBS, University of Leeds. The electrodes were cut into small sizes (approx. 2 cm × 2 cm) and glued with carbon paste onto a one inch metal stub. For better conductivity and less damage of bacteria due to the electron beam, a thin platinum coating was applied. A platinum coating of 5 nm thickness was evaporated onto the sample before inserting the sample inside the SEM chamber.

2.2.16 Fluorescence microscopy

Bacteria bound to immunosensors were visualized using a modified protocol from Mannoor (Mannoor et al., 2010). First, a stock of propidium iodide (PI) was made in dH_2O at 1 mg/ml concentration and kept at 4 °C. After the final incubation of the immunosensors with *S. pyogenes*, they were dipped in PI solution (1:500 dilution of PI stock in PBS) for 15 min. After incubation in PI the sensors were washed with PBS and dH_2O and was imaged on an EVOS FL Digital Inverted Fluorescence Microscope. The output image was further processed in ImageJ.

2.2.17 Statistical and graphical software

Data from different electrochemical experiments were imported to either Origin Pro or GraphPad Prism. Image compilation and schematics were drawn in CorelDraw software. Chemical structures were drawn using ChemDraw Pro v13.0. Optical images were adjusted using ImageJ software.

Chapter Three

Preliminary sensor fabrication and optimization

Chapter 3 Preliminary sensor fabrication and optimization

3.1 Introduction

Biosensor construction is a multi-step process which requires strict optimization on each possible step. Depending on the type of electrode, bioreceptor and target analyte, critical parameters may vary. However, in the first place, choice of electrode material is crucial. In this thesis, commercial screen printed gold electrodes were used (**section 2.1.6**). Electrochemical and microscopic investigation of these electrodes were routinely carried out. This is important as batch to batch, or even intra-batch variation, was observed. Clean electrode surfaces provide better electrochemistry and facilitate immobilization of base layer and bioreceptors. Different cleaning protocols were tried and the cleaned electrodes were electrochemically evaluated before biosensor construction.

As an initial approach, self-assembled monolayers (SAMs) and mixed SAMs (mSAMs) were deposited on these electrodes, to check the feasibility of SAM formation on this surface. A conducting copolymer of polyaniline (PANI) and 2-aminobenzylamine (2-ABA) was also explored as a base layer. However, several key issues connected with this copolymer, e.g. impedance drift due to change in oxidation state, long deposition time and non-abundance of surface amines led us to eventually use a different polymer.

Deposition of non-conducting inert polytyramine (Ptyr) was optimized on these electrodes and taken forward for biosensor construction. The Ptyr surface amine was also characterized by an on-sensor blot method termed as ‘Midland blotting’ (**section 2.2.12**). In addition, off-sensor binding interaction of different biosensor

components were routinely checked by a dot blot method before using on the biosensor surface. These preliminary data on sensor optimizations are presented in this chapter.

3.2 Characterization of bare electrodes

3.2.1 CV and EIS profile of new bare electrodes

A CV study (Heinze, 1984) of bare electrodes in the presence of a redox couple gives critical information about oxidation and reduction current (**section 1.8**). Two important features obtained from a CV are; (1), the potential difference between the two peaks known as ΔEp which is the difference between oxidation and reduction potential and (2), the magnitude of the peak currents for both oxidation and reduction (Ip).

The bare DS gold electrodes, opened from a new box were tested for the characteristic CV pattern of bare gold electrodes. The CV showed a sharp reversible peak profile both at the oxidation and reduction points of redox couple (**Figure 3.1, A**). The grey shaded area (average of 3 working electrodes) exhibited slight variation from electrode to electrode, which is due to the surface roughness and variability during screen printing. The average oxidation and reduction peak was observed at 0.184 V and 0.081 V respectively whilst the average currents for oxidation and reduction were 48 µA and -51 µA respectively.

In general, atomically flat, smooth gold surface are supposed to produce better reversible CV profiles compared to screen printed rougher surfaces. However, in a comparative electrochemical study of six commercially available carbon electrodes, the opposite feature was observed (Kadara et al., 2009). They have shown that, the roughest surface produced the best reversible CV profile, which was due to an

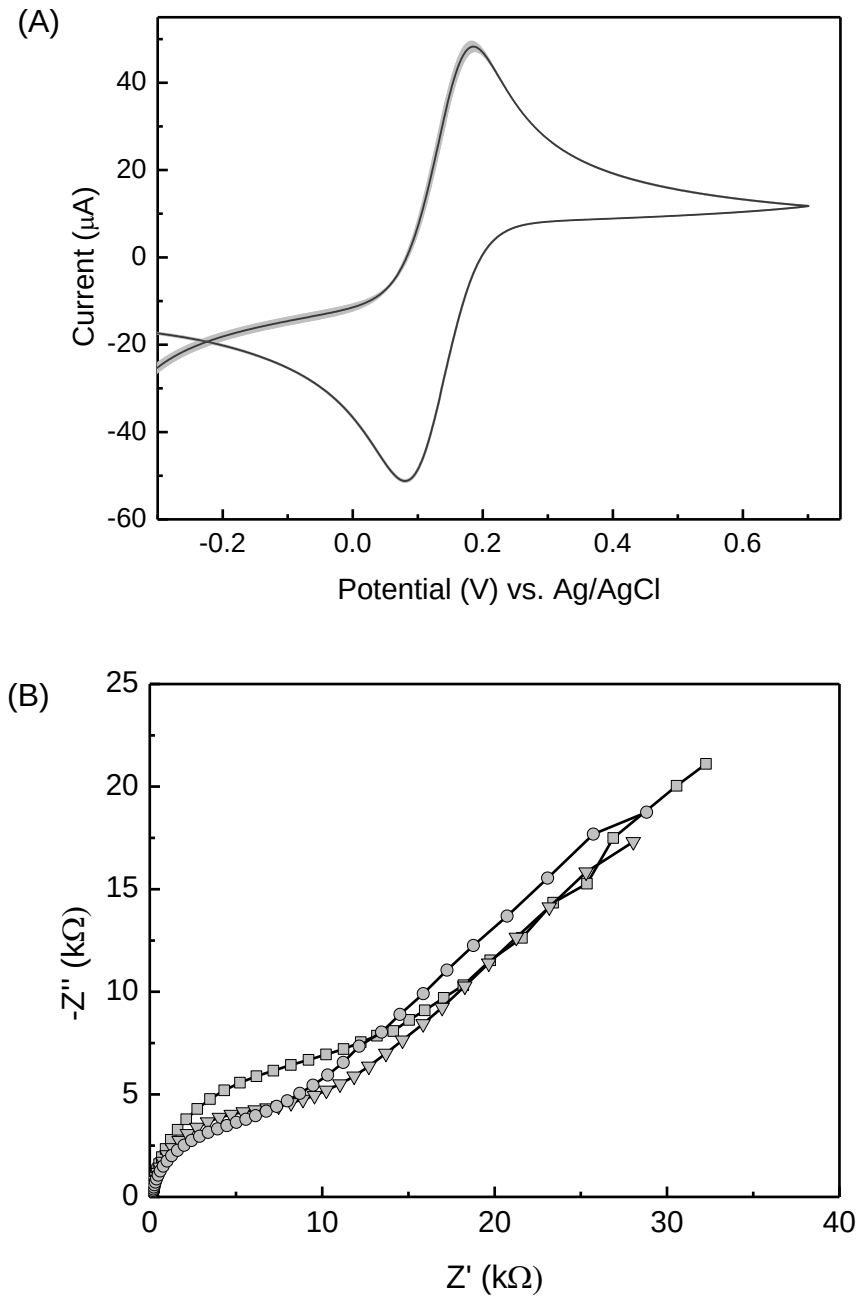

Figure 3.1: Electrochemical profile of bare DS electrodes

(A) CV of pristine bare DS gold electrodes at a sweep rate of 50 mV/s in redox couple. Data are the average of three electrodes (black line) with the standard deviation (n=3) shown in grey shadow, (B) Nyquist plot of three separate working electrodes. CV and EIS readings were taken using a 10 mM $[Fe(CN)_6]^{3-/4-}$ redox couple in PBS, pH 7.0.

increased number of exposed edges. However, other factors like deposition technique and the type of graphite used in the ink can affect this property. They also pointed out that a reversible CV on a rough surface does not necessarily contribute to electrode reproducibility, which is another important requirement of the transducer surface. In a similar type of study, commercial carbon paste and screen printed electrodes were tested with commonly used redox couples (Fanjul-Bolado et al., 2008). They also demonstrated the relationship of high peak current to rough surface in all redox couple except hexa-amine ruthenium chloride. They showed the same behaviour with commercial gold screen printed electrodes where DS gold electrodes showed higher redox reversibility (Garcia-Gonzalez et al., 2008). On these grounds, it can be concluded that, although DS gold electrodes have a good reversible CV profile, their rough surface property can be a critical limiting attribute towards reproducible biosensor construction.

EIS is also another commonly used technique to understand the feature of a bare gold electrode surface. The Nyquist plot gives information of the resistive (real) and capacitive (imaginary) components of the surface impedance (**Figure 3.1, B**). Three representative Nyquist plots are presented here. They showed a typical small semi-circular arc (*R*ct) in the high frequency zone followed by long Warburg (W) component as fairly straight line in the low frequency zone. The small *R*ct (average 15 kΩ) indicated the high conductivity of the bare gold surface which did not hinder the electron transfer to and from the redox couple. Compared to CV profiles, EIS showed slightly more variability (n=3) being sensitive method over CV. The rough electrode surface was also observed in electron microscopy (**section 3.2.2**).

3.2.2 Cleaning and characterization of screen printed electrodes

To obtain optimum biosensor results, the electrode surface must be clean. There is no established standard method to clean screen printed gold electrodes. To optimize the cleaning procedure, random electrodes were subjected to microscopic examination and electrochemical characterization by EIS. Three different cleaning methods were employed; (1), sonication in 100% ethanol for 5 min in a bath sonicator; (2), careful pipetting of 1.5 µl of piranha solution [3:7 of 30% (v/v) H_2O_2 and 98% (v/v) H_2SO_4] onto each circular working electrode area (please note that piranha solution is highly corrosive and proper care need to be taken) and (3), electrochemical cleaning by running 15 cycles CV from 0 to +1.4 V in 0.1M H_2SO_4 solution at a scan rate of 50 mV/s. After each cleaning method applied, impedance readings were taken and *R*ct values were calculated.

The change in *R*ct (%) compared to bare gold electrode was plotted (**Figure 3.2, A**). After sonication a slight increase in *R*ct was observed which was due to possible recontamination of dielectric material onto the gold surface. Piranha treated electrodes showed a higher *R*ct change, as the dielectric not completely resistant to it. Some deposition of dissolved dielectric might occur on the electrode surface. In contrast, CV cleaning came out as best cleaning method as it reduced the *R*ct value indicating increased conductivity of the cleaned gold surface.

When SEM was performed, bare electrodes looked porous, with an irregular granular pattern (**Figure 3.2, B and C**). This also matched data provided by D. J. Pike (personal communication, School of Mechanical Engineering, University of Leeds), who did coherence scanning inferometry of DS gold electrodes surfaces using an NPFLEX Optical Profiler. The data showed X and Y axis average surface topography of around 2 µm and 2.5 µm respectively denoting a highly rough surface. In particular, large crystals observed in the SEM along the surface

contributed most of the roughness. However, visual observations of a CV cleaned surface showed a smoother surface probably due to gold oxide formation (**Figure 3.2, D**). Bare pristine and sonicated electrodes were equally suitable for polymer depositions, as rough surfaces are better for polymer anchorage than very smooth one. However, for SAM deposition, CV cleaned surfaces were used. Piranha cleaned surfaces were not suitable for any applications with these electrodes.

Different types of cleaning methods have been reported in the literature for screen printed gold electrodes. CV mediated cleaning in acidic solution is a widely reported method used to clean DS gold electrodes, e.g. prior to diazonium coating (Radi et al., 2009), and for 3,3-dithiodipropionic acid di(N-succinimidyl ester) (DTSP) SAM formation (Escamilla-Gomez et al., 2008). DS electrodes were also cleaned using methanol for molecularly imprinted polymer formation (Moreira et al., 2013). To develop a DNA based sensor for algae detection, DS gold electrodes were cleaned by two methods; CV running in H_2SO_4 and chemical treatment in Piranha solution (Orozco and Medlin, 2011). Piranha treatment resulted in damaged electrodes with very poor performance whereas the CV cleaned surface favoured thiol-terminated oligonucleotide layer formation. Custom-made screen printed gold electrodes on clean ceramic substrate were cleaned by Piranha solution for 2 h prior to SAM deposition (Susmel et al., 2003). However, they did not report details of the fate of insulating ink (from Agmet, USA) and the base ceramic after long exposure to Piranha solution. From these reports, acidic CV cleaning emerged as the best method for cleaning screen printed gold electrodes.

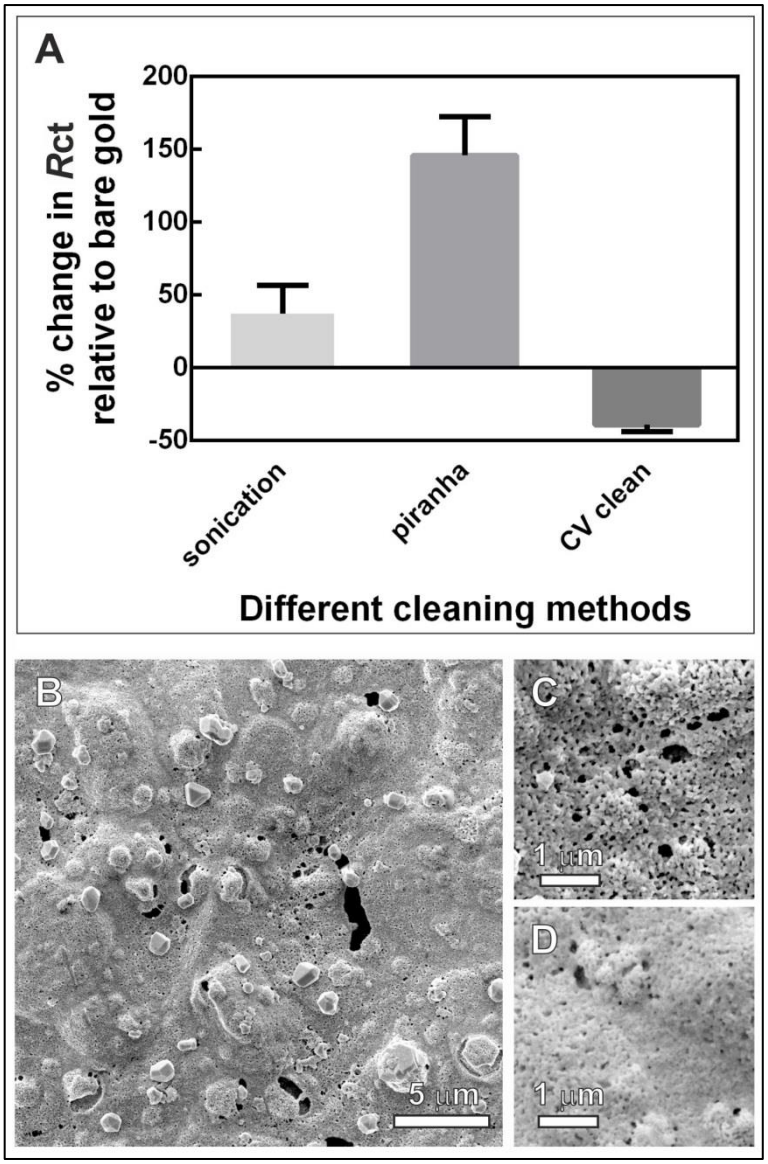

Figure 3.2: Effect of different cleaning methods on DS gold electrodes

(A) Percent change in *R*ct over bare gold electrodes upon different cleaning methods (n=3, average with ± SEM), reproduced from (Ahmed et al., 2013) (B) SEM image of pristine DS electrodes direct from box, (C) same as B at higher magnification and (D) SEM of DS gold electrode surface after CV cleaning.

3.3 Preliminary study with SAM/ mSAM as base layer

Self-assembled monolayers (SAMs) and mixed SAMs (mSAMs) are widely used base layers for different type of biosensor construction. If the electrode surface is clean and smooth, a complete coverage of SAMs can be achieved with different functional groups for bioreceptor conjugation. However, as screen printed electrodes are very rough on the nano-scale, few studies use these electrodes for SAM on it. In addition, as the analyte in the research was bacteria, which are micron sized and contain multiple epitopes on their surfaces, the feasibility of a SAM as the base layer was investigated. Two types of self-assembled surface were tested; (1), a SAM of 4-aminothiophenol (4-ATP) and (2), an mSAM of long chain alkane thiol (MHDA) with biotin tagged lipid (biotin-caproyl-DPPE) (**Figure 3.3**). 4-ATP assembles a SAM via its phenyl rings in a side-by-side fashion with sulphur attached to the gold surface, leaving free primary amine groups facing upwards. 4-ATP is a very small molecule and the SAM is predicted to be less than 1 nm thick. The mSAM format on the other hand, intercalate the biotinylated lipid in between MHDA layer. This leaves a free biotin standing out of the surface and aids in biotin-avidin mediated conjugation approaches. Thus mSAM is fairly long, around 2 nm from the surface.

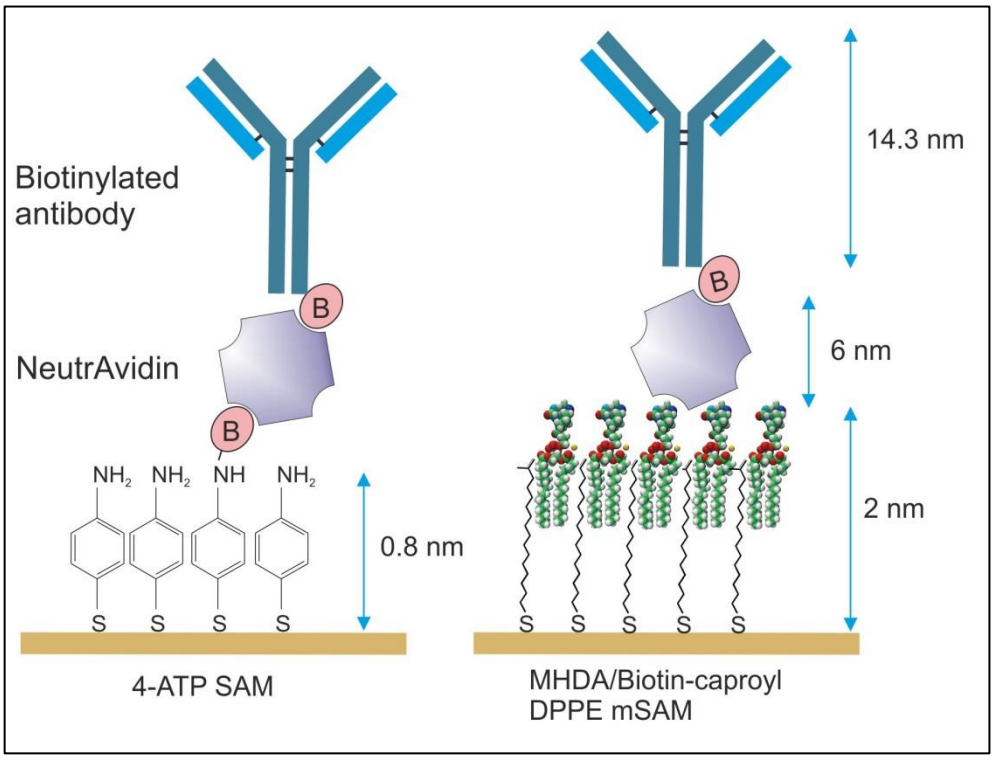

Figure 3.3: Schematic of SAM and mSAM based biosensor construction

4-ATP SAM on gold surface, biotinyl antibodies conjugated to amine via NeutrAvidin and biotin-NHS (left). mSAM of MHDA and biotin-caproyl-DPPE (right). Drawing is not in scale and approximate distance of bioreceptor to the gold surface are shown.

3.3.1 CV profile of SAM and mSAM formation

Before deposition of SAM/ mSAM, all the electrodes were cleaned by CV in 0.1 M sulphuric acid solution, followed by washing with sufficient amount of dH_2O. Both the sensors were functionalized with NeutrAvidin and biotin tagged antibodies. CV characteristics before and after SAM or mSAM deposition were observed. The 4-ATP derived SAM showed a reduction of both oxidation and reduction current (**Figure 3.4, A**). However, the CV profile observed was quasi-reversible which indicates impurity in SAM formation or some chemical reaction between the SAM and surface contaminants. On the other hand, the mSAM showed a reversible CV profile after deposition. However, here the current drop in oxidation and reduction peak due to deposition was much smaller (**Figure 3.4, B**). This might correlate with the electrode surface roughness, as incomplete deposition was achieved. In addition, when full sensors were constructed on the mSAM surfaces, the impedance signal collapsed to the bare gold level meaning the mSAM formation was unstable (data not shown). For this reason, only the 4-ATP SAM based study was continued.

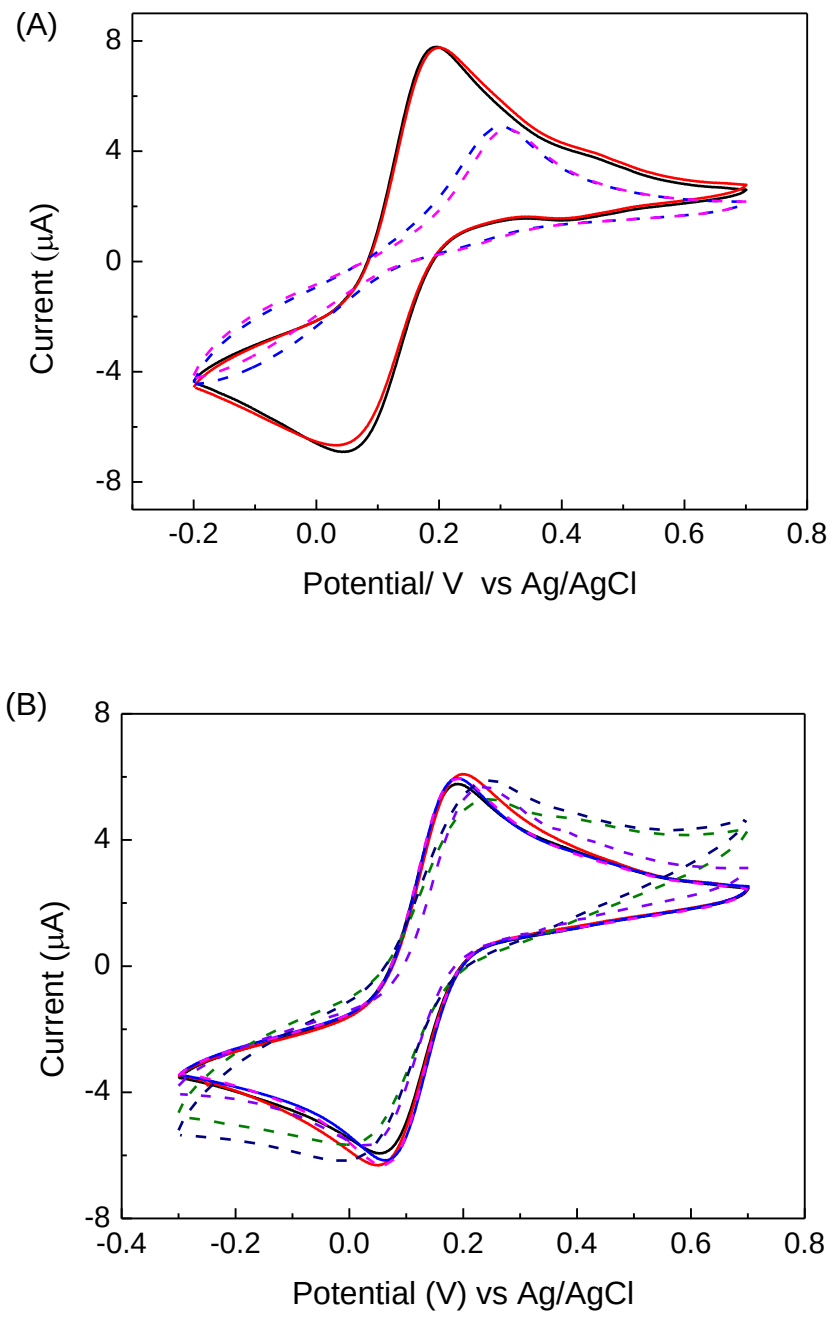

Figure 3.4: CV data of SAM and mSAM on clean DS electrode

(A) 4-ATP SAM (n=2) and (B) mSAM of MHDA and biotin-caproyl-DPPE (n=3). Solid lines are the CV of independent bare gold electrode surfaces, dashed lines are the same electrodes after SAM/ mSAM deposition. CV reading was taken in 2 mM $[Fe(CN)_6]^{3-/4-}$ redox couple in PBS, pH 7.0.

3.3.2 Nyquist plot of SAM based bacterial detection

As mSAM based sensor construction was not feasible on DS gold electrodes, preliminary studies with a 4-ATP based complete biosensor to detect *S. pyogenes* were performed. Sensor chips were fabricated with biotinylated anti-*S.pyogenes* full antibodies immobilized onto 4-ATP SAM via biotin-NeutrAvidin link (**section 2.2.5**). Control sensors were made following the same protocol using biotinylated anti-digoxin antibodies. Then three concentrations of *S. pyogenes* (10^3, 10^5 and 10^7 cells/ml) were incubated onto both sensor surfaces and their EIS were recorded. One representative Nyquist plot from each group is presented in **Figure 3.5.**

All of the sensors showed semi-circular Nyquist plots (*R*ct value ~75 kΩ) after 4-ATP deposition. They were reproducible on different sensor chips. Immobilization of antibodies were also consistent on all the chips confirmed by EIS data. Both antibodies were deposited via a biotin NeutrAvidin link with increasing *R*ct value (~ 150 kΩ). In the specific sensor, *R*ct was increased upon incubation of 10^3 cells/ml of *S. pyogenes* indicating immune binding between antibodies and bacteria. When higher concentration of bacterial cells were incubated, the *R*ct then dropped. This can be due to two distinct behaviours on the sensor surface; First, as bacteria have multiple antigens on their cell surface, upon binding to antibodies on the sensor, pinholes were generated with increased electron transfer and lower impedance and second, as SAM formation might be faulty due to the roughness of the printed gold surface, successive binding of bacteria could disrupt the SAMs resulting in more current flow.

In the control sensor, however, a different scenario was observed. None of the bacterial incubation showed any consistent *R*ct change. Even after second and third incubations, the impedance dropped below the initial sensor level. This might suggest that there was no direct immune binding on surface and subsequent

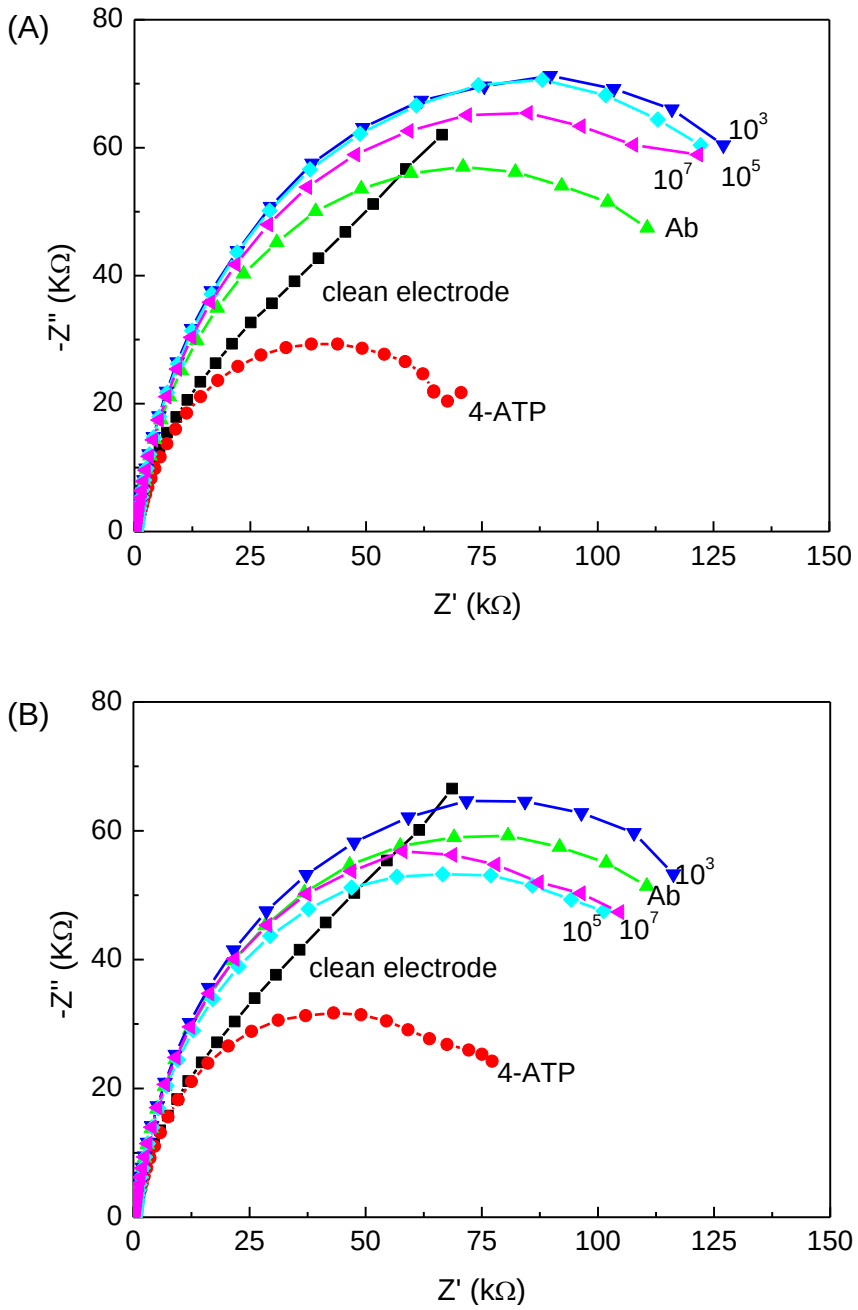

Figure 3.5: EIS data of specific and non-specific 4-ATP SAM based sensor upon *S. pyogenes* incubation

(A) Biotinylated anti-*S. pyogenes* antibodies and (B) biotinylated anti digoxin antibodies were immobilized onto a 4-ATP SAM based sensor. Three concentration of *S. pyogenes* were incubated on both sensors and Nyquist data are shown. EIS reading was taken in 10 mM $[Fe(CN)_6]^{3-/4-}$ redox couple in PBS, pH 7.0. Clean electrode (-♦-); 4-ATP SAM (-●-); constructed sensor (-▲-); 10^3, 10^5 and 10^7 cells/ml (-▲-, -♦-, and -▲- respectively).

incubation and washing had disrupted the base layer and its impedance. These nonlinear impedance shifts were consistent in multiple repeats. From these findings it was concluded that, on a SAM/ DS gold surface, it was very difficult to get a linear relationship between impedance signals and bacterial concentration, and so they were not suitable for SAM based bacterial detection.

The nature of SAM and/or mSAM on transducer surface has two implications to be considered; First, the behaviour of SAM deposition on a relatively rough electrode surface, e.g. DS gold electrode and second, the fate of SAM/ mSAM layer upon binding analytes with multiple binding sites, e.g. oligosaccharides, bacteria, viruses both in smooth and rough electrodes. From the literature it is well established that flat, smooth and clean surfaces are suitable for anchoring monolayers (Schreiber, 2000). There are several reports of SAM/ mSAM based biosensor constructions on flat electrodes targeting different type of analytes including the small molecule chloramphenicol (Chullasat et al., 2011), cardiac biomarker myoglobin (Billah et al., 2008), and bacteria (Geng et al., 2008; Mantzila et al., 2008). These sensors were constructed using flat electrodes on nanoscale with single or combined pre cleaning methods like treating with piranha solution, physical polishing, CV cleaning etc. However, SAM/ mSAM based bacterial detection publications do not report any issues regarding effect of binding via multiple epitopes on the monolayer.

There are very few reports of SAM based biosensor prepared using screen printed electrodes (Loaiza et al., 2008; Shen and Liu, 2007). Also they term these layers as ‘interrupted monolayer’ or ‘non-insulating layer with irregular pores’, which in theory does not reflect pure SAM formation. Again, the effect of these interrupted monolayers on analyte detection is not clearly investigated or reported. In a study, photosynthetic reaction centre Photosystem II (PS II) was immobilized onto an intentionally ‘defective’ SAM layer formed on DS gold electrodes (Bhalla and

Zazubovich, 2011). However, they used an amperometric method to test the effects of photosynthetic inhibitors, which were not supposed to alter the SAM on the surface. Impedimetric detection of antioxidant activity of garlic extracts using a SAM on a DS gold electrodes was reported (Cortina-Puig et al., 2009). In their study, they optimized deposition time and composition of different SAMs and mSAMs. However, they did not report any issues related to faulty deposition or smoothness of the SAM layer.

In our research group, during optimization of impedimetric detection of carbohydrates, it was observed that binding of a multivalent sugar moiety to lectins immobilized on a SAM surface tends to disrupt that SAM (Shahidan, 2012). This was also supported by SECM and CV data. Although the SAM was on a smooth gold surface, the exact reason behind this phenomenon still demands further research with different SAMs, bioreceptors and analytes. In this context, it was a better choice to select more robust base layer like polymers to start with. Hence, polymer based sensor construction was investigated.

3.4 Preliminary study with a PANI/ 2-ABA copolymer

As previously in our group copolymer of PANI/ 2-ABA has been used to construct immunosensors against adenovirus (Caygill et al., 2012), preliminary work was started with this copolymer as base layer. Sensors made with this copolymer were tested for MS2 and *S. pyogenes* as a model organism. Polyaniline (PANI) is a widely used conducting polymer, however incorporation of additional amine containing analogue 2-aminobenzylamine (2-ABA) increased the amount of pendant amine on the surface (Caygill et al., 2012). The copolymer was made from equal molar ratio of two monomers in HCl solution by cyclic voltammetry of 20 cycles. This polymerization process was well characterized in our group by CV (Shahidan, 2012).

PANI itself has several oxidation states and is prone to interconvert from one stage to another (Lux, 1994). This inter-conversion is due to slight pH change, and can be unsuitable for certain biosensor application. In the initial stage when biosensors were constructed using PANI/ 2-ABA copolymer for both MS2 and *S. pyogenes* as model microorganisms, both specific and non- specific signal was changing in the same magnitude. Several repeats of this scenario generated few possibilities; (1), the amount of surface amine is not abundant, thus copolymer to analyte charge interaction is overtaking the immune reaction; (2), the inherent inter-conversion of polymer is affecting sensor signal, as long processing time from sensor making to interrogation triggers the inter-conversion easily. With these hypotheses in mind, several aspects of this copolymer was investigated and compared with alternative amine containing polymers to select a suitable base layer for sensor construction.

3.4.1 PANI/ 2-ABA copolymer impedance drift

The first investigation was done to check the copolymer impedance stability over time and different conditions. To do this, impedance readings were taken at three different time points; (1), as fresh, just after polymerization; (2), after keeping freshly prepared polymers at room temperature for 24 h and (3), after soaking the 24 h aged polymers in 10 mM $[Fe(CN)_6]^{3-/4-}$ solution for 1 h. The fresh polymer Nyquist plot showed its capacitive nature (~70 kΩ) with less resistance (~30 kΩ) (**Figure 3.6, A**). When the same electrodes were kept at room temperature, their impedance behaviour changed again. The capacitive feature of freshly prepared copolymers dropped significantly to ~12 kΩ, making the polymer more conducting (**Figure 3.6, B**). This can be described as aging of the polymer over time. However, when these electrodes were kept for an hour in redox mediator, the polymer became highly capacitive and resistive, which is evident from the Nyquist plots (**Figure 3.6, C**). Although the clear mechanism behind the changes in impedance cannot be concluded from EIS data, the unstable impedance observed here made this system less suitable for biosensor construction.

To further check impedance behaviour of copolymer in redox mediator, consecutive impedance reading of polymer on two different electrode chips were tested. As shown in **Figure 3.7** the impedance increased with successive impedance measurements. After three to four measurement the drift became less indicating the stabilization of the polymer in the testing redox mediator solution. However, it is very hard to differentiate this impedance drift from the change due to immune binding on a full sensor surface. To further investigate the issue, the magnitude of impedance change on different biosensor layers was tested with MS2 incubation.

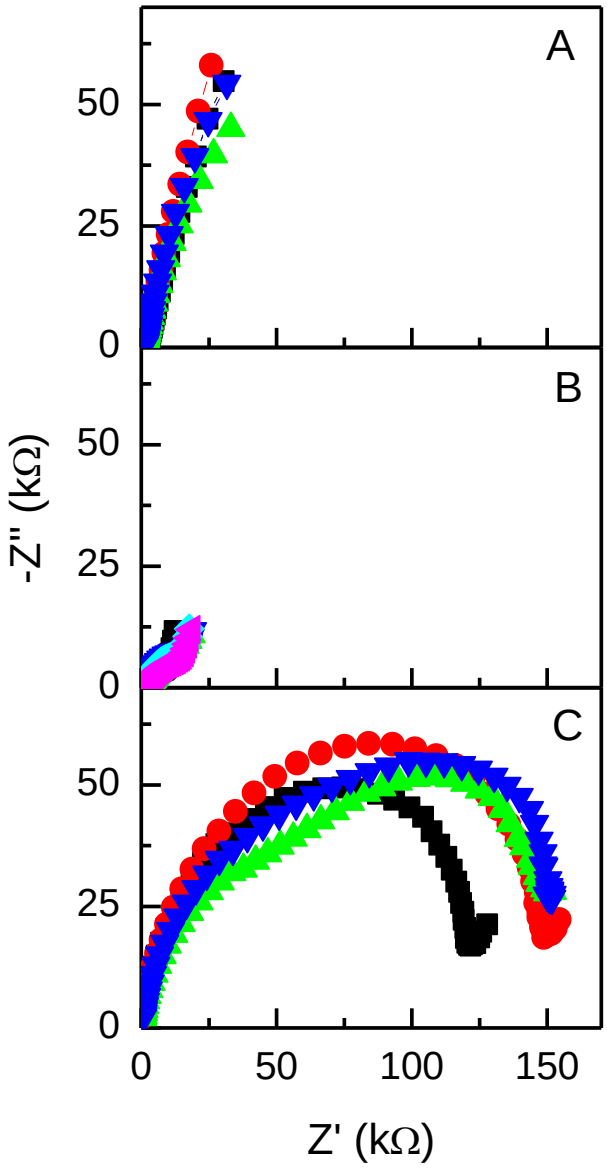

Figure 3.6: PANI/ 2ABA copolymer EIS variability over time

(A) Fresh copolymer, (B) after 24 h at room temperature and (C) 24 h with additional one hour soaking in redox mediator (10 mM 1:1 ratio of $[Fe(CN)_6]^{3-/4}$ in PBS, pH 7.0). For each graph data from four individual electrode surfaces are presented.

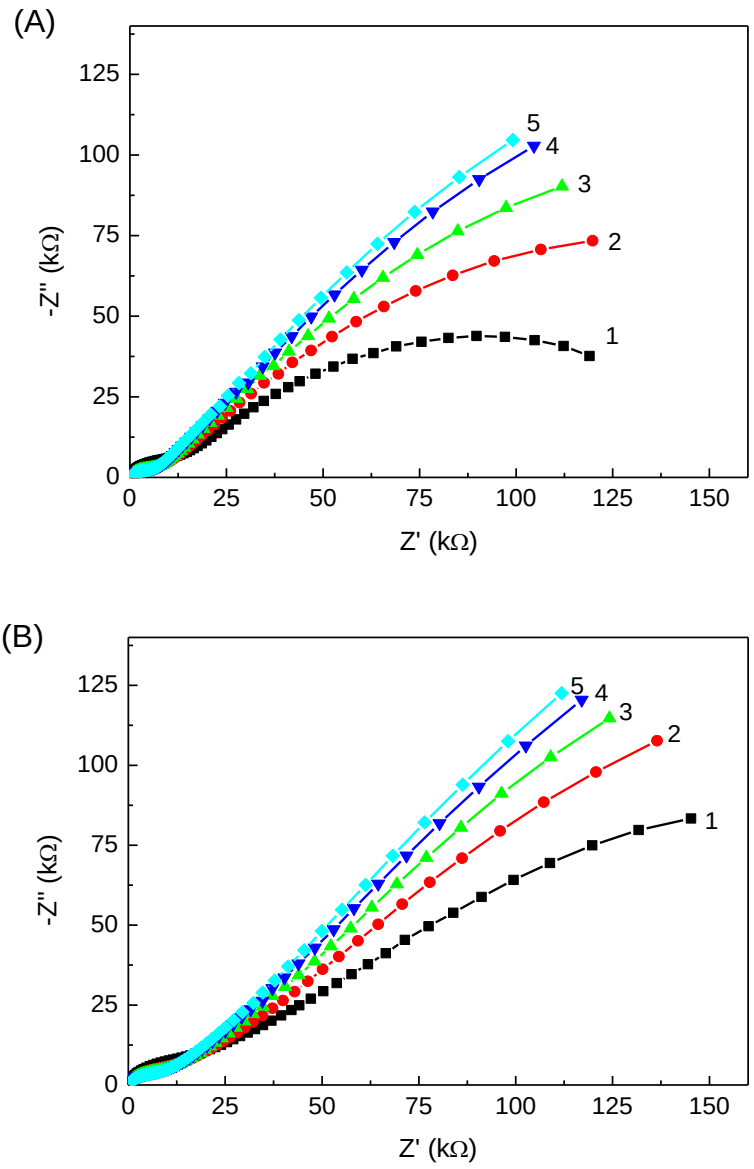

Figure 3.7: Consecutive EIS of PANI/ 2ABA copolymer on two DS electrodes

Five consecutive EIS reading of copolymer on gold electrodes in redox mediator (10 mM $[Fe(CN)_6]^{3-/4}$ in PBS pH 7.0. Two independent working electrodes are shown in A and B. Numbering (1-5) indicates the sequence of EIS reading with ~2 minutes of data collection and 30 s of gap between them.

The four types of surfaces prepared were; (1), only copolymer; (2), sulfo-SMCC added to copolymer amine; (3), reduced MS2 antibodies conjugated to copolymer via sulfo-SMCC and (4), reduced anti digoxin antibodies conjugated same way on the surface as control. On all of these sensors, increasing concentration of MS2 were incubated and the impedance readings were recorded to see the impact of MS2 incubation on the different copolymer based layers.

On the copolymer only surface successive incubation of MS2 resulted in an increase in impedance (**Figure 3.8, A**). This change in impedance could be the effect of impedance drift along with some non-specific absorption of MS2 on the polymer surface. However, as previously observed, the dominant change might be due to impedance drifts of the polymer itself. On the second surface, where sulfo-SMCC was conjugated, the change was slightly lower (**Figure 3.8, B**), possibly due to some coverage of the surface amine which reduced non-specific absorbance of MS2.

On both surfaces with specific and non-specific antibodies the change in impedance was not larger compared to other two surfaces (**Figure 3.8, C and D**). This could be due to the coverage of polymer with antibodies thus reducing the impedance change. However, the shape of the Nyquist plots after full sensor construction and analyte incubation became more linear, due to complex polymer layer. The difficulty of these Nyquist plot shape was to derive the equivalent circuit component and construct sensor calibration. Based on these findings, a search for a more inert and stable polymer with abundant amines was carried out and optimization of tyramine polymerization was performed.

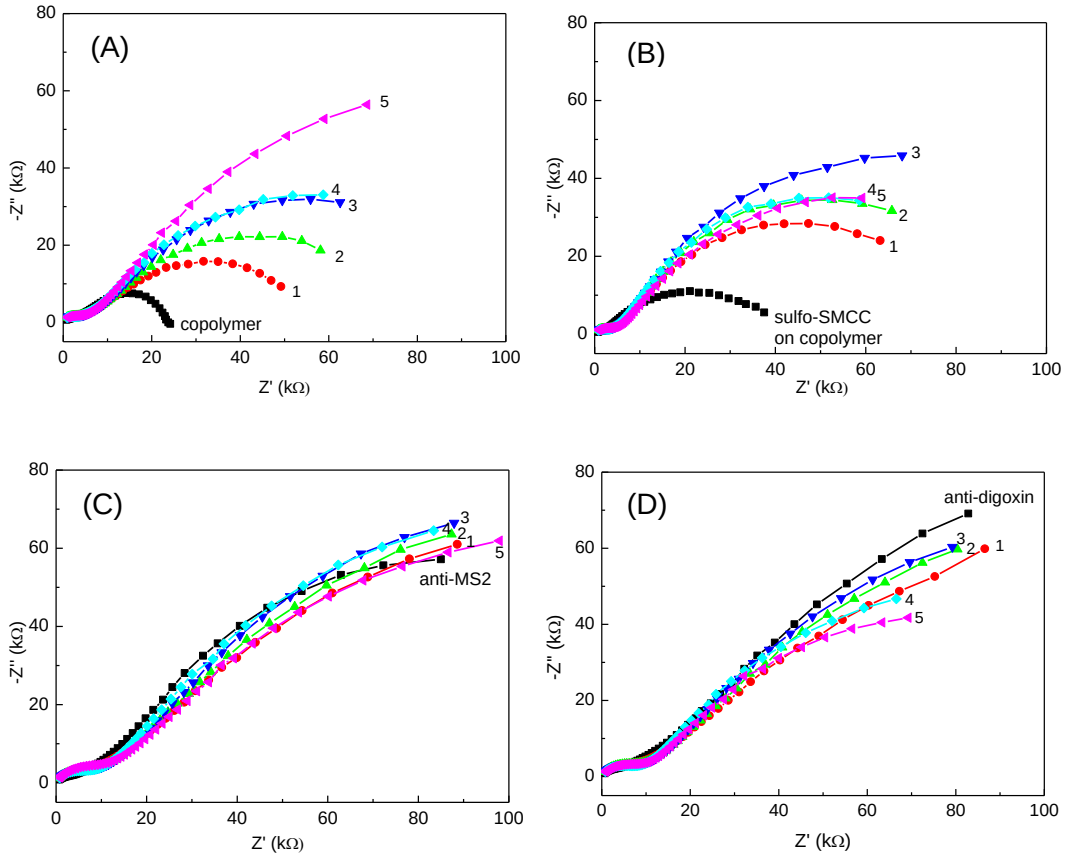

Figure 3.8: Impedance behaviour of different layers of PANI-2ABA copolymer based sensor

Increasing concentration of MS2 (from 1-5, 10^2, 10^4, 10^6, 10^{12} and 10^{14} pfu/ml) were incubated onto; (A), PANI/ 2-ABA copolymer; (B), sulfo SMCC conjugated onto copolymer; (C), anti-MS2 half antibodies and (D), anti-digoxin half antibodies immobilized on copolymer via sulfo-SMCC. EIS was taken in 10 mM $[Fe(CN)_6]^{3-/4}$ in PBS pH 7.0.

3.5 Dot blots to monitor compatibility of the individual biosensor components

When an unexpected sensor response was observed with copolymer based studies, the compatibility of the different sensor components were also checked. Dot blotting is a very easy, quick and semi-quantitative off-sensor technique to assess individual components' binding ability. For this reason the dot blots were done at regular intervals to check the binding profile of sensor components. This data also helped to check stock to stock variability of sensor components.

In full antibody based sensor construction, NeutrAvidin was used as a bridge between SAM or polymer amines to the biotinylated bioreceptors. A dot blot was performed to check two different batches of NeutrAvidin purchased at two different time points and to confirm their biotin binding activity. Two nitrocellulose membranes were spotted with 2 µl of two NeutrAvidin stocks and one negative control ovalbumin. The first membrane was blocked and incubated with biotinylated anti-*S. pyogenes* antibodies, which were raised in rabbit. Then goat anti-rabbit HRP conjugated antibodies were incubated followed by adding ECL substrates and imaging. In the second membrane no primary biotinylated antibodies were used. The signal was visible in only two spots on the first membrane, indicating both the NeutrAvidin stock were functional to bind biotinylated antibodies (**Figure 3.9, A**). In the absence of primary antibodies, however, no signal was seen, confirming that the signal in first membrane was due to bound biotinylated antibodies only.

In the second experiment, biotinylated antibodies were spotted onto the membrane. Two forms of biotinylated anti-*S. pyogenes* antibodies (LC, long chain and SC, short chain biotin-NHS tagged to the antibodies) along with LC anti-digoxin

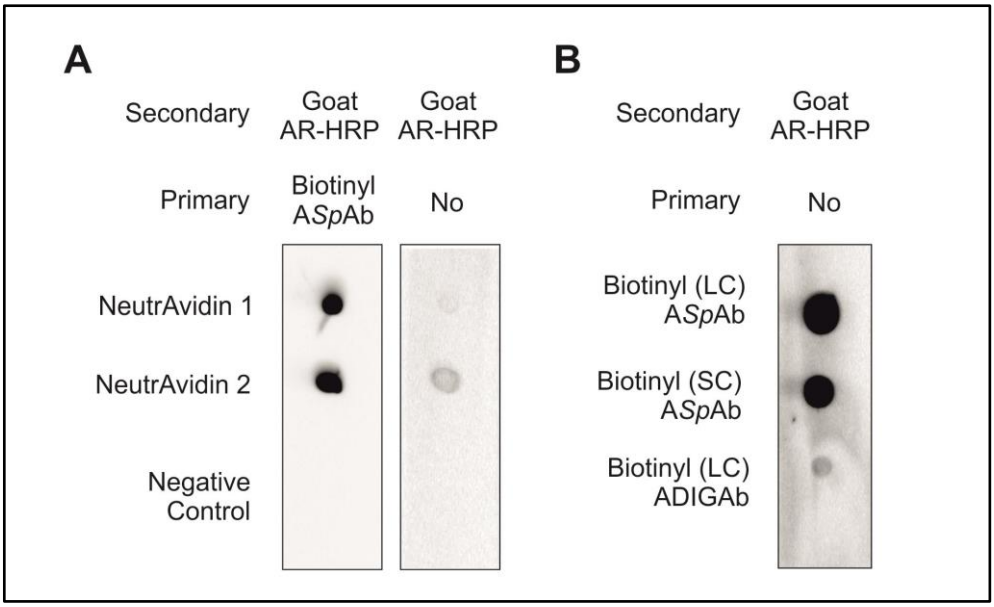

Figure 3.9: Dot blot characterization of NeutrAvidin and antibodies

(A) NeutrAvidin from two different stocks and negative control, ovalbumin (2µl each) was spotted on both membranes. On the first strip biotinylated anti-*S. pyogenes* antibody was incubated followed by goat anti-rabbit HRP in PBS. On the second membrane no primary antibody was used, (B) Biotinylated antibodies were spotted followed by goat anti-rabbit HRP (1:1000 dilution of 1mg/ml stock). Anti-*S. pyogenes* and anti-digoxin antibodies were raised in rabbit and sheep host respectively. AR= anti-rabbit, A*Sp*Ab= anti-*S. pyogenes* antibodies, ADIGAb= anti-digoxin antibodies.

antibodies were spotted. The anti-digoxin antibody was raised in sheep. No primary antibodies were used, instead goat anti rabbit HRP conjugated antibodies were incubated. Two antibodies against *S. pyogenes* showed signal, with no signal from anti-digoxin antibodies (**Figure 3.9, B**). This experiment reconfirmed the host in which antibodies were raised, as this information is very critical in characterization experiments, where different host derived antibodies were regularly used.

S. pyogenes stocks were also tested using dot blots to check the off-sensor binding feature with a set of different antibodies. To check this, 2 µl of bacterial sample (10^7 cells/ml) were spotted on five different membranes. Two different dilution of biotinylated anti-*S. pyogenes* antibodies, biotinylated anti-MS2 antibodies, biotinylated anti-digoxin antibodies and a blank incubation were performed. This was followed by streptavidin-HRP and ECL reagent. The data showed that, *S. pyogenes* were sensitive to only biotinylated anti-*S. pyogenes* antibodies (**Figure 3.10**). The result also suggested the antibodies successfully bound bacteria and streptavidin HRP interacted with biotins attached to those antibodies. Thus, both the bacteria-antibody interaction and biotin-streptavidin interaction was active.

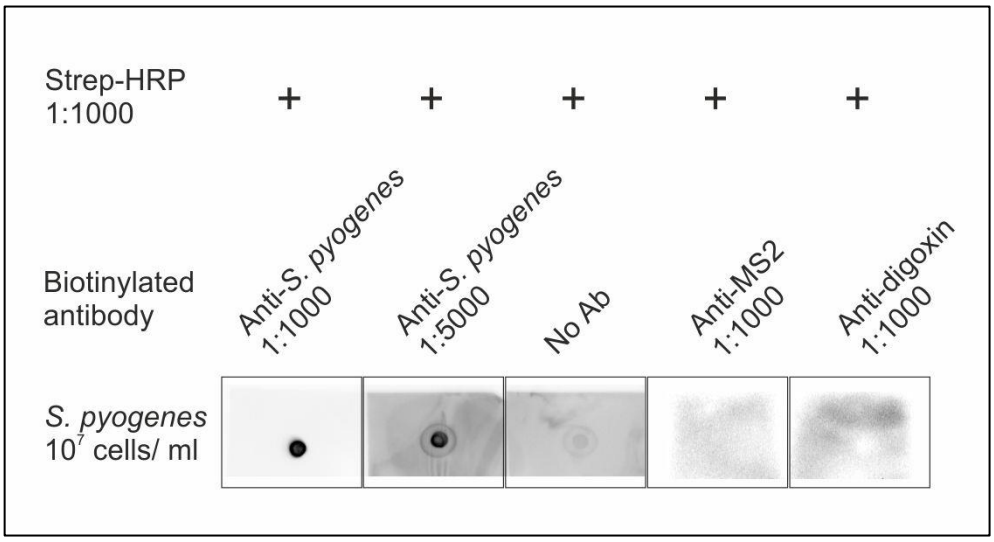

Figure 3.10: Dot blot of *S. pyogenes* with different antibodies

S. pyogenes (10^7 cells/ml) sample of 2 µl were spotted on each membrane. All biotinylated antibodies were diluted from 1 mg/ml stock. Appropriate blocking and washing was performed on each step as described in **section 2.2.14**. After adding ECL reagents the membranes were imaged in imager and the photographs were processed in ImageJ software.

3.6 Optimization of polytyramine deposition

As PANI/ 2-ABA copolymer showed impedance instability, and difficulties with impedance data acquisition, an alternative amine-abundant stable polymer was investigated. Tyramine is an amine containing phenol and electropolymerization of tyramine has been reported from basic, neutral and acidic media. This leaves the aliphatic chain terminated with pendant amines from the polymer surface, which do not take part in the polymerization. Polytyramine has been used for several biosensor applications including capacitive immunosensors (Wu et al., 2005), enzyme sensors (Suprun et al., 2004; Tsuji et al., 1990), and impedance sensors (Pournaras et al., 2008; Yang et al., 2012). Generally, polytyramine is an inert polymer with non-conducting properties. It shows high pH stability and solvent compatibility over a wide range of potentials, making it suitable for sensor applications (Losic et al., 2005). The thickness and porosity of this polymer can also be controlled by several parameters including solvent, concentration of tyramine, number of CV deposition cycles and the deposition scan speed.

The published literature on polytyramine are mainly of two types; 1), polytyramine used in biosensor applications and 2), characterization of polytyramine deposition and its morphology. However, in our impedimetric sensor application, the impedance property of the deposited polymer is crucial as highly capacitive or resistive polymer could produce an insensitive signal. The literature reports substantial variation in different parameters of polytyramine deposition including the base material (platinum, gold, carbon, silicon and diamond), solvent for polymerization (PBS, PBS-methanol mixture, methanol/ NaOH and H_2SO_4), and different number of CV deposition cycles (2 to 250). A representative example of the variety of polytyramines in the literature is shown in **Table 3.1** below.

Table 3.1: Parameters for polytyramine electrodeposition

Solvent used for polymerization	CV parameters	Application	Base electrode	Reference(s)
Tyramine, 1.5% (w/v) in PBS	–0.3 to +1.8 V, 10 cycles at 50 mV/s	Glucose sensor, amperometric	Platinum coated carbon paste electrode	(Liu et al., 2007)
Methanol solution containing 0.3 M NaOH and 0.1 M tyramine	+0 to +1.5 V at a rate of 50 mV/s.	Capacitive immunosensor to detect HSA	Gold wire electrode	(Wu et al., 2005)
0.01 M tyramine in ethanol/ PBS mixture (1:3, pH 7.0)	+ 0.6 to + 1.8 V at the scan rate of 50 mV/s five cycles	Bi-enzyme sensor to detect pollutants	Carbon	(Suprun et al., 2004)
0.1 M tyramine in (a) aqueous 0.1 M H^2S0^4 (b) aqueous 0.2 M NaOH and (c) methanol containing 0.3 M NaOH	Passing a constant current of 50 pA for 1 h	Glucose sensor, amperometric	Platinum	(Tsuji et al., 1990)
0.1 M tyramine in methanol/ 0.050 M phosphate buffer pH 7.40 (1:3)	−0.1 to 1.7 V at 100 mV/s	Glucose sensor	Carbon	(Miscoria et al., 2006)
2.5 mM tyramine in PBS (pH = 4.1)	-0.2 V to +1 V at 50 mV/s 50 scans (25 cycles),	Dopamine and ascorbic acid amperometric detection	GCE	(Khudaish et al., 2012)
Solution of 50mM tyramine in a degassed 1:3 mixture of ethanol/ sodium phosphate buffer saline (PBS, 2.0 mM phosphate buffer, pH 7.0 + 100mM NaCl)	0.0 to 0.8V at scan rate of 50 mV/s	Capacitive glucose biosensor	Sputtered gold surface	(Labib et al., 2010)
Methanol solution containing 0.3 M NaOH and 0.1 M tyramine	0 V to +1.5 V at a scan rate of 50 mV/s for 16 cycles	impedance sensing of PEP gene	GCE	(Yang et al., 2012)

Solvent used for polymerization	CV parameters	Application	Base electrode	Reference(s)
0.1 M tyramine and $HClO_4$, pH 2	10-250 cycles	Oligonucleotide hybridization	Glassy carbon or Pt disk	(Tran et al., 2003)
10 mM tyramine, solvent not mentioned	-0.3V to 1.6V	Glucose biosensor	SPGE	(Miao et al., 2005)
Tyramine solution (15 mM) in $HClO_4$ (0.5 M), pH adjusted with NaOH	-0.4 to 1.2 V, several cycles	Characterization of nickel incorporation	Graphite	(de Castro et al., 2008)
0.1 M tyramine in phosphate buffer/ methanol solution (3:1) 0.05 M, pH 6.8,	0.0 V to +1.5 V, scan rate 10 mV/s to 500 mV/s and 1, 5, 10 and 20 sweep cycles	Ptyr deposition on silicon electrodes	Silicon	(Losic et al., 2005)
0.025 M tyramine in 0.1 M H_2SO_4	−0.10 to 1.05 V 50 cycles from	To study polymerization mechanism	Pt	(Tenreiro et al., 2007)
Tyramine hydrochloride (0.1 M) dissolved in methanol containing 0.3 M NaOH	-0.1 V to +1.7 V *vs.* Ag/AgCl at 500 mV/s for 20 cycles	Dopamine detection	Boron doped diamond electrode	(Shang et al., 2009)

Considering these parameters, the polytyramine was extensively optimized for the particular impedimetric use to detect bacteria using DS gold electrodes.

3.6.1 CV mediated electrodeposition of Polytyramine

Initially, polytyramine was electropolymerized from methanol containing NaOH (**section 2.2.4**). The methanol solution containing 0.3 M NaOH and 0.025 M tyramine was cycled from 0 V to +1.6 V at scan speed of 100 mV/s. **Figure 3.11** shows the CV during polymer formation. The oxidation peak in the first cycle (**Figure 3.11, A**) was observed at around +0.5 V indicating the polymer chain formation via oxidative ether formation. However, In the second cycle the polymer growth was self-limited and the drop in current can be observed. When cycle 1 to cycle 8 were co plotted (**Figure 3.11, B**) it can be seen that as the cycles progress, the self-limiting property of polymer continued with gradual reduction in the current. However, deposition of polymer with 2 cycles was selected as it provided sufficient surface amines for antibody conjugation. Keeping two cycles constant, several other parameters were also checked, including the effect of different solvents and effect of deposition scan speed. Alternatively, the scan speed was kept constant while the effect of different number of cycles on the deposited polymer impedance was observed. These observations are described in the following sections.

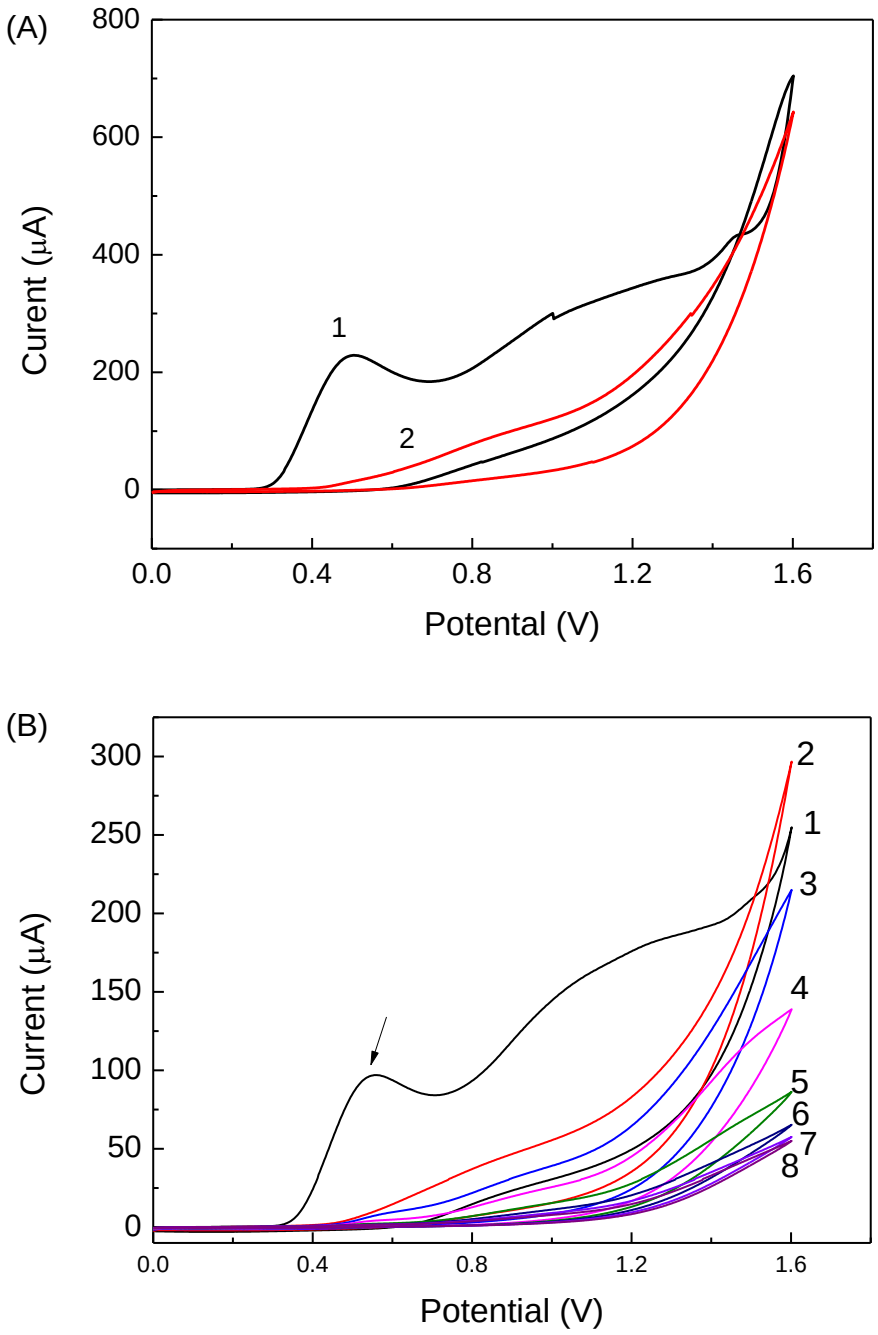

Figure 3.11: CV mediated electrodeposition of Ptyr on DS gold electrodes

(A) Cyclic voltammetry showing two cycles during polytyramine deposition, two working electrodes connected at a time and (B) CV of Ptyr deposition from cycle 1-8, data from single working electrode. The arrow shows oxidation peak of first scan. These data are published in (Ahmed et al., 2013)**.**

3.6.2 Different solvent for Ptyr formation

Although there are several reports in the literature of polytyramine deposition from different solvents, the majority of them are from methanol containing NaOH. Sodium hydroxide helps in the ionization of the monomer, thus promoting polymerization. Here, different solvents were used to deposit polytyramine and the polymer impedance and surface amine were analysed by Midland blot. The benefit of the Midland blotting data is that, it confirms the 3D orientation of pendant amine which are capable of binding to streptavidin. Impedance data alone only provides confirmation of deposition on the surface but is not an indication of proper orientation of amine groups on the polymer surface.

Tyramine (25 mM) was dissolved in five different solvents; 1), PBS, pH 7.0; 2), methanol; 3), 1 M HCl; 4), 1 M H_2SO_4 and 5), methanol with 0.3 M NaOH. After deposition CV was carried out which showed that HCl and H_2SO_4 mediated polymer was poorly deposited, which is also evident from Nyquist plot (**Figure 3.12, A and B**). However, all other polymers passivated the surface, indicated by a low current in CV and high impedance. When these sensors were exposed to HRP conjugated streptavidin and ECL reagents for Midland blotting, it was observed that, only methanol with and without NaOH mediated polymers had abundant surface amines (**Figure 3.12, C**). This indicated that, although some solvent mediated polymers showed high a impedance, indicating some sort of deposition, the surface amine might not be at the right orientation to be available for conjugation. This could be due to the globular nature and 3D packing of the polymer which could alter the position of the free amines on the polymer. Considering these data, it was found that methanol with NaOH was a suitable solvent for polytyramine deposition and provided abundant surface amines.

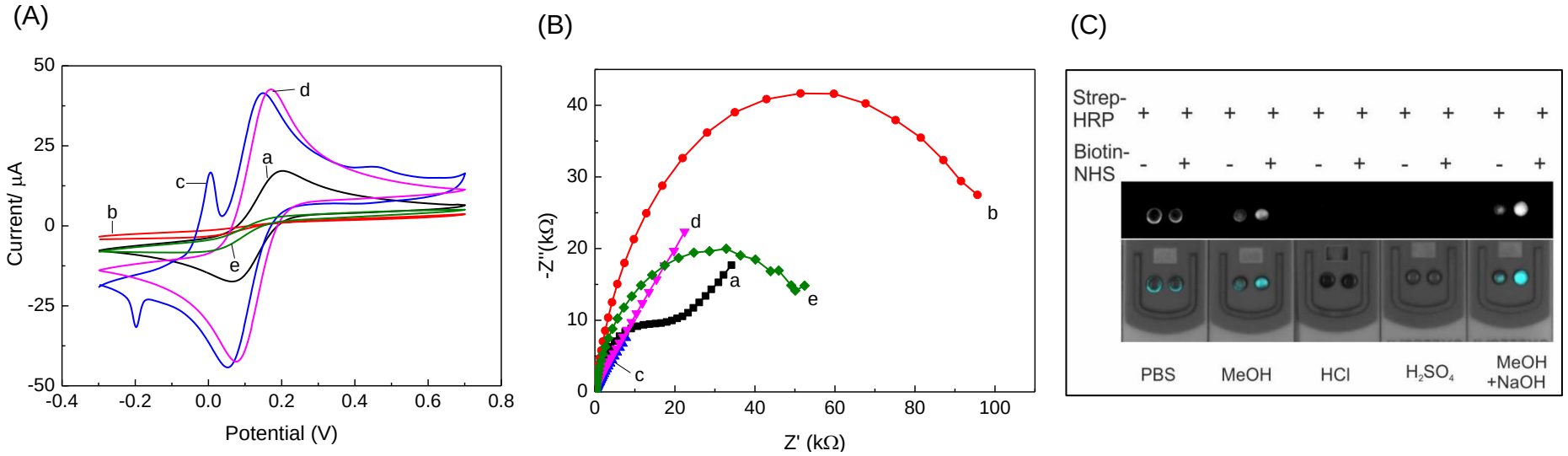

Figure 3.12: Selection of solvent for Ptyr deposition

(A) CV of Ptyr deposited from different solvents; (a), PBS; (b), MeOH; (c), HCl; (d), H_2SO_4 and (e), MeOH and NaOH, (B) Corresponding EIS data of the polymers and (C) Midland blotting of primary amine in the same polymers. Midland blot upper panel is the illumination captured from the imager and lower panel is the superimposed image of electrodes and false cyan colour illumination. All the polymers were deposited with 2 cycles from 0 to +1.6 V, CV and impedance data were recorded in 10 mM $[Fe(CN)_6]^{3-/4}$ in PBS pH 7.0 (1:1 ratio). Data published in (Ahmed et al., 2013).

3.6.3 Effect of scan speed and number of cycle on deposition

When it was confirmed that, tyramine can be polymerized in methanol/ NaOH and provide sufficient accessible surface amines, its impedance properties were further characterized. The dependence of scan speed with constant number of cycles (2 cycles) was observed. It was found that scan speed was inversely proportional to *R*ct of deposited polymers (**Figure 3.13, A**). Depending on the sensor construction format either 100 mV/s or 200 mV/s scan rate was selected. For full antibody based sensors usually 200 mV/s scan speed was used, and for antibody fragments 100 mV/s was used. The main goal was to keep full sensor level Nyquist plot in a semi-circular shape, so that equivalent circuit data acquisition could be accurately calculated.

When keeping the scan speed at 100 mV/s, the number of cycles was varied (2, 4, 6 and 8 cycles). It was found that, above 2 cycles, the sensors became highly capacitive and resistive and tended to lose the semi-circular Nyquist shape (**Figure 3.13, B**). Thus from these findings, 2 cycle mediated depositions at 100 or 200 mV/s scan rate was used depending on the type of sensor construction.

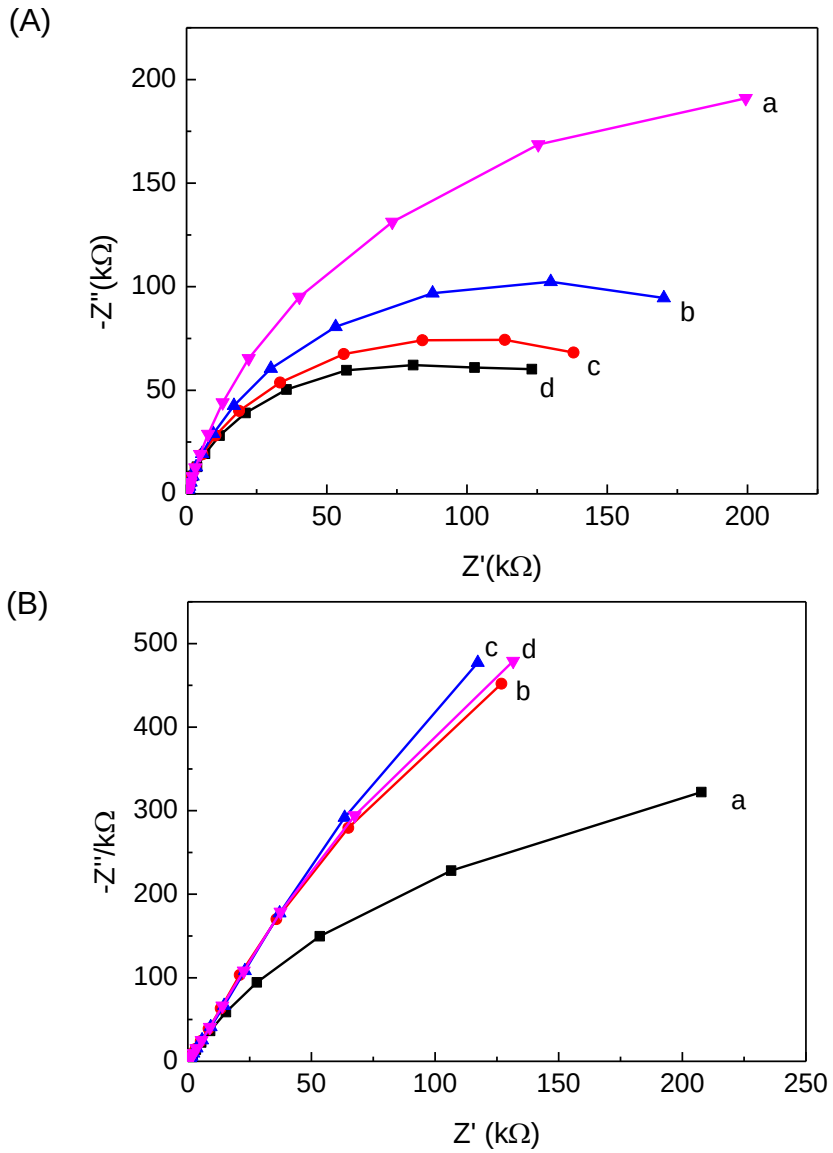

Figure 3.13: Effect of scan rate and scan number on Ptyr deposition

(A) Ptyr EIS with different scan rates (2 scans), a=100, b= 200, c =300 and d= 400 mV/s, all on single chip, EIS was measured from 0.25 Hz to 25 kHz, with 25 points in 2 mM $[Fe(CN)_6]^{3-/4}$ in PBS pH 7.0 and (B) Nyquist plot of 0.025 mM tyramine with different scan cycles (scan rate 100 mV/s), a= 2, b= 4, c= 6 and d= 8 scans from 0.25 Hz to 10 kHz with 20 points (Ahmed et al., 2013).

3.6.4 Effect of NaOH concentration on Ptyr deposition

It has been already shown that the presence of NaOH affected the 3D availability of surface amines. However, according to the literature NaOH also enhances the conductivity of polymer itself. Three different solvents; 1), methanol; 2) methanol with 0.3 M NaOH and 3), methanol with 0.6 M NaOH were used. After polymerization, the impedance data showed that, as the concentration of NaOH increased, the impedance of the polymer dropped indicating an increase in conductivity (**Figure 3.14**). However, the conductivity of polytyramine can also be increased by changing the solvent from basic to acidic medium (Abrahao et al., 2013). In this study, for all biosensor construction, polytyramine was deposited from methanol with 0.3 M NaOH which showed consistency both in impedance and Midland blot data.

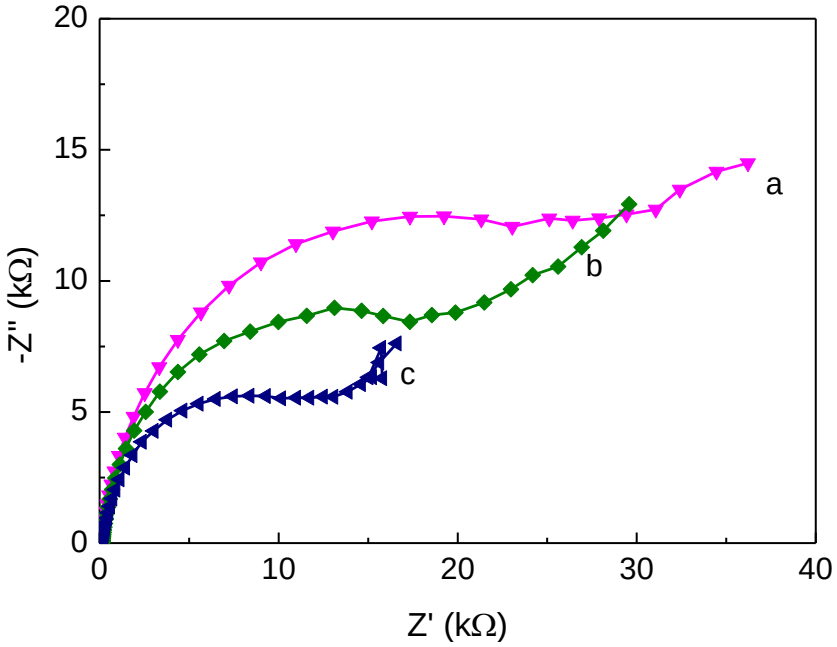

Figure 3.14: Effect of NaOH concentration on Ptyr conductivity

Three different conditions were used; (a), methanol; (b), methanol with 0.3 M NaOH and (c), methanol with 0.6 M NaOH. They were electropolymerized with two cycles and impedance reading was taken after deposition. Impedance reading was taken in standard redox mediator solution 10 mM $[Fe(CN)_6]^{3-/4}$ in PBS pH 7.0 .

3.6.5 Midland blot to compare available surface amine of copolymer and Ptyr

When impedance drift and non-specific binding was observed in PANI/ 2-ABA copolymer, visual changes in the PANI/ 2-ABA solution in 1 M HCl was detected with aging. After optimization of tyramine, different stocks of PANI/ 2-ABA solutions were used to generate copolymer along with polytyramine. These surfaces were exposed for Midland blotting to check comparative surface amine availability. Five different stock solutions used were; 1), freshly prepared tyramine in methanol with NaOH; 2), freshly prepared PANI/ 2-ABA clear stock solution; 3), one week old PANI/ 2-ABA solution, which was light brown in colour; 4), two month old stock solution of PANI/ 2-ABA, which was dark brown in colour and 5), a six month old very dark brown PANI/ 2-ABA stock. The Midland blot data showed that fresh polytyramine deposited by 2 cycles had abundant surface amines compared to all other samples of PANI/ 2-ABA (**Figure 3.15**). Among the PANI/ 2-ABA samples only freshly prepared polymer showed some signs of surface amines compared to the polytyramine surface. This finding suggested a few key points. First, with aging, the PANI/ 2-ABA solution tended to oxidise and the resulting polymer did not show sufficient surface amines. Second, even in case of the freshly prepared polymer, 2-ABA itself was prone to oxidation. However, the exact chemical mechanism of 2-ABA incorporation in to the PANI/ 2-ABA copolymer is also not well characterized. The Midland data clearly demonstrated that, due to either self-oxidization of 2-ABA or poor copolymerization of 2-ABA with aniline, or due to aging the polymer had insufficient surface amines compared to polytyramine. This observation also strengthened the choice of polytyramine over the PANI/ 2-ABA copolymer.

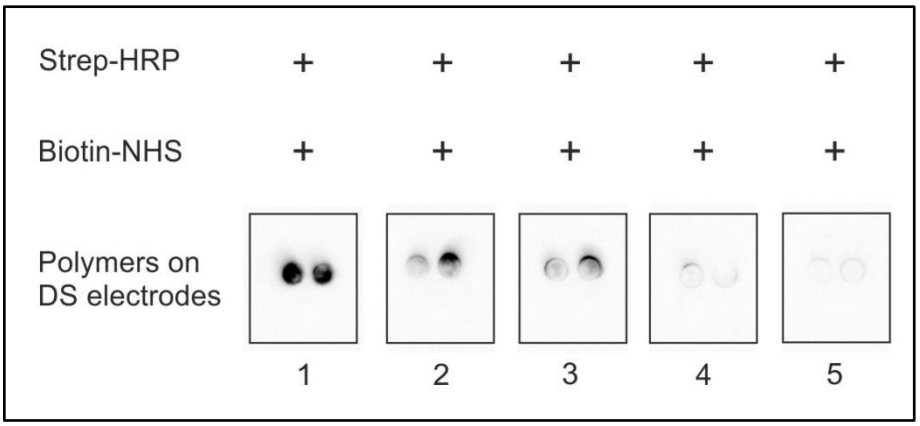

Figure 3.15: Midland blot data of available surface amines on different polymer surfaces

Five different polymer solutions were used, two working electrode for each type of polymer. Polymers were prepared using 1), freshly prepared tyramine in methanol with NaOH, two CV cycles; 2), freshly prepared PANI/ 2-ABA stock; 3), one week old PANI/ 2-ABA solution, light brown in colour; 4), two month old stock solution of PANI/ 2-ABA, dark brown in colour and 5), six month old very dark brown PANI/ 2-ABA stock. All PANI/ 2-ABA were cycled 20 times for polymer deposition. All surfaces were exposed to biotin-NHS, followed by streptavidin-HRP and ECL reagents before imaging. Inverted image of the Midland blot is presented here.

3.6.6 Midland blot of Ptyr surface amine deposited with various deposition cycles

Midland blotting was performed on polytyramine films made with different number of deposition cycles, keeping all other parameters as optimised. Four different polymer layers were obtained from 2, 4, 6 and 8 CV cycles. Then they were incubated with biotin-NHS, followed by streptavidin-HRP and ECL reagents before imaging. Polymer made from 2, 4 and 6 cycles showed presence of abundant surface amines, whereas after 8 cycle amine loading was slightly reduced (**Figure 3.16**). As a 2 cycle deposition could reduce the overall sensor fabrication time, it was selected as the optimum for polytyramine deposition. Also from the impedance data (**Figure 3.13, B**) it was observed that over 2 cycles the Nyquist plot tended to be highly resistive and capacitive, making it less suitable for subsequent sensor fabrication.

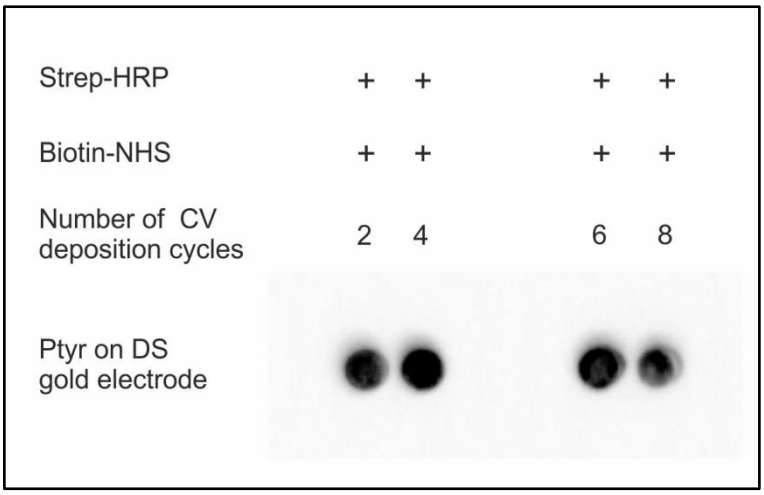

Figure 3.16: Midland blot of Ptyr surface amine deposited by different deposition cycle

Electrodes were coated with polymer by cycling them 2, 4, 6 and 8 times in 0.025 M tyramine methanol solution with 0.3 M NaOH. The scan speed was 100 mV/s. After deposition, the electrodes were exposed to biotin-NHS (1 mg/ml for 30 min), followed by streptavidin HRP. Then ECL reagents were added and the electrodes were imaged in the imager. Inverted light signals are presented in this data.

3.6.7 Consecutive polytyramine impedance showed higher stability

After optimization of polytyramine deposition, the effect of consecutive impedance reading in 10 mM $[Fe(CN)_6]^{3-/4}$ in PBS pH 7.0 redox mediator was checked. Five impedance scans were taken in redox mediator with intermediate wash and gentle drying in argon stream. The five scans (**Figure 3.17**) showed that, after the first scan, the second and the third scan had a slightly lower impedance. This could be due to washout of non-specifically bound monomer from the surface. After that, the impedance was quite stable. And most importantly, it retained the semi-circular Nyquist plot shape which facilitated the correct extraction of equivalent circuit components within the Autolab FRA module.

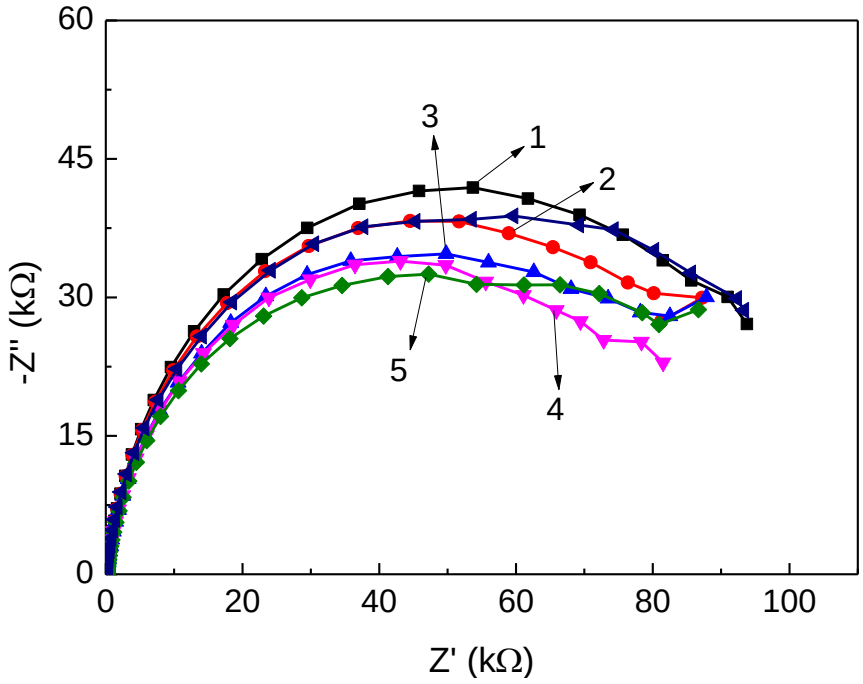

Figure 3.17: Consecutive impedance signal of electrodeposited Ptyr in redox mediator

After deposition of polytyramine on a single working electrode, five consecutive impedance reading (1 to 5) was taken in redox mediator (10 mM 1:1 ratio of $[Fe(CN)_6]^{3-/4}$ in PBS pH 7.0). After each reading the electrodes were washed in dH_2O and the next reading was then recorded.

3.7 Reproducibility of polymer deposition and impedance

After optimization of polytyramine deposition scans and solvent conditions, deposited polymers were assessed for reproducibility during deposition and after deposition. To do this, a large number of independent data of polymerization CV during polymer formation was superimposed. The first cycle was the indicative of oxidation peak and amount of current at where the cycle was reversed. Twenty individual data of first cycles were superimposed and presented in **Figure 3.18, A**. It was observed that, the standard deviation (grey shade) of the average first CV cycle (black line) on twenty electrodes was reproducible.

Then the polymer impedance reproducibility (**Figure 3.18, B**) of the same electrodes were superimposed with the variability shown for both X and Y axis (red and blue error bars showed standard error of mean/ SEM of resistance and capacitance component respectively). The data indicated that although the deposition CV profile showed lower variation, post deposition impedance showed more variability. The red error bars showed the SEM of resistance components from average at each frequency. The blue error bars showed the SEM of capacitance part of the polymer from average at each frequency. At very high frequency the error bars were very small indicating less variability at that region. However, at lower frequencies both the resistance and capacitance varied within 20 electrodes. This again reflected the fact that manufacturing of these screen printed electrodes created variability on surface area and conductivity, which was also reflected on impedance data after polymer formation.

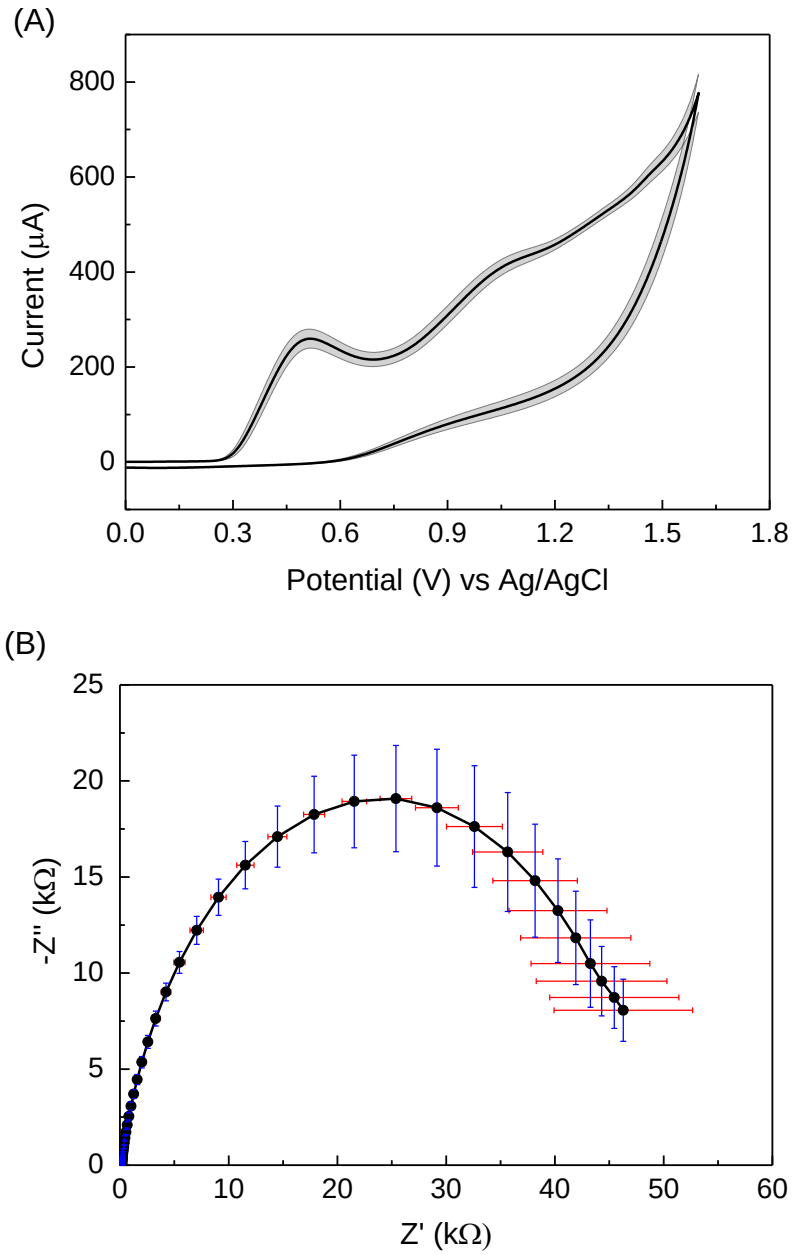

Figure 3.18: Reproducibility of polytyramine deposition and impedance

(A) First CV cycle during tyramine polymerization (n=20, black line showing average with grey shaded area showing standard deviation) and (B) superimposed EIS data of the same 20 electrodes, red error bar showing SEM of resistance and blue error bars showing SEM of capacitive component respectively. CV and EIS reading was recorded in 10 mM 1:1 ratio of $[Fe(CN)_6]^{3-/4}$ according to standard protocol.

3.8 Conclusions

Commercial screen printed gold electrodes were used and optimized for biosensor construction. Bare electrodes were electrochemically examined and a reversible CV profile was observed. However the surface roughness contributed to electrode variability. Different cleaning methods were also explored for polymer or SAM deposition.

To construct a biosensor against bacteria with multiple epitopes, polymer layer was considered to be better choice over a SAM surface. The SAM formation was not suitable on rough screen printed surface, and upon bacterial binding the stability of SAM base layer seems to be low. The PANI/ 2-ABA conductive copolymer showed a drift in impedance signal with slight changes in pH and thus the non-conducting polymer, polytyramine, was optimized as biosensor base layer. The effect of scan speed, number of scans and different solvents was considered while optimizing electrodeposition with respect to the impedance profile of polymer layer and fully constructed biosensor.

Off sensor dot blot and on-sensor blot (Midland blot) was used to confirm several parameters during sensor fabrication. The optimization helped to pick key parameters of electrode cleaning and polymer which were maintained all through the research. With optimized polymer deposition, full antibody based sensor fabrication and testing was performed and presented in the following chapter.

Chapter Four

Whole antibody based immunosensor fabrication to detect *S. pyogenes*

Chapter 4 Whole antibody based immunosensor fabrication to detect *S. pyogenes*

4.1 Introduction

As discussed in the previous chapter, polytyramine (Ptyr) was selected and optimized as the sensor base polymer after observing impedance drift, non-specific signal due to inter-conversion of different PANI/ 2-ABA oxidation states and incompatibility of SAM or mSAM formation on rough electrode surfaces. Immunosensors were constructed using whole antibody which was raised against intact heat killed *S. pyogenes* cells. The conjugation protocol used was followed from previous biosensor developed for the detection of the cardiac biomarker myoglobin (Billah et al., 2008). That project was implemented using SAM or mSAM on atomically flat photolithographic gold electrodes. The present study was completely based on commercially produced screen printed gold electrodes and the base layers were mainly electrochemically deposited polymers onto the electrodes.

Data presented in this chapter are based on biotinylated whole antibodies immobilized onto Ptyr coated surface via biotin-NeutrAvidin interaction. These data helped to establish the proof-of-concept of immunosensors using commercially produced electrodes against large analyte, e.g. *S. pyogenes*. Although a previously used protocol was followed, strict optimization of NeutrAvidin and antibody concentration were performed to maximise the output signal. A general schematic of the immunosensor is presented in **Figure 4.1.** Typically, optimized Ptyr (0.025 M tyramine in methanol with 0.3 M NaOH) was electro polymerized onto gold electrodes by cyclic voltammetry (CV) with 2 cycles from +0 V to +1.6 V. Then

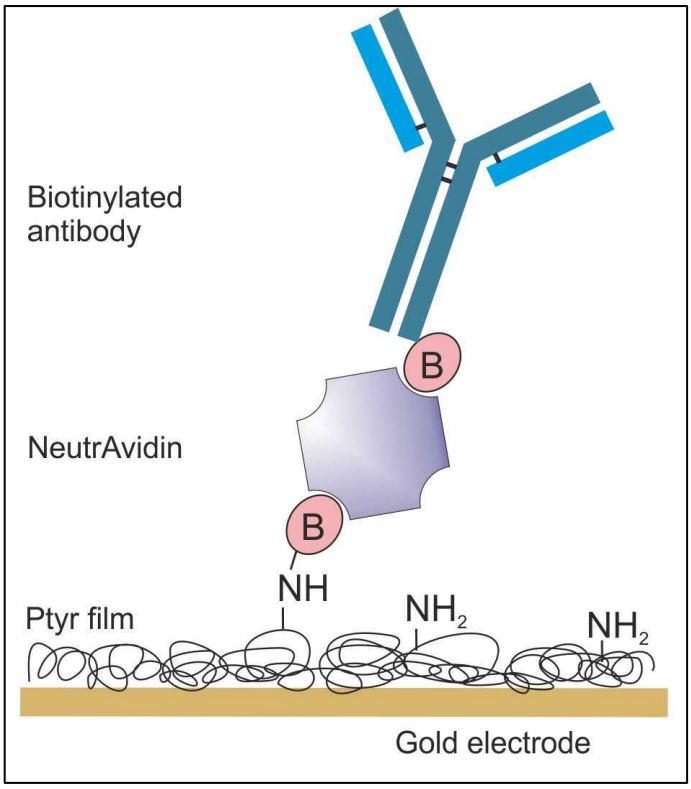

Figure 4.1: Schematic of whole antibody based immunosensor to detect *S. pyogenes*

Ptyr was electropolymerized onto gold electrode. Biotinylated anti-*S. pyogenes* antibodies were conjugated to the free amine of Ptyr film via biotin-NeutrAvidin interaction. Incubation with biotin-NHS provided pendant free biotin which interacted with NeutrAvidin. Biotinylated antibodies were then conjugated via remaining binding sites of NeutrAvidin. The drawing is not to scale. Adapted from (Ahmed et al., 2013).

biotin-NHS (1 mg/ml in PBS, pH 7.0) was incubated for 30 min. After washing with PBS, NeutrAvidin in PBS (6 µg/ml) was incubated for 45 min followed by wash and incubation of biotinylated antibodies (10 µg/ml in PBS) for 1 h. These fully constructed sensors were used for bacterial binding analysis. Appropriate non-specific antibodies and/or non-specific bacteria were used as control.

Each level of sensor construction was monitored by EIS and Midland blotting. The immunosensors' ability to detect *S. pyogenes* was then monitored both in PBS and biological media i.e. human saliva. To further prove bacterial capture on the sensor surface, a post binding fluorescence study and SEM was also performed as supporting techniques. To address non-specific binding, a blocking study was performed and is presented in this chapter.

4.2 Sensor fabrication characterized by EIS and Midland blotting

Electrochemical impedance spectroscopy (EIS) has been widely used to monitor step by step sensor construction. In this study the immunosensors constructed onto gold electrodes were monitored by EIS reading in $[Fe(CN)_6]^{3-/4-}$ redox couple (10 mM each, 1:1 molar ratio) in PBS. The impedance spectrum was generated over a range of frequencies and was analysed as Nyquist plot where the complex impedance was plotted. The x axis is the resistance component and the y axis represents capacitance. The semi-circular shape of the curve intersect x axis and charge transfer resistance (*R*ct) can be measured. The Nyquist plot can be further modelled to an equivalent circuit where individual component can be separately distributed in the model (**section 1.7.3**).

In **Figure 4.2, A**, a representative layer by layer Nyquist plot can be seen where the Ptyr had ~35 kΩ of resistance using redox mediator. When biotin-NHS and NeutrAvidin were immobilized on top of the Ptyr amines, the impedance increased and *R*ct value reached ~150 kΩ. This resistance reflected the binding of NeutrAvidin onto Ptyr via biotin-NHS. After addition of biotinylated antibody on top of NeutrAvidin, the impedance again increased up to 230 kΩ. The Nyquist plot generated was further modelled by a Randle's equivalent circuit (**Figure 4.2, B)**. As in the Nyquist plot, none of the layers showed any straight line generally observed in lower frequency (Warburg component), the model was further simplified neglecting the Warburg component. The EIS was also used to monitor the impedance behaviour after adding each concentration of analyte. This will be discussed in the following section.

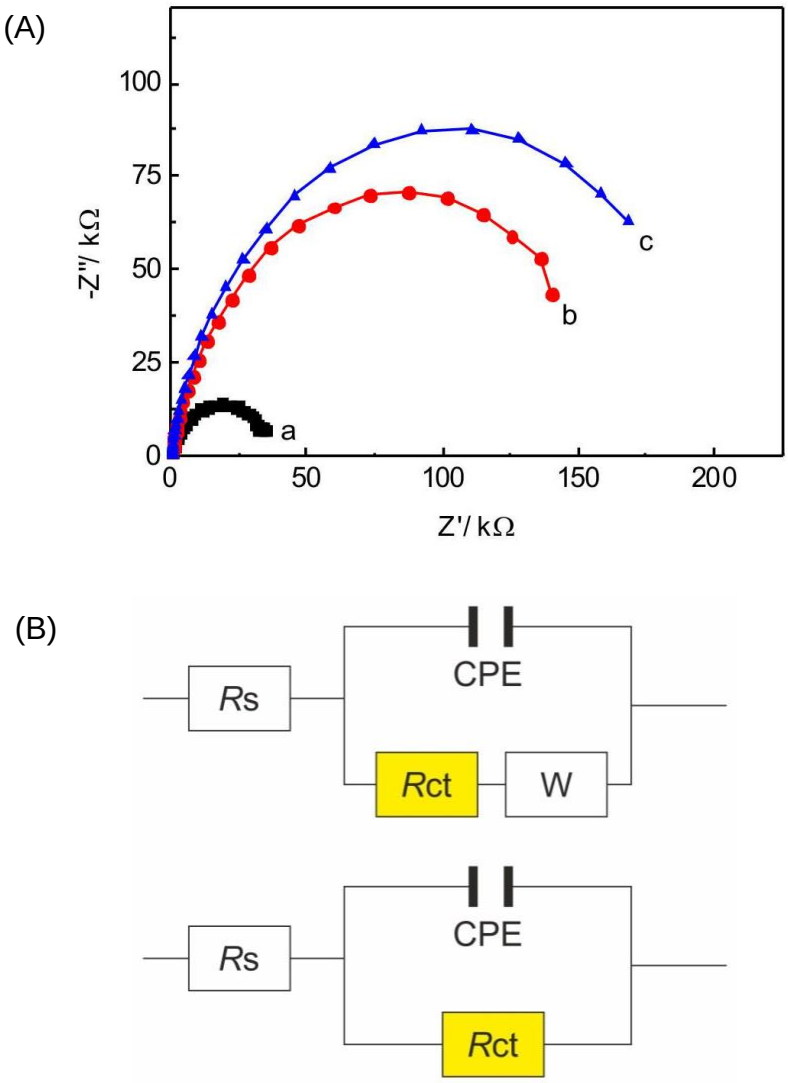

Figure 4.2: EIS profiling of layer-by-layer sensor construction and equivalent circuit model

(A) Nyquist plot of (a), Ptyr; (b), biotin-NHS and NeutrAvidin on Ptyr and (c), biotinylated antibodies on NeutrAvidin. Ptyr deposition at 200 mV/s, NeutrAvidin 6 µg/ml, antibodies 10 µg/ml. EIS reading was taken in $[Fe(CN)_6]^{3-/4-}$ redox mediator (10 mM 1:1 ratio) (Ahmed et al., 2013) and (B) general Randle's equivalent circuit model (top), modified model without Warburg component (below). *R*s= solution resistance, *R*ct= charge transfer resistance, CPE= constant phase element and W= Warburg component.

Although EIS is a very sensitive way to characterize sensor layers during construction and analyte binding, detailed chemical information on each surface (e.g. presence of amine on deposited Ptyr and presence of antibody on surface) is limited. Increase or decrease in EIS does not necessarily explain the actual 3D presence of a particular group or moiety on the surface which is important to know before conjugation. After the successful use of Midland blotting (**section 2.2.12**) it was used to check the presence of amines on Ptyr and also to confirm the availability of bound antibodies. As Midland blotting provides semi quantitative data, it is useful to compare the signal intensity using different experimental conditions applied and the corresponding signal can be corroborated with EIS data.

For the determination of surface amines on Ptyr surface, two sets of electrodes (100 and 200 mV/s scan rate) were prepared. The control electrode was bare gold. They were incubated either in the presence or absence of biotin-NHS (1 mg/ml, 30 min) followed by a wash in PBS and incubation with 1:25 dilution of streptavidin-HRP (10 µg/ml stock) for 30 min. After several washes, ECL reagent mix was placed onto the electrode and image was taken inside G:box imager. The data (**Figure 4.3, A**) showed no signal on bare electrode, and in other controls. It showed a strong signal on Ptyr deposited with a 100 mV/s scan speed and slight fade signal at 200 mV/s. The scan rate of polymer deposition is inversely proportional to the polymer density. At lower scan speed, the deposited Ptyr was more dense, presenting more surface amines and hence more light signal. Another important feature of this experiment was that, as streptavidin-HRP was able to bind surface amine via biotin-NHS, during sensor construction NeutrAvidin would be able to bind the same way meaning the surface accessibility of Ptyr prepared at both of these scan rates were suitable for biotin-NeutrAvidin mediated immunosensor construction.

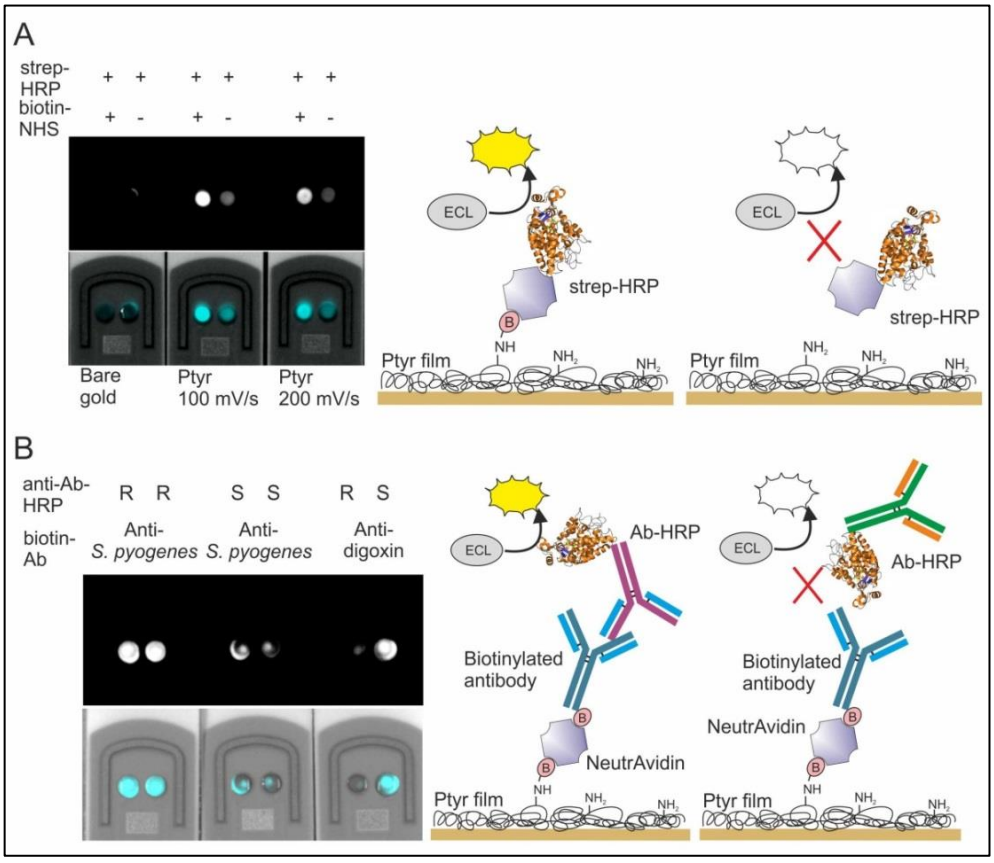

Figure 4.3: Midland blot to confirm polymer amine and immobilized antibodies on sensor surface

(A) ECL image of bare gold and polymers (upper panel) and superimposed image with cyan false colour (lower panel) after incubating with biotin NHS and Streptavidin-HRP and (B) immobilized anti-*S .pyogenes* and anti-digoxin antibodies were detected by Midland blotting with appropriate anti-antibody-HRP conjugates. (R= anti-rabbit and S= anti-sheep HRP antibodies). The images were processed in ImageJ software. Side drawing illustrate the corresponding detection principle. Adapted from (Ahmed et al., 2013).

To confirm the presence of bound biotinylated antibodies (both specific and non-specific) on top of electrodes, two electrodes were prepared with anti-*S. pyogenes* antibodies and one with anti-digoxin antibodies. Then appropriate anti-rabbit and anti-sheep antibodies conjugated with HRP were incubated for 1h. After appropriate washes and incubation of ECL reagent the sensors were imaged. From **Figure 4.3, B,** it can be seen that, anti-rabbit-HRP antibodies bound to anti-*S. pyogenes* antibodies (raised in rabbit host) and anti-sheep-HRP bound to anti-digoxin antibodies (raised in sheep host). The control working electrodes showed no signal apart from very little non-specific signal due to absorption of HRP tagged antibodies onto the surface. These fully characterized sensors were then finally used for optimization studies and to produce calibration of bacterial binding.

4.3 Reproducibility of fully constructed sensor impedance

To understand the electrochemical stability of fully constructed sensors, repeat impedance measurements were taken. This information is helpful to know whether the measuring $[Fe(CN)_6]^{3-/4-}$ redox mediator solution has any particular influence on changing the impedance. Also, whilst taking multiple measurement with different bacterial concentration, electrodes were being repeatedly washed and tested. Thus, the impedance stability of polymer base layer during multiple measurements can help to achieve consistent results. To test this effect, two types of impedance reading were taken. In the first case, five consecutive impedance was recorded with a fully constructed and protein A blocked sensor surfaces without any washing step. In the second approach, sensors were washed and dried in argon stream before each new measurement.

The five consecutive impedance measurements without taking the electrode out of the measuring solution showed very reproducible and consistent Nyquist plots (**Figure 4.4, A**). However, when intermediate wash and drying was performed a slight increase in impedance was observed (**Figure 4.4, B**). However, this change was very small compared to impedance change due to antigen-antibody interaction and was consistent for both specific and non-specific sensor surfaces. Most importantly, this change did not influence the discrimination of specific and non-specific signals. The drying step is difficult to avoid in research work as a dry surface helped to incubate next incubation aliquot as a droplet onto the working electrode. In an ideal point of care scenario, usually single shot testing will be performed, thus this drying step can be avoided and the slight change in impedance can be removed.

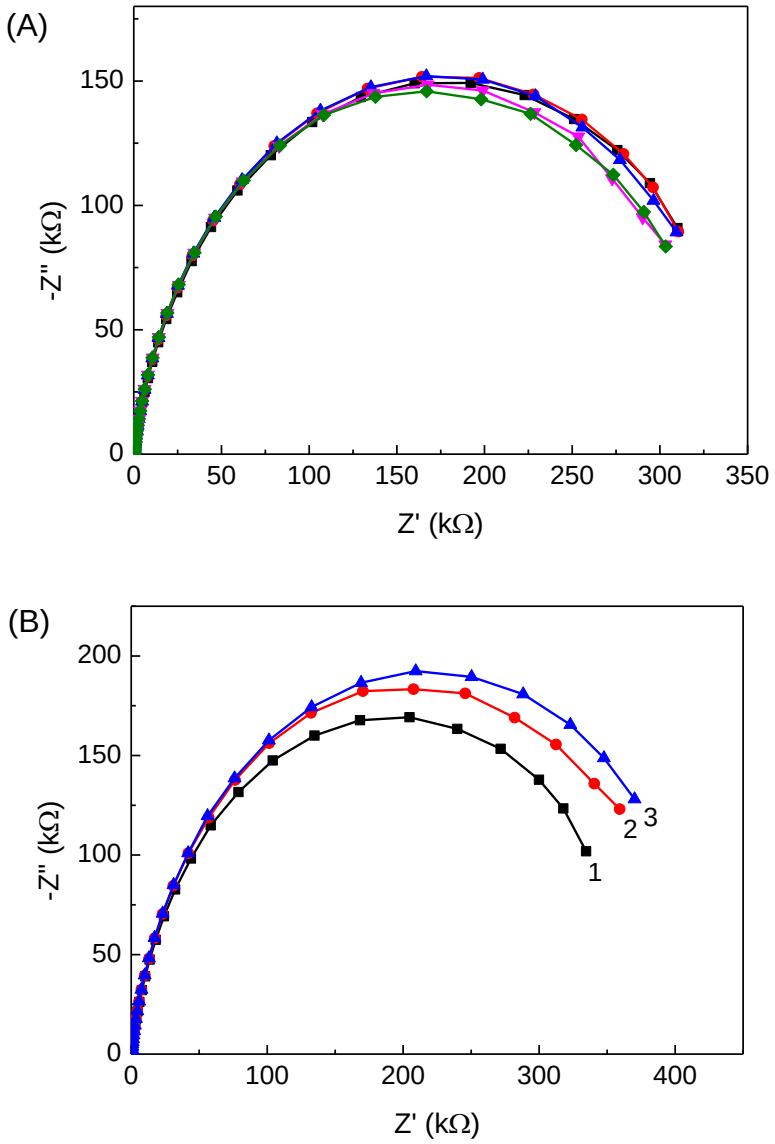

Figure 4.4: Reproducibility of impedance in fully constructed sensors

(A) Five consecutive impedance spectra of fully constructed sensor surface (10 µg/ml antibody and 1 mg/ml protein A blocking). The reading was taken without intermediate washing steps. The scans were performed on single working electrode and (B) three impedance readings (numbered 1-3) with intermediate washing and drying step. Single working electrode was used. Impedance readings were taken in 10 mM $[Fe(CN)_6]^{3-/4-}$ redox couple in PBS, pH 7.0.

4.4 Optimum antibody concentration determination

It is very important to determine the optimum bioreceptor concentration tethered to the sensor surface to achieve maximum analyte binding. Both the spacing of antibodies on the sensor surface and their comparative size and orientation with respect to the analyte can affect binding. Considering the macro level roughness of commercial screen printed electrodes, the coverage of the surface with antibody cannot be atomically flat and homogeneous. In addition, biotin tagged antibodies which bind NeutrAvidin can generate a mixed orientation of antibodies on the surface. Microorganisms, like bacteria and viruses ranges from tens of nm to µm, and are much larger than antibodies (~14 × 8.5 × 4 nm). In such case, too much dense antibodies might hinder the availability of binding sites to microorganisms.

To get the optimum antibody concentration for *S. pyogenes* detection, a range of immunosensors were constructed with varying antibody concentration. Two control sensors were also constructed, one with no antibody conjugated and the other one with non-specific anti-digoxin antibodies at a concentration of 10^{-2} mg/ml. For all concentrations and controls, a set of 4 individual electrodes were prepared by the protocol described in **section 2.2.7** and then 10 µl of *S. pyogenes* (10^6 cells/ml) were incubated before washing and EIS measurement. NeutrAvidin concentration was kept constant at 6 µg/ml for all experiments.

The average *R*ct values of sensors calculated after immobilization of different concentrations of antibodies can reflect the corresponding impedance behaviour upon bioreceptor binding. A general trend of increasing *R*ct with increasing concentration of antibodies was observed (**Figure 4.5, A**). However, at 1 mg/ml antibody the signal dropped from its peak. This supports the hypothesis that highly concentrated antibodies can self-limit their binding on the sensor surface

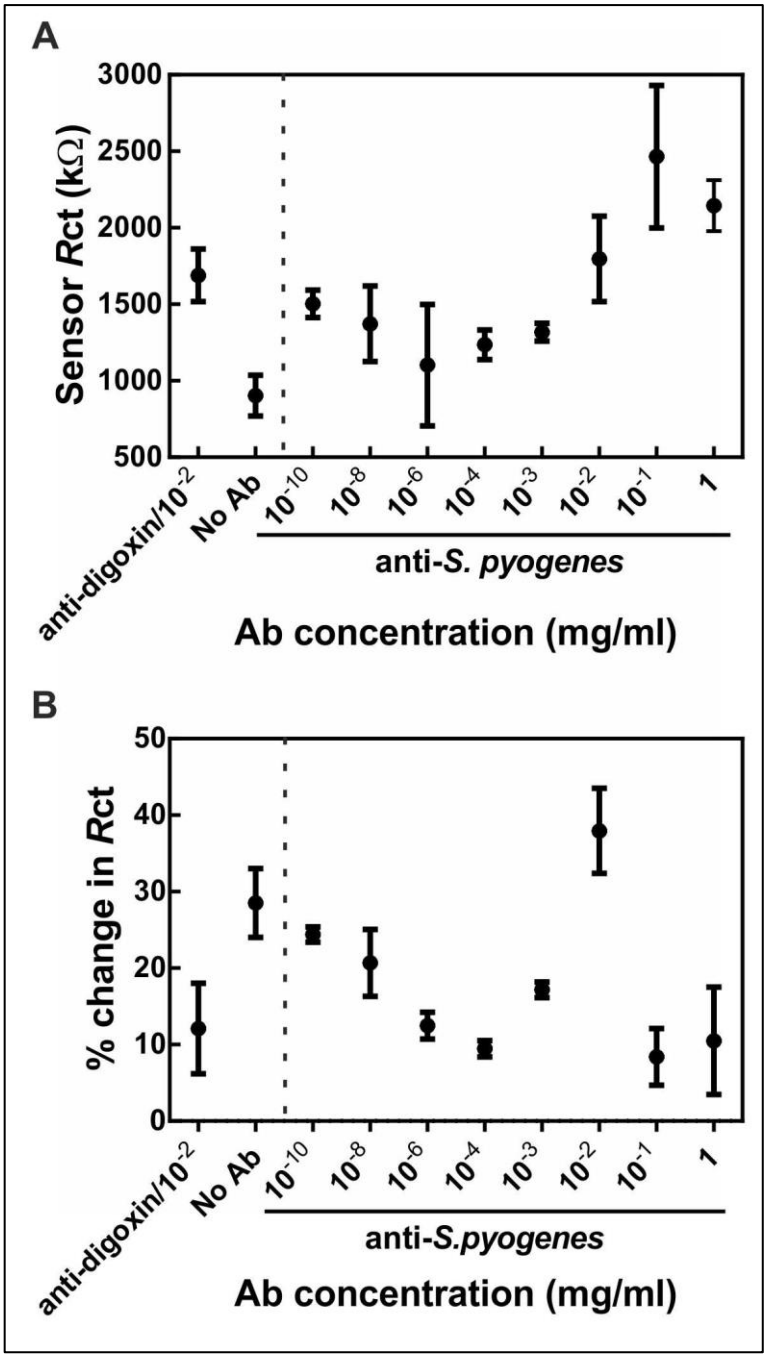

Figure 4.5: Antibody concentration optimization

(A) Fully constructed sensor *R*ct values with varying Ab concentrations. NeutrAvidin concentration was kept constant at 6 µg/ml. Differences between means are statistically significant in ANOVA (**p=0.0028) (B) Percent change in *R*ct after analyte (10^6 cells/ml) binding at those sensors of (A). Differences between means are statistically significant in ANOVA (***p=0.0002). All data points were average ± SEM (n=3). Data were published in (Ahmed et al., 2013).

because of steric hindrance. This was also supported by Holford et al. (2013), where too dense antibodies decreased sensor sensitivity due to steric hindrance (Holford et al., 2013). Sensors incubated with anti-*S. pyogenes* and anti-digoxin at the same concentration (10^{-2} mg/ml) showed close *R*ct values (~1700 kΩ) indicating same level of binding and impedance behaviour. Although the observed trend of absolute *R*ct values differed slightly from antibody to antibody.

When these sensors were incubated with *S. pyogenes* (10^{6} cells/ml) for 30 min and the percentage change of impedance was calculated after the bacterial incubation, optimum antibody concentration could be found. From **Figure 4.5, B** it was observed that highest binding (~40%) was achieved at an antibody concentration of 10^{-2} mg/ml. Surprisingly, a good amount of binding was observed (~30%) in the negative control where no antibody was conjugated to the surface NeutrAvidin. This observed non-specific binding supports to the idea of NeutrAvidin's ability to bind bacterial surface via its RYD motif (Alon et al., 1990). This non-specific binding was masked (dropped from ~30% to ~10%) when NeutrAvidin gradually bound to more and more antibodies (from 10^{-10} to 10^{-4} mg/ml). Again in the case of sensors covered with anti-digoxin antibodies (10^{-2} mg/ml), this non-specific signal was reduced to ~12%.

4.5 Optimum NeutrAvidin concentration determination

The packaging of NeutrAvidin on to the polymer layer also play important role to have an optimum coating of antibodies onto the sensor surface. The correct spacing between them relies on the amount of NeutrAvidin and antibodies bound. If insufficient NeutrAvidin is on the surface, enough of antibody will not bind. On the other hand, too much NeutrAvidin can accommodate extra antibodies creating steric hindrance to bacterial binding.

To test this, several concentrations of NeutrAvidin were immobilized onto the polymer surface via biotin-NHS. Then the optimum amount of antibody (10 µg/ml) was incubated on all of the electrodes. At this stage the average *R*ct value of all sensors was calculated (**Figure 4.6, A**). It can be seen that from 10^{-4} mg/ml NeutrAvidin, the sensor *R*ct values increased with increasing concentration of NeutrAvidin up to 10^{-1} mg/ml. The highest *R*ct was observed at 10^{-1} mg/ml of NeutrAvidin where the maximum amount of antibody was bound.

The same sensors were then incubated with *S. pyogenes* (10^6 cells/ml) for 30 min before taking impedance data. Then the change of impedance due to bacterial binding was plotted (**Figure 4.6, B**). Although the highest sensor *R*ct was observed at NeutrAvidin concentration of 10^{-1} mg/ml (**Figure 4.6, A**), the lowest change in impedance due to bacterial binding was observed in the same sensors. This indicated that the highest loading of antibodies did not help in bacterial binding. This could be due to tight packing of antibodies creating rigidity in the antigen binding sites. Binding was observed both in 10^{-2} mg/ml and 10^{-3} mg/ml NeutrAvidin concentrations (~20% to 40% impedance change), with a slight drop using 10^{-4} mg/ml NeutrAvidin. The percentage change in *R*ct observed at 10^{-5} mg/ml NeutrAvidin (> 40%) was mainly due to charge interaction between polytyramine

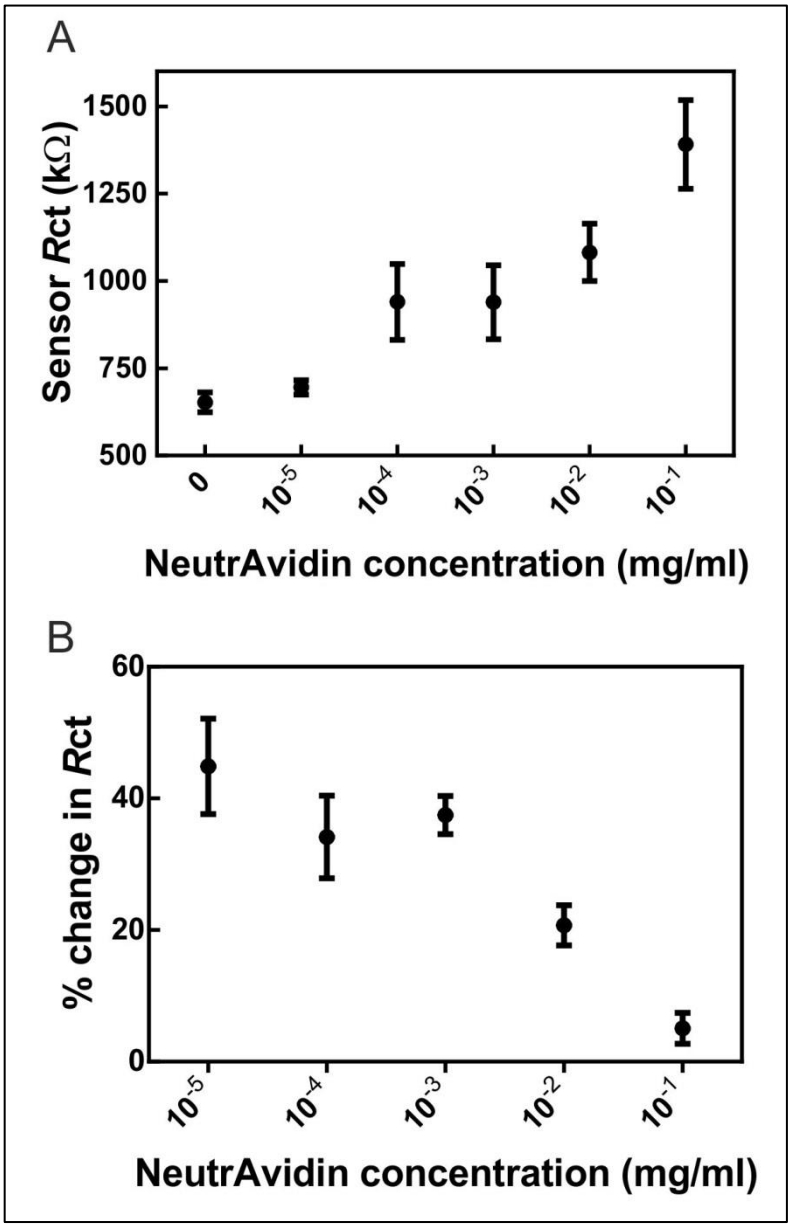

Figure 4.6: Determination of optimum NeutrAvidin concentration

(A) *R*ct values of fully constructed sensor with varying NeutrAvidin concentrations. Antibody concentration was kept constant at 10 µg/ml. Differences among means were statistically significant by ANOVA (**p=0.0034) (B) Percent change in *R*ct after *S. pyogenes* (10^6 cells/ml) binding on the same sensors of (A). Differences among means are statistically significant (***p=0.0004). All data presented are average ± SEM (n=3).

and bacteria, and not due to the antigen antibody interaction. From sensor *R*ct data it was observed that almost no antibody deposition was achieved at that concentration (**Figure 4.6, A**) and the *R*ct was close to the *R*ct of control without any NeutrAvidin.

In the literature the amount of NeutrAvidin used varied from 6 µg/ml to 200 µg/ml, with incubation times from 30 min to 2 h (Hleli et al., 2006; Hou et al., 2006; Tully et al., 2008). In a study to detect influenza A virus, which is 80-120 nm in size, 200 µg/ml of NeutrAvidin was used for 2 h with 100 µg/ml of antibodies (Hassen et al., 2011). In another study, the small calcium binding protein psoriasin was detected using sensors constructed with 10 µg/ml of NeutrAvidin for 1 h at room temperature (Holford et al., 2013).

After analysing these data, it was concluded that a NeutrAvidin concentration in a range of 10^{-2} mg/ml to 10^{-3} mg/ml was optimum to achieve a maximum signal in our system. Accordingly, in all experiments 06 µg/ml of NeutrAvidin was used (equivalent to 10^{-7} M NeutrAvidin). This optimum concentration of NeutrAvidin ensured proper distribution of antibodies on the sensor surface creating maximum flexibility and access to bind bacteria.

4.6 Calibrating sensor in PBS

After optimization of NeutrAvidin and antibody concentrations on the sensor surface a range of bacterial samples were tested in PBS. Usually, on a single sensor chip increasing concentration of bacteria were incubated with an intermediate wash and impedance measurement. The same procedure was repeated in several sensors and average data presented. However, a typical point of care diagnostic chip will handle one sample at a time i.e. be a 'one-shot' system. Between these two methods, the first approach is termed cumulative incubation whilst the latter one (single shot) is termed single shot incubation. In single shot incubation, separate sensors were used to incubate a particular concentration of bacterial sample. Multiple chips were used for a single concentration and the average data obtained. However, the single shot incubation protocol required many more sensor chips compared to cumulative incubation approach. For the two methods, incubation time was kept exactly same.

4.6.1 Cumulative incubation

As described earlier, cumulative incubation is a widely used approach for sensor calibration. Typically, six sensor chips (12 working electrodes) were prepared, three with specific antibodies on surface and the rest with non-specific antibodies. Bacterial cells were serially diluted from stock and five concentrations (10^4 to 10^8 cells/ml) were used for the interrogation. In brief, starting from lowest concentration, 10µl of bacterial samples were incubated for 30 min, washed and impedance measurements were taken. A representative Nyquist plots of the sensor surface and five concentrations of bacterial samples is shown in **Figure 4.7**. The equivalent circuit component value for each stage was obtained using Autolab software FRA module (**Table 4.1**).

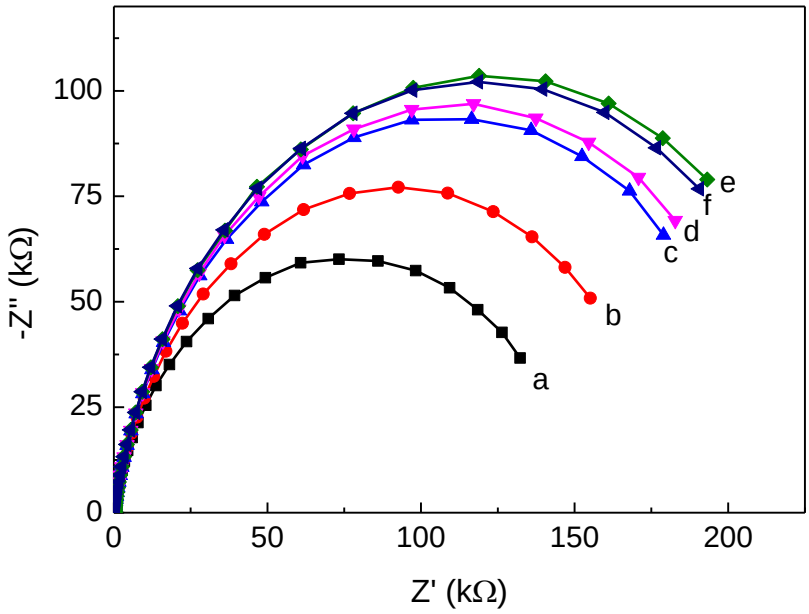

Figure 4.7: Representative Nyquist plots with increasing concentration of *S. pyogenes*

(a), Fully constructed sensors were incubated with (b-f), increasing concentration of bacterial cells from 10^4 to 10^8 cells/ml Impedance readings were taken in 10 mM (1:1 ratio) $[Fe(CN)_6]^{3-/4-}$ redox mediator in PBS, pH 7.0. Reproduced from (Ahmed et al., 2013)

Table 4.1: Equivalent circuit value for each level of sensor fabrication in cumulative incubation

		***R*s (Ω)**	***R*ct (kΩ)**	**CPE (nF)**
Full sensor		147	152	137
***S. pyogenes* (cells/ml)**	**10^4**	148	181	274
	10^5	160	213	348
	10^6	156	218	396
	10^7	155	239	300
	10^8	162	234	325

*R*s= solution resistance, *R*ct= charge transfer resistance and CPE= constant phase element. The data presented in this table are collected from Autolab software and from a representative electrode. Reproduced from (Ahmed et al., 2013).

It can be seen that, as a general trend, impedance (CPE and *R*ct) increased with exposure to increasing number of bacterial cells on the surface. However, the change in *R*ct was more linear and consistent than CPE. The full sensor *R*ct was ~150 kΩ. The first two bacterial concentration caused maximum change in *R*ct. The change in the following incubations were comparatively smaller. Gradually, due to bound bacteria on surface, the available space became limited. In addition, when high concentration of bacterial samples were applied, due to their dense population, steric hindrance could create further problems in binding to antibodies. At the highest concentration, slight decrease in *R*ct was observed. This might be due to the effect of dissociation of some bound cells or new 3D packing of cells onto the surface which facilitated the electron transfer. The solution resistance (*R*s), was almost unchanged and the magnitude was way smaller than *R*ct (**Table 4.1**).

4.6.2 Single shot incubation

In contrast to cumulative incubation, single shot incubation allows the sensors to be incubated only once. Calibration curves in cumulative incubation and single shot incubation are shown in **Figure 4.8, A and B.** It can be seen that, the percentage change in *R*ct was higher in cumulative incubation than single shot. This was expected as cumulative incubation received multiple incubations on a single chip. The linear increase in cumulative incubation was observed from 10^4 to 10^7 cells/ml. However in single shot incubation the linear increase was only up to 10^6 cells/ml. The reproducibility of the signal was less in the single shot protocol. This is linked to the fact that, both irregular surface and random orientation of biotinylated antibodies induced variability in the sensor coverage on different electrodes.

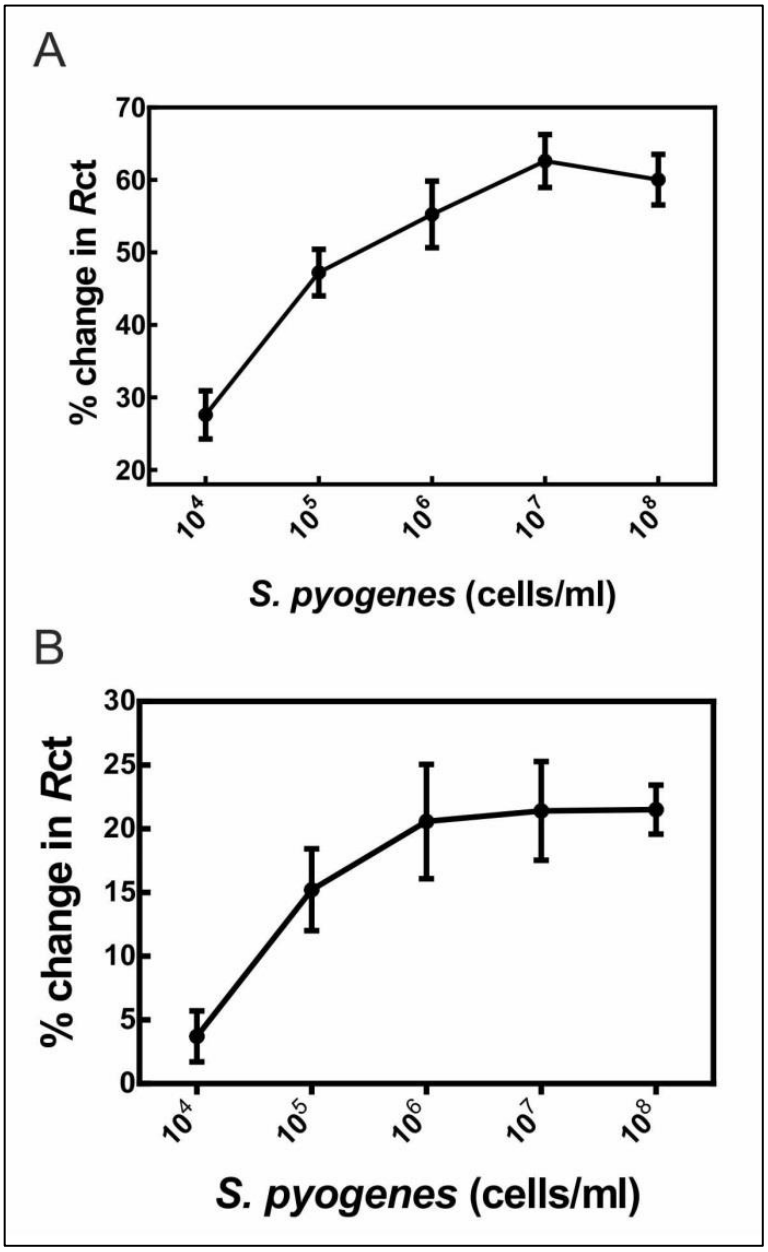

Figure 4.8: Calibration curves of *S. pyogenes* detection in PBS

(A) Cumulative incubation of increased bacterial cells were performed on the same sensor surface. Change in impedance (%) over fully constructed sensor upon incubation of a particular concentration was plotted. Data presented with average ± SEM (n=3) and (B) single shot incubation of each concentration of bacteria. Data presented are the average ± SEM (n=6). Figure A is reproduced and B is adapted from (Ahmed et al., 2013).

4.7 Confirmation of bacterial binding by microscopy

Visual confirmation of bacterial binding onto sensor surface was achieved by two methods. In the first method, sensors with bound bacterial cells were incubated in propidium iodide (PI), a reagent which can penetrate the cell wall and bind to the DNA of dead cells. This can be achieved in two ways, either by incubating the bacteria with PI before application onto immunosensor, or sensor bound bacteria can be incubated with PI solution after they were bound by the antibodies on the sensor surface. Both systems worked well and showed the presence of individual bacteria bound to the biosensor. A representative micrograph of *S. pyogenes* bound onto full antibody based sensors is shown in **Figure 4.9, A**. The red dots are either individual cells or small clusters of bacterial cells.

In the second approach, SEM images were obtained after incubating sensors with bacteria. However, it was observed that if SEM was taken without any coating the cells were found to be fade due to poor conductivity (**Figure 4.9, B, upper panel**). However, the visualization was highly improved with 5 nm platinum coating before imaging (**Figure 4.9, B, lower panel**). The shrinking morphology of cells was due to the heat killing and freeze drying process of *S. pyogenes* cells.

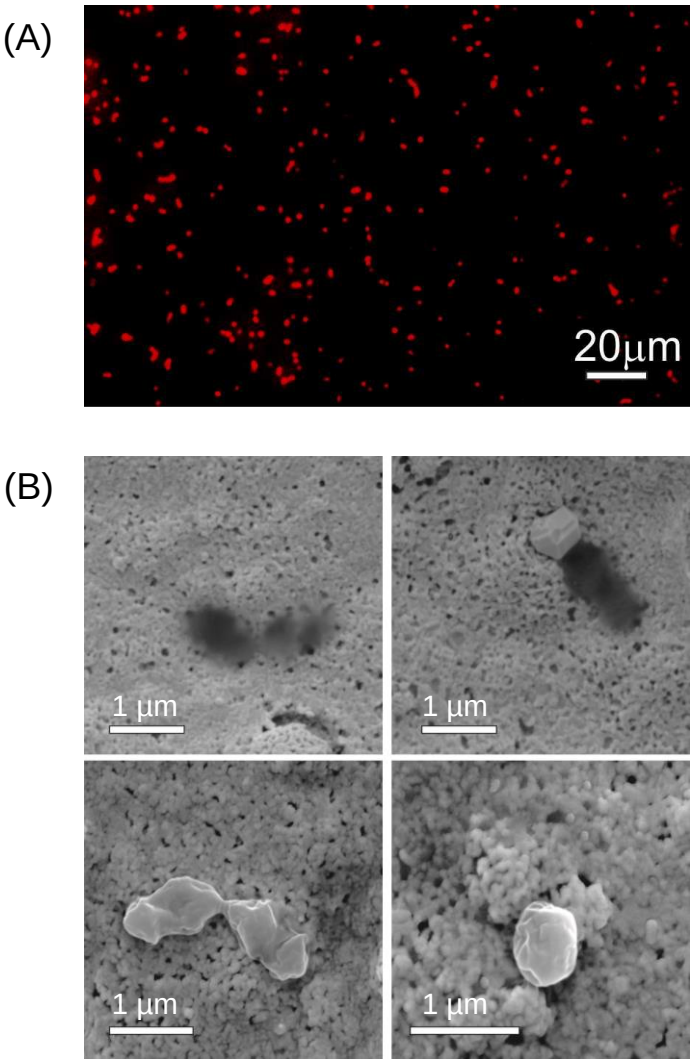

Figure 4.9: Fluorescence and SEM image of captured bacterial cells onto immunosensor

(A) Fluorescence micrograph of PI tagged bacteria *S. pyogenes* captured onto sensor surface, reproduced from (Ahmed et al., 2013) and (B) SEM image of captured *S. pyogenes* on sensor surface, without any coating (upper panel) and with 5 nm platinum coating (lower panel).

4.8 Minimization of non-specific binding by blocking the Fc of IgG with protein A

At this point, it was observed that the non-specific binding profile also increased along with the specific binding although it was significantly lower than that of the specific interaction. As the bacterial surface is much more complex than a small protein analyte we hypothesized that surface proteins might bind non-specifically to the immunosensor. While searching for more detail about *S. pyogenes* surface, an interesting feature of its two surface proteins, M and H, was found. Both of these proteins can bind the Fc of IgG. First, the genetic closeness of Fc receptor and M protein of GAS was discovered, and they were products of a gene duplication (Heath and Cleary, 1989). Then Gomi et al (1990) cloned the gene of protein H and expressed it in *E. coli* which showed the affinity towards Fc portion of human IgG (Gomi et al., 1990). Later on, other reports also confirmed the capacity of the H protein to bind both Fc and albumin (Akesson et al., 1994; Frick et al., 1994). In recent years, it has been further revealed that this unusual mode of binding of *S. pyogenes* to Fc of IgG is an escape route to avoid antibody mediated killing of *S. pyogenes* (Nordenfelt et al., 2012). These critical information correlates with our finding. When *S. pyogenes* was incubated on the surface with non-relevant antibodies (anti-digoxin or anti-*E. coli*) a certain level of binding was always observed which might be due to binding of *S. pyogenes* surface proteins to Fc of IgG on the sensor surface (**Figure 4.10)**.

To test this hypothesis, the following experiment was designed. After fabricating sensors with anti-*S. pyogenes* antibodies, they were incubated with 1 mg/ml protein A as blocking agent for 30 min. It was hoped that it would block the available Fc on the surface without blocking the Fab regions. Other three control sensors were

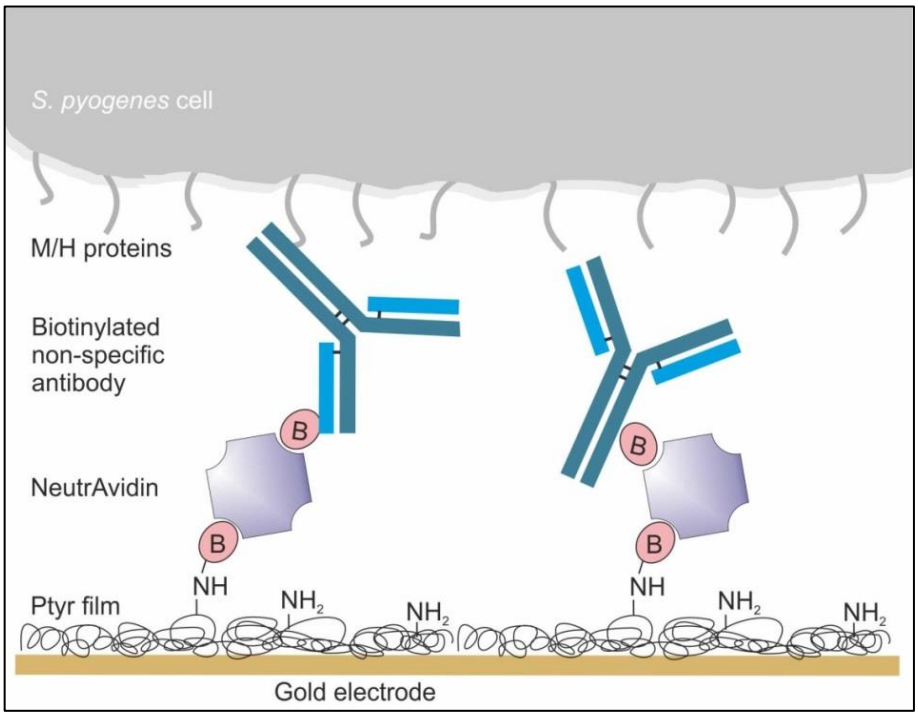

Figure 4.10: Hypothesis of *S. pyogenes* surface M and H protein mediated non-specific binding

S. pyogenes (top grey) surface protein M and protein H are homologous to Fc binding protein/ receptor. They therefore can bind Fc region of any antibody. In case of non-specific antibodies on sensor surface, this binding may contribute to increased non-specific signal. The schematic is not drawn in scale.

prepared with anti-digoxin antibodies on surface. The first one was without any blocking, the second one was blocked with 1 mg/ml BSA and the third one was blocked with 1 mg/ml protein A. Then all of these sensors were exposed to *S. pyogenes* (10^7 cells/ml) and the percentage *R*ct change was plotted.

From data in **Figure 4.11, A** it can be observed that, even after the sensor was blocked with protein A, specific sensors had ~20% *R*ct change upon bacterial binding. In the control sensors, where no blocking was applied around 10% of non-specific signal was found. Blocking with BSA dropped this down to around 5%, however blocking with protein A significantly reduce the non-specific binding down to 1%. These results strongly suggested that, *S. pyogenes* were non-specifically binding to any non-relevant antibodies on surface via Fc and blocking with protein A can almost minimize that binding. When a full calibration curve was done using protein A blocking, data showed that it could significantly lower the non-specific curve down to the base level (**Figure 4.11, B**).

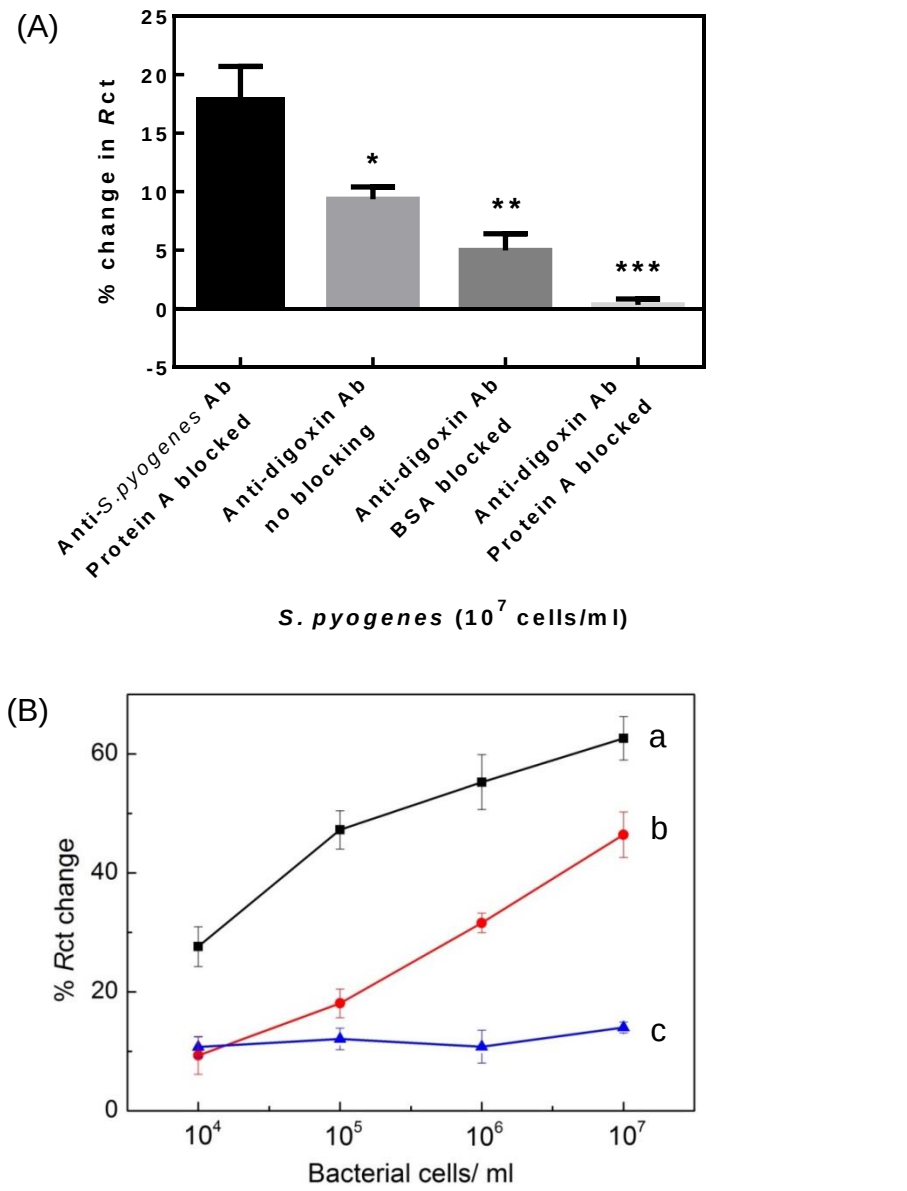

Figure 4.11: Protein A blocking to reduce non-specific binding

(A) Effect of sensor blocking to reduce non-specific signal with full biotinylated antibodies on sensor surface. Single shot *S. pyogenes* (10^7 cells/ml) were incubated on each type of sensors for 30 min, then impedance change (%) was plotted. Dunnett's multiple comparison test showed the statistical significance compared to first column and (B) improvement of non-specific binding in cumulative incubation when sensors were blocked by protein A; (a), Incubation of *S. pyogenes* on anti-*S. pyogenes* surface without any blocking; (b), *S. pyogenes* on anti-digoxin surface without blocking and (c), with 1 mg/ml protein A blocking. Data presented with average ± SEM (n=3).

4.9 Effect of protein A blocking on *S. pyogenes* binding on both specific and non-specific sensors

Although it was observed that protein A blocking could reduce the non-specific binding significantly (**Figure 4.11, B**), its effect of blocking on both specific and non-specific sensors was further investigated. It was hypothesized that, the blocking will have some non-specific and steric effects on a specific sensor surface. Thus the signal may decrease on specific sensors too. In that case, the signal difference between specific and non-specific sensors after blocking is critical.

Initially two concentrations of protein A (1 mg/ml and 0.5 mg/ml) were applied to block both types (specific and non-specific) of sensors surfaces. Then three concentration of *S. pyogenes* samples (10^4, 10^5 and10^6 cells/ml) were incubated in cumulative incubation and change in impedance was plotted. It was observed that, at 0.5 mg/ml concentration blocking, the separation between specific and non-specific was lower than that with 1 mg/ml protein A blocking (**Figure 4.12**). However, in 1 mg/ml blocking the absolute signal value was very low. This could be due to fact that, high concentrations of protein A blocked many antibody binding sites too. Further investigation is required to evaluate the effect of protein A/G blocking. With the available data, effect of blocking in both full antibody and half antibody based sensors have been further discussed in **section 5.6** and in **section 7.1.4**.

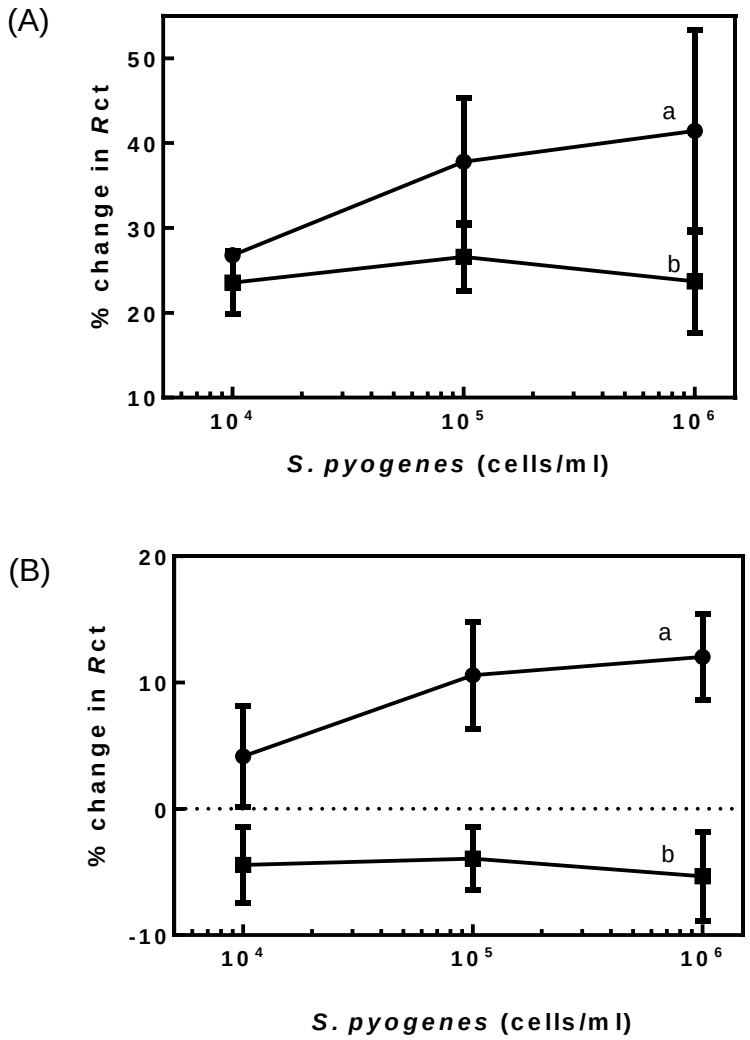

Figure 4.12: Effect of *S. pyogenes* binding after protein A blocking in specific and non-specific sensors

(A) Fully constructed sensors were blocked with 0.5 mg/ml of protein A and (B) with 1 mg/ml of protein A for 30 min. The specific (a) and non-specific sensors (b) were constructed using biotinylated anti-*S. pyogenes* and anti-*E. coli* antibodies respectively. Impedance reading was taken in 10 mM (1:1 ratio) of $[Fe(CN)_6]^{3-/4-}$ redox couple, in PBS, pH 7.0. Data presented are average ± SEM (n=3).

4.10 Sensor performance in 50% (v/v) human saliva

From all of the results observed on impedance signals with protein A blocking, BSA was considered the best blocking choice to test sensors in biological media. *S. pyogenes* acts as a biomarker in throat sample. Thus, saliva is a better choice over blood or urine and being non-invasive easy to collect the sample. Human saliva was collected from healthy individual and spiked with 10^7 cells/ml of *S. pyogenes* or *S. pneumoniae* (used as a negative control). Two different types of sensors were prepared: (1), biotinylated anti-*S. pyogenes* antibodies on the sensor surface and (2), biotinylated anti-digoxin antibodies immobilized onto the sensors. Three incubation conditions were prepared; (1), *S. pyogenes* incubated on to anti-*S. pyogenes* sensor; (2), *S. pneumoniae* incubated onto anti-*S. pyogenes* sensor and (3), *S. pyogenes* incubated onto anti-digoxin sensor. All electrodes were blocked with 1 mg/ml BSA in PBS for 30 min. This was followed by 30 min of bacterial incubation in 50% (v/v) human saliva in PBS before impedance readings were taken.

From the data it was observed that, specific interaction produced ~45% change in signal (**Figure 4.12**). This signal comprised specific antigen-antibody interaction along with some non-specific interaction due to salivary components. When *S. pneumoniae* was incubated there was still some increase in signal (~20%), which is probably due to the fact that they are very closely related bacteria and share some common antigens on the cell surface. When *S. pyogenes* were incubated onto a nonspecific anti-digoxin antibodies the change in signal was minimal (~5%). So, from these data it can be seen that, BSA blocking can still reduce the Fc mediated non-specific binding even in real biological fluids.

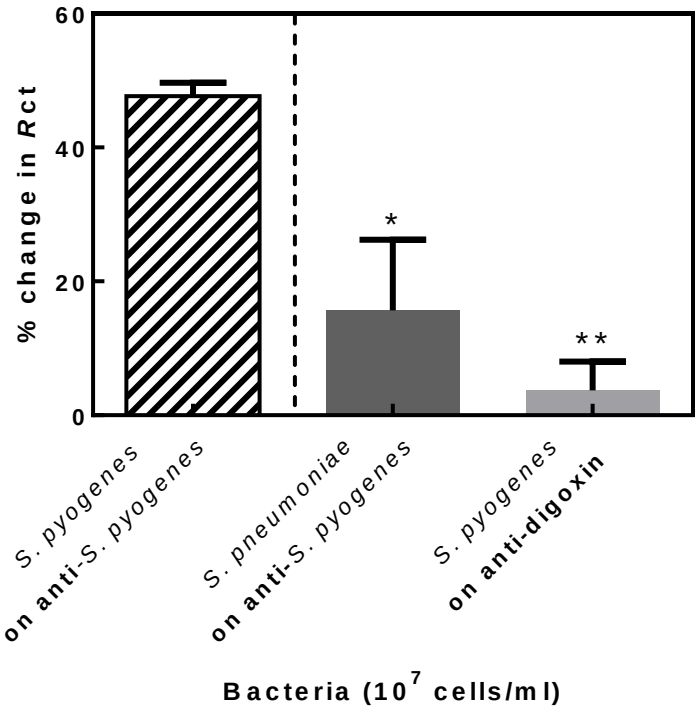

Figure 4.13: Sensor performance in 50 % (v/v) human saliva

Sensors were constructed with biotinylated full antibodies. Single shot incubation of bacterial cells (10^7 cells/ml) for 30 min were performed and change in impedance (%) was plotted. Dunnett's multiple comparison test showed the statistical significance of each condition compared to the control (left column). Data presented as average ± SEM (n=3). (Ahmed et al., 2013)

4.11 Conclusion

From the electrochemical data and Midland blot it was clear that the polytyramine surface had sufficient free surface amines for conjugation and biotinylated antibodies can be successfully tethered onto the surface. The reproducibility of fully constructed sensors in the measuring solution was also observed. Strict optimization of NeutrAvidin and antibody concentration allowed achievement of maximum signal output. Two types of incubation and calibration was performed. However, the single shot calibration was limited by the need for multiple electrodes per experiment.

Non-specific binding of target bacteria *S. pyogenes* onto non-relevant antibodies on surface appeared to be a serious issue. General blocking (i.e. BSA) and specially targeted blocking of Fc of IgG (i.e. via protein A) reduced sensor non-specific signal. However, protein A blocking also caused lowered specific signal and further investigations are needed to improve this behaviour.

When sensors were tested in human saliva sample spiked with bacteria, it showed good specificity and selectivity. As a starting point, where sensors were prepared with biotinylated full antibodies it helped to isolate the key parameters to improve the sensors and these information were equally helpful while constructing the sensors using antibody fragments which will be discussed in the following Chapter.

Chapter Five

Reduced antibody based sensor for *S. pyogenes*

Chapter 5 Reduced antibody based sensor for *S. pyogenes*

5.1 Introduction

In the previous chapters, fabrication of whole antibody based sensors to detect *S. pyogenes* is described. The fabrication included immobilization of biotinylated antibodies onto screen printed gold electrodes via NeutrAvidin. The surface base polymer i.e. polytyramine was also extensively studied. However, in these immunosensors the antibody was not highly oriented as the biotinylation site is random. In addition, the antibody recognition sites are far away from the electrode surface. To address these issues a more oriented and close to surface configuration is required.

Different fragments of antibodies can be generated by targeting multiple reactive sites in an antibody. One of the most widely used methods is the mild reduction of the hinge region disulphide bonds to produce two identical half antibody fragments. Two different reducing agents, 2-mercaptoethylamine. HCl (2-MEA) and tris (2-carboxyethyl) phosphine (TCEP) were explored to split antibodies. Their reduction efficiency and usefulness in biosensor construction was also tested. As a quick purification method, spin filters were used to separate half antibody fragments before applying onto the electrode surface. In preliminary studies, biosensors were constructed with non-purified reduction products (a mix of full antibody and other possible fragments) and then purified half antibodies were found to improve immobilization of antibodies and bacteria binding. The general scheme for half antibody based sensor construction is shown in **Figure 5.1.** In brief, polytyramine was deposited onto gold electrodes. Then the hetero-

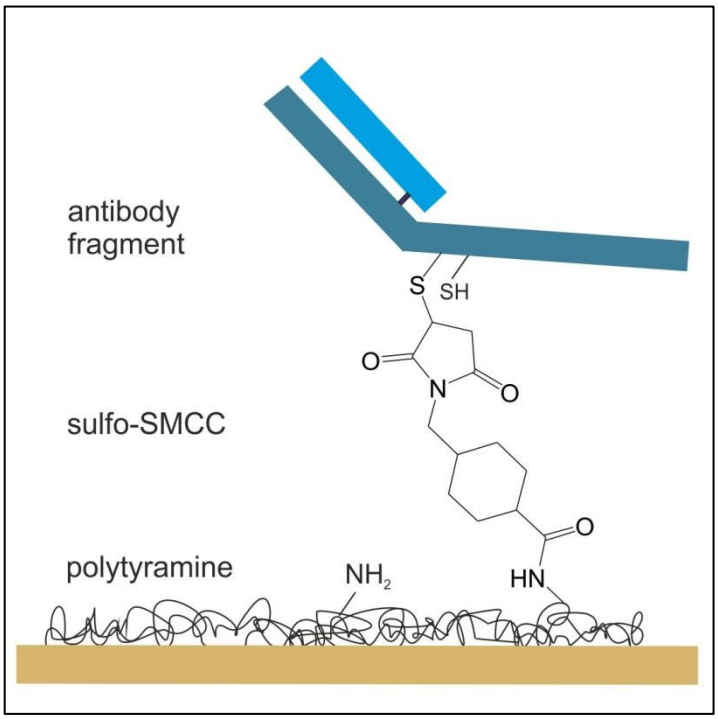

Figure 5.1: Schematic of half antibody based immunosensor construction

Polytyramine (Ptyr) was deposited on DS gold electrodes, then the surface amine was conjugated with linker sulfo-SMCC. Free maleimide group was then coupled to the sulfhydryl group of reduced (by 2-MEA or TCEP) half antibody fragments. The drawing is not to scale.

bifunctional cross linker sulfosuccinimidyl-4-(N-maleimidomethyl) cyclohexane-1-carboxylate (sulfo-SMCC) was used to link the polymer surface amine to the free sulfhydryl of the half antibodies. In contrast, to full antibody based sensor construction, this allows close proximity of the bioreceptor to the electrode surface. And, as the conjugation is only via free sulfhydryl groups in the hinge region, the fragments are expected to be highly oriented, compact and the distance of binding sites from the electrode is around 5-8 nm (Billah et al., 2010) which is almost half to the full antibody format.

The effect of protein A/G blocking, which was used in full antibody format, also helped in the half antibody format. Altogether, half antibody sensors showed higher signals and sensitivity over full antibody based sensors. The effect of protein G on blocking Fc in half antibody based sensors were more significant compared to full antibody based sensors.

5.2 Optimization of 2-MEA and TCEP reduced antibodies

5.2.1 Antibody fragment generation

Reducing agents that selectively target the hinge region of antibodies are used to generate two identical copies of half antibody per antibody molecule. However, 2-MEA is known to be more gentle and selective towards hinge region disulphide bonds. The other reducing agent TCEP is stronger and less selective. 2-MEA is a thiol containing compound, so if not purified after the reduction of antibodies, it will compete with maleimide coupling. In contrast, TCEP is thiol free, so its presence in the reaction product does not cause such problem.

Generally, when antibodies are treated with reducing agents, depending on the concentration of both antibody and reducing agent, temperature, and incubation time an initial mixture of several antibody fragments can be generated (**Figure 5.2**). Generally, the hinge region disulphides are separated first and half antibodies were produced (~75 kDa). Further reduction of this fragment can happen resulting in one heavy chain (~50 kDa) and one light chain (~25 kDa). However, although the chances are less, other types of fragments can also be present, e.g. full antibody missing one light chain (~125 kDa) and without two light chains (~100 kDa).

After successful reduction of antibodies by 2-MEA, purification was necessary. Although TCEP reduced antibodies can be directly applied onto sensor surfaces, purification helps towards better immobilization. When reduction mixture are incubated onto sensor surfaces, the unwanted fragments or non-reduced whole antibodies create steric hindrance affecting optimum binding. For this reason, in both cases, purification of the half antibody fragments is helpful before fabricating the immunosensor.

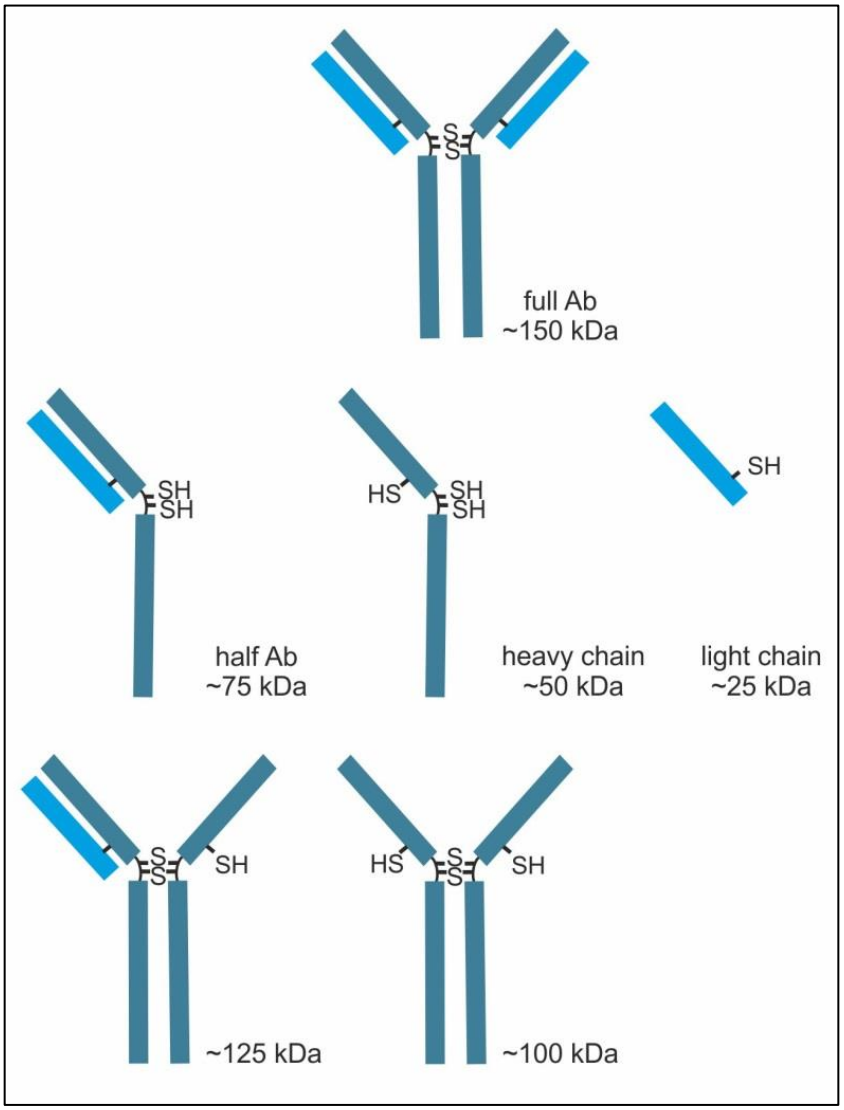

Figure 5.2: Antibody fragments generated by selective reduction

Gentle reduction of antibodies selectively cleaves hinge region to produce half antibodies (~75 kDa). Further reduction can produce heavy chains and light chains. Other less likely but possible fragments are full antibody missing one or two light chains.

Usually, reduced antibody fragments are separated by size exclusion chromatography. However, the collected fraction were usually very diluted and needed additional concentration step. To avoid this, spin filters with different molecular weight cut off were used directly to isolate half antibody fragments in less time. This also helped in controlling volumes to get the desired final concentration of half antibodies. Starting from antibody reduction, followed by purification, sensor construction and testing could be done in one single day when spin filters were used. As reduced half antibody fragments cannot be stored for further use, fresh fragments were prepared and purified on each experimental day. Thus, a consistent protocol was developed to maintain reproducibility and quality of fragment generation for biosensor application. This is schematically presented in **Figure 5.3**. In brief, the antibodies were treated either with 2-MEA or TCEP according to method (**section 2.2.8**) and then was first centrifuged through 100 kDa cut off filters. The filtrate which is devoid of full antibodies, was then taken onto a 50 kDa filter and centrifuged to concentrate the half antibody fragments. This remaining solution was then recovered and was ready to use for biosensor applications or further analysis e.g. SDS-PAGE.

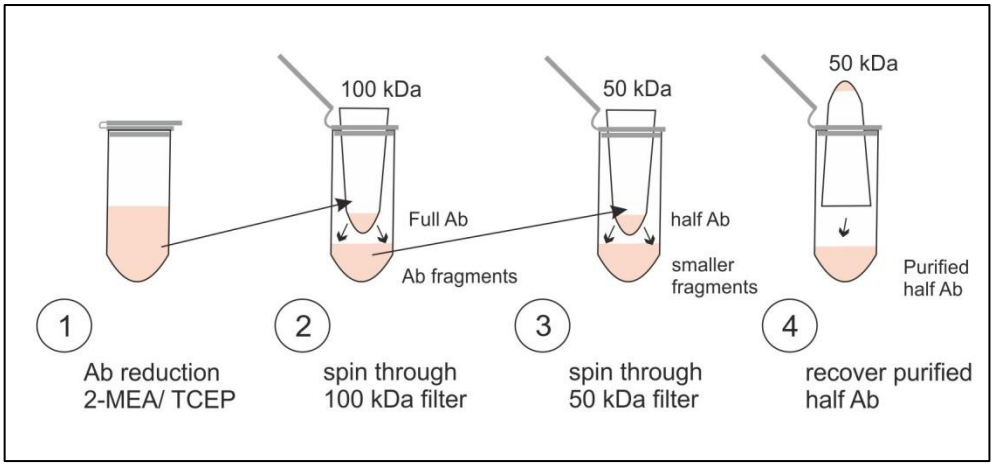

Figure 5.3: General scheme of reduced antibody purification

Antibody reduction was performed in the presence of either 2-MEA or TCEP. Then the reduction product was centrifuged using 100 kDa cut off spin filter to remove unreacted full antibodies. The filtrate with remaining antibody fragments was further purified using 50 kDa cut off filters to retain half antibody fragments (~75 kDa). The purified half antibody fragments were then used directly to fabricate sensor surface.

5.2.2 Determination of optimum TCEP molar ratio

Before incubation of antibodies with TCEP, the optimum molar ratio of TCEP to antibodies was optimized. To generate sufficient half antibodies without generating other fragments (light and heavy chains), TCEP was incubated with antibodies at different molar ratio and the reaction product was subjected to SDS-PAGE. TCEP with five different molar ratio were used (100 to 1000) and was incubated for 30 min. Then the reaction products were run on SDS-PAGE with a control lane (no TCEP) and a protein marker lane (**Figure 5.4**).

It was observed that from a 500:1, molar ratio onwards significant production of half antibodies occurred with a clear band in the gel. However, above a 750 molar ratio, other fragments (heavy and light chain) started to appear. When the approximate percentage of these fragments was analysed from band intensities using ImageJ software, it was found that a maximum of ~30% half antibodies could be produced at a 750:1 molar ratio of TCEP to antibody. This molar ratio was then used for both sensor applications and further SDS-PAGE experiments.

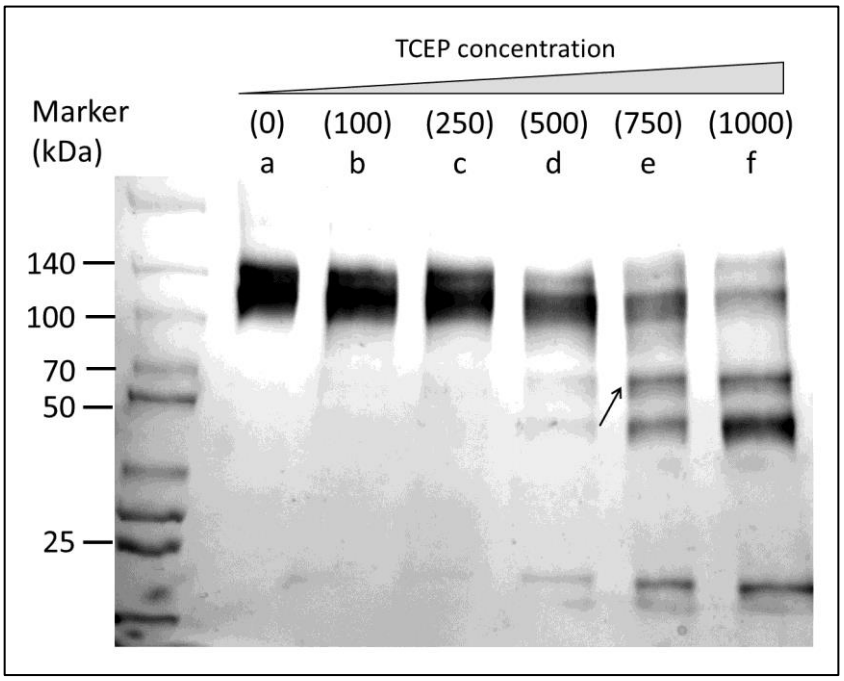

Figure 5.4: Optimization of TCEP molar ratio by SDS-PAGE for half antibody production

Different molar ratio of TCEP: antibodies (100, 250, 500, 750 and 1000:1) were incubated at room temperature for 30 min. Then control (no TCEP, full antibodies, lane a) and reacted samples (TCEP reaction products, lane b-f) were loaded onto 4%-15% (w/v) resolving gel with loading dye, stained and imaged with Syngene G:Box. The half antibody band is marked with small arrow.

5.2.3 SDS-PAGE of TCEP and 2-MEA reduced antibodies after optimization

As mentioned earlier, after selective reduction, purification was performed using spin filters with 50 kDa and 100 kDa cut off. The TCEP to antibodies molar ratio was optimized (750:1) and 2-MEA concentration had been previously optimized in our group (50 mM 2-MEA with 16 µM antibodies). Using these two optimized conditions two different polyclonal antibodies (anti-*S. pyogenes* and anti-*E. coli*) were reduced and SDS-PAGE was carried out to see corresponding bands in the gel (**Figure 5.5**).

Lane 1 and 2 showed the untreated antibodies of anti-*S. pyogenes* and anti-*E. coli* respectively. Then for each antibody samples were run in two lanes for 2-MEA and two lanes for TCEP treatments. In all cases the first lane (1a) was the reaction product and the following one (1b) was the spin filter purified product. As the incubation time were different for 2-MEA and TCEP and one lane contained reaction product (non-purified) and the other lane had the purified fragments, the timing were adjusted accordingly so that all lane products were ready to put in the gel at the same time.

From **Figure 5.5** it was observed that for both the antibodies, TCEP was harsher than 2-MEA producing more unwanted fragments. Although, half antibody band was visible in the lane with purified sample, it was faint as the amount of half antibody was only ~30% of total fractions. However, starting from 2.5 mg/ml full IgG, the purified half antibody concentration was found to be 0.025 mg/ml when the same starting volume was maintained. This concentration was close to the optimum antibody concentration required for surface immobilization.

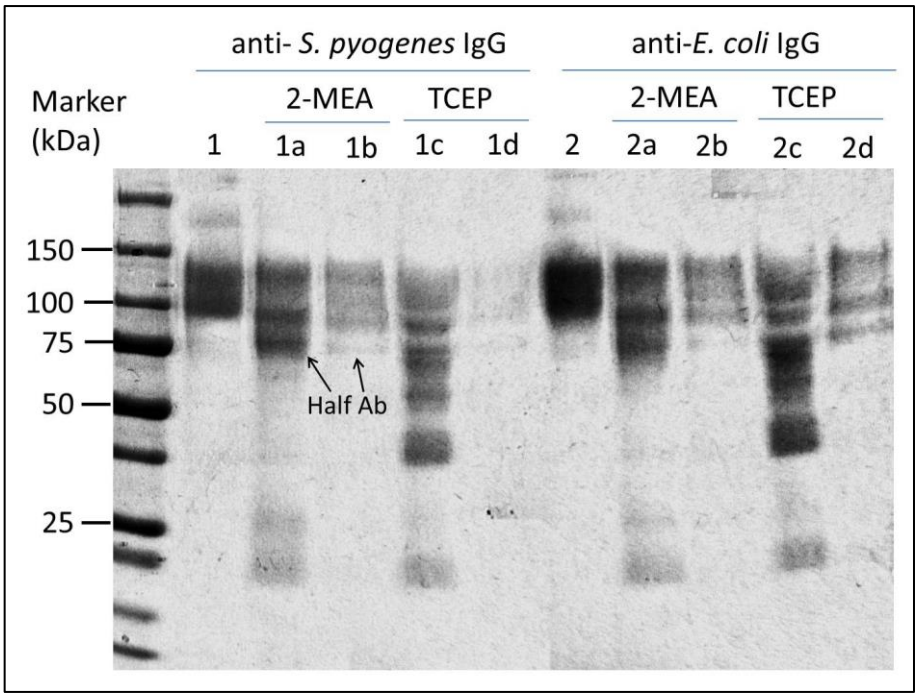

Figure 5.5: SDS-PAGE of optimized 2-MEA and TCEP reduced antibody fragments

Antibodies (2.5 mg/ml or 16 µM) were treated with 50 mM 2-MEA for 90 min in 37ºC water bath and with TCEP at 750:1 molar ratio to antibodies, for 30 min at room temperature before loading to the gel. Lane 1 and 2 were unreacted antibodies. Lane 1a, 1c, 2a and 2c were reaction products without purification. The rest of the lane samples were purified by two step spin filtering. All the reactions were timed before applying to the lanes. The image was taken in a Fujifilm dark box and contrast was optimized in ImageJ software.

Antibody fragments are becoming a popular choice in biosensor applications. However, the key challenges are the choice of reducing agent, efficiency and amount of fragments generated, purification and storage. The most studied fragments are half antibody fragments and F(ab´). They benefit from small size, without losing immune reactivity. Depending on the fragments generated, the immobilization techniques also vary. Both the half antibodies and F(ab´) contain free SH groups, that can be either directly assembled onto gold surface or can be chemically linked to a base layer.

In our group, biosensors have been constructed against myoglobin (Billah et al., 2010) and adenoviruses (Caygill et al., 2012) using half antibody fragments. Anti-myoglobin half antibodies were immobilized onto a 4-aminothiophenol (4-ATP) SAM amines via sulfo-SMCC. The electrodes were almost atomically flat gold electrodes, which are particularly useful for SAM deposition. Anti-adenovirus half antibodies were immobilized onto a mixed copolymer of aniline and 2-aminobenzylamine (2-ABA) via the same linker. In this case, the electrodes used were screen printed gold electrodes commercially purchased from DropSens. In both cases, 2-MEA was used as reducing agent and their purification was performed via size exclusion chromatography. The confirmation of antibody fragment generation was carried out with HPLC, atomic force microscopy (AFM) and SDS-PAGE analysis.

There are few other published research that used antibody fragments for biosensor construction. Antibodies against *E. coli* were reduced via TCEP for quartz crystal microbalance (QCM) based biosensor (Sharma and Mutharasan, 2013a). To reduce antibodies they used a 757:1 molar ratio of TCEP to antibodies for 1 h and directly immobilized the fragments onto a gold chip. They also reported that fragments could retain their biological activity and the response was higher compared to physically absorbed and protein-G mediated immobilization. However,

they claimed that as TCEP is not specific towards the hinge region, a good portion of other fragments were also generated along with the half antibodies.

In another study, half antibodies were prepared by TCEP and then immobilized onto nanoparticle for drug delivery, targeting cancer cells (Hu et al., 2010). They used 3 a fold molar excess of TCEP over monoclonal antibodies and reacted 4h. This low molar ratio for prolonged exposure helped to split the desired amount of half antibodies which was confirmed by SDS-PAGE. Apart from the benefit that TCEP does not need to be removed after the reaction, it is still difficult to produce a selective reduction. As 2-MEA and TCEP reacted antibodies needed purification for better immobilization, then considering the greater specificity of 2-MEA towards the hinge region, it was selected as a better choice of reducing agent.

5.3 Preliminary studies with TCEP reduced non purified antibodies

Initially, before optimizing the TCEP: IgG molar ratio, a non-purified TCEP reduced reaction mix was directly used to construct the biosensors. This was performed to observe the general performance of TCEP to produce viable half antibodies and their ability to bind bacteria onto the sensor surface when immobilized without purification. To achieve this, antibodies (2.5 mg/ml) were incubated with TCEP at a final concentration of 5 mM, which is ~300 molar excess to antibodies for 30 min at room temperature. Then, this reaction product was immediately incubated on a sulfo-SMCC modified polytyramine surface. After incubation the surfaces were thoroughly washed and were ready for interrogation. Two types of sensor surfaces were constructed; 1), with anti-*S. pyogenes* antibodies and 2), with anti-digoxin antibodies. After immobilization of antibodies the sensors were blocked with 2 mg/ml BSA for 30 min. Three experimental conditions were prepared, 1) *S. pyogenes* tested on anti- *S. pyogenes* surface, 2) *S. pyogenes* tested on anti-digoxin surface and 3) blank PBS (without any bacteria) onto anti- *S. pyogenes* surface. Three concentrations of bacteria (10^3, 10^5 and 10^7 cells/ml) were applied onto the sensor surfaces, incubated for 25 min before washing and the impedance readings were taken.

The effect of these three conditions are presented in **Figure 5.6**. It was observed that when increasing concentrations of *S. pyogenes* were incubated, a gradual increase in the Nyquist curve was indicative of specific immune interaction (**Figure 5.6, A**). When the same bacteria were incubated onto surface with anti-digoxin antibodies, no increase in the Nyquist curve was observed (**Figure 5.6, B**).

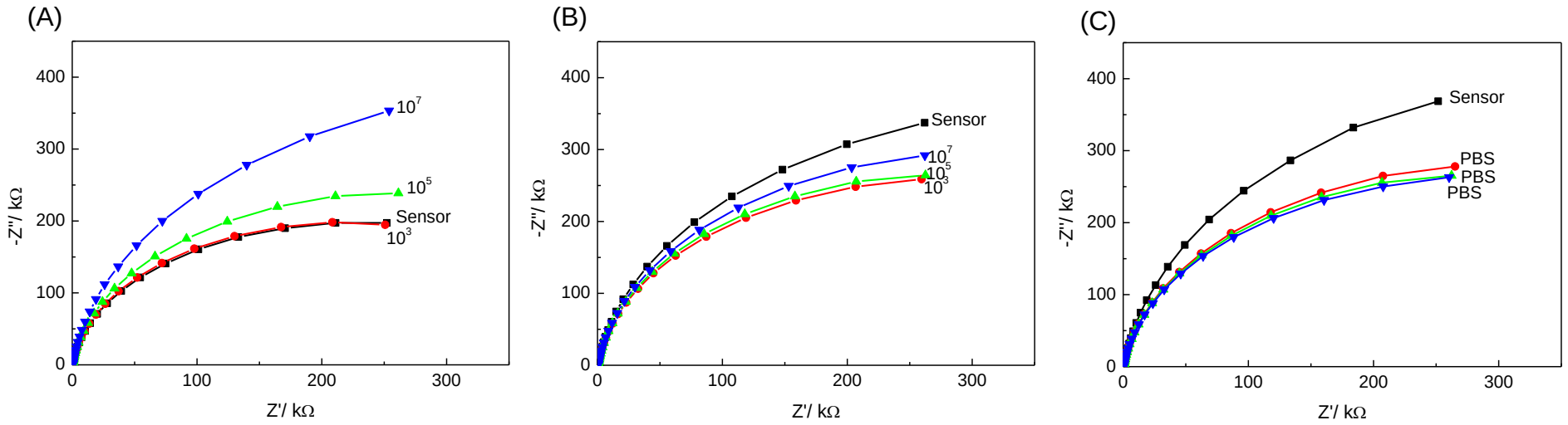

Figure 5.6: Preliminary sensor response with non-purified TCEP reduced antibodies

Sensors were constructed with TCEP reduced antibodies against *S. pyogenes* and digoxin. The Ptyr was deposited at 100 mV/s scan speed for 2 cycles. (A) *S. pyogenes* were incubated onto reduced anti-*S. pyogenes* antibodies immobilized surface. (B) *S. pyogenes* were incubated onto sensor surface with reduced anti-digoxin antibodies and (C) Blank PBS (no bacteria) were incubated onto anti-*S. pyogenes* surface. EIS was taken in presence of 10 mM (1:1 molar ratio) of $[Fe(CN)_6]^{3-/4-}$ redox mediator in PBS, pH 7.0 in each step of analyte addition. Three different concentrations of *S. pyogenes* were used (10^3, 10^5 and 10^7 cells/ml) in (A) and (B). All sensors were blocked with 2 mg/ml BSA after immobilization of antibodies for 30 min.

Instead, all of the impedance was below the sensor impedance, which indicated loss of impedance mostly due to some non-specific BSA washed away from the surface. However, with increasing bacterial concentration, there was slight increase, but all of them fell below the full sensor value. When the sensor surface was tested with repeating incubation of PBS only (**Figure 5.6, C**), it was also found that all three repeats were below the sensor level and they did not vary even after three PBS incubations. This also indicated that in the specific condition, the antibody-bacteria interaction was the main event for the increase of impedance. With PBS only incubations, the steady impedance also indicated the stability of sensor impedance. However, from these data it was observed that as non-purified product was used, the absolute impedance value of the sensor surface was non-reproducible. This implies that, the surfaces were not equally coated from chip to chip, and thus BSA blocking was also not equally distributed from sensor to sensor. Another drawback of using non-purified antibodies was that other -SH containing fragments (heavy and light chain) could also be immobilized without contributing towards the immune reaction.

Thus, from the primary finding it was concluded that, as a reducing agent TCEP can be used. However, the limitations of using non-purified products and random generation of other fragments made it less suitable choice compared to 2-MEA. To produce more reproducible sensor surfaces with similar impedance values to start with, purification of reaction product is recommended and thus comparing these two reducing agents, 2-MEA was taken further for use in biosensor construction. The BSA blocking worked well with TCEP based sensors. However, in 2-MEA based sensors at first the sensors were tested without any blocking and then protein G blocking was carried out to compare the results with full antibody based sensors.

5.4 Sensor construction and calibration using 2-MEA reduced half antibodies

5.4.1 Midland blot of immobilized half antibodies

As previously performed with full antibody based sensors, presence of immobilized half antibody fragments were also specifically detected by Midland blotting. The sensors were prepared according to the standard protocol and then incubated with specific and non-specific anti-HRP antibodies. As anti-*S. pyogenes* antibodies were raised in rabbit host, anti-rabbit HRP conjugated antibodies were used for specific interaction and anti-sheep HRP antibodies were used as negative control.

The midland blot data showed that, chemiluminescence signal was observed when appropriate HRP conjugated antibodies were incubated (**Figure 5.7**). Compared to that in the control working electrode, there was no signal indicating that the light signal in WE 1 was due to presence of immobilized half antibodies against *S. pyogenes* which interacted with HRP conjugated antibodies and emitted light when exposed to ECL reagent. However the signal here was not strong compared to full antibody based sensors (**Figure 4.3, B**). This could be due to the fact that, HRP conjugated antibodies cannot bind half antibodies efficiently on the surface because of compact 3D packaging of half antibodies. Another possible reason could be the fact that this electrode was subjected to Midland blotting with other electrodes tested for different parameters, which created a relative intensity difference among electrodes. However, when the electrode was cropped and brightness and contrast was corrected a clear difference between two working electrode was observed. In addition, anti-HRP antibodies are less sensitive towards half antibody fragments than full antibodies according to the manufacturer product description.

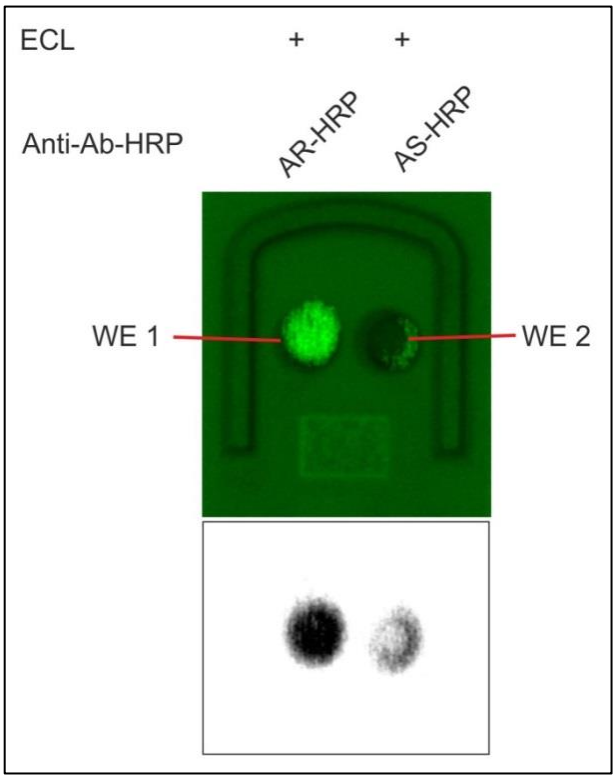

Figure 5.7: Midland blot to detect immobilized half antibodies onto sensor surface

Electrode was coated with polytyramine. Then, 2-MEA reduced and purified half antibodies against *S. pyogenes* were immobilized onto both working electrode 1 (WE 1) and working electrode 2 (WE 2) via sulfo-SMCC. Then anti-rabbit HRP (AR-HRP) and anti-sheep HRP (AS-HRP) antibodies were incubated onto WE 1 and WE 2 respectively. A chemiluminescent image was taken after exposure to ECL reagents. The upper panel is the superimposed image of the electrode and the light green false coloured signal. Lower panel is the inverted light signal.

5.4.2 Sensor EIS using 2-MEA reduced antibodies after optimization

Biosensors were prepared with 2-MEA reduced half antibodies and cumulative incubation of increasing concentration of *S. pyogenes* were performed. For this, three types of antibodies were used; 1), anti-*S. pyogenes*; 2), anti-*E. coli* and 3), anti-digoxin. Then 10 µl sample of bacterial cells with increasing concentrations from 10^3 to 10^8 cells/ml were incubated on all the sensors with replication. Impedance was recorded after each incubation.

A sample of layer by layer impedance of a specific sensor is shown in **Figure 5.8, A**. It was observed that, a regular increase in impedance took place with increasing concentration of bacteria. The percent change in impedance over fully constructed sensor level with three antibodies was plotted against increasing concentration of bacteria (**Figure 5.8, B**). It was observed that, in case of specific interaction linear increase in signal was observed with increased bacterial concentration. The maximum change was achieved (~150% with highest bacterial incubation). Anti-*E. coli* surface showed same linear increase, but the signal change was much lower at all concentrations except 10^6 cells/ml. In case of anti-digoxin surface, the rise in signal was much lower and almost unchanged from 10^5 cells/ml incubation onwards. This single variance from antibody to antibody could be due to several reasons. Anti-*E. coli* antibodies were raised against a mixture of five *E. coli* strains, which may share some similar cellular epitopes to *S. pyogenes* surface that contributed to non-specific signal. Moreover, anti-*E. coli* antibodies were very fresh compared to anti-digoxin and thus some Fc of anti-digoxin could be damaged over time and produced less non-specific binding to *S. pyogenes* via Fc binding.

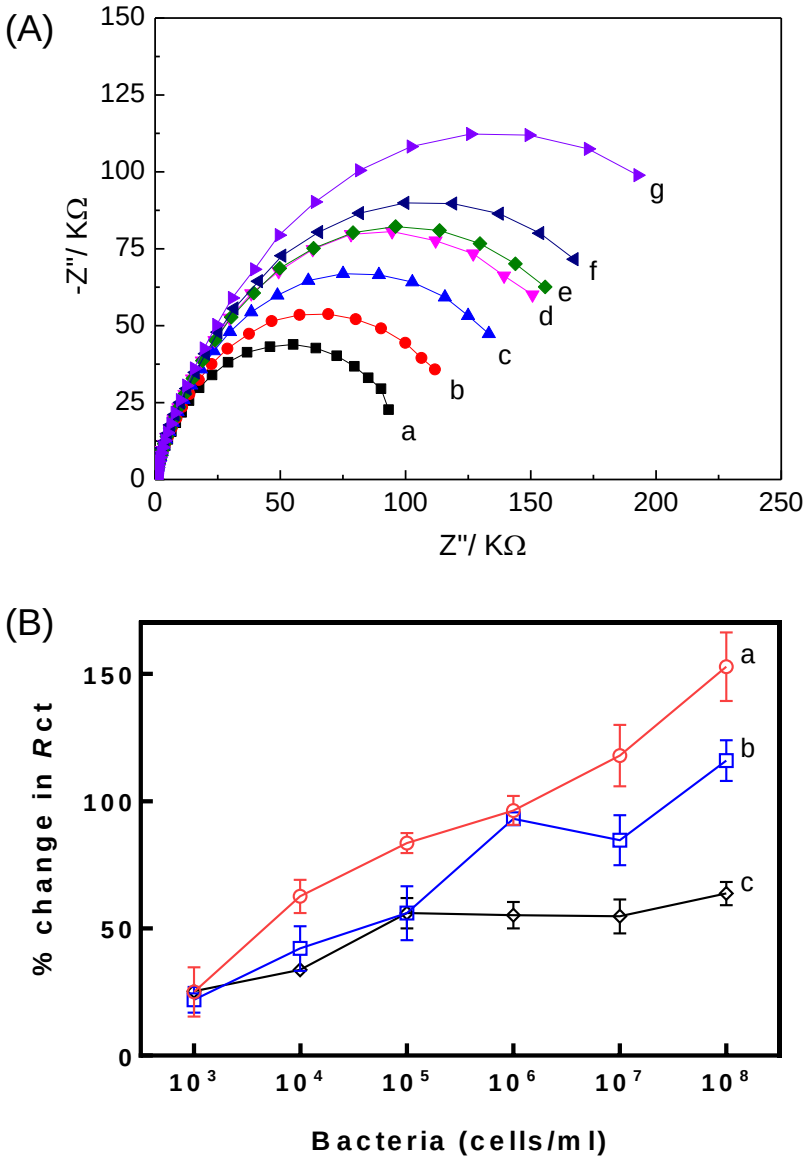

Figure 5.8: Impedance profile of 2-MEA reduced half antibody based sensors

(A) Representative layer by layer sensor impedance of half antibody based sensors (a) and *S. pyogenes* 10^3 to 10^8 cells/ml (b-g). Impedance was recorded in 10 mM $[Fe(CN)_6]^{3-/4-}$ redox couple in PBS, pH 7.0. (B) Calibration of increasing concentration *S. pyogenes* incubation on (a), anti-*S. pyogenes* surface; (b), anti-*E. coli* surface and (c), anti-digoxin surface. Data presented are average ± SEM (n=3) and incubation were performed in cumulative fashion.

5.5 Effect of protein G blocking in half antibody sensors

The effect of protein A blocking was tested in full antibody format. Here, in half antibody format, sensors were blocked with 1 mg/ml recombinant protein G and both specific and control sensors were exposed to four bacterial concentrations (from 10^4 to 10^7 cells/ml) by cumulative incubation. 2-MEA reduced anti-digoxin antibodies were used as control sensor surface.

From the calibration curve (**Figure 5.9**), it was observed that in half antibody sensor format the signal dropped compared to non-blocked surface as it happened in full antibody format. The signal at highest bacterial concentration dropped from the linear rise. Until that point, specific and non-specific interaction signal was different. The comparative effect of protein A/G blocking on sensors have been further analysed with the available data and will be discussed in **section 5.6 and section 7.1.4**.

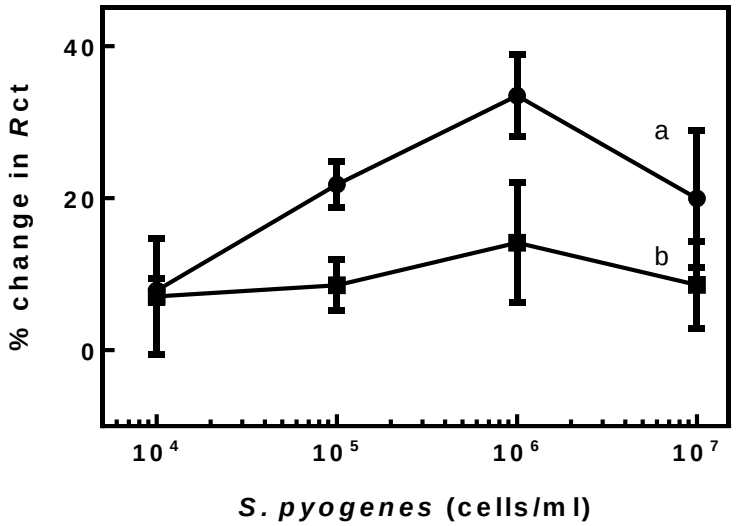

Figure 5.9: Recombinant protein G blocked half antibody based sensor calibration

Increasing concentration of S. pyogenes cells were incubated on surfaces with anti-*S. pyogenes* half antibodies (a) and anti-digoxin half antibodies (b). The sensor were blocked with 1 mg/ml recombinant protein G for 30 min. Impedance was recorded at each level and % change in *R*ct over protein G blocked surfaces were plotted against increasing bacterial concentrations. Data presented here are average ± SEM (n=3)

5.6 Comparative sensor sensitivity using protein A/G blocking

It was observed both in full antibody format (**Figure 4.12**) and in half antibody format (**Figure 5.9**) that use of protein A/G as blocking agent reduced the average signal. But it was important to know the relationship of signals between specific and non-specific surfaces before and after blocking. To get a greater insight on how these blocking agents influenced signal sensitivity, pre and post blocking data were further analysed in both formats (**Figure 5.10**). Data were collected when a particular concentration of bacteria (i.e. here 10^5 cells/ml) was incubated onto the sensor surfaces and the ratio of the percentage change in Rct of specific and non-specific interaction was plotted. It was observed that, in full antibody format, blocking with protein A decreased the ratio by 1.6 times, whereas in half antibody format it increased by 2-fold. Depending on these data, further hypothesis is discussed in **section 7.1.4**.

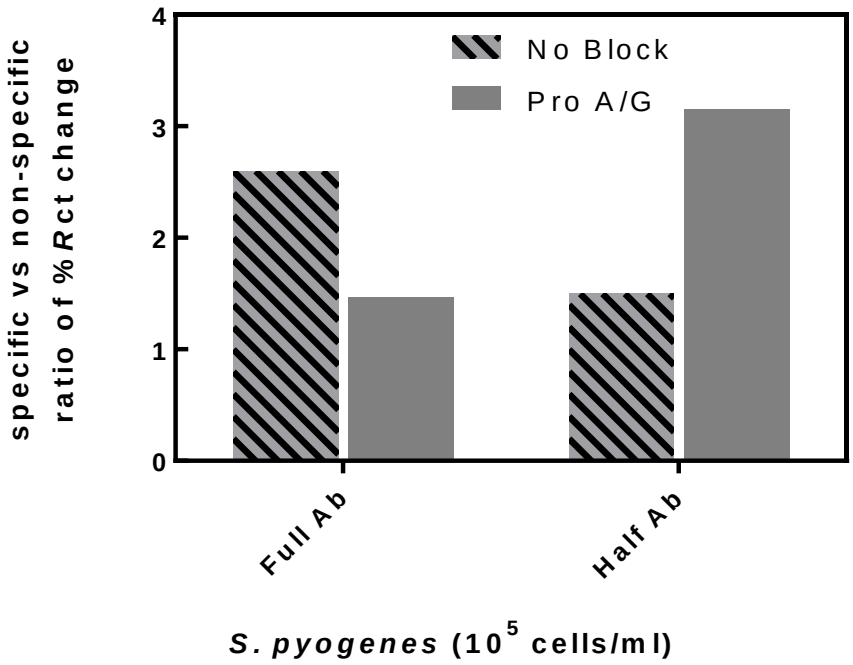

Figure 5.10: Effect of protein A/G blocking on sensor sensitivity both in full and reduced antibody immobilized surfaces

Values were calculated from calibration curves, when 10^5 cells/ml bacteria were exposed in cumulative incubation. The ratio of percentage change in *R*ct in specific and control sensor with or without blocking is presented. The ratio is obtained from the data where n≥3 ± SEM. Full antibody based sensors were blocked with protein A and half antibody based sensors were blocked with recombinant protein G.

5.7 Conclusion

Reduced antibody fragments was immobilized onto electrode surface after cleaving whole antibodies using reducing agents. Parameters of antibody reduction was optimized and SDS PAGE was performed to monitor selective reduction. With the optimized condition, the constructed sensors were exposed to increasing concentration of bacterial cells. The change in impedance signal with half antibody based sensor was a lot higher than that of biotinylated full antibody based sensors. It was observed that both signal value and reproducibility improved with antibody fragments. This also supports the compact packaging of antibody fragments close to gold electrode surface enabling its electrochemistry more sensitive.

Non-specific signal due to Fc portion of any antibody was also observed here. Blocking the Fc using recombinant protein G was performed. However, the same trend of some signal loss manifested the problems of blocking in general. If flatter surfaces can be used as starting electrode material, the sensitivity can be increased manifold. Antibody fragments as bioreceptor proved to be effective to capture target bacteria. However, further research should focus on more efficient reduction and purification of antibodies and stability of immobilized antibody fragments on sensor surfaces. In the following chapter, the scope and possible use of mixed polymers of phenol derivatives to reduce non-specific signal in human serum has been discussed.

Chapter Six

Hybrid polymer surface to reduce non-specific signal in biological sample

Chapter 6 Hybrid polymer surface to reduce non-specific signal in biological sample

6.1 Introduction

From the full antibody and half antibody based system, it was observed that non-specific signal minimization is a critical step for optimum response. This non-specific interaction may arise at the bioreceptor level. However, the base layer itself can contribute to non-specific binding creating unwanted signal. Most of the amine containing polymers are positively charged. Most of the biological samples (e.g. blood, saliva) contain many proteins that have low isoelectric points and at physiological pH are negatively charged. So, apart from the antibody-antigen interaction substantial non-specific charge interaction can occur (**Figure 6.1**).

To address this, usually different blocking agents are used after the immobilization of the bioreceptors. However, coverage of the blocking agents on the surface is difficult to control and sometimes reduces the specific binding event to a certain level. To tackle this problem an alternative could be the selective introduction of negatively charged monomers into the polymer (**Figure 6.2**). To detect an Alzheimer's disease biomarker we have already used a mixed polymer of tyramine (Tyr) and phloretic acid (PA) at 3:1 molar ration in basic medium (Rushworth et al., 2014). However, in that study a critical characterization of copolymer was not performed.

To develop this concept further for sensor applications, a study of the copolymer has been performed. Along with phloretic acid, a neutral analogue of tyramine, 4-propyl phenol (4-PP) has also been studied. The capacity of these polymers to

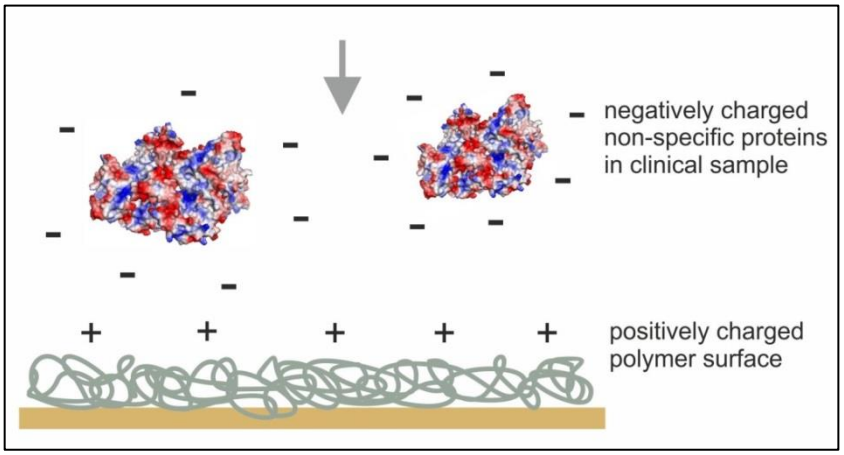

Figure 6.1: Schematic of non-specific binding of sample proteins to biosensor surface

Most of the non-target proteins in biological samples are negatively charged at physiological pH. Positively charged polymers tend to attract these proteins non-specifically creating a substantial amount of non-specific signal. Introducing negatively charged species into polymer may reduce this background noise by repelling most of the negatively charged non-target proteins.

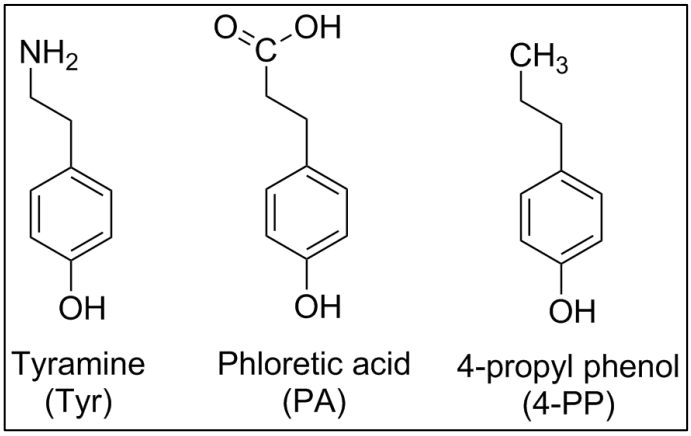

Figure 6.2: Phenolic monomers used in copolymer synthesis

Tyramine and its two analogues, phloretic acid with negatively charged carboxylic acid and 4-propylphenol with neutral methyl group. Introducing negatively charged or neutral monomers into polymer can reduce non-specific protein binding onto biosensor.

immobilize bioreceptors were analysed by impedance. This also indicated the extent of amine presence after copolymerization. Later on, the non-specific effect of human serum onto these polymers were examined. Copolymer base layers were also prepared from acidic medium to check their ability to repel non-specific serum proteins. These findings have been presented in this chapter which can be a starting point to tune polymer surfaces for reduction of the non-specific signal in impedimetric biosensor development.

6.2 Preparation of mixed charged copolymer

To introduce negatively charged or neutral monomers into copolymer different methods were followed and are presented in **Table 6.1**. In brief, to electropolymerize tyramine and PA, two different mixing methods were applied. In Method 1, the total molar concentration (25 mM) was kept constant and both the monomers were adjusted to give different molar ratios between them (e.g. 3:1, 1:1 and 1:3). In Method 2, the tyramine was kept constant (25 mM) and PA was adjusted to have different molar ratio in the mixture. To synthesize copolymer of tyramine and 4-PP, Method 2 was applied to create different molar mixtures.

All of the monomers were mixed in ethanol containing 0.3 M NaOH. The deposition was achieved using 2 CV cycles from 0 V to +1.6 V. First, a copolymer of tyramine and PA were electropolymerized according to Method 1 and the polymerization process was analysed with CV and EIS. From the deposition CV graph (**Figure 6.3, A**) it can be seen that the oxidation peak shifted from higher potential (0.56 V) to a lower potential (0.32 V) as PA increased and tyramine decreased in the solution. The oxidation peak current however did not change that much. However, the current at the first reverse point (i.e. at 1.6 V) increased with the increasing amount of PA in solution.

This was also evident in CV and EIS data. From CV data (**Figure 6.3, B**) it was found that the first two polymers (a and b) had reduced current and peak separation indicating deposition. The last three polymers (c, d and e) had CV graphs almost close to bare gold indicating very poor deposition with increasing PA. The impedance data (**Figure 6.3, C**) also showed that *R*ct dropped with the increase of PA and decrease of tyramine. At this point, with impedance data it was

Table 6.1: Molar ratio of different phenolic monomers for polymerization

Tyramine and phloretic acid: Method 1				
Polymer conditions	Tyramine (Tyr) mM	Phloretic acid (PA) mM	Copolymer (mM)	Molar ratio
a	25	0	25	Pure Tyr
b	18.75	6.25	25	3:1
c	12.50	12.50	25	1:1
c	6.25	18.75	25	1:3
e	0	25	25	Pure PA
Tyramine and phloretic acid: Method 2				
Polymer conditions	Tyramine (Tyr) mM	Phloretic acid (PA) mM	Copolymer (mM)	Molar ratio
a	25	0	25	Pure Tyr
b	25	8.3	33.3	3:1
c	25	25	50	1:1
d	25	75	100	1:3
Tyramine and 4-propylphenol				
Polymer conditions	Tyramine (Tyr) mM	4-propylphenol (4-PP) mM	Copolymer (mM)	Molar ratio
a	25	8.3	33.3	3:1
b	25	25	50	1:1
c	25	75	100	1:3
d	0	25	25	Pure 4-PP

All the polymers were deposited with 2 potential cycles from 0 to 1.6 V at 100 mV/s scan speed. The solvent was ethanol containing 0.3 M NaOH.

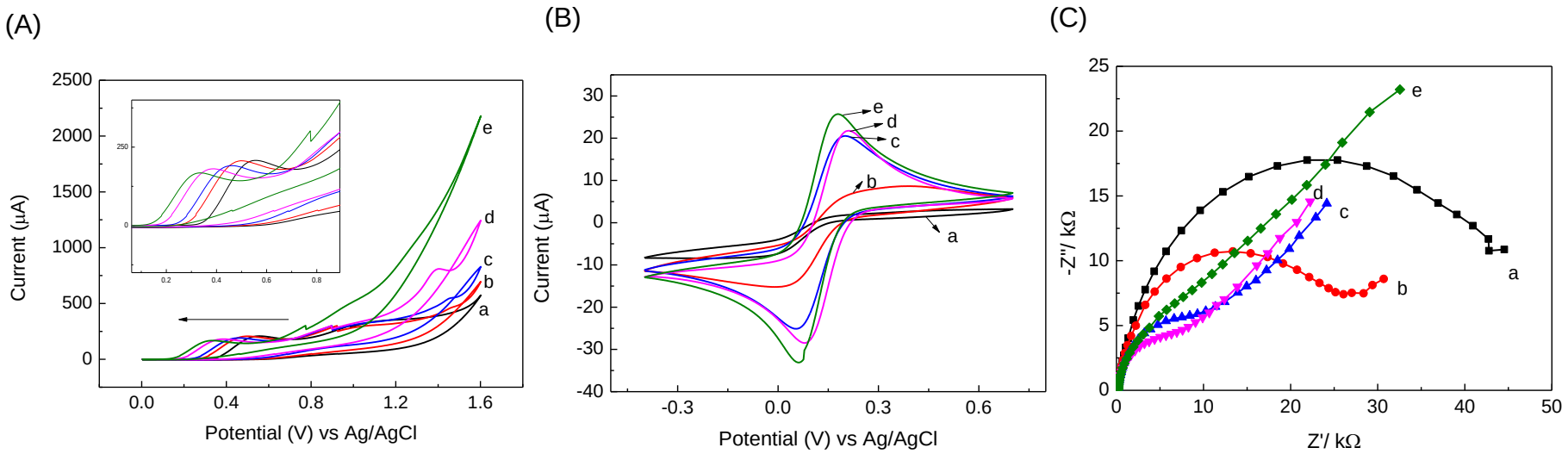

Figure 6.3: Electropolymerization profile of copolymer of tyramine and phloretic acid, CV and EIS using Method 1

(A) Electropolymerization of (a), 25 mM tyramine; (b), 18.75 tyramine and 6.25 mM PA; (c), 12.50 mM tyramine and 12.50 mM PA; (d) 6.25 mM tyramine and 12.75 mM PA and (e), 25 mM PA dissolved in ethanol containing 0.3 M NaOH. The electrodes were cycled from 0 V to +1.6 V for 2 cycles at 100 mV/s scan speed. Inset shows the enlarged oxidation peak area (B) CV of above mentioned polymers in 10mM $[Fe(CN)_6]^{3-/4-}$ redox couple. Scan speed was 50 mV/s. (C) EIS reading of the deposited polymers in the same redox couple.

not clear whether the low impedance was due to less polymer deposition or the deposited polymer was more porous and had high conductivity. The other important observation was as amount of tyramine was reduced with increasing PA, a low amount of tyramine could slow polymerization. Accordingly, Method 2 was designed to keep tyramine constant.

In Method 2 (**Figure 6.4, A**), the deposition CV showed that unlike Method 1, the oxidation peak potential did not shift. However, the peak current increased with increasing concentration of PA in solution. From the CV and EIS data (**Figure 6.4, B and C**) it was clear that impedance dropped with increasing PA. In this case, as the tyramine concentration was constant, increase in PA concentration had some effect on the deposited polymer since the impedance fell and current increased. Two things were important at this stage; (a), the amine availability in those polymers after introduction of PA; and (b), interaction of these polymers with non-specific proteins. Considering the data obtained via Method 1 and 2, Method 2 was then taken forward. Then the copolymers were used to see how much antibody could be conjugated onto the surface which acts as an indication of surface amine availability. Non-specific serum binding was also analysed on antibody immobilized surfaces to find out the effectiveness of the new copolymers (**section 6.3**).

Using Method 2, a copolymer of tyramine and 4-PP was also polymerized. It was observed from the CV deposition profile that introduction of 4-PP into polymer increased the oxidation peak current (**Figure 6.5, A**). However, 4-PP alone had a lower current compared to three copolymers. From impedance data (**Figure 6.5, B**) it was observed that all of the copolymers gave impedance reading with very high resistance and capacitance compared to copolymer of tyramine and PA. This indicated the 4-PP copolymerized better with tyramine than PA. For further study, a molar ratio of 1:1 was selected for tyramine and 4-PP.

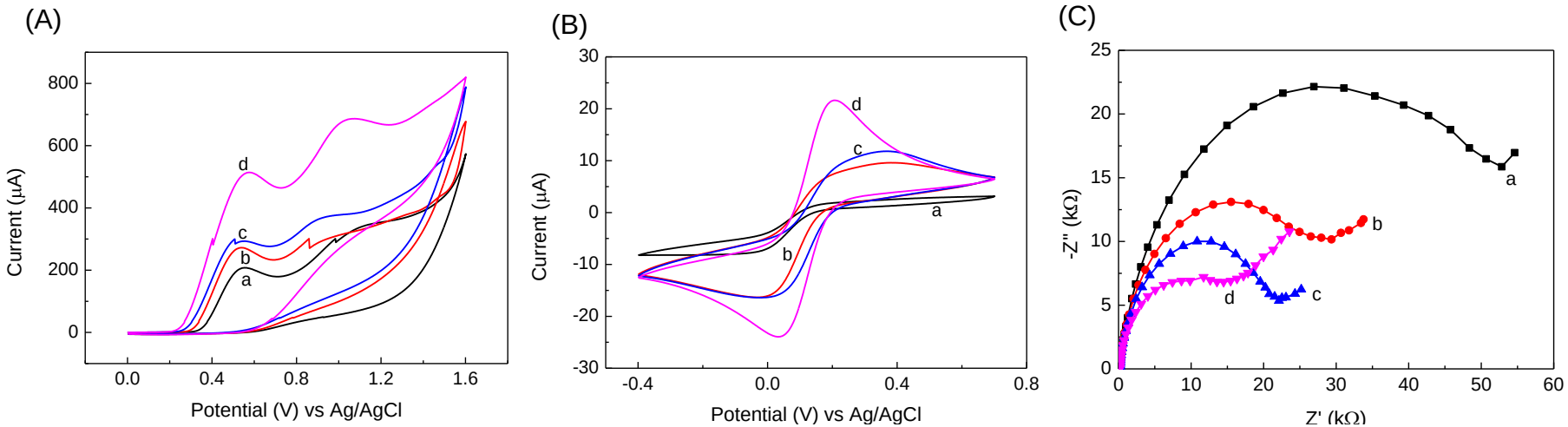

Figure 6.4: Electropolymerization profile of copolymer of tyramine and phloretic acid, CV and EIS using Method 2

(A) Electropolymerization of (a), 25 mM tyramine; (b), 25 mM tyramine and 8.3 mM PA; (c), 25 tyramine and 25 mM PA; and (d), 25 mM tyramine and 75 mM PA dissolved in ethanol containing 0.3 M NaOH. The electrodes were cycled from 0 V to +1.6 V for 2 cycles at 100 mV/s scan speed. Inset shows the enlarged oxidation peak area for clear view (B) CV of above mentioned polymers in 10mM $[Fe(CN)_6]^{3-/4-}$ redox couple. Scan speed was 50 mV/s. and (C) EIS reading of the polymers in the same redox couple. Impedance reading was taken from 25 mHz to 25000 Hz with 51 points with modulation voltage of 10 mV at 0V.

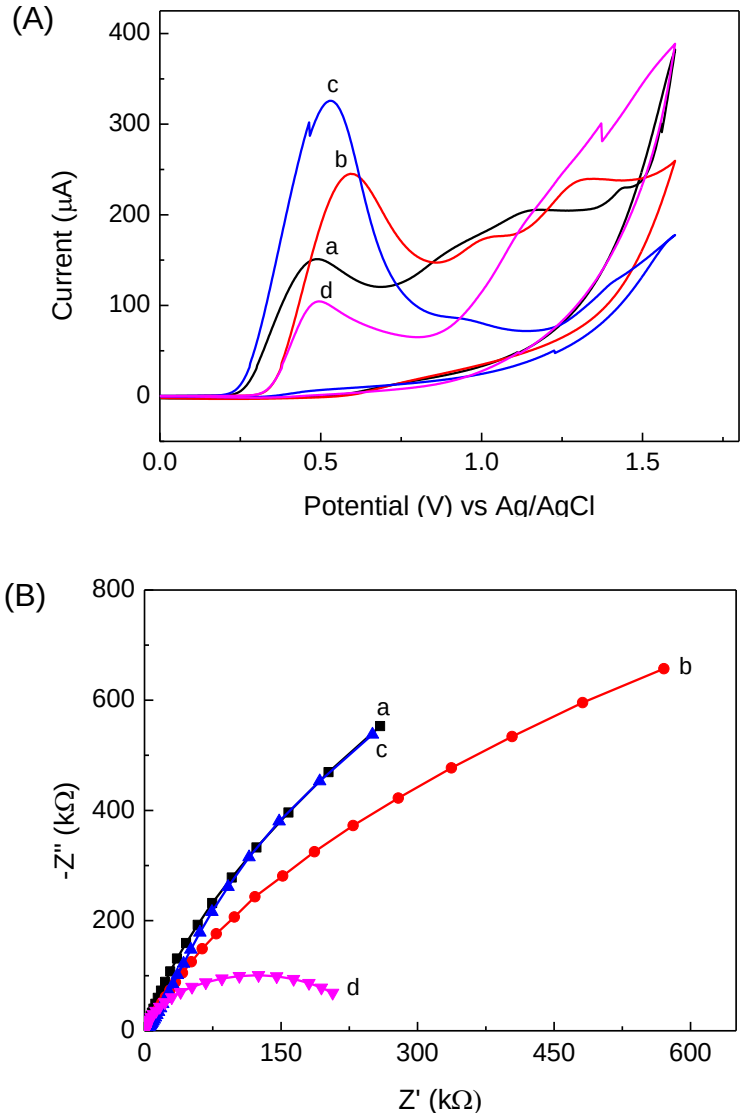

Figure 6.5: CV and EIS profile of electrodeposited copolymers from tyramine and 4-propylphenol

(A) CV profile of deposited copolymer of tyramine and 4-PP. Polymer of (a), 25 mM tyramine and 8.3 mM of 4-PP; (b), 25 mM tyramine and 25 mM 4-PP; (c), 25 tyramine and 75 mM 4-PP; (d), and 25 mM 4-PP and (B) Nyquist curve of above mentioned polymers. Reading was taken in 10 mM $[Fe(CN)_6]^{3-/4-}$ redox probe.

6.3 Antibody deposition and serum binding on different polymers

To test the effectiveness of new copolymers for antibody conjugation, four conditions were selected; 1), 100% tyramine (25 mM); 2), tyramine/ PA (9:1); 3), tyramine/ PA (3:1) and 4), tyramine/ 4-PP (1:1). Then biotinylated antibodies were conjugated onto these surfaces which were then incubated in human serum for 30 min. EIS was recorded after antibody and serum incubation. The data (

Figure 6.6) showed that when a one third molar ratio of PA to tyramine was introduced into the polymer, both antibody deposition and serum binding was reduced. This indicated that there were not enough accessible amines on the surface to successfully conjugate to the antibodies. This result was interesting as only ~33% of PA reduced the surface amine substantially. On the other hand, the 4-PP mixed copolymer had a very high *R*ct value. However, subsequently there was a decrease in impedance after antibody incubation suggesting the polymer was water soluble and washed away in subsequent incubations.

So from the data, a few key points were concluded. First, the monomers (PA and 4-PP) polymerized differently when mixed with tyramine. Initially, it was thought that PA or 4-PP would copolymerize in the similar mechanism of polytyramine formation alone. In polytyramine the main polymerization occurs through the *ortho* and *meta* positions relative to OH group. But the data suggested that PA and 4-PP did not follow a simple polyphenol polymerization mechanism.

Although there are no reports on copolymerization of tyramine with PA or 4-PP from basic media, some publications describe homo-polymerization of carboxyl group

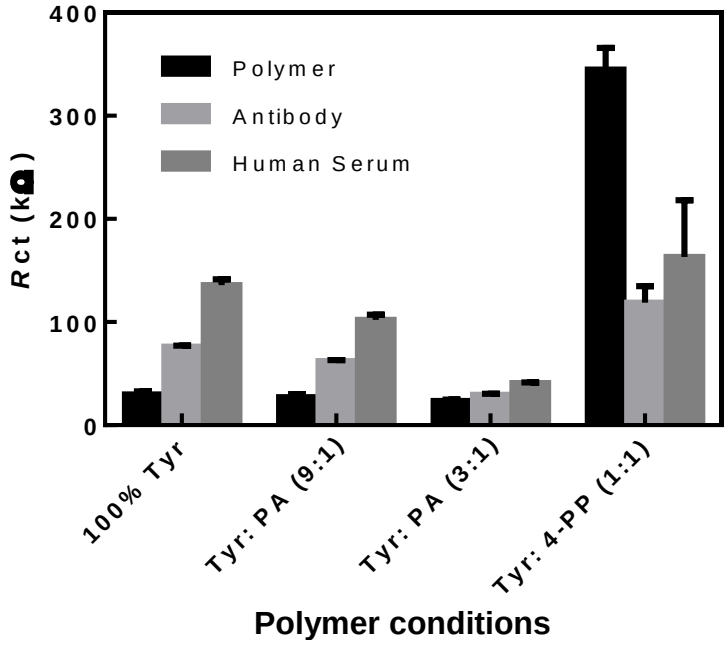

Figure 6.6: Change in layer-by-layer impedance with mixed charged polymers Polymers were prepared keeping tyramine molar concentration fixed and changing the other monomer. Then full biotinylated antibodies were deposited followed by incubation in human serum for 30 min. Average *R*ct values ± SEM (n=3) were presented for each layer of construction. Impedance was recorded using 10 mM $[Fe(CN)_6]^{3-/4-}$ redox couple.

containing phenolic compounds in acidic media. In one study, polymerization of 4-hydroxybenzoic acid (4-HBA) was performed from perchloric acid onto graphite electrodes (Ferreira et al., 2011). They compared three pH conditions and concluded that both *R*ct and mass deposition was higher in acidic pH compared to basic and neutral pH. In basic pH both -OH and carboxyl group are negatively charged. In our study, in basic medium both carboxyl and -OH of PA can be negatively charged and interact with tyramine amine and –OH to form amide and polyester.

Another molecular modelling and research study explained the concept of polyester formation and ring-ring interaction (Ferreira et al., 2012). They polymerized 3-hydroxyphenylacetic acid (3-HPAA) and showed that apart from normal polyether chain formation at *ortho* and meta position, non-electrochemical polyester and ring-ring interaction can take place (Ferreira et al., 2012). It was also unclear that which mechanism dominated at a particular condition. This hypothesis also explained our finding, that during copolymer formation of tyramine and PA in basic medium, beside the electrochemical polyether formation, polyester, ring-ring interaction and amide bond could take place (**Figure 6.7**). These two additional linking chemistry might result in different 3D folding of the polymer which reduced the amine accessibility on surface.

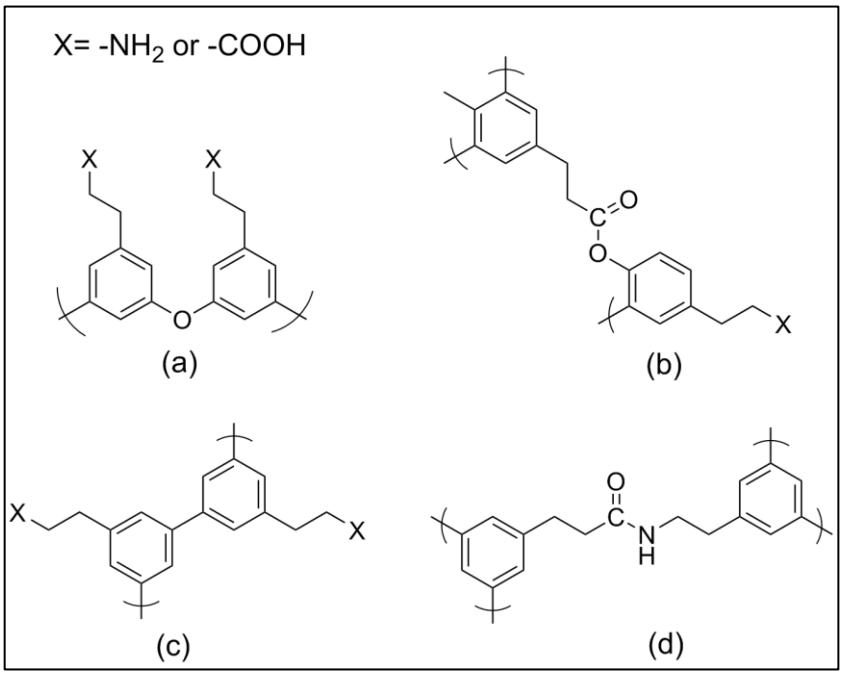

Figure 6.7: Possible copolymerization mechanism between tyramine and phloretic acid

During copolymerization, four types of bond can take place; (a), typical ether bond due to electrochemical polymerization; (b), head to tail ester formation; (c), ring-ring interaction and (d), head to head amide formation. Multiple mechanisms can also take place simultaneously. According to the Ferreira et al (2012), these bonded structures (a-c) can form octamer and construct globular shapes.

6.4 Polymer deposited from acidic media

As there are reports within literature, in which acidic condition for the homopolymerization of carboxyl containing phenolic compounds were used, an experiment was conducted to see the efficacy of copolymer formation and antibody conjugation when polymers were deposited from sulphuric acid. Two different molar ratio of tyramine and PA were used (3:1 and 2:1, keeping tyramine at 25 mM) and the *R*ct values of the polymer and then antibody covered surface were analysed.

The data (**Figure 6.8**) showed that, the extent of polymer deposition was different for the two conditions. However, none of the copolymer showed significant conjugation of antibodies onto the surface. This finding again demonstrated that even in acidic media, introduction of PA with tyramine reduced the amine availability. The exact chemistry and chemical composition of these copolymers needs to be further investigated to find out the optimum conditions where the required amount of carboxyl group incorporation can be ensured whilst keeping surface amine level optimum to conjugate sufficient bioreceptors.

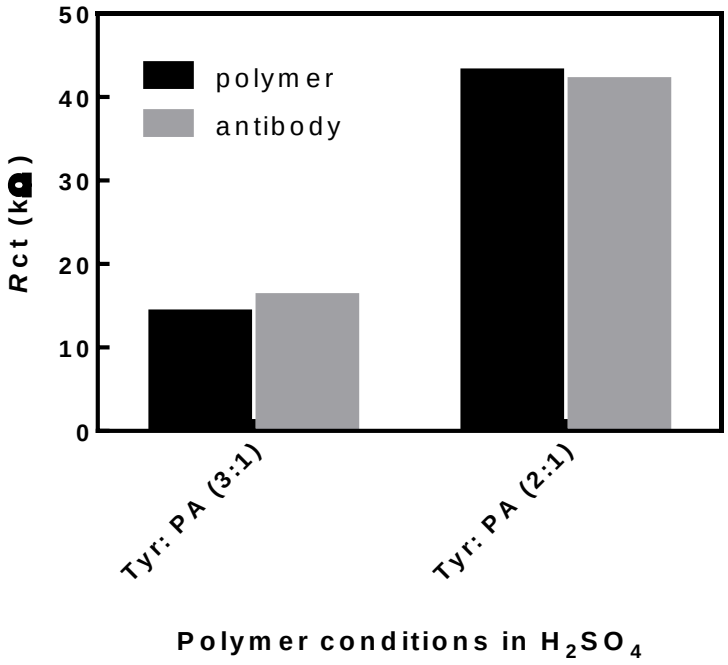

Figure 6.8: Impedance value of polymer and antibody level developed from acidic media

Polymers were deposited in 1M H_2SO_4 with 2 scans at 100 mV/s. The impedance was measured at polymer and antibody level. Each data presented here are the average values of two individual electrodes for each condition.

6.5 Conclusion

In this chapter, monomers with negatively charged or neutral group were introduced along with amine containing tyramine to synthesize a copolymer. The hypothesis was to reduce non-specific signal that was due to charge interaction between polymer free amines and negatively charged non-target proteins in blood or saliva sample. However, the negatively charged monomer PA and methyl group containing 4-PP did not polymerize in the same manner. In pure polytyramine, the main bonds are polyether, originated in the phenol ring near the -OH groups. However, when PA was mixed, head to tail ester or head to head amide formation and ring-ring interaction may took place and changed the polymer growing chemistry affecting surface amine availability. Tyramine to PA molar ratio of 3:1 had very few amines compared to pure tyramine.

The methyl group containing monomer 4-PP copolymerized quite strongly, but the polymer was water soluble and the impedance data showed the possible wash out of this polymer from the surface with subsequent washing and incubation. Thus it was not suitable at all to construct the immunosensor. In another attempt, copolymers of tyramine and PA were deposited from acidic media. However, the polymer had less amine to conjugate antibodies, which was also observed in polymers from a basic medium.

It was evident that, introduction of PA significantly reduced non-specific human serum binding. So, further research needs to be focused to tune the polymerization where ether bond formation can be made as dominant bond. The preliminary results presented in this chapter showed some promise that a copolymer condition with optimum amine to conjugate antibodies along with negative or neutral moiety would help to produce a surface suitable for biosensor applications.

Chapter Seven

General discussion

Chapter 7 General discussion

7.1 General discussion

The overall aim of the project was to develop and optimize immunosensor fabrication to achieve successful detection of the bacterium *S. pyogenes*. In the overall project, commercial screen printed electrodes were used. Starting from the surface nanostructure, base layer polymer optimization and antibody immobilization strategies were explored. Each of the important technical observations, consideration and recommendation will be further discussed in this chapter with a final outlook on future research.

7.1.1 Electrodes and fabricated sensor reproducibility

The commercial screen printed dual electrodes used in the study raised both positive and negative concerns in terms of sustainable and reproducible research. The best feature of these electrodes are that all three electrodes are printed onto one base which helps to keep the inter electrode distance constant. Two independent readings can also be taken without removing the electrode from the measuring solution. In contrast, single working electrodes such as P3 and P4 (**Figure 1.10, h and i**) are very difficult to handle, reference and counter electrode positioning is always manual, connection is fiddly and few electrodes can be managed in a single day. DropSens electrode connection was robust and easy to work with, and the electrode chip was of a decent size to be comfortably handled during washing, drying and incubation steps.

Although the technical features and electrochemical property of bare surface of these electrodes were satisfactory, the real surface area was very rough on the

nano scale (**Figure 3.2, B**). Intra electrode variability was less as compared to inter electrode variability. This was reflected in data observed at every level of sensor fabrication, e.g. EIS data obtained from the bare electrode, after polymer deposition (**Figure 3.18**) and after antibody immobilization. After polytyramine deposition the average *R*ct value observed was 46.30 kΩ with SD ± 6.37 kΩ, (n=20, polymers on each electrode was deposited with same parameters). However, when biotinylated antibodies were immobilized the variation further increased. Anti- *S. pyogenes* and anti-digoxin antibodies showed average *R*ct value of 180 kΩ with SD ± 62 kΩ and 91 kΩ with SD ± 40 kΩ respectively (n=20 for each antibody). The variation observed in polymer and antibody levels were not only due to electrode surface variability, but also due to variation in the monomer solution and random orientation of antibodies onto surface. Tyramine tends to precipitate in solution very quickly during deposition and stick to the glass container. Batch to batch product variability of purchased tyramine was also a major concern. The physical colour of tyramine powder was very different ranging from pure white to light brownish, resulting in difference in their polymerization capacity. The half antibody immobilized surface was more reproducible than that with biotinylated whole antibodies. This was likely due to biotinylated antibodies having different orientation upon conjugation whereas half antibodies only conjugate via the hinge region sulfhydryl group.

The cost of electrodes is still a limiting factor for large number of replicates. One electrode chip costs around £ 3 to 4, depending on design. Although the cost can be minimized, manual sensor fabrication and measurement lengthen the overall testing time, thus managing too many electrodes became difficult. However, to analyse important parameters single shot incubations with the maximum number electrodes possible was performed. Introduction of robotic automated deposition and simultaneous data reading facility of n>20 would be very useful for producing

more robust and significant data. Another limiting factor of DropSens electrodes was box to box variation. Within a box (usually 75 electrodes) inter electrode variation was low. However, difference was observed between electrodes from different boxes. These variations included visual diameter differences in the working electrode area and differences in CV and EIS data. Keeping this under consideration, critical data pool was usually acquired using electrodes from a single box.

There was no chance to assess the effect of relative electrode size on EIS signal sensitivity. Smaller electrode area is considered better for detect small numbers of bacteria, but this can also be a limiting factor when too many bacteria are present in the sample. Thus, an optimum electrode area is also important if certain range of detection is required. Miniaturization can help in getting a better signal, as one study suggested 50 µm as the lower limit of electrode diameter for optimum bio-impedance study (Rahman et al., 2007). However, as the size of microelectrodes decreases, the chance of increased noise may arise depending on the study parameters (Pliquett et al., 2010).

7.1.2 Antibody coverage and use of fragments

It was observed that the optimum density of bioreceptor on the sensor surface has a vital influence on analyte binding. This vary depending on the size and shape of analyte and due to the roughness of electrode surface. As screen printed electrodes were relatively rough, the roughness also dictated the antibody orientation and successful immobilization. If almost atomically flat surface are available, the effect of optimum antibody concentration could be measured more accurately with better reproducibility.

Although the use of antibody fragments helped to orient them closer to the electrode surface and give a better signal, it was always a challenge to get desired amount of reduced purified product keeping it bioactive. However, antibody cleavage can be optimized by adjusting reduction buffer pH (personal communication, Asta Makaraviciute). It was observed that a greater yield of reduction was produced using low pH acetate buffer. However, the stability of these fragments, their binding efficiency on to the sensor surface and bioactivity has not yet been fully tested.

7.1.3 Midland blotting as a supporting method

Successfully designed optical on-sensor chemiluminescence (Midland blotting) helped at every layer of sensor fabrication (**section 2.2.12**). It enabled to obtain critical chemical and biological information directly about sensor surfaces. The only critical step was to select the samples in such a way that the highest light emitting sample did not interfere with the low emitting samples. When unknown samples are to be analysed, it is always useful to use a known sample with high signal as a reference. When two low signal samples needed to be analysed, they were photographed in isolation so that their comparative emission could be easily visualized and compared. As a semi-quantitative optical method it was useful in sensor fabrication and to corroborate impedance data.

7.1.4 Sensor surface blocking

During the sensor fabrication process, a number of empty spaces can be generated on the sensor surface. These include unreacted chemical moieties in the polymer and gaps between immobilized antibodies. Thus, blocking these areas reduced the non-specific signal and enhanced the sensitivity of sensor. In full antibody based sensor format, it was observed that without blocking substantial non-specific

binding took place (**section 4.8**). The main reason behind this was found to be the interaction of the antibody Fc region with the M/H protein of *S. pyogenes*. Thus, protein A was employed as a blocking agent to specifically block the Fc region. However, like with any blocking agent, this decreased signal intensity as it also hindered some antibody binding sites. Later on, using BSA as a blocking agent was found to be useful when bacteria were detected in spiked human saliva.

In half antibody sensor format, instead of protein A, recombinant protein G was used as this was smaller in size and could serve the same purpose by blocking the free Fc of half antibodies. Similar patterns of decreased change in impedance was observed in half antibody based system. When the comparative sensitivity was analysed (**section 5.6, Figure 5.10**), the finding led to a hypothesis that in full antibody as the orientation of antibody is random, Fc bound protein A created blockade to many active sites (**Figure 7.1, A**). For this reason the signal ratio dropped. In contrast, as half antibodies are completely oriented and protein G is smaller than protein A, blocking of Fc did not occlude the binding site (**Figure 7.1, B**). Thus, blocking the sensor surface is very critical and specific attention is required to avoid unnecessary blocking of active sites on sensor surfaces.

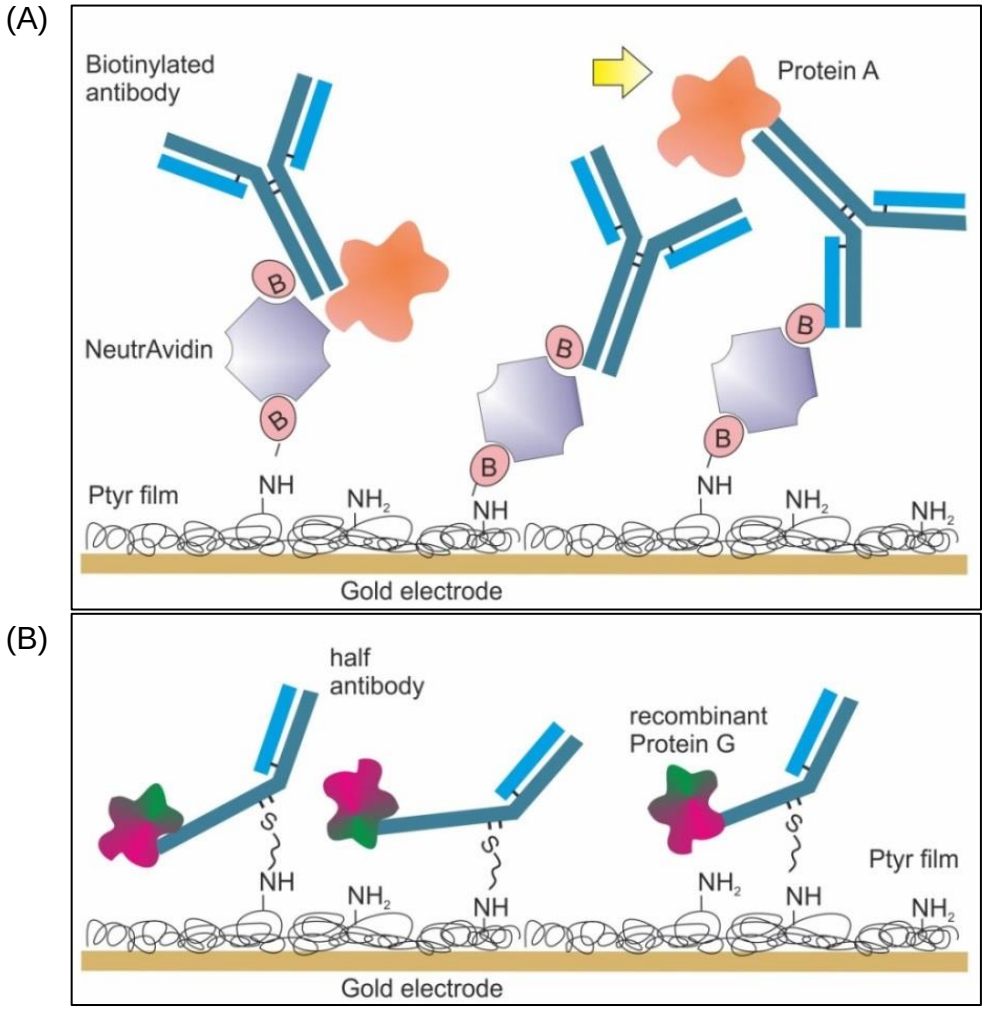

Figure 7.1: Plausible effect of protein A/G blocking in sensor construction

(A) Hypothesis describing the effect of protein A blocking in full antibody based sensors. Protein A bound to Fc portion of antibody can hinder the active site of other antibodies (arrow marked) and (B) the effect of recombinant protein G blocking in half antibody based sensors. Protein A bound to Fc of an antibody can hinder the antigen binding site of another antibody as the biotinylated antibodies are randomly oriented (arrow marked). In contrast, recombinant protein G are small and as the antibodies are highly oriented, the steric hindrance are expected to be minimum.

7.1.5 Software and data acquisition

During this project, Autolab GPES and FRA modules were used for data generation of CV and EIS respectively. These software cannot be operated side by side, and are incapable of data fitting while data collection is live. Because of this problem, additional time is required for data file conversion, data fitting with equivalent circuit model. Usually twelve hour data collection is followed by next day couple of hours of data conversion and another couple of hours post processing in another software. However, very recently our group has installed new Autolab software NOVA, which has the capability to support data acquisition while background measurement is progressing. The EIS data fitting is also real time and can be processed while data collection is active.

7.1.6 Point-of-care design perspective

How successfully the present system can be taken forward toward point of care device and can be commercialised? From the present available data, it can be strongly stated that, the quantitative data obtained from EIS can be enhanced by further optimizing several parameters like sensor surfaces, robotic incubation, and more trial with real patient samples. However, as funding in impedimetric sensor development is still overlooked, from the experience of glucose biosensor development it can be assumed that it will take long years of research and funding to reach market.

In terms of practical design perspective, several improvement should take place. How the sample will be incubated onto sensor surface (with or without a single step dilution or modification), its volume, post measurement disposal system are very critical. The accuracy, measurement capacity of hand held device and its cost are also of prime important. But, it can be achievable with rapid development of

miniaturization and large scale quality control provided money and research skill are not a limiting factor.

7.1.7 Future outlook

The success behind any biosensor project is all about precision and reproducibility. This can be critical during manufacturing, optimization or measurement. With the advent of nano level real time microscopy, it would be possible to monitor real time nano topographical changes on sensor surfaces. Imprinting bioreceptor in desired orientation is still the biggest challenges of all. It is also very tricky to design every layer so that real life samples have minimum interference with signal. Intelligent regeneration process along with multiplexing would enable to reduce overall costs. However, as biosensor is multi parametric system, ‘one optimization, fits all’ strategy will not work. Every individual target demands its own design and general findings can assist in specific decision making. It is hoped that the data derived knowledge from this thesis will be helpful for any future research in designing chip based sensor platform to detect whole organisms.

References

References

Abrahao, O., Machado, A.E.D., Silva, F.F.S., Madurro, J.M., de Castro, C.M., Sonoda, M.T., 2013. Tyramine electropolymerization revisited by DFT and experimental study. Journal of Molecular Structure, 1037, 200-208.

Ahmad, Z.A., Yeap, S.K., Ali, A.M., Ho, W.Y., Alitheen, N.B.M., Hamid, M., 2012. scFv Antibody: Principles and Clinical Application. Clinical & Developmental Immunology, 2012, 1-15.

Ahmed, A., Rushworth, J.V., Hirst, N.A., Millner, P.A., 2014. Biosensors for Whole-Cell Bacterial Detection. Clinical Microbiology Reviews, 27, 631-646.

Ahmed, A., Rushworth, J.V., Wright, J.D., Millner, P.A., 2013. Novel Impedimetric Irnmunosensor for Detection of Pathogenic Bacteria *Streptococcus pyogenes* in Human Saliva. Analytical Chemistry, 85, 12118-12125.

Akesson, P., Schmidt, K.H., Cooney, J., Bjorck, L., 1994. M1-Protein and Protein-H - IgG Fc-Binding and Albumin-Binding Streptococcal Surface-Proteins Encoded by Adjacent Genes. Biochemical Journal, 300, 877-886.

Alon, R., Bayer, E.A., Wilchek, M., 1990. Streptavidin Contains an RYD Sequence Which Mimics the RGD Receptor Domain of Fibronectin. Biochemical and Biophysical Research Communications, 170, 1236-1241.

Arlett, J.L., Myers, E.B., Roukes, M.L., 2011. Comparative advantages of mechanical biosensors. Nature Nanotechnology, 6, 203-215.

Arwin, H., Poksinski, M., Johansen, K., 2004. Total internal reflection ellipsometry: principles and applications. Applied Optics, 43, 3028-3036.

Aziz, R.K., Kotb, M., 2008. Rise and persistence of global M1T1 clone of *Streptococcus pyogenes*. Emerging Infectious Diseases, 14, 1511-1517.

Baccar, H., Mejri, M.B., Hafaiedh, I., Ktari, T., Aouni, M., Abdelghani, A., 2010. Surface plasmon resonance immunosensor for bacteria detection. Talanta, 82, 810-814.

Bamberger, D.M., 2010. Diagnosis, initial management, and prevention of meningitis. Am Fam Physician, 82, 1491-1498.

Bard, A.J., Faulkner, L.R., 2001. Electrochemical methods: fundamentals and applications. Wiley.

Barletta, F., Mercado, E.H., Lluque, A., Ruiz, J., Cleary, T.G., Ochoa, T.J., 2013. Multiplex real-time PCR for detection of campylobacter, salmonella, and Shigella. Journal of Clinical Microbiology, 51, 2822-2829.

Barreiros dos Santos, M., Agusil, J.P., Prieto-Simón, B., Sporer, C., Teixeira, V., Samitier, J., 2013. Highly sensitive detection of pathogen Escherichia coli O157:H7 by electrochemical impedance spectroscopy. Biosensors and Bioelectronics, 45, 174-180.

Bhalla, V., Zazubovich, V., 2011. Self-assembly and sensor response of photosynthetic reaction centers on screen-printed electrodes. Analytica Chimica Acta, 707, 184-190.

Billah, M., Hays, H.C.W., Millner, P.A., 2008. Development of a myoglobin impedimetric immunosensor based on mixed self-assembled monolayer onto gold. Microchimica Acta, 160, 447-454.

Billah, M.M., Hodges, C.S., Hays, H.C.W., Millner, P.A., 2010. Directed immobilization of reduced antibody fragments onto a novel SAM on gold for myoglobin impedance immunosensing. Bioelectrochemistry, 80, 49-54.

Bisno, A.L., Brito, M.O., Collins, C.M., 2003. Molecular basis of group A streptococcal virulence. Lancet Infectious Diseases, 3, 191-200.

Boehme, C.C., Saacks, S., O'Brien, R.J., 2013. The changing landscape of diagnostic services for tuberculosis. Semin Respir Crit Care Med, 34, 17-31.

Borisov, S.M., Wolfbeis, O.S., 2008. Optical biosensors. Chemical Reviews, 108, 423-461.

Brogan, K.L., Wolfe, K.N., Jones, P.A., Schoenfisch, M.H., 2003. Direct oriented immobilization of F(ab ') antibody fragments on gold. Analytica Chimica Acta, 496, 73-80.

Buchapudi, K.R., Huang, X., Yang, X., Ji, H.F., Thundat, T., 2011. Microcantilever biosensors for chemicals and bioorganisms. Analyst, 136, 1539-1556.

Campbell, G.A., Mutharasan, R., 2005. Detection of pathogen Escherichia coli O157 : H7 using self-excited PZT-glass microcantilevers. Biosensors & Bioelectronics, 21, 462-473.

Campbell, G.A., Mutharasan, R., 2007. A method of measuring Escherichia coli O157 : H7 at 1 cell/ml in 1 liter sample using antibody functionalized

piezoelectric-excited millimeter-sized cantilever sensor. Environmental Science & Technology, 41, 1668-1674.

Carapetis, J.R., Steer, A.C., Mulholland, E.K., Weber, M., 2005. The global burden of group A streptococcal diseases. Lancet Infectious Diseases, 5, 685-694.

Carroll, K.C., 2002. Laboratory diagnosis of lower respiratory tract infections: Controversy and conundrums. Journal of Clinical Microbiology, 40, 3115-3120.

Caygill, R.L., 2012. Developing an electrochemical assay to detect and quantify virus particles, PhD Thesis, University of Leeds.

Caygill, R.L., Hodges, C.S., Holmes, J.L., Higson, S.P.J., Blair, G.E., Millner, P.A., 2012. Novel impedimetric immunosensor for the detection and quantitation of Adenovirus using reduced antibody fragments immobilized onto a conducting copolymer surface. Biosensors & Bioelectronics, 32, 104-110.

Chan, K.Y., Ye, W.W., Zhang, Y., Xiao, L.D., Leung, P.H.M., Li, Y., Yang, M., 2013. Ultrasensitive detection of E. coli O157:H7 with biofunctional magnetic bead concentration via nanoporous membrane based electrochemical immunosensor. Biosensors & Bioelectronics, 41, 532-537.

Charlermroj, R., Oplatowska, M., Gajanandana, O., Himananto, O., Grant, I.R., Karoonuthaisiri, N., Elliott, C.T., 2013. Strategies to improve the surface plasmon resonance-based immmunodetection of bacterial cells. Microchimica Acta, 180, 643-650.

Chaubey, A., Malhotra, B.D., 2002. Mediated biosensors. Biosensors & Bioelectronics, 17, 441-456.

Cheng, I.F., Chang, H.C., Chen, T.Y., Hu, C.M., Yang, F.L., 2013. Rapid (<5 min) Identification of Pathogen in Human Blood by Electrokinetic Concentration and Surface-Enhanced Raman Spectroscopy. Scientific Reports, 3.

Chiang, W.H., Chen, P.Y., Nien, P.C., Ho, K.C., 2011. Amperometric detection of cholesterol using an indirect electrochemical oxidation method. Steroids, 76, 1535-1540.

Chullasat, K., Kanatharana, P., Limbut, W., Numnuam, A., Thavarungkul, P., 2011. Ultra trace analysis of small molecule by label-free impedimetric immunosensor using multilayer modified electrode. Biosensors & Bioelectronics, 26, 4571-4578.

Clark, L.C., Lyons, C., 1962. Electrode systems for continuous monitoring in cardiovascular surgery. Annals of the New York Academy of Sciences, 102, 29-45.

Cole, J.N., Barnett, T.C., Nizet, V., Walker, M.J., 2011. Molecular insight into invasive group A streptococcal disease. Nature Reviews Microbiology, 9, 724-736.

Conroy, D.J.R., Millner, P.A., Stewart, D.I., Pollmann, K., 2010. Biosensing for the Environment and Defence: Aqueous Uranyl Detection Using Bacterial Surface Layer Proteins. Sensors, 10, 4739-4755.

Cortina-Puig, M., Munoz-Berbel, X., Calas-Blanchard, C., Marty, J.L., 2009. Electrochemical characterization of a superoxide biosensor based on the co-immobilization of cytochrome c and XOD on SAM-modified gold electrodes and application to garlic samples. Talanta, 79, 289-294.

Croxen, M.A., Law, R.J., Scholz, R., Keeney, K.M., Wlodarska, M., Finlay, B.B., 2013. Recent Advances in Understanding Enteric Pathogenic Escherichia coli. Clinical Microbiology Reviews, 26, 822-880.

Cunningham, M.W., 2000. Pathogenesis of group A streptococcal infections. Clinical Microbiology Reviews, 13, 470-511.

Davis, F., Higson, S.P.J., 2012. Practical applications and protocols for enzyme biosensors. Biosensors for Medical Applications, 135-160.

Davis, F., Higson, S.P.J., 2013. Arrays of microelectrodes: technologies for environmental investigations. Environmental Science-Processes & Impacts, 15, 1477-1489.

de Avila, B.E.F., Pedrero, M., Campuzano, S., Escamilla-Gomez, V., Pingarron, J.M., 2012. Sensitive and rapid amperometric magnetoimmunosensor for the determination of Staphylococcus aureus. Analytical and Bioanalytical Chemistry, 403, 917-925.

de Castro, C.M., Vieira, S.N., Goncalves, R.A., Brito-Madurro, A.G., Madurro, J.M., 2008. Electrochemical and morphologic studies of nickel incorporation on graphite electrodes modified with polytyramine. Journal of Materials Science, 43, 475-482.

de la Rica, R., Baldi, A., Fernandez-Sanchez, C., Matsui, H., 2009. Selective Detection of Live Pathogens via Surface-Confined Electric Field Perturbation on Interdigitated Silicon Transducers. Analytical Chemistry, 81, 3830-3835.

Dweik, M., Stringer, R.C., Dastider, S.G., Wu, Y.F., Almasri, M., Barizuddin, S., 2012. Specific and targeted detection of viable Escherichia coli O157:H7 using a sensitive and reusable impedance biosensor with dose and time response studies. Talanta, 94, 84-89.

Escamilla-Gomez, V., Campuzano, S., Pedrero, M., Pingarron, J.M., 2008. Electrochemical immunosensor designs for the determination of Staphylococcus aureus using 3,3-dithiodipropionic acid di(N-succinimidyl ester)-modified gold electrodes. Talanta, 77, 876-881.

Fan, X.D., White, I.M., Shopova, S.I., Zhu, H.Y., Suter, J.D., Sun, Y.Z., 2008. Sensitive optical biosensors for unlabeled targets: A review. Analytica Chimica Acta, 620, 8-26.

Fanjul-Bolado, P., Hernandez-Santos, D., Lamas-Ardisana, P.J., Martin-Pernia, A., Costa-Garcia, A., 2008. Electrochemical characterization of screen-printed and conventional carbon paste electrodes. Electrochimica Acta, 53, 3635-3642.

Ferreira, D.C., Machado, A.E.H., Tiago, F.D., Madurro, J.M., Madurro, A.G.B., Abrahao, O., 2012. Molecular modeling study on the possible polymers formed during the electropolymerization of 3-hydroxyphenylacetic acid. Journal of Molecular Graphics & Modelling, 34, 18-27.

Ferreira, L.F., Souza, L.M., Franco, D.L., Castro, A.C.H., Oliveira, A.A., Boodts, J.F.C., Brito-Madurro, A.G., Madurro, J.M., 2011. Formation of novel polymeric films derived from 4-hydroxybenzoic acid. Materials Chemistry and Physics, 129, 46-52.

Fischetti, V.A., 1989. Streptococcal M-Protein - Molecular Design and Biological Behavior. Clinical Microbiology Reviews, 2, 285-314.

Fisher, A.C., 1996. Electrode dynamics. Oxford university press, New York.

Frick, I.M., Akesson, P., Cooney, J., Sjobring, U., Schmidt, K.H., Gomi, H., Hattori, S., Tagawa, C., Kishimoto, F., Bjorck, L., 1994. Protein-H - a Surface Protein of Streptococcus-Pyogenes with Separate Binding-Sites for Igg and Albumin. Molecular Microbiology, 12, 143-151.

Fronczek, C.F., You, D.J., Yoon, J.-Y., 2013. Single-pipetting microfluidic assay device for rapid detection of Salmonella from poultry package. Biosensors and Bioelectronics, 40, 342-349.

Garcia-Gonzalez, R., Fernandez-Abedul, M.T., Pernia, A., Costa-Garcia, A., 2008. Electrochemical characterization of different screen-printed gold electrodes. Electrochimica Acta, 53, 3242-3249.

Gasparyan, V.K., Bazukyan, I.L., 2013. Lectin sensitized anisotropic silver nanoparticles for detection of some bacteria. Analytica Chimica Acta, 766, 83-87.

Geng, P., Zhang, X., Meng, W., Wang, Q., Zhang, W., Jin, L., Feng, Z., Wu, Z., 2008. Self-assembled monolayers-based immunosensor for detection of Escherichia coli using electrochemical impedance spectroscopy. Electrochimica Acta, 53, 4663-4668.

Geng, T., Uknalis, J., Tu, S.I., Bhunia, A.K., 2006. Fiber-optic biosensor employing Alexa-Fluor conjugated antibody for detection of Escherichia coli O157 : H7 from ground beef in four hours. Sensors, 6, 796-807.

Gerber, M.A., Shulman, S.T., 2004. Rapid diagnosis of pharyngitis caused by group A streptococci. Clinical Microbiology Reviews, 17, 571-580.

Gerber, M.A., Spadaccini, L.J., Wright, L.L., Deutsch, L., 1984. Latex Agglutination Tests for Rapid Identification of Group-a Streptococci Directly from Throat Swabs. Journal of Pediatrics, 105, 702-705.

Getz, E.B., Xiao, M., Chakrabarty, T., Cooke, R., Selvin, P.R., 1999. A comparison between the sulfhydryl reductants tris(2-carboxyethyl)phosphine and dithiothreitol for use in protein biochemistry. Analytical Biochemistry, 273, 73-80.

Golmohammadi, R., Valegard, K., Fridborg, K., Liljas, L., 1993. The Refined Structure of Bacteriophage-MS2 at 2.8 Angstrom Resolution. Journal of Molecular Biology, 234, 620-639.

Gomi, H., Hozumi, T., Hattori, S., Tagawa, C., Kishimoto, F., Bjorck, L., 1990. The Gene Sequence and Some Properties of Protein-H - a Novel Igg-Binding Protein. Journal of Immunology, 144, 4046-4052.

Grieshaber, D., MacKenzie, R., Voros, J., Reimhult, E., 2008. Electrochemical biosensors - Sensor principles and architectures. Sensors, 8, 1400-1458.

Guo, X., Lin, C.S., Chen, S.H., Ye, R., Wu, V.C.H., 2012a. A piezoelectric immunosensor for specific capture and enrichment of viable pathogens by quartz crystal microbalance sensor, followed by detection with antibody-functionalized gold nanoparticles. Biosensors & Bioelectronics, 38, 177-183.

Guo, X.F., Kulkarni, A., Doepke, A., Halsall, H.B., Iyer, S., Heineman, W.R., 2012b. Carbohydrate-Based Label-Free Detection of Escherichia coli ORN 178 Using Electrochemical Impedance Spectroscopy. Analytical Chemistry, 84, 241-246.

Hao, R., Wang, D., Zhang, X.e., Zuo, G., Wei, H., Yang, R., Zhang, Z., Cheng, Z., Guo, Y., Cui, Z., Zhou, Y., 2009. Rapid detection of Bacillus anthracis using monoclonal antibody functionalized QCM sensor. Biosensors and Bioelectronics, 24, 1330-1335.

Hassanzadeh-Ghassabeh, G., Devoogdt, N., De Pauw, P., Vincke, C., Muyldermans, S., 2013. Nanobodies and their potential applications. Nanomedicine, 8, 1013-1026.

Hassen, W.M., Duplan, V., Frost, E., Dubowski, J.J., 2011. Quantitation of influenza A virus in the presence of extraneous protein using electrochemical impedance spectroscopy. Electrochimica Acta, 56, 8325-8328.

Hays, H.C.W., Millner, P.A., Prodromidis, M.I., 2006. Development of capacitance based immunosensors on mixed self-assembled monolayers. Sensors and Actuators B-Chemical, 114, 1064-1070.

Heath, D.G., Cleary, P.P., 1989. Fc-Receptor and M-Protein Genes of Group-a Streptococci Are Products of Gene Duplication. Proceedings of the National Academy of Sciences of the United States of America, 86, 4741-4745.

Heinze, J., 1984. Cyclic Voltammetry - Electrochemical Spectroscopy. Angewandte Chemie-International Edition in English, 23, 831-847.

Hermanson, G.T., 2008a. Bioconjugate Techniques. Academic Press.

Hermanson, G.T., 2008b. Chapter 5 - Heterobifunctional Crosslinkers. In: Hermanson, G.T. (Ed.), Bioconjugate Techniques (Second Edition). Academic Press, New York, pp. 276-335.

Hirst, N.A., Hazelwood, L.D., Jayne, D.G., Millner, P.A., 2013. An amperometric lactate biosensor using H2O2 reduction via a Prussian Blue impregnated poly(ethyleneimine) surface on screen printed carbon electrodes to detect anastomotic leak and sepsis. Sensors and Actuators B-Chemical, 186, 674-680.

Hleli, S., Martelet, C., Abdelghani, A., Burais, N., Jaffrezic-Renault, N., 2006. Atrazine analysis using an impedimetric immunosensor based on mixed biotinylated self-assembled monolayer. Sensors and Actuators B-Chemical, 113, 711-717.

Holford, T.R.J., Holmes, J.L., Collyer, S.D., Davis, F., Higson, S.P.J., 2013. Label-free impedimetric immunosensors for psoriasin-Increased reproducibility and sensitivity using an automated dispensing system. Biosensors & Bioelectronics, 44, 198-203.

Hong, J.M., Lee, A., Han, H., Kim, J., 2009. Structural characterization of immunoglobulin G using time-dependent disulfide bond reduction. Analytical Biochemistry, 384, 368-370.

Hou, Y.X., Helali, S., Zhang, A.D., Jaffrezic-Renault, N., Martelet, C., Minic, J., Gorojankina, T., Persuy, M.A., Pajot-Augy, E., Salesse, R., Bessueille, F., Samitier, J., Errachid, A., Akimov, V., Reggiani, L., Pennetta, C., Alfinito, E., 2006. Immobilization of rhodopsin on a self-assembled multilayer and its specific detection by electrochemical impedance spectroscopy. Biosensors & Bioelectronics, 21, 1393-1402.

Hu, C.M.J., Kaushal, S., Cao, H.S.T., Aryal, S., Sartor, M., Esener, S., Bouvet, M., Zhang, L.F., 2010. Half-Antibody Functionalized Lipid-Polymer Hybrid Nanoparticles for Targeted Drug Delivery to Carcinoembryonic Antigen Presenting Pancreatic Cancer Cells. Molecular Pharmaceutics, 7, 914-920.

Huang, J.L., Yang, G.J., Meng, W.J., Wu, L.P., Zhu, A.P., Jiao, X.A., 2010. An electrochemical impedimetric immunosensor for label-free detection of Campylobacter jejuni in diarrhea patients' stool based on O-carboxymethylchitosan surface modified Fe3O4 nanoparticles. Biosensors & Bioelectronics, 25, 1204-1211.

Ivnitski, D., Abdel-Hamid, I., Atanasov, P., Wilkins, E., 1999. Biosensors for detection of pathogenic bacteria. Biosensors & Bioelectronics, 14, 599-624.

Ji, H.F., Yan, X.D., Zhang, J., Thundat, T., 2004. Molecular recognition of biowarfare agents using micromechanical sensors. Expert Review of Molecular Diagnostics, 4, 859-866.

Jiang, X.S., Wang, R.H., Wang, Y., Su, X.L., Ying, Y.B., Wang, J.P., Li, Y.B., 2011. Evaluation of different micro/nanobeads used as amplifiers in QCM immunosensor for more sensitive detection of E. coli O157:H7. Biosensors & Bioelectronics, 29, 23-28.

Joung, C.-K., Kim, H.-N., Im, H.-C., Kim, H.-Y., Oh, M.-H., Kim, Y.-R., 2012. Ultra-sensitive detection of pathogenic microorganism using surface-engineered

impedimetric immunosensor. Sensors and Actuators B-Chemical, 161, 824-831.

Joung, C.-K., Kim, H.-N., Lim, M.-C., Jeon, T.-J., Kim, H.-Y., Kim, Y.-R., 2013. A nanoporous membrane-based impedimetric immunosensor for label-free detection of pathogenic bacteria in whole milk. Biosensors and Bioelectronics, 44, 210-215.

Kadara, R.O., Jenkinson, N., Banks, C.E., 2009. Characterisation of commercially available electrochemical sensing platforms. Sensors and Actuators B-Chemical, 138, 556-562.

Khudaish, E.A., Al-Ajmi, K.Y., Al-Harthi, S.H., Al-Hinai, A.T., 2012. A solid state sensor based polytyramine film modified electrode for the determination of dopamine and ascorbic acid in a moderately acidic solution. Journal of Electroanalytical Chemistry, 676, 27-34.

Kim, H.J., Bennetto, H.P., Halablab, M.A., Choi, C.H., Yoon, S., 2006. Performance of an electrochemical sensor with different types of liposomal mediators for the detection of hemolytic bacteria. Sensors and Actuators B-Chemical, 119, 143-149.

La Belle, J.T., Shah, M., Reed, J., Nandakumar, V., Alford, T.L., Wilson, J.W., Nickerson, C.A., Joshi, L., 2009. Label-Free and Ultra-Low Level Detection of Salmonella enterica Serovar Typhimurium Using Electrochemical Impedance Spectroscopy. Electroanalysis, 21, 2267-2271.

Labib, M., Hedstrom, M., Amin, M., Mattiasson, B., 2010. A novel competitive capacitive glucose biosensor based on concanavalin A-labeled nanogold colloids assembled on a polytyramine-modified gold electrode. Analytica Chimica Acta, 659, 194-200.

Laczka, O., Maesa, J.M., Godino, N., del Campo, J., Fougt-Hansen, M., Kutter, J.P., Snakenborg, D., Munoz-Pascual, F.X., Baldrich, E., 2011. Improved bacteria detection by coupling magneto-immunocapture and amperometry at flow-channel microband electrodes. Biosensors & Bioelectronics, 26, 3633-3640.

Lamagni, T.L., Darenberg, J., Luca-Harari, B., Siljander, T., Efstratiou, A., Henriques-Normark, B., Vuopio-Varkila, J., Bouvet, A., Creti, R., Ekelund, K., Koliou, M., Reinert, R.R., Stathi, A., Strakova, L., Ungureanu, V., Schalen, C.,

Jasir, A., Grp, S.-E.S., 2008. Epidemiology of severe Streptococcus pyogenes disease in Europe. Journal of Clinical Microbiology, 46, 2359-2367.

Lang, H.P., Gerber, C., 2008. Microcantilever sensors. Stm and Afm Studies on (Bio)Molecular Systems: Unravelling the Nanoworld, 285, 1-27.

Li, Y., Fang, L.C., Cheng, P., Deng, J., Jiang, L.L., Huang, H., Zheng, J.S., 2013. An electrochemical immunosensor for sensitive detection of Escherichia coli O157:H7 using C-60 based biocompatible platform and enzyme functionalized Pt nanochains tracing tag. Biosensors & Bioelectronics, 49, 485-491.

Ligler, F.S., Sapsford, K.E., Golden, J.P., Shriver-Lake, L.C., Taitt, C.R., Dyer, M.A., Barone, S., Myatt, C.J., 2007. The array biosensor: portable, automated systems. Analytical Sciences, 23, 5-10.

Lisdat, F., Schafer, D., 2008. The use of electrochemical impedance spectroscopy for biosensing. Anal Bioanal Chem, 391, 1555-1567.

Liu, M.Q., Jiang, J.H., Feng, Y.L., Shen, G.L., Yu, R.Q., 2007. Glucose biosensor based on immobilization of glucose oxidase in electrochemically polymerized polytyramine film and overoxidised polypyrrole film on platinized carbon paste electrode. Chinese Journal of Analytical Chemistry, 35, 1435-1438.

Loaiza, O.A., Campuzano, S., Pedrero, M., Pingaron, J.M., 2008. Designs of enterobacteriaceae lac Z gene DNA gold screen printed biosensors. Electroanalysis, 20, 1397-1405.

Losic, D., Cole, M., Thissen, H., Voelcker, N.H., 2005. Ultrathin polytyramine films by electropolymerisation on highly doped p-type silicon electrodes. Surface Science, 584, 245-257.

Lu, L., Chee, G., Yamada, K., Jun, S., 2013. Electrochemical impedance spectroscopic technique with a functionalized microwire sensor for rapid detection of foodbornepathogens. Biosensors & Bioelectronics, 42, 492-495.

Lux, F., 1994. Properties of Electronically Conductive Polyaniline - a Comparison between Well-Known Literature Data and Some Recent Experimental Findings. Polymer, 35, 2915-2936.

Maalouf, R., Fournier-Wirth, C., Coste, J., Chebib, H., Saikali, Y., Vittori, O., Errachid, A., Cloarec, J.P., Martelet, C., Jaffrezic-Renault, N., 2007. Label-free detection of bacteria by electrochemical impedance spectroscopy:

Comparison to surface plasmon resonance. Analytical Chemistry, 79, 4879-4886.

Macdiarmid, A.G., Chiang, J.C., Richter, A.F., Epstein, A.J., 1987. Polyaniline - a New Concept in Conducting Polymers. Synthetic Metals, 18, 285-290.

Macdonald, D.D., 2006. Reflections on the history of electrochemical impedance spectroscopy. Electrochimica Acta, 51, 1376-1388.

Makaraviciute, A., Ramanaviciene, A., 2013. Site-directed antibody immobilization techniques for immunosensors. Biosensors & Bioelectronics, 50, 460-471.

Mandler, D., Kraus-Ophir, S., 2011. Self-assembled monolayers (SAMs) for electrochemical sensing. Journal of Solid State Electrochemistry, 15, 1535-1558.

Manjappa, A.S., Chaudhari, K.R., Venkataraju, M.P., Dantuluri, P., Nanda, B., Sidda, C., Sawant, K.K., Murthy, R.S.R., 2011. Antibody derivatization and conjugation strategies: Application in preparation of stealth immunoliposome to target chemotherapeutics to tumor. Journal of Controlled Release, 150, 2-22.

Mannoor, M.S., Zhang, S.Y., Link, A.J., McAlpine, M.C., 2010. Electrical detection of pathogenic bacteria via immobilized antimicrobial peptides. Proceedings of the National Academy of Sciences of the United States of America, 107, 19207-19212.

Mantzila, A.G., Maipa, V., Prodromidis, M.I., 2008. Development of a faradic impedimetric immunosensor for the detection of Salmonella typhimurium in milk. Analytical Chemistry, 80, 1169-1175.

Massad-Ivanir, N., Shtenberg, G., Tzur, A., Krepker, M.A., Segal, E., 2011. Engineering Nanostructured Porous SiO2 Surfaces for Bacteria Detection via "Direct Cell Capture". Analytical Chemistry, 83, 3282-3289.

Mejri, M.B., Baccar, H., Baldrich, E., Del Campo, F.J., Helali, S., Ktari, T., Simonian, A., Aouni, M., Abdelghani, A., 2010. Impedance biosensing using phages for bacteria detection: Generation of dual signals as the clue for in-chip assay confirmation. Biosensors and Bioelectronics, 26, 1261-1267.

Miao, Y.Q., Chen, J.R., Hu, Y., 2005. Electrodeposited nonconducting polytyramine for the development of glucose biosensors. Analytical Biochemistry, 339, 41-45.

Miscoria, S.A., Barrera, G.D., Rivas, G.A., 2006. Glucose biosensors based on the immobilization of glucose oxidase and polytyramine on rodhinized glassy carbon and screen printed electrodes. Sensors and Actuators B-Chemical, 115, 205-211.

Moreira, F.T.C., Dutra, R.A.F., Noronha, J.P.C., Sales, M.G.F., 2013. Electrochemical biosensor based on biomimetic material for myoglobin detection. Electrochimica Acta, 107, 481-487.

Mouffouk, F., Rosa da Costa, A.M., Martins, J., Zourob, M., Abu-Salah, K.M., Alrokayan, S.A., 2011. Development of a highly sensitive bacteria detection assay using fluorescent pH-responsive polymeric micelles. Biosensors and Bioelectronics, 26, 3517-3523.

Muyldermans, S., 2013. Nanobodies: Natural Single-Domain Antibodies. Annual Review of Biochemistry, Vol 82, 82, 775-797.

Neufeld, T., Schwartz-Mittelmann, A., Biran, D., Ron, E.Z., Rishpon, J., 2003. Combined phage typing and amperometric detection of released enzymatic activity for the specific identification and quantification of bacteria. Analytical Chemistry, 75, 580-585.

Nordenfelt, P., Waldemarson, S., Linder, A., Morgelin, M., Karlsson, C., Malmstrom, J., Bjorck, L., 2012. Antibody orientation at bacterial surfaces is related to invasive infection. Journal of Experimental Medicine, 209, 2367-2381.

O'Neill, R.D., Chang, S.C., Lowry, J.P., McNeil, C.J., 2004. Comparisons of platinum, gold, palladium and glassy carbon as electrode materials in the design of biosensors for glutamate. Biosensors & Bioelectronics, 19, 1521-1528.

Orozco, J., Medlin, L.K., 2011. Electrochemical performance of a DNA-based sensor device for detecting toxic algae. Sensors and Actuators B-Chemical, 153, 71-77.

Owen, V., 1997. Real-time optical immunosensors, a commercial reality. Biosensors and Bioelectronics, 12, i-ii.

Pfeiffer, M.L., DuPont, H.L., Ochoa, T.J., 2012. The patient presenting with acute dysentery--a systematic review. J Infect, 64, 374-386.

Pliquett, U., Frense, D., Schonfeldt, M., Fratzer, C., Zhang, Y., Cahill, B., Metzen, M., Barthel, A., Nacke, T., Beckmann, D., 2010. Testing miniaturized

electrodes for impedance measurements within the beta-dispersion – a practical approach. Journal of Electrical Bioimpedance, 1, 41-55.

Pournaras, A.V., Koraki, T., Prodromidis, M.I., 2008. Development of an impedimetric immunosensor based on electropolymerized polytyramine films for the direct detection of Salmonella typhimurium in pure cultures of type strains and inoculated real samples. Analytica Chimica Acta, 624, 301-307.

Prodromidis, M.I., 2010. Impedimetric immunosensors-A review. Electrochimica Acta, 55, 4227-4233.

Qi, P., Wan, Y., Zhang, D., 2013. Impedimetric biosensor based on cell-mediated bioimprinted films for bacterial detection. Biosensors & Bioelectronics, 39, 282-288.

Radi, A.E., Munoz-Berbel, X., Cortina-Puig, M., Marty, J.L., 2009. An electrochemical immunosensor for ochratoxin A based on immobilization of antibodies on diazonium-functionalized gold electrode. Electrochimica Acta, 54, 2180-2184.

Rahman, A.R.A., Price, D.T., Bhansali, S., 2007. Effect of electrode geometry on the impedance evaluation of tissue and cell culture. Sensors and Actuators B-Chemical, 127, 89-96.

Randles, J.E.B., 1947. Kinetics of Rapid Electrode Reactions. Discussions of the Faraday Society, 1, 11-19.

Ray, P.C., Khan, S.A., Singh, A.K., Senapati, D., Fan, Z., 2012. Nanomaterials for targeted detection and photothermal killing of bacteria. Chemical Society Reviews, 41, 3193-3209.

Read, P.J., Donovan, B., 2012. Clinical aspects of adult syphilis. Intern Med J, 42, 614-620.

Report, 2011. Group A streptococcal infections: seasonal activity 2010/11. In, Health Protection Report, Vol. 5. Health Protection Agency, City.

Richman, S., Kranz, D., Stone, J., 2009. Biosensor Detection Systems: Engineering Stable, High-Affinity Bioreceptors by Yeast Surface Display. In: Rasooly, A., Herold, K. (Eds.), Biosensors and Biodetection, Vol. 504. Humana Press, pp. 323-350.

Rushworth, J.V., Ahmed, A., Griffiths, H.H., Pollock, N.M., Hooper, N.M., Millner, P.A., 2014. A label-free electrical impedimetric biosensor for the specific

detection of Alzheimer's amyloid-beta oligomers. Biosensors & Bioelectronics, 56, 83-90.

Rushworth, J.V., Ahmed, A., Millner, P.A., 2013a. Midland blotting: a rapid, semi-quantitative method for biosensor surface characterization. Journal of Biosensors and Bioelectronics, 4, 1-7.

Rushworth, J.V., Hirst, N.A., Goode, A.J., Pike, D.J., Ahmed, A., Millner, P.A., 2013b. Impedimetric Biosensors for Medical Applications: Current Progress and Challenges. ASME and Momentum Press, 2, Park Avenue, NY 10016, USA.

Saerens, D., Huang, L., Bonroy, K., Muyldermans, S., 2008. Antibody fragments as probe in biosensor development. Sensors, 8, 4669-4686.

Salam, F., Uludag, Y., Tothill, I.E., 2013. Real-time and sensitive detection of Salmonella Typhimurium using an automated quartz crystal microbalance (QCM) instrument with nanoparticles amplification. Talanta, 115, 761-767.

Salleh, M.H.M., Glidle, A., Sorel, M., Reboud, J., Cooper, J.M., 2013. Polymer dual ring resonators for label-free optical biosensing using microfluidics. Chemical Communications, 49, 3095-3097.

Scallan, E., Hoekstra, R.M., Angulo, F.J., Tauxe, R.V., Widdowson, M.A., Roy, S.L., Jones, J.L., Griffin, P.M., 2011. Foodborne illness acquired in the United States--major pathogens. Emerging Infectious Diseases, 17, 7-15.

Schirhagl, R., 2014. Bioapplications for Molecularly Imprinted Polymers. Analytical Chemistry, 86, 250-261.

Schreiber, F., 2000. Structure and growth of self-assembling monolayers. Progress in Surface Science, 65, 151-256.

Schwabe, L.D., Gobbo, A.F., Gottschall, R.L., Randall, E.L., 1991. Comparison of Testpack Plus Strep-a with Selective and Nonselective Culture Media for Detection of Group-a Streptococci. Diagnostic Microbiology and Infectious Disease, 14, 367-372.

Sepulveda, B., Angelome, P.C., Lechuga, L.M., Liz-Marzan, L.M., 2009. LSPR-based nanobiosensors. Nano Today, 4, 244-251.

Shabani, A., Zourob, M., Allain, B., Marquette, C.A., Lawrence, M.F., Mandeville, R., 2008. Bacteriophage-Modified Microarrays for the Direct Impedimetric Detection of Bacteria. Analytical Chemistry, 80, 9475-9482.

Shahidan, M.A., 2012. Development of impedimetric biosensors for carbohydrate detection, PhD Thesis, University of Leeds.

Shang, F.J., Liu, Y.L., Hrapovic, S., Glennon, J.D., Luong, J.H.T., 2009. Selective detection of dopamine using a combined permselective film of electropolymerized (poly-tyramine and poly-pyrrole-1-propionic acid) on a boron-doped diamond electrode. Analyst, 134, 519-527.

Sharma, H., Mutharasan, R., 2013a. Half Antibody Fragments Improve Biosensor Sensitivity without Loss of Selectivity. Analytical Chemistry, 85, 2472-2477.

Sharma, H., Mutharasan, R., 2013b. Rapid and sensitive immunodetection of Listeria monocytogenes in milk using a novel piezoelectric cantilever sensor. Biosensors and Bioelectronics, 45, 158-162.

Sharma, H., Mutharasan, R., 2013c. Review of biosensors for foodborne pathogens and toxins. Sensors and Actuators B: Chemical, 183, 535-549.

Shen, J., Liu, C.C., 2007. Development of a screen-printed cholesterol biosensor: Comparing the performance of gold and platinum as the working electrode material and fabrication using a self-assembly approach. Sensors and Actuators B-Chemical, 120, 417-425.

Siddiqui, S., Dai, Z.T., Stavis, C.J., Zeng, H.J., Moldovan, N., Hamers, R.J., Carlisle, J.A., Arumugam, P.U., 2012. A quantitative study of detection mechanism of a label-free impedance biosensor using ultrananocrystalline diamond microelectrode array. Biosensors & Bioelectronics, 35, 284-290.

Smeesters, P.R., McMillan, D.J., Sriprakash, K.S., 2010. The streptococcal M protein: a highly versatile molecule. Trends Microbiol, 18, 275-282.

Stockley, P.G., Stonehouse, N.J., Valegard, K., 1994. Molecular Mechanism of Rna Phage Morphogenesis. International Journal of Biochemistry, 26, 1249-1260.

Stumpp, M.T., Amstutz, P., 2007. DARPins: A true alternative to antibodies. Current Opinion in Drug Discovery & Development, 10, 153-159.

Su, L., Jia, W., Hou, C., Lei, Y., 2011a. Microbial biosensors: A review. Biosensors & Bioelectronics, 26, 1788-1799.

Su, W.-H., Tsou, T.-S., Chen, C.-S., Ho, T.-Y., Lee, W.-L., Yu, Y.-Y., Chen, T.-J., Tan, C.-H., Wang, P.-H., 2011b. Are we satisfied with the tools for the diagnosis of gonococcal infection in females? Journal of the Chinese Medical Association, 74, 430-434.

Sumby, P., Porcella, S.F., Madrigal, A.G., Barbian, K.D., Virtaneva, K., Ricklefs, S.M., Sturdevant, D.E., Graham, M.R., Vuopio-Varkila, J., Hoe, N.P., Musser, J.M., 2005. Evolutionary origin and emergence of a highly successful clone of serotype M1 group A Streptococcus involved multiple horizontal gene transfer events. Journal of Infectious Diseases, 192, 771-782.

Sungkanak, U., Sappat, A., Wisitsoraat, A., Promptmas, C., Tuantranont, A., 2010. Ultrasensitive detection of Vibrio cholerae O1 using microcantilever-based biosensor with dynamic force microscopy. Biosensors and Bioelectronics, 26, 784-789.

Suprun, E.V., Budnikov, H.C., Evtugyn, G.A., Brainina, K.Z., 2004. Bi-enzyme sensor based on thick-film carbon electrode modified with electropolymerized tyramine. Bioelectrochemistry, 63, 281-284.

Susmel, S., Guilbault, G.G., O'Sullivan, C.K., 2003. Demonstration of labeless detection of food pathogens using electrochemical redox probe and screen printed gold electrodes. Biosensors & Bioelectronics, 18, 881-889.

Tamayo, J., Kosaka, P.M., Ruz, J.J., San Paulo, A., Calleja, M., 2013. Biosensors based on nanomechanical systems. Chemical Society Reviews, 42, 1287-1311.

Tan, F., Leung, P.H.M., Liu, Z.B., Zhang, Y., Xiao, L.D., Ye, W.W., Zhang, X., Yi, L., Yang, M., 2011. A PDMS microfluidic impedance immunosensor for E. coli O157:H7 and Staphylococcus aureus detection via antibody-immobilized nanoporous membrane. Sensors and Actuators B-Chemical, 159, 328-335.

Tawil, N., Sacher, E., Mandeville, R., Meunier, M., 2012. Surface plasmon resonance detection of E. coli and methicillin-resistant S. aureus using bacteriophages. Biosensors & Bioelectronics, 37, 24-29.

Tedeschi, L., Domenici, C., Ahluwalia, A., Baldini, F., Mencaglia, A., 2003. Antibody immobilisation on fibre optic TIRF sensors. Biosensors & Bioelectronics, 19, 85-93.

Tenreiro, A.M., Nabais, C., Correia, J.P., Fernandes, F.M.S.S., Romero, J.R., Abrantes, L.M., 2007. Progress in the understanding of tyramine electropolymerisation mechanism. Journal of Solid State Electrochemistry, 11, 1059-1069.

Tiede, C., Tang, A.A.S., Deacon, S.E., Mandal, U., Nettleship, J.E., Owen, R.L., George, S.E., Harrison, D.J., Owens, R.J., Tomlinson, D.C., McPherson, M.J.,

2014. Adhiron: a stable and versatile peptide display scaffold for molecular recognition applications. Protein Engineering Design and Selection, 27, 145-155.

Tlili, C., Sokullu, E., Safavieh, M., Tolba, M., Ahmed, M.U., Zourob, M., 2013. Bacteria Screening, Viability, And Confirmation Assays Using Bacteriophage-Impedimetric/Loop-Mediated Isothermal Amplification Dual-Response Biosensors. Analytical Chemistry, 85, 4893-4901.

Tolba, M., Ahmed, M.U., Tlili, C., Eichenseher, F., Loessner, M.J., Zourob, M., 2012. A bacteriophage endolysin-based electrochemical impedance biosensor for the rapid detection of Listeria cells. Analyst, 137, 5749-5756.

Torun, O., Boyaci, I.H., Temur, E., Tamer, U., 2012. Comparison of sensing strategies in SPR biosensor for rapid and sensitive enumeration of bacteria. Biosensors & Bioelectronics, 37, 53-60.

Tothill, I.E., Newman, J.D., White, S.F., Turner, A.P.F., 1997. Monitoring of the glucose concentration during microbial fermentation using a novel mass-producible biosensor suitable for on-line use. Enzyme and Microbial Technology, 20, 590-596.

Tran, L.D., Piro, B., Pham, M.C., Ledoan, T., Angiari, C., Dao, L.H., Teston, F., 2003. A polytyramine film for covalent immobilization of oligonucleotides and hybridization. Synthetic Metals, 139, 251-262.

Tripathi, S.M., Bock, W.J., Mikulic, P., Chinnappan, R., Ng, A., Tolba, M., Zourob, M., 2012. Long period grating based biosensor for the detection of Escherichia coli bacteria. Biosensors and Bioelectronics, 35, 308-312.

Tsuji, I., Eguchi, H., Yasukouchi, K., Unoki, M., Taniguchi, I., 1990. Enzyme Immunosensors Based on Electropolymerized Polytyramine Modified Electrodes. Biosensors & Bioelectronics, 5, 87-101.

Tully, E., Higson, S.P., Kennedy, R.O., 2008. The development of a 'labeless' immunosensor for the detection of Listeria monocytogenes cell surface protein, Internalin B. Biosensors & Bioelectronics, 23, 906-912.

Uygun, Z.O., Uygun, H.D.E., 2014. A short footnote: Circuit design for faradaic impedimetric sensors and biosensors. Sensors and Actuators B-Chemical, 202, 448-453.

Vo-Dinh, T., Cullum, B., 2000. Biosensors and biochips: advances in biological and medical diagnostics. Fresenius Journal of Analytical Chemistry, 366, 540-551.

Wan, Y., Lin, Z., Zhang, D., Wang, Y., Hou, B., 2011. Impedimetric immunosensor doped with reduced graphene sheets fabricated by controllable electrodeposition for the non-labelled detection of bacteria. Biosensors & Bioelectronics, 26, 1959-1964.

Wan, Y., Zhang, D., Hou, B.R., 2010a. Selective and specific detection of sulfate-reducing bacteria using potentiometric stripping analysis. Talanta, 82, 1608-1611.

Wan, Y., Zhang, D., Wang, Y., Hou, B., 2010b. A 3D-impedimetric immunosensor based on foam Ni for detection of sulfate-reducing bacteria. Electrochemistry Communications, 12, 288-291.

Wang, C., Irudayaraj, J., 2008. Gold Nanorod Probes for the Detection of Multiple Pathogens. Small, 4, 2204-2208.

Wang, J., 2002. Electrochemical nucleic acid biosensors. Analytica Chimica Acta, 469, 63-71.

Wang, J., 2006. Analytical electrochemistry. John Wiley and Sons, Inc., New Jersey and Canada.

Wang, Y., Knoll, W., Dostalek, J., 2012a. Bacterial Pathogen Surface Plasmon Resonance Biosensor Advanced by Long Range Surface Plasmons and Magnetic Nanoparticle Assays. Analytical Chemistry, 84, 8345-8350.

Wang, Y., Ye, Z., Si, C., Ying, Y., 2013a. Monitoring of Escherichia coli O157:H7 in food samples using lectin based surface plasmon resonance biosensor. Food Chemistry, 136, 1303-1308.

Wang, Y.X., Ping, J.F., Ye, Z.Z., Wu, J., Ying, Y.B., 2013b. Impedimetric immunosensor based on gold nanoparticles modified graphene paper for label-free detection of Escherichia coli O157:H7. Biosensors & Bioelectronics, 49, 492-498.

Wang, Y.X., Ye, Z.Z., Ying, Y.B., 2012b. New Trends in Impedimetric Biosensors for the Detection of Foodborne Pathogenic Bacteria. Sensors, 12, 3449-3471.

Wu, Z.S., Li, J.S., Deng, T., Luo, M.H., Shen, G.L., Yu, R.Q., 2005. A sensitive immunoassay based on electropolymerized films by capacitance measurements for direct detection of immunospecies. Analytical Biochemistry, 337, 308-315.

Yakovleva, M.E., Moran, A.P., Safina, G.R., Wadstrom, T., Danielsson, B., 2011. Lectin typing of Campylobacter jejuni using a novel quartz crystal microbalance technique. Analytica Chimica Acta, 694, 1-5.

Yang, T., Zhou, N., Li, Q.H., Guan, Q., Zhang, W., Jiao, K., 2012. Highly sensitive electrochemical impedance sensing of PEP gene based on integrated Au-Pt alloy nanoparticles and polytyramine. Colloids and Surfaces B-Biointerfaces, 97, 150-154.

Yang, X., Gu, C., Qian, F., Li, Y., Zhang, J.Z., 2011. Highly sensitive detection of proteins and bacteria in aqueous solution using surface-enhanced Raman scattering and optical fibers. Anal Chem, 83, 5888-5894.

Zakikhany, K., Degail, M.A., Lamagni, T., Waight, P., Guy, R., Zhao, H., Efstratiou, A., Pebody, R., George, R., Ramsay, M., 2011. Increase in invasive Streptococcus pyogenes and Streptococcus pneumoniae infections in England, December 2010 to January 2011. Eurosurveillance, 16, 6-9.

Zelada-Guillen, G.A., Sebastian-Avila, J.L., Blondeau, P., Riu, J., Rius, F.X., 2012. Label-free detection of Staphylococcus aureus in skin using real-time potentiometric biosensors based on carbon nanotubes and aptamers. Biosensors & Bioelectronics, 31, 226-232.

Zhang, J., Ji, H.F., 2004. An anti E. coli O157:H7 antibody-immobilized microcantilever for the detection of Escherichia coli (E. coli). Analytical Sciences, 20, 585-587.

Zhou, W.Z., Huang, P.J.J., Ding, J.S., Liu, J., 2014. Aptamer-based biosensors for biomedical diagnostics. Analyst, 139, 2627-2640.

Zhu, Q., Shih, W.Y., Shih, W.H., 2007. In situ, in-liquid, all-electrical detection of Salmonella typhimurium using lead titanate zirconate/gold-coated glass cantilevers at any dipping depth. Biosensors & Bioelectronics, 22, 3132-3138.

Zhu, T., Pei, Z.H., Huang, J.Y., Xiong, C.Y., Shi, S.G., Fang, J., 2010. Detection of bacterial cells by impedance spectra via fluidic electrodes in a microfluidic device. Lab on a Chip, 10, 1557-1560.